Topics in Medicinal Chemistry 8

Michael D. Wendt *Editor*

Protein-Protein Interactions

Springer

8

Topics in Medicinal Chemistry

Protein-Protein Interactions

Volume Editor: Michael D. Wendt

With contributions by

Angelo Aguilar · Paramjit S. Arora · Denzil Bernard · Kurt Deshayes · Stephen T. Joy · John Kadow · Sanjeev Kumar · David R. Langley · Andrew B. Mahon · Nicholas A. Meanwell · Stephen E. Miller · Jeremy Murray · Richard Pracitto · Domagoj Vucic · Michael A. Walker · Shaomeng Wang · Michael D. Wendt · Kap-Sun Yeung · Yujun Zhao

Springer

Editor
Michael D. Wendt
Dept R4N6 Bldg AP10
Cancer Research
Abbott Laboratories
100 Abbott Park Road
Abbott Park, IL 60064
USA

ISSN 1862-2461 ISSN 1862-247X (electronic)
ISBN 978-3-642-28964-4 ISBN 978-3-642-28965-1 (eBook)
DOI 10.1007/978-3-642-28965-1
Springer Heidelberg New York Dordrecht London

Library of Congress Control Number: 2012942189

Printed on acid-free paper

Springer is part of Springer Science+Business Media (www.springer.com)

Volume Editor

Michael D. Wendt

Dept R4N6 Bldg AP10
Cancer Research
Abbott Laboratories
100 Abbott Park Road
Abbott Park, IL 60064
USA

Editorial Board

Topics in Medicinal Chemistry Also Available Electronically

Topics in Medicinal Chemistry is included in Springer's eBook package *Chemistry and Materials Science*. If a library does not opt for the whole package the book series may be bought on a subscription basis. Also, all back volumes are available electronically.

For all customers who have a standing order to the print version of *Topics in Medicinal Chemistry*, we offer the electronic version via SpringerLink free of charge.

If you do not have access, you can still view the table of contents of each volume and the abstract of each article by going to the SpringerLink homepage, clicking on "Browse by Online Libraries", then "Chemical Sciences," and finally by selecting *Topics in Medicinal Chemistry*.

You will find information about the

- Editorial Board
- Aims and Scope
- Instructions for Authors
- Sample Contribution

at springer.com using the search function by typing in *Topics in Medicinal Chemistry*.

Color figures are published in full color in the electronic version on SpringerLink.

Aims and Scope

Drug research requires interdisciplinary team-work at the interface between chemistry, biology and medicine. Therefore, the new topic-related series *Topics in Medicinal Chemistry* will cover all relevant aspects of drug research, e.g. pathobiochemistry of diseases, identification and validation of (emerging) drug targets, structural biology, drugability of targets, drug design approaches, chemogenomics, synthetic chemistry including combinatorial methods, bioorganic chemistry, natural compounds, high-throughput screening, pharmacological in vitro and in vivo investigations, drug-receptor interactions on the molecular level, structure-activity relationships, drug absorption, distribution, metabolism, elimination, toxicology and pharmacogenomics.

In general, special volumes are edited by well known guest editors.

In references *Topics in Medicinal Chemistry* is abbreviated *Top Med Chem* and is cited as a journal.

Preface to the Series

Medicinal chemistry is both science and art. The science of medicinal chemistry offers mankind one of its best hopes for improving the quality of life. The art of medicinal chemistry continues to challenge its practitioners with the need for both intuition and experience to discover new drugs. Hence sharing the experience of drug discovery is uniquely beneficial to the field of medicinal chemistry.

The series Topics in Medicinal Chemistry is designed to help both novice and experienced medicinal chemists share insights from the drug discovery process. For the novice, the introductory chapter to each volume provides background and valuable perspective on a field of medicinal chemistry not available elsewhere. Succeeding chapters then provide examples of successful drug discovery efforts that describe the most up-to-date work from this field.

The editors have chosen topics from both important therapeutic areas and from work that advances the discipline of medicinal chemistry. For example, cancer, metabolic syndrome and Alzheimer's disease are fields in which academia and industry are heavily invested to discover new drugs because of their considerable unmet medical need. The editors have therefore prioritized covering new developments in medicinal chemistry in these fields. In addition, important advances in the discipline, such as fragment-based drug design and other aspects of new lead-seeking approaches, are also planned for early volumes in this series. Each volume thus offers a unique opportunity to capture the most up-to-date perspective in an area of medicinal chemistry.

Dr. Peter R. Bernstein
Prof. Dr. Armin Buschauer
Prof. Dr. Gunda J. Georg
Prof. Dr. Yoshiaki Kiso
Dr. John Lowe
Dr. Hans Ulrich Stilz

Preface

The last decade has been a difficult one for the pharmaceutical industry. The rate of new compound registrations has slowed from its peak in the 1990s, and efforts to shorten discovery times and streamline clinical paths have not resulted in increased efficiency overall. Moreover, biologics have become an increasingly large part of the field, and their higher success rate over the last several years has further disappointed prospects for small-molecule drug discovery going forward. Several explanations for this downturn have been put forward; one of the most commonly accepted is the idea that the 'low hanging fruit' has been picked, and the drug targets remaining are simply more challenging. With the synthetic, analytical, and structural technologies present today, the far greater understanding of relevant biology, and the vast and ever-growing historical knowledge of drug discovery at our fingertips, it is difficult to imagine that current practitioners in the field of small-molecule drug discovery are simply not as proficient as those of yesterday. While regulatory issues are more challenging than ever, it seems certain that the drug targets and biological mechanisms that the industry is focusing on are simply more difficult than those of 20 or 30 years ago. Thus the identification of high-quality drug targets – targets that are not only druggable, but of high biological relevance – is more crucial than ever.

Over roughly this same period of time, better understanding of biological systems – in particular of signaling pathways and various aspects of structural biology – has brought to the fore a new type of drug target for consideration. In addition to the enzymes, ion channels, and receptors that traditionally have comprised the domain of small-molecule drug targets, protein-protein interactions (PPIs) began to gain consideration. In the last two decades, the industry has taken on many PPIs, but few compounds have gained FDA approval, the vast majority of compounds that reached clinical trials have failed in the early stages, and the overall impression is one of higher-than-average failure in the discovery stage as well. Additionally, approved compounds have for the most part been intravenously delivered, and for narrow indications, and none have achieved 'blockbuster' status. All this has served to maintain and perhaps strengthen a common view of PPIs as being undruggable. PPIs are often seen as being part of the problem, rather than part of a possible way forward.

It is certainly true that thus far, the overall effort to modulate PPIs with small molecules has not constituted a successful venture. However, comparing the last two decades of PPI-targeted drug research to the success of earlier eras, or even to more conventionally targeted work over the same period, should not be of paramount concern. The important question is whether PPIs represent viable small-molecule drug targets now, and into the future. In order to answer this, it is necessary to look at what has been learned from two decades of work on PPIs in the pharmaceutical industry, and to consider how this experience can improve prospects for PPI-targeted drug discovery in coming years.

In this volume, we look at some of the most prominent and successful campaigns within the PPI field. In an introductory chapter, the field as a whole is appraised, with short summaries of several targeted PPIs. Classification of PPIs into structural types leads to some generalizations about the small-molecule inhibitors that emerge from projects targeting them; from a drug discovery standpoint, each type also has unique positive and negative aspects. Additionally, themes of the importance of structural and mechanistic understanding of targets are highlighted.

Chapter 2 surveys the field of inhibitors of the MDM2/p53 interaction, which essentially began with the high-profile disclosure of Nutlins, and quickly and steadily grew through programs at a number of pharmaceutical companies. The MDM2/p53 interaction constitutes a paradigm example of a relatively large, hydrophobic interaction surface for which lead compounds can easily be found. The success of several programs in deriving potent, orally bioavailable small molecules attests to the druggability of this target, and compounds have begun to enter clinical trials. Additionally, the use of many of these small molecules in elucidating additional biology around the MDM2/p53 axis is described. Chapter 3 covers IAP antagonists, also referred to as Smac mimetics, which are well-represented in the clinic for the treatment of cancer. The PPI targeted here involves recognition of a short peptide sequence, and is much different in character from the MDM2/p53 interaction. Drug discovery groups consequently had very different experiences in the course of finding and optimizing chemical matter. Additionally, this chapter, like Chap. 2, illustrates the complexity of signal transduction networks, and the complementary manner in which drug discovery programs are made more difficult by this complexity of relevant biological pathways, and can be of great aid in understanding them.

Chapters 4 and 5 look at PPIs in the field of antiinfective agents, with summaries of work targeted to inhibitors of various HIV-1-related processes, and to RSV fusion inhibitors. Many of these interactions are notable for being involved in structural recognition and reorganization processes instead of signaling pathways. Therapeutic compounds modulating these interactions can operate via a number of mechanisms, from simple blockade of a necessary conformational change or of the formation of a temporary complex, to

alteration of a pre-fusion oligomeric protein into a less-functional conformation. Defining these mechanisms of action adds to the difficulty of drug design. An additional complication, deriving from mutations leading to resistant varieties of targeted proteins, further hinders discovery efforts.

Many of the most challenging PPI interfaces involve widely separated contact points, which are particularly difficult to engage with a druglike small molecule. Therefore, general methods for reproducing this family of epitopes, and thereby substituting for or augmenting the usual drug discovery process, would be of great utility. Chapter 6 presents several approaches that have been taken in the area of α-helical peptide mimetics, primarily by academic laboratories. Designed molecules of this type have already proven valuable as biological probes and have attracted attention from major pharmaceutical companies, but questions remain as to their viability as drugs. The primary obstacles to these approaches concern stability and cell permeability of the mimetics, which continue to be addressed by researchers. However, it is expected that conventional small molecules directed to this type of PPI will tend to possess particularly difficult pharmacokinetic problems of their own. In the final chapter, a small-molecule effort directed at one of these PPIs is presented. Chapter 7 is a detailed case study of the Bcl-2 family inhibitors project at Abbott. Bcl-xL and Bcl-2 have much larger binding epitopes than conventional drug targets, larger even than many other PPIs, including MDM2/p53, and this program provides a rare example of a PPI with well-separated binding pockets that has yielded a fully optimized small-molecule clinical candidate. In this chapter, the particular challenges related to this type of PPI, such as lead identification and appropriate physicochemical characteristics of inhibitors are highlighted.

I thank the authors for their contributions to this volume, and hope that in total this book presents a suitably clear picture of where the field of PPI-directed small-molecule drug discovery has been, what lessons we can take from the past, and, armed with this experience, where the field might be headed.

February 2012 Michael D. Wendt

Contents

Contributors

Angelo Aguilar Comprehensive Cancer Center and Departments of Internal Medicine, Pharmacology and Medicinal Chemistry, University of Michigan, Ann Arbor, MI, USA

Paramjit S. Arora Department of Chemistry, New York University, New York, NY, USA

Denzil Bernard Comprehensive Cancer Center and Departments of Internal Medicine, Pharmacology and Medicinal Chemistry, University of Michigan, Ann Arbor, MI, USA

Kurt Deshayes Department of Early Discovery Biochemistry, Genentech Inc., South San Francisco, CA, USA

Stephen T. Joy Department of Chemistry, New York University, New York, NY, USA

John Kadow Department of Medicinal Chemistry, Bristol-Myers Squibb Research and Development, Wallingford, CT, USA

Sanjeev Kumar Comprehensive Cancer Center and Departments of Internal Medicine, Pharmacology and Medicinal Chemistry, University of Michigan, Ann Arbor, MI, USA

David R. Langley Department of Computer-Aided Drug Design, Bristol-Myers Squibb Research and Development, Wallingford, CT, USA

Andrew B. Mahon Department of Chemistry, New York University, New York, NY, USA

Nicholas A. Meanwell Department of Medicinal Chemistry, Bristol-Myers Squibb Research and Development, Wallingford, CT, USA

Stephen E. Miller Department of Chemistry, New York University, New York, NY, USA

Jeremy Murray Department of Structural Biology, Genentech Inc., South San Francisco, CA, USA

Richard Pracitto Department of Medicinal Chemistry, Bristol-Myers Squibb Research and Development, Wallingford, CT, USA

Domagoj Vucic Department of Early Discovery Biochemistry, Genentech Inc., South San Francisco, CA, USA

Michael A. Walker Department of Medicinal Chemistry, Bristol-Myers Squibb Research and Development, Wallingford, CT, USA

Shaomeng Wang Comprehensive Cancer Center and Departments of Internal Medicine, Pharmacology and Medicinal Chemistry, University of Michigan, Ann Arbor, MI, USA

Michael D. Wendt Dept R4N6 Bldg AP10, Cancer Research, Abbott Laboratories, Abbott Park, IL, USA

Kap-Sun Yeung Department of Medicinal Chemistry, Bristol-Myers Squibb Research and Development, Wallingford, CT, USA

Yujun Zhao Comprehensive Cancer Center and Departments of Internal Medicine, Pharmacology and Medicinal Chemistry, University of Michigan, Ann Arbor, MI, USA

Top Med Chem 8: 1–56
DOI: 10.1007/978-3-642-28965-1_1

Protein-Protein Interactions as Drug Targets

Michael D. Wendt

Contents

M.D. Wendt (✉)
Dept R4N6 Bldg AP10, Cancer Research, Abbott Laboratories, 100 Abbott Park Road, Abbott Park, IL 60064, USA
e-mail: mike.d.wendt@abbott.com

Abstract Over the last two decades, a number of protein-protein interactions (PPIs) have been targeted by the pharmaceutical industry. Pharma as a whole has historically considered PPIs to be undruggable or at the very least high-risk targets, and the relative lack of success in modulating PPIs with small molecules has done little to change this prevailing view. However, many compounds are now in clinical trials, and the experiences of the last 20 years have at the very least led to improved understanding of how to approach these challenging targets. This chapter discusses some of the issues that PPIs present as targets for small molecule modulation, with emphasis on the structural characteristics of PPIs in general, and also of classes of PPIs that share specific attributes. Grouping PPIs by structural class produces a clearer picture of both the characteristics of optimized small molecules, and the relative merits and drawbacks of various PPIs as drug targets. Within this framework, much of the past work in the PPI area is summarized through capsule descriptions of efforts directed against individual targets. Some contributors to individual successes and failures, and some insights gained from the many avenues of research followed within the PPI field are put forward. Themes of the importance of understanding the structural basis of mechanism of action and of structural support for drug discovery emerge, and guidelines for future study are offered.

Keywords Drug discovery • Inhibitors • Protein-protein interactions • Protein surface

1 Introduction

It has been estimated that roughly 10% of the human genome is involved in some type of disease state, resulting in a corresponding ~3,000 potential drug targets [1]. To that one could add a number of proteins belonging to infectious organisms. However, in order to be considered suitable targets for small-molecule drug discovery, proteins also need to be "druggable" in the sense that sufficiently potent compounds can be found that also possess the physicochemical properties necessary to be orally bioavailable. Current estimates have also converged on a value of ~3,000 for the number of druggable proteins [1, 2]. The intersection of these two groups, estimated at 600–1,500 [2], defines an approximate number of exploitable small-molecule drug targets available to the pharmaceutical industry. To date, roughly 300 proteins belonging to about 130 protein families have been successfully targeted by approved drugs [3]. These numbers are dwarfed by estimates of the numbers of protein folds (1–10,000) and protein families (16–60,000) [4–6]. Historically, the vast majority of biological targets for small-molecule drug discovery have been enzymes, ion channels, and G-protein coupled and nuclear hormone receptors [1–3].

Recent advances in genomics and proteomics have brought to light vast networks of protein-protein interactions (PPIs), termed the interactome [7]. As a result, we now have a far greater understanding of signaling pathways and host-pathogen

interactions, potentially opening up a large number of new targets for pharmaceutical intervention [8–10]. However, the pharmaceutical industry has been reluctant to focus on this extremely diverse and far-reaching class of potential drug targets, at least within the framework of finding small-molecule drugs. Pharma has both recognized and successfully demonstrated the biological and commercial validity of many of these targets through the application of therapeutic antibodies, the market for which continues to lead the growth of the prescription drug market as a whole [11]. While therapeutic antibodies possess some outstanding qualities as drugs, including high stability and outstanding specificity, they also suffer from a number of serious drawbacks. Biologics are both expensive and difficult to produce, are not orally bioavailable, and are unable to antagonize intracellular protein targets. Thus, even taking into account the anticipated expansion of biologicals into additional markets, PPIs as a group remain compelling targets from a biological standpoint. Yet, while there has been a large increase in the number of small-molecule programs targeting PPIs over the last 20 years, particularly in the cancer, immunology, and antiinfective areas, a general wariness of these targets remains, stemming primarily, but by no means completely, from a negative assessment of their druggability. Moreover, the successes in this area, whether measured by the number of clinical candidates or marketed drugs, have been few in number.

This chapter will discuss what has been learned about PPIs and their viability as drug targets over the last two decades. Following a general section on the defining aspects of PPIs, highlighting the challenges that PPIs present to drug discovery groups, this chapter then looks specifically at several of the most prominent pharma-targeted PPIs over the last two decades, focusing primarily on structural characteristics of binding sites, and the issues associated with them.

2 PPIs as Drug Targets

Beyond druggability challenges, PPIs have created other complications for drug discovery programs [12–19]. These include issues of identification and characterization of small-molecule binding sites, the lack of natural ligands that can be easily used as a starting point for drug discovery, and various problems associated with compound screening – relying on screening sets that are poor matches for PPIs, separating real from artifactual hits, and verifying the proper binding location of hit compounds. All of these issues ultimately relate back to the fundamentally different endogenous interactions of PPIs, compared to enzyme-substrate or receptor-substrate interactions. Close examination of this class of interactions follows.

2.1 Structural Characteristics of Protein-Protein Interfaces

While in principle binding between proteins can be driven by widely varying mixtures of polar and electrostatic interactions (H-bonds and salt bridges),

in practice the binding energies are largely derived from the mutual burying of largely complementary hydrophobic surfaces [20]. The interfaces formed normally have a hydrophobic core, with a more polar border which remains solvent-accessible after binding [21]. These interface cores are often the most hydrophobic patches on the individual protein surfaces [22]. Both theory and observation have established that a rough minimum of 1,200 $Å^2$ of interface area, or 600 $Å^2$ per monomer, is required to stabilize a PPI [20]. Most PPIs of interest will involve somewhat larger surface areas, between 750 and 1,500 $Å^2$ for each protein [23]. It has been suggested that the minimum area corresponds to that required to make a water-tight seal around a set of interactions that are strong enough to carry out biological activity [21].

It is important to make a distinction between obligate, permanent dimer or oligomer interfaces forming a stable structure, and transient interfaces formed by separate proteins capable of carrying out independent functions. Members of the former group bind much more strongly, and their interfaces are larger and less flat, with tighter packing and very few water molecules trapped between monomers [20, 23–25]. Also, the energetic dominance of hydrophobic surface matching for obligate protein-protein complexes is more overt than for temporary complexes [23, 26, 27]. Accordingly, the amino acid compositions of obligate interaction surfaces are much more hydrophobic than overall protein exteriors, sometimes closely resembling those of protein cores [26–30], while transient complex surfaces are roughly halfway between interior and surface by this measure [23, 24]. This is to be expected given the amounts of time the two types of surface spend exposed to solvent.

Relative to solvent-accessible surfaces, permanent interfaces contain an over-abundance of nonpolar amino acids, both aromatic and aliphatic, particularly near the center of the contact surface. Temporary interfaces do not feature a much higher percentage of nonpolar residues, but do contain more neutral polar residues at the expense of charged amino acids, with the exception of arginine, which is also overrepresented in obligate complex surfaces [21, 23, 24]. Hydrogen bonds are not uncommon in temporary interfaces, with, on average, one hydrogen bond per 170 $Å^2$ of interacting surface [23]. About one third involve a charged side chain, and salt bridges comprise just over one in ten polar interactions. Among obligate complexes, the density of hydrogen bonds is not very different [20], but a far greater percentage involve one or two charged species, in keeping with relative surface amino acid compositions [30].

Among nonpolar residues, the larger amino acids, and in particular the aromatic residues, are overrepresented in the hydrophobic cores of transient PPI surfaces [21, 23, 31–33]. While still lipophilic, aromatic side chains have lower transfer free energies per atom than aliphatic side chains [34–36]. Methionine, while not a major component of interfaces, is also often more frequently found there than in permanently exposed or buried surfaces, and also has a low transfer free energy. Methionine is known to interact very favorably with aromatic groups, probably due to the polarizability of both aromatic systems and sulfur atoms. Together, these residues also feature the most flexibility and size among nonpolar residues, and thereby have

the greatest capacity to change the shape of a local surface; their overrepresentation enhances the well-known mobility of many hydrophobic patches.

To the medicinal chemist, then, a first-order description of protein-protein interfaces paints a picture of two very large interacting surfaces, mostly devoid of small, polar features that could by themselves, bound to an appropriate structure, produce large amounts of affinity. The surfaces instead achieve sufficient affinity only through summing weak interactions over a very large area. Optimization of antagonists of this type of interaction are expected to yield very large, hydrophobic, and atom-inefficient compounds.

An important refinement to this view was put forth by Clackson and Wells [37], who demonstrated, through the use of alanine scanning [38], that certain key residues in a growth hormone system had a very disproportionate effect on binding, and the corresponding subregions of binding surfaces were referred to as "hot spots." Similarly, multiple studies have established that a very limited number of residues at protein-protein interfaces are crucial, and a single point mutation can often greatly reduce affinity or even completely block a PPI without changing the overall integrity of the protein [39–41]. Hot spots have since become the subject of a great deal of study, particularly through their interactions with small-molecule inhibitors of PPIs [21, 23, 24, 42–46]. Hot spots tend to be of small-molecule size and are normally located near the center of PPI surfaces. Hot spots also commonly have a capacity to adapt conformationally, producing more concave local topologies and increasing their ability to accommodate more conventionally drug-sized ligands. Many studies using phage display of small peptides have shown strong preferences for binding at hot spots [47–49], which illustrates their propensity for binding a variety of small molecules. Finally, a number of publications have demonstrated the robustness of the hot spot paradigm by using hot spot-based models to rationally predict small-molecule binding sites on proteins [42, 50–54].

While the conformational flexibility of hot spots is not expected to greatly reduce the lipophilicity of a corresponding small-molecule inhibitor, it does improve the prospects for a viable antagonist of a reasonable size. By forming a better defined pocket, a hot spot may allow more protein surface to be buried by a smaller ligand. Still, due to the relative lack of high-energy polar interactions between protein and ligand, efficiencies of binding [55, 56] of optimized PPI-directed compounds will still be lower than those of most receptor- or enzyme-targeted compounds. However, the differences, while meaningful, are not so extreme. In one study, a group of optimized PPI inhibitors had an average ligand efficiency (LE) of 0.24, compared to 0.25–0.35 for protease inhibitors, and 0.3–0.4 for kinase inhibitors [16]. A more recently derived figure gives a value of 0.27 for advanced PPI inhibitors [57]. Thus, while the view that PPI binding is primarily driven by hydrophobic surface-matching is largely correct, the impact of this on the druggability of many PPI sites is commonly lessened due to the presence of small subsites within the contact surfaces.

2.2 Physical Characteristics of Small-Molecule PPI Antagonists

As alluded to above, the characterization of PPIs as undruggable rests on a view of their binding surfaces as being in general too large and too hydrophobic for their constituent interactions to be inhibited by druglike molecules. Rules of thumb such as Lipinski's Rule of Five [58], polar surface area (PSA) restriction [59], and the "golden triangle" [60] seek to quantify measurable aspects of orally bioavailable molecules in order to provide guidance to future medicinal chemistry efforts. Compounds in violation of these measures of druglikeness are expected to be particularly prone to preclinical and clinical failures associated with various ADMET issues.

As the amount of work targeting PPIs has grown, many researchers have analyzed data from the literature, from both academic and industrial research groups, to derive chemotypes for PPI inhibitors [57, 61–63]. Many different interactions, involving most protein fold classes, have been included in these efforts. As a result, a general picture is emerging of the molecular properties of advanced PPI inhibitors. These compounds, as expected, usually fall outside the standard realm of druggable compound space, having higher molecular weight and logP values than rules of thumb recommend. Even early hits and leads often suffer by comparison to similar guidelines established for these compounds [64–66]. This is a particular problem because early project molecules tend to become more lipophilic throughout the optimization process [64]. Interestingly, advanced PPI inhibitors also tend to be relatively rigid and are more highly aromatic than other optimized compounds, also in keeping with what is known about the makeup of hot spots [19, 57, 61, 62].

The failure of optimized PPI antagonists to fall within desirable ranges of compound space has reinforced the concerns of pharmaceutical discovery programs over the druggability of PPIs. Yet implicit in these assessments are a number of assumptions. First, the common physicochemical guidelines defining "druglike" molecules may be too restrictive, leading to a similarly restrictive view of how many druggable proteins exist. Second, the definition of some potential targets as undruggable due to either a lack of precedent, or previous failures to find compounds from screening efforts, lacks sufficient rigor, and is dependent on an assumption of the future of drug discovery looking very similar to the past.

Good aqueous solubility and high permeability are optimal qualities for a compound to have in order to possess good oral bioavailability. In practice, candidate molecules, particularly larger compounds, must try to strike a balance between these two characteristics. It comes as no surprise that PPI inhibitors usually fail on these grounds. If limits on polar surface area (PSA) and logP are adhered to, then molecules above a certain size are mathematically almost certain to run afoul of one of those two guidelines. A noted study by Veber [67] demonstrated that low PSA and low rotatable bond count are by themselves good predictors of oral bioavailability, suggesting that molecular weight is primarily a proxy for other characteristics, especially molecular flexibility. Additionally, several papers have

shown that oral absorption can be predicted with a high degree of accuracy from surface properties such as PSA and the number of hydrogen bonding groups alone [59, 68–70]. Interestingly, these correlates roughly describe the set of advanced PPI inhibitors discussed above, which are relatively rigid and have low PSA values and few hydrogen bonding groups in spite of their size. It may be that by keeping these parameters low, higher than recommended logP values and molecular weights may be tolerated. Finally, PPI inhibitors, by virtue of their larger size, will in general be expected to have a greater tendency to reduce their effective size and polarity through hydrophobic collapse or internal hydrogen bonding [71], further enhancing their membrane permeability.

Oral bioavailability rules are based on successfully developed compounds discovered years or decades ago. However, current and recent medicinal chemistry work has not been targeting the same therapeutic modalities as in past decades, and compounds designed toward current targets often do not and cannot occupy the same chemical space as older marketed drugs. Several studies over the past decade have demonstrated that advanced compounds have become larger and more hydrophobic as the industry has moved on to different targets [72–75]. Additionally, compounds directed to individual targets have also tended to increase in size over time [76, 77]. A number of explanations for this phenomenon have been put forward [75], among them the dominance of the target-based drug discovery paradigm, an increasing focus on selectivity, the need to find new patentable space, and reliance on high-throughput screening (HTS) for chemical matter.

The foregoing is not meant to suggest that concerns over the likely physical properties of PPI inhibitors should be ignored. Several studies have shown that clinical attrition rates of compounds correlate with size and lipophilicity [72, 74, 78], and the trend within pharma toward deriving compounds with that profile has certainly contributed to difficulties in getting clinical candidates to market. It is only meant to point out that comparison of current targets of any type to those responsible for populating recommended chemical space places an – unfortunately – unrealistic burden on them. A more appropriate and important comparison is between PPIs and other current potential drug targets. Targets such as HIV protease, and peptide-liganded GPCRs such as the angiotensin II and chemokine receptors, have become increasingly popular, and inhibitors directed to these targets are often near or beyond desired ranges for prediction of good oral bioavailability. Many kinase inhibitors, particularly inactive-conformation-targeting compounds, also share these traits. These high molecular weight compounds often have very low aqueous solubility but fair to good lipid solubility and adequate oral pharmacokinetics [79]. Against this background, the higher-than-historical size and lipophilicity of PPI-modulating compounds, while far from optimal and of legitimate concern, need not be seen as an overriding obstacle, but as one complicating factor – among many that are inevitably presented by a given drug target – common to PPIs, as well as several non-PPI targets currently under examination by the pharmaceutical industry.

Compounds with these physicochemical characteristics will normally fit into the FDA Class II or IV pharmacokinetic classifications. Many may be expected to exhibit dissolution rate-limited absorption, due to their low solubility and high lipophilicity. One analysis has shown that poorly soluble drugs that have nevertheless reached the market tend to have low solubility driven by lipophilicity, and not high crystallinity, and this type of compound is also most susceptible to enhancement of absorption by the implementation of various excipient additions or advanced formulation techniques [80]. A number of formulation technologies have been introduced in recent years that address pharmacokinetic liabilities such as this, among them protein nanoparticles [81], gels [82], microemulsions [83], dendrimers [84], liposomal nanocarriers [85], and melt extrusions and other solid dispersion technologies [86]. Increasing numbers of compounds entering the clinic, not only PPI inhibitors, will inhabit a different region of chemical space than older compounds, and enabling technologies will increasingly be of value in enhancing their oral bioavailability. Further experience will be necessary to determine whether poorly soluble, high logP compounds can frequently enough achieve acceptable oral bioavailability through maintenance of PSA, and application of formulation technologies.

2.3 Identification of Small-Molecule Binding Sites

Identifying chemical matter for a PPI can be particularly challenging. An early difficulty associated with some PPI drug targets is the identification of the proper location of intervention by a small molecule. Unlike traditional drug targets, for which the natural ligand is of small-molecule size and the location of binding is known, the small-molecule binding site of a PPI – if it exists at all – must be determined. Usually, the endogenous substrate is of such a size that there is still a question as to where within that interaction surface a small molecule might bind.

The average volume of concave pockets at PPI interfaces is very small, with an average of six sites of roughly 50 $\mathring{A}^3$ per interface [54]. It is extremely difficult to identify from simple inspection which of these are hot spots exploitable by small molecules. This is particularly evident from comparisons of unbound and complexed structures of a number of proteins involved in PPIs [46, 87]. A given protein surface should be considered to be able to assume a number of different local conformations, with only some of them featuring well-defined, deep binding pockets capable of a strong interaction with a given ligand. An excellent illustration of this is a study using picosecond time-scale molecular dynamics simulations on MDM2, IL-2, and Bcl-xL that showed the unbound proteins forming transient conformations similar to their inhibitor-bound states [88]. Thus, it is usually not clear from inspection of a given apoprotein or endogenous protein-ligand crystal structure where hot spots are, nor what their local conformations would be given the presentation of an appropriate small molecule [89, 90]. Methods to determine hot spot locations include mutagenesis studies, including the aforementioned phage display

methodology [47–49]. Alanine scanning in particular has been useful in determining which parts of a peptide epitope are responsible for key contacts [45, 47]. Additionally, both molecular dynamics studies and computational methods based on small-molecule docking or surface scoring functions [42, 50–54, 91], can aid in predicting hot spots, but these latter methods by themselves may not provide the assurance of druggability necessary to begin a drug discovery program.

2.4 Compound Screening Methods

The PPI inhibitor discovery process often begins with attempts at dissection of the 'lock' member of the binding pair into a minimal binding peptide. Some PPIs center on a short peptide binding motif; for these, epitope mapping of this sort is often successful. In most cases, however, this approach is not possible, as there is no single dominant part of the binding surface that can be located to a continuous peptide sequence. The key contacting amino acid residues – hot spots – are widely separated, both spatially and in terms of secondary structure, and the impracticality of using an α-helical or β-sheet fold as a starting point for small-molecule drug discovery means that other avenues must be sought. For these reasons, HTS is often applied to the problem.

Many types of assay are available to be used in HTS protocols to identify inhibitors of PPIs, but a competition assay, in which inhibition of complex formation is measured, is most common. Fluorescence polarization (FPA), fluorescence resonance energy transfer (FRET), enzyme-linked immunosorbent assays (ELISA), and other assay formats have been used. The interacting proteins can be used in their full-length forms; though, more frequently only the interacting domains are employed, and if possible the excised interacting peptide is usually preferred.

PPIs often confront HTS with a number of complications. First, the matter of separating true hits from artifacts, compounds that cause precipitation or aggregation of the protein, can be particularly difficult. When screening against a hydrophobic PPI, there is virtually no chance of finding very high affinity (sub-micromolar) compounds, so the best hits will be at or below an affinity level where artifact compounds are more common. Moreover, for well-established target types, screening will normally yield a group of compounds among which some contain a functionality that is known to, or can easily be identified to, interact strongly with a key moiety within the target. Compounds without such a moiety can often be excluded with a high degree of confidence. For PPI targets, compounds that are aggregators [92, 93] or denaturants – acting via a detergent effect – may not be separable from true hits by inspection, especially in light of the fact that both types of promiscuous hits tend to be populated by large hydrophobic compounds. Careful modification of assay conditions can often diagnose aggregation; alternately, analytical ultracentrifugation (AUC) can be used [94–96]. Additionally, AUC, isothermal titration calorimetry (ITC) [97, 98], surface plasmon resonance (SPR) [99, 100], and other methods can determine binding stoichiometry. Also, questions

of inhibition through allosteric mechanisms can require additional experiments. At any rate, when investigating a PPI, it is often very complicated to perform the necessary verification of screening hits with secondary approaches.

Normal high-throughput screening (HTS) often fails to yield results for PPI targets. Pharmaceutical company compound repositories, being reflections of their history, consist mainly of larger molecules tailored to bind to a specific enzyme or receptor. As such, most of these compounds feature a specific, usually highly polar group chosen to interact with an active site or recognition element. This polar group, coupled with the larger size of more fully elaborated compounds, will prevent most compounds from efficiently binding to a hot spot. Additionally, even less polar compounds rarely have the proper shape to bind effectively to the protein target, but can still appear as moderate-affinity binders through indiscriminate hydrophobic interactions.

Fragment screening [101–106] would seem to be a complementary approach, particularly suited for small, isolated hot spots, though this method has still not quite achieved a ubiquity in pharma commensurate with that of HTS. Fragment screening uses libraries of smaller molecules, usually with an average molecular weight of 150–250. These compounds are of a more appropriate size and level of complexity to bind to many hot spots, and once bound, the molecules are better able to find the most complementary geometry for a given binding site. Smaller compounds normally result in lower-affinity hits (10–100 μM or more), so particularly robust screening methodologies are required. The most popular technique has been NMR spectroscopy [101, 107], though surface plasmon resonance (SPR) has been gaining wide acceptance [108, 109], and mass spectroscopy and even X-ray crystallography have been successfully employed [106, 110–112].

The variety of complications that can result from insufficient knowledge of the targeted protein-small-molecule interaction can be largely avoided by using a structure-based screening method, such as NMR screening [113–115] or X-ray crystallography [116, 117], or at least by using analytic structural methodologies to verify other screening results. It is in practice impossible to carry out these types of screening on larger compound libraries due to the low-to-medium throughput of these methods. However, screening libraries are often suitably truncated through the prior application of in silico screening methods [118–121], or the functional assays discussed above. Alternately, after lead compounds have been found, site-directed mutagenesis studies can be performed to confirm the site of binding.

3 PPIs with Noncontinuous Epitopes

The following group of drug targets most closely exemplifies the standard structural picture of PPIs. All feature a large interaction surface with a hydrophobic core and a more polar rim that is minimally involved in interactions with small-molecule inhibitors. However, members of this group of targets vary greatly in the precise nature of their binding surfaces. The shape, size, and relative locations of

hydrophobic hot spots dominate the character of the binding sites, and thereby in large part determine the physicochemical qualities of inhibitors resulting from compound optimization, producing small molecules that have little in common other than a tendency toward large size and hydrophobicity. Related to this, the discontinuity of the natural ligand epitopes requires drug discovery programs to derive chemical matter through chemical screening techniques, such as HTS, fragment screening or in silico screening. As a result of the mobility of the protein surfaces involved, and the adaptive conformations that can result from presentation of differently structured inhibitors, it is particularly valuable to have structural support for programs targeting one of this family of PPIs.

3.1 IL-2/IL-2Rα

The cytokine IL-2 plays a key role in growth, differentiation, and activation of T-cells. The antibodies daclizumab and basiliximab, which recognize the α5 subunit of the IL-2 receptor (IL-2Rα) and block binding of IL-2, have been clinically effective as immunosuppressive agents [122]. However for reasons of cost, administration, and possible side effects, they are used only pre- and post-transplantation, and in the acute phase of transplant rejection. This state of affairs has precipitated interest in small-molecule inhibition of this interaction.

IL-2 has a typical four-helix bundle cytokine fold [123]. Site-directed mutagenesis identified several residues important for receptor binding on the AB loop and the B helix [124]. Roche used this data to target a series of acylphenylalanines designed to bind to IL-2Rα by mimicking Arg38 and Phe42 of IL-2. A modest medicinal chemistry effort resulted in compound **1**, with an IC_{50} of 3 μM [125]. Surprisingly, ELISA and NMR studies showed that these compounds bind to IL-2 rather than IL-2Rα.

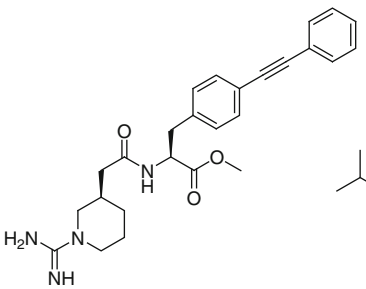

1

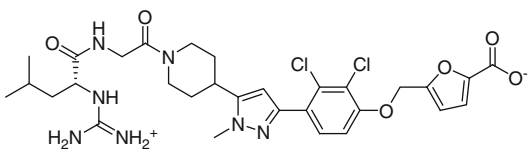

SP4206

Sunesis, using their tethering methodology [126], employed a fragment-based approach to explore two subregions of the binding site. Their medicinal chemistry work started with two fragments derived from the Roche compound **1** [127]. The excised biaryl amino acid was coupled to a small library of surrogates for the

guanidine fragment, after which the new polar fragment was used as a coupling partner for a library of hydrophobic monomers. The resulting synthetically tractable compound served as a lead for conventional optimization. Throughout this process, compounds were analyzed by SPR, analytical ultracentrifugation (AUC), and NMR in order to verify that the inhibition of the IL-2/IL-2Rα interaction correlated with reversible, stoichiometric binding to IL-2 at the IL-2Rα binding site. IL-2-bound X-ray structures were obtained for some compounds, including the optimized SP4206 [128, 129]. Subsequently, a structure of the IL-2/IL-2Rα complex was disclosed [130]. As anticipated, the receptor and inhibitor bound to the region of IL-2 between the A and B helices. While the receptor contacts IL-2 much more extensively, with a total buried surface of 1,868 $Å^2$, the affinity of SP4206 ($K_i = 60$ nM) is nevertheless comparable to that of the receptor, and consequently far more ligand-efficient.

Further comparison of the two IL-2 complexes is very interesting. The receptor uses parts of four β-strands to contact the IL-2 surface (Fig. 1a), illustrating the impossibility of using a peptide/peptidomimetic approach for this target. Most side chains make purely hydrophobic contacts with two complementary lipophilic subregions of IL-2, while a ring of edge residues make polar interactions with the IL-2 surface. In particular, Lys35 and Arg38 of IL-2 contact a highly acidic region of IL-2Rα, while Glu62 forms a salt bridge with Arg36 of the receptor. Similarly, the guanidine group of SP4206 forms a salt bridge with Glu62 of IL-2, while the terminal furanoic acid is situated between the Arg38 and Asp35 side chains (Fig. 1b). The D-leucine side chain and the two central aromatic rings make good contact with the well-separated hydrophobic regions. In particular, the dichlorobiphenyl group fills a very well-defined subpocket that is not present in the IL-2/IL-2Rα structure.

Structural aspects of the hydrophobic interactions are quite different in the two complexes. Though the IL-2 backbone is essentially identical in the two structures, the IL-2 surface complexed to SP4206 achieves greater concavity through rearrangement of side chains of Lys35, Arg38, Met39, and especially Phe42. The deeper penetration of the dichlorophenyl group resulting from this may be partly responsible for the superior efficiency of SP4206 binding relative to that of the receptor. By contrast, the IL-2/IL-2Rα structure shows Tyr45 and especially Phe42 pointed away from the rest of the IL-2 surface, fitting into complementary subpockets on IL-2Rα. The authors of the IL-2/IL-2Rα X-ray paper describe IL-2 in general, and Phe42 and Tyr45 in particular, as taking the "convex" role of the ligand in the interaction, and not the "concave" role of the receptor. This illustrates the relative flatness of the endogenous interaction as a whole, and the complexed surfaces are best described as being complementary without either partner taking on a clear structural role within the ligand/receptor paradigm. The small molecule, by comparison, without an extended surface to engulf the hydrophobic surface of IL-2, is instead effective by inducing more local concavity, and locking in a low-energy conformation of IL-2 which increases the enthalpy of interaction at little additional

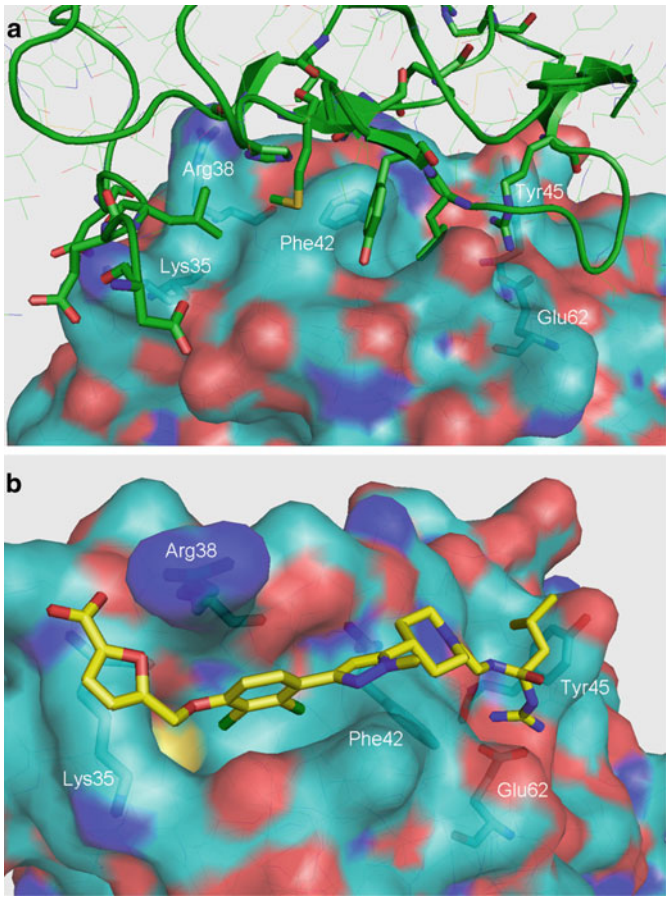

Fig. 1 (**a**) X-ray crystal structure of IL-2/IL-2Rα interface, with important IL-2Rα residues shown (**b**) X-ray crystal structure of SP4206 bound to IL-2. Key IL-2 residues are *highlighted* in both structures (pdb 1z92, 1py2)

entropic cost [131]. Nevertheless, SP4206 does an excellent job of broadly mimicking the key interactions found in the native complex. Interestingly, alanine scanning of IL-2 identified Phe42, Tyr45, and Glu62 as by far the most important residues for binding either SP4206 or the receptor, with replacement of each causing >100-fold reductions in affinity.

Several other X-ray structures of IL-2 complexes attest to its surface malleability [127]. This serves as an excellent example of the capacity of a hydrophobic hot spot to undergo rearrangement to focus its surface into a shape more complementary to a small molecule.

3.2 HPV E1/E2

Human papillomavirus (HPV) is the cause of a number of benign and malignant epithelial lesions, including most cervical cancers. The HPV vaccine Gardasil, introduced in 2006, is effective in removing the threat from some of the most high-risk variants of HPV, and Cervarix, a second vaccine, was recently given FDA approval [132, 133]. Still, HPV infection-related lesions remain common, particularly in the developing world. Therapies are usually cytodestructive, and there are no small-molecule HPV antivirals available.

Papillomaviruses are nonenveloped viruses with genomes encoding eight proteins [134]. The interaction between the viral transcription factor E2 and the viral initiator helicase E1 forms a prereplication complex, and is necessary to the viral cycle. E2 temporarily blocks oligomerization of E1, and guides E1 to the DNA origin of HPV, where E2 dissociates, allowing E1 hexamer formation and commencement of DNA replication. Boehringer Ingleheim initiated a program directed to this interaction as a means of treating benign warts caused by low-risk variants HPV6 and -11, as this condition involves continuous DNA replication [135]. A group of indanediones was identified through HTS, using radiolabeled origin DNA in a scintillation proximity assay [136, 137]. This assay had the potential to identify inhibitors of any interaction between the three members of the E1–E2-DNA complex, but further experiments demonstrated that the assay was only likely to identify E1–E2 interaction inhibitors. Counterscreens were also implemented to eliminate nonspecific compounds, and functional assays were developed to serve as proxies for viral replication, due to the complexity of the viral lifecycle. Optimization of leads afforded compounds with DNA replication inhibition in vitro and in vivo, with **2** possessing an $IC_{50} = 6$ nM [136–139]. Multiple biochemical assays, NMR, and isothermal titration calorimetry (ITC) experiments showed that these molecules bound to the transactivation domain (TAD) of E2. A second series was found through rescreening the BI compound repository with an automated ligand displacement assay. Extensive SAR work led to compound **3**, with IC_{50} values of 20 and 123 nM against HPV11 and -6, respectively [140]. Inhibitors have high affinity to HPV6 and -11, but not the key high-risk variants HPV16 and -18 [137]. This is in part attributable to His32, which in the high-risk HPV variants is a tyrosine. Substitution of His32 by the larger residue is predicted to prevent complete opening of a deep hydrophobic pocket.

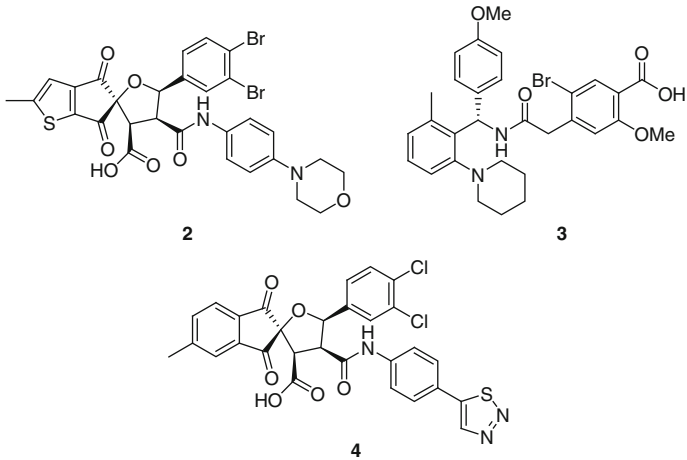

During the course of this work, structures of TADs from HPV16 and HPV18 were obtained [141, 142], and shortly afterward, the structure of an E2 TAD in complex with E1 from HPV18, the most prevalent variant, was disclosed [143]. In the E1/E2 complex, the three helices of the N-terminal domain of E2, plus a linker connecting the N- and C-terminal domains, contact several small helices and a long loop of the E1 protein. The periphery of the E1/E2 interface contains a mix of polar and nonpolar interactions, most importantly the highly conserved E1 Arg454-E2 Glu39 salt bridge. At a late stage of the Boehringer-Ingleheim project, an X-ray structure of an E2 TAD/**4** complex was also determined (Fig. 2). Interestingly, this showed two molecules of the inhibitor bound to the E2 TAD surface, with one making much better surface contact [138]. The large contact surface of the E1/E2 complex, 940 $Å^2$ per protein, completely engulfs that of the E2/**4** interaction surface, with 20 E2 residues involved in binding to E1 compared to seven for the **4** complex. The E2 surface is also much more concave in the latter structure, with the primary hydrophobic hot spot roughly in the center of the larger E1 binding surface. The protein backbone conformation is not significantly altered, but residues Tyr19 and His32 rotate their side chains ~90°, and Leu94 and Glu100 also make adjustments to form the hydrophobic pocket into which the main indanedione is buried. The ring system forms a sandwich complex with side chains of His32 and Trp33, while the carboxylate group forms hydrogen bonds to backbone amides.

While the second inhibitor molecule in the crystal structure does not make the same degree of contact with the surface of E2, and was shown to be a crystallization artifact, the chlorophenyl ring of the second molecule does appear to bind into a well-defined small pocket. An isobutyric acid also found in the crystal structure binds in a small cleft on the other side of the main pocket, and forms a salt bridge with His32. Interestingly, these two additional subsites were identified by a computational probe mapping study as secondary hot spots [43]. The two extra molecules in the binding site are clearly interacting not only with the E2 surface but also with the surface of the first molecule of **4**; the concavity of both secondary sites is

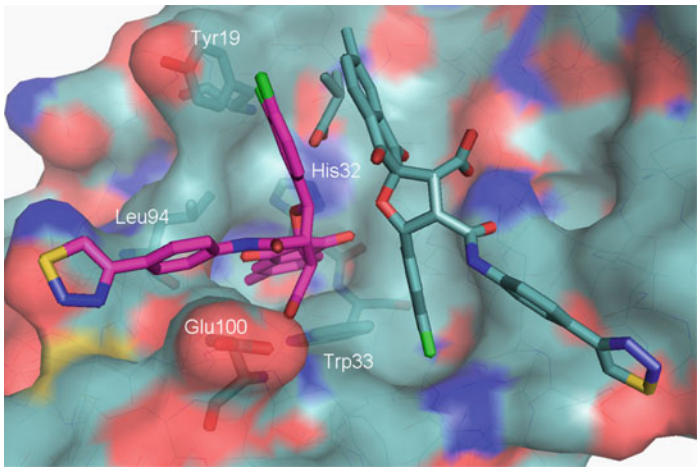

Fig. 2 Crystal structure of **4** bound to HPV-11 E2. Primary ligand is in *magenta*. Secondary hot spots are at positions of isobutyric acid and chlorophenyl group of second inhibitor molecule. Conformationally mobile binding pocket residues are *highlighted* (pdb 1r6n)

improved by the presence of the first inhibitor molecule, and the two inhibitor molecules make excellent π–π interactions with their aromatic groups above the isobutyric acid. Nevertheless, accessing the two small subsites flanking the deep indanedione pocket could prove a source of additional or alternate binding energy. The isobutyric acid site in particular could conceivably impart a great deal more affinity to a small molecule. Accessing all of these interactions would produce a much larger and more undruglike molecule; this tradeoff is endemic to the types of binding sites exhibited by this class of PPI.

The Boehringer Ingleheim HPV project was discontinued during lead optimization [140]; nevertheless, this effort shows how in the absence of structural validation, a variety of assays can be used to identify and verify inhibitors. It also illustrates the importance of information gained through crystal structures and structural analysis, and the ability of small molecules to exploit the conformational mobility of hydrophobic hot spots.

3.3 ZipA/FtsZ

Cell division in bacteria is mediated by an organelle called the septal ring. At the outset of cell division, Z-interacting protein A (ZipA) helps to form this structure through binding to FtsZ, another protein component of the ring. Inhibitors of the ZipA/FtsZ interaction have been sought as potential antibiotics. An X-ray structure of ZipA complexed to a 17-amino acid peptide from the C-terminal region of FtsZ showed the partially β-stranded, partly α-helical peptide placing several

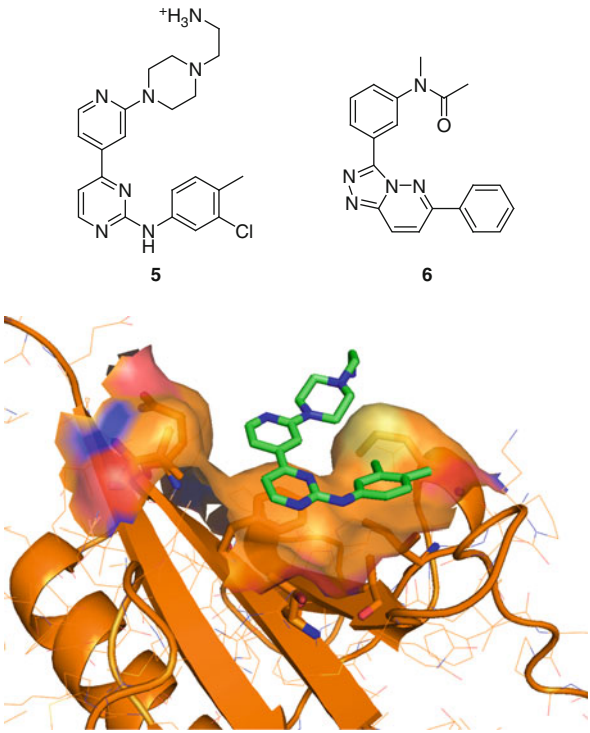

Fig. 3 Crystal structure of **5** bound to ZipA. Hydrophobic residues and associated surfaces are *highlighted*. Phe269 is in the *center* (pdb 1y2f)

side chains in a groove on the ZipA surface [144]. Contacting residues span roughly 20 Å, with residues closer to the ends of the groove (Asp370 and Gln381) making polar interactions with the surface, while central, hydrophobic residues (Tyr371, Leu372, Ile374, Phe377, and Leu378) contact a broad, flat region of ZipA, and account for a large percentage of the total contact surface. Alanine scanning established that three of the hydrophobic residues (Ile374, Phe377, and Leu378) accounted for almost all of the binding affinity to the peptide. The unbound ZipA structure is very similar overall to peptide-bound ZipA, particularly in the hydrophobic region, but a few side chain displacements in the binding site were made in the latter structure to accommodate the peptide, most notably rotation of an arginine to better interact with Tyr371.

A small-molecule effort at Wyeth used NMR screening to find several hits [145], though subsequent optimization did not result in meaningful improvements [146]. More extensive HTS yielded compound **5**, with a K_i of 12 μM [147], and modeling-based scaffold hopping led to **6** [148]. X-ray structures of ZipA complexes with several compounds, including both **5** and **6**, were obtained. All of them show the compounds covering the same central, flat area as the key hydrophobic side chains of the FtsZ peptide, and the overall structure of ZipA is very similar to the peptide-bound structure (Fig. 3). However, none of the interactions involve very deep

penetration. Interestingly, the FtsZ peptide itself was reported to have a K_D of 7 μM, while the complete protein has roughly 100-fold higher affinity.

For ZipA, it may not be difficult to find large, flat compounds with moderate affinity, but this is likely to be the case for many hydrophobic surfaces, particularly flatter surface presentations. Unless the ZipA hydrophobic region is capable of forming a more well-defined pocket than it has displayed to date, it will be far more difficult to engineer high-affinity compounds. Not only does the FtsZ peptide bind without a major conformational change occurring to the ZipA surface, but small-molecule screening and optimization also failed to find a ligand capable of inducing a more concave surface. It may be that efforts were simply not comprehensive enough; however, the computational screening study mentioned in connection with the HPVE2 surface above also noted a lack of probe compound binding for this site, uncharacteristic of hot spot behavior [43]. It is of course difficult to estimate what the energetic costs would be of rotating the side chains making up the ZipA hydrophobic surface. Only Phe269 appears able to substantially change the shape of the pocket without a great deal of backbone displacement, and flipping the side chain up would uncover a β-sheet backbone. This may be an instance of an interaction where the primary hydrophobic surface does not behave like a hot spot; that is, it is not capable of concentrating enough surface matching into a small enough space to efficiently bind small molecules.

3.4 MDM2/p53

Mouse double minute protein 2 (MDM2, human analogue HDM2) is an oncoprotein regulating the amount and activity of the tumor suppressor p53. MDM2 binds to p53, blocking the transactivation domain and thereby p53 transcription. MDM2 also exports p53 from the nucleus and acts via its E3 ubiquitination ligase activity to promote proteasome-mediated degradation of p53. MDM2 is often overexpressed in tumors; this overexpression correlates well with the presence of wild-type p53, which is found in roughly half of human tumors. For these reasons, MDM2 has been of considerable interest as a target for cancer therapy [149].

The interaction between MDM2 and p53 was characterized by crystal structures of MDM2 complexed with peptides derived from the N-terminal domain of p53. The structures showed an amphipathic α-helix interacting through the three hydrophobic side chains of residues Phe19, Trp23, and Leu26, which insert into a very localized and very well-defined hydrophobic cleft on MDM2 (Fig. 4) [150]. Mutational analysis [151] and alanine scanning [152] had previously uncovered the importance of these residues and highlighted a fourth, Leu22, which binds in a shelf adjacent to the Trp23 site.

This arrangement of hydrophobic side chains has proven to be compact enough for several groups to have found hit compounds from HTS [153–156], focused library screening [157, 158], and computational screening [159–161]. Many of

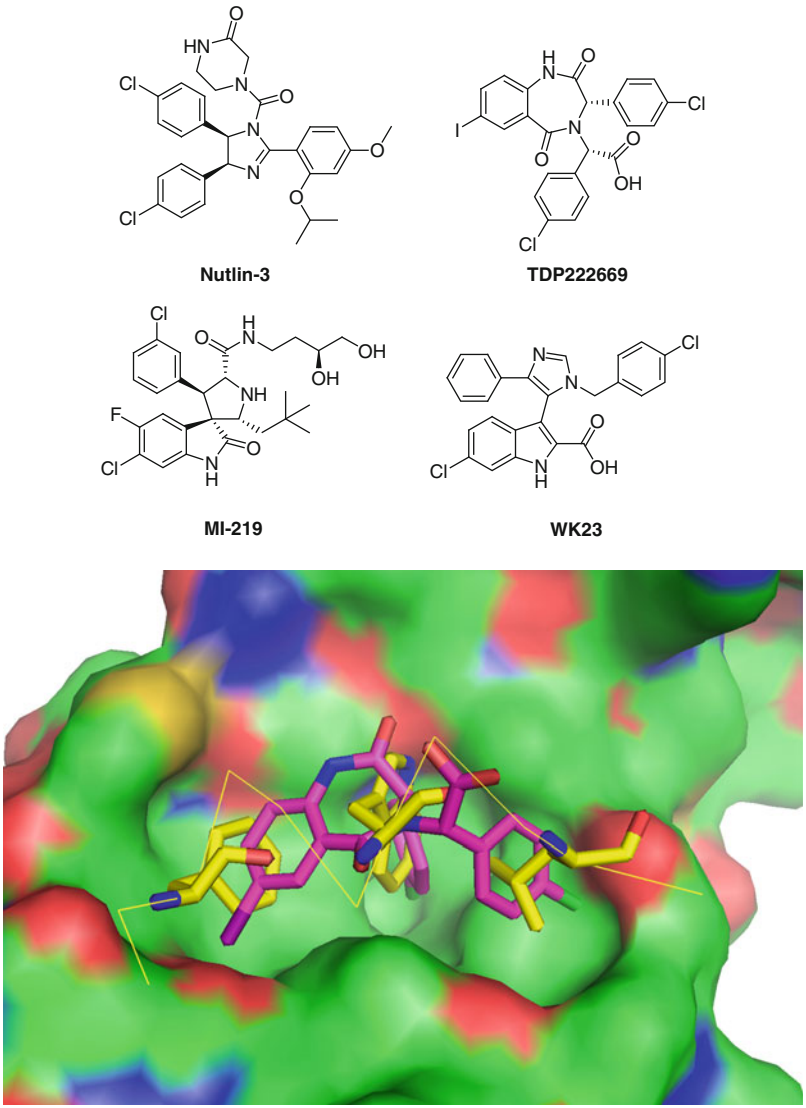

Fig. 4 Crystal structure of HDM2-p53 15-mer peptide complex. Helical ribbon and Phe19, Trp23 and Leu26 are shown in *yellow*. Benzodiazepinedione TDP222669 from HDM2 cocrystal is superimposed in *magenta*, showing effective mimicry of all three hydrophobic contacts (pdb 1ycr, 1t4e)

these compounds possess a motif comprised of two adjacent aromatic groups extending off of a rigid scaffold. X-ray and NMR structures of two members of the first group of potent MDM2/p53 inhibitors called Nutlins [153, 162], plus the benzodiazepinedione TDP222669 [154] bound to MDM2 show their aryl groups

mimicking Trp23 and Leu26. The Phe19 pocket is occupied by alkoxy groups of the third aryl ring by the Nutlins, and by the third aryl group itself in the case of TDP222669. Recently, bound structures of a spirooxindole related to MI-219, developed by the Wang group at Michigan, and of WK23, a compound from a series developed at Novartis have appeared [163, 164]. In both, the largest, central group fits into the main Trp23 pocket, with flanking groups occupying the other two sites [165]. Once again, the small-molecule contact surfaces are in the center of a much larger peptide-binding epitope. In these and other crystal structures of MDM2/p53 inhibitors, MDM2 always presents very similar binding surfaces, with only very small additional movements of side chains to accommodate slightly larger structures [165, 166]. However, the structure of unliganded MDM2 is essentially flat in the p53-binding region, with only a very small dimple corresponding to the position of the Trp23 binding site [167]. It appears that this hot spot has a very sharply defined open conformation that can be "found" by a number of different chemical structures.

Compounds from some of the above series have been optimized to low nanomolar affinity levels. The Johnson and Johnson group disclosed Nutlin-3 with a K_i of 36 nM [153], and Nutlins have shown anticancer effects in vitro and in vivo [168]. Further development of spirooxindoles produced MI-219 [169], which has a 5 nM K_i, and also shows effects in vitro and in vivo. Many compounds exhibit potent cellular activity and good pharmacokinetics. Several other series have appeared in recent years [170], and a few compounds have reached clinical trials [171].

3.5 Bcl-2 Family Proteins

B-cell lymphoma 2 (Bcl-2) family members are regulators of the intrinsic apoptosis (programmed cell death) pathway, and anti-apoptotic family members have been strongly implicated in cancer [172]. Heterodimer-forming interactions between anti-apoptotic family members such as Bcl-xL or Bcl-2, and α-helical domains of pro-apoptotic proteins control the ability of cells to carry out the apoptotic program. Several compounds have been reported to bind to and inhibit various anti-apoptotic Bcl-2 family members, but for most of these compounds reported affinities are poor, and structural information is unavailable [15].

NMR structures of Bcl-xL bound to two amphipathic α-helical peptides excised from pro-apoptotic Bcl-2 family members Bak and Bad were obtained by a group at Abbott Laboratories [41, 173]. The Bcl-xL interaction surface consists of a wide binding cleft with a very long contact surface extending through several helical turns. The Bak and Bad peptides are highly charged on their exposed surfaces, with large hydrophobic residues directed into the Bcl-xL surface. Alanine scanning determined that Leu78 and Ile85 of the Bak peptide were particularly important for good binding, with their hydrophobic side chains making deep contact with the Bcl-xL surface. Along with these key hydrophobic residues separated by two turns

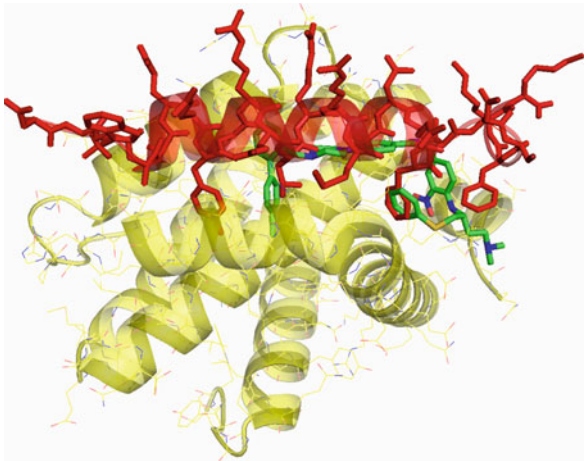

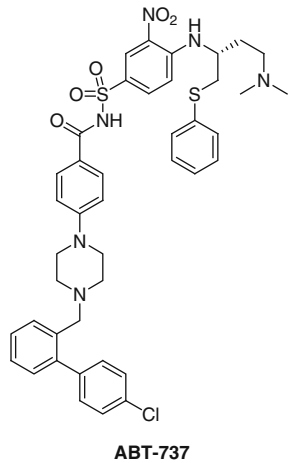

ABT-737

Fig. 5 Crystal structure of ABT-737 bound to Bcl-xL overlaid with Bad peptide (pdb 2yxj)

of the α-helix, a third important contact point on the other face of the Bak α-helix consisted of a conserved aspartic acid that interacted with an arginine residue on Bcl-xL.

This was followed by the disclosure of ABT-737, a very large (mol. wt. 813), hydrophobic, sub-nanomolar i.v.-only inhibitor of Bcl-xL and Bcl-2, which binds in the broad cleft [174]. Initially, NMR fragment screening found compounds that bound in the two hydrophobic hot spots. Derivation of compounds that interacted with both hot spots, followed by structure-guided optimization eventually led to ABT-737. An X-ray structure of ABT-737 bound to Bcl-xL shows two deep, widely separated hydrophobic binding regions, again corresponding to the hydrophobic hot spots (Fig. 5) [175]. In spite of its large size, the contact surface of ABT-737 is much smaller than that of either peptide, and the corresponding groove is narrower. Pronounced cavities corresponding to the two hydrophobic hot spots are similar in the ABT-737 and native peptide structures; however, early, not fully optimized compounds often induced different presentations of the hot spots, formed by intermediate amounts of displacement of hydrophobic side chains. Subsequently, an orally bioavailable analogue of ABT-737, navitoclax (ABT-263) was disclosed [176]. Navitoclax is even larger (mol. wt. 974) and is currently in Phase II trials for cancer.

This PPI stands out from most other examples with discontinuous epitopes, due to the greater distance between hot spots, resulting in two discrete binding sites requiring inhibitors to be separately optimized to both sites, and necessitating an exceedingly large compound. Accessing only one of the two hydrophobic pockets would not produce a small molecule with competitive potency, as the endogenous heterodimers bind in the picomolar range. The Abbott compounds have affinities toward Bcl-xL and Bcl-2 that are similar to the endogenous ligands, and the oral bioavailability of navitoclax was sufficient for development of a clinically viable formulation in spite of its size.

3.6 TNF-a Dissociators

Tumor necrosis factor-α (TNF-α) is a proinflammatory cytokine that is an important mediator of inflammation, and of responses to infection and cancer. TNF-α has been successfully targeted by a number of commercial engineered antibodies, including Enbrel, Remicade, and Humira, for treatment of rheumatoid arthritis. However, small-molecule antagonists of the interaction of TNF-α with its receptor TNFR1 have not been described. Instead, indirect approaches seeking to inhibit expression or processing of TNF-α, or to interrupt downstream signaling events, have been popular [177]. TNF-α has a trimeric structure, with the β-pleated sheet monomers associating about a threefold symmetry axis [178]. The trimer is extremely stable; urea/guanidinium dissociation involves simultaneous denaturation of monomers, and the trimer interface buries 2,200 $Å^2$ per subunit. The top of the trimer core features a number of polar interactions, while the middle is dominated by an extensive cluster of tyrosine residues that make concerted edge-to-face interactions, and the bottom, which forms an interaction surface with TNFR1, is extensively hydrophobic, with a preponderance of aliphatic residues.

A small molecule that inhibits the activity of TNF-α was found through fragment screening [179]. This molecule, SPD304, displaces one of the monomers from the TNF-α trimer by binding in the center of the trimer interface (Fig. 6). The resulting dimer sequesters SPD304 through a hydrophobic interface made up of 16 residues, six of which are tyrosines. The most central residues, the two Tyr119 amino acids from the two remaining monomers that normally form the pinwheel arrangement in the center of the interface, rotate down to make room for part of SPD304. This is accompanied by a minimal outward displacement of monomers. The interaction is purely hydrophobic, involving no hydrogen bonds. Interestingly, the compound is able to not only block trimer association, but also to dissociate one subunit of biologically active trimeric TNF-α. This access to the buried center of the trimer presumably occurs through very fast conformational dynamics of the protein.

SPD304 has a cellular $IC_{50} = 4.6$ μM, and no subsequent optimization work was reported. This compound is clearly far from being a drug, and is already quite large, though it is possible that improved potency could be attained. Nevertheless, SPD304 is very interesting in that it is able to disrupt a very strong, obligate protein-protein interaction.

Several other small-molecule modulators of PPIs operate on structural proteins, including a number of targets belonging to the antiviral field, specifically HIV-1, hepatitis C virus (HCV) and respiratory syncytial virus (RSV). Targeted proteins are responsible for various aspects of viral entry or fusion processes. While some small molecules act in a conventional manner – via mimicry of one binding partner, such as those inhibiting the HIV-1 gp120/CD4 interaction – others, like HIV-1 gp41 antagonists, block formation of a six-helix bundle [180–182]. Still others, like the RSV fusion inhibitor TMC353121 [183], seem to modify the conformation of a six-helix bundle to a less biologically active form, and many work through mechanisms not yet determined.

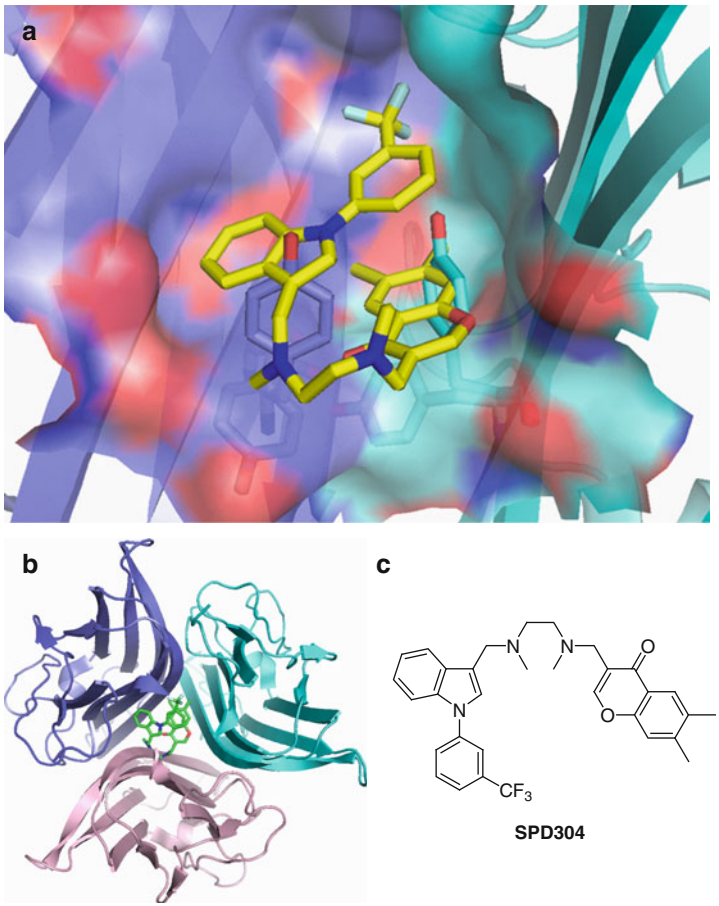

Fig. 6 (**a**) SPD304 bound to TNF-α dimer. Tyrosine residues rotated out of binding site are shown below compound, forming part of binding pocket. Corresponding residues from native TNF-α trimer are superimposed. (**b**) Overhead view of TNF-α trimer with SPD304 (**c**) superimposed (pdb 2az5)

3.7 Summary

The success of high-throughput screening for MDM2 programs, the moderate success of it for HPV E1/E2, and the failure of it with regard to Bcl-xL are almost certainly related to the disposition of hot spots for these targets. The hydrophobic region of MDM2 features hot spots that coalesce into a single dominant binding site, while for HPV the hot spots flanking the main hydrophobic crevice on the HPV surface are more distant, and the Bcl-xL (and Bcl-2) surface has two very discrete, well-separated concavities. By comparison, fragment screening was more appropriate and more successful for Bcl-xL, and for HPV E1/E2 – based on the X-ray

structure above – it may also have found small ligands to individual hot spots. In general, the applicability of various methods for derivation of chemical matter are very dependent on the particular character of surfaces and hot spots for this class of PPI.

Drug discovery programs targeting members of this class of PPIs benefit enormously from the availability of X-ray or NMR structures, as attested to by the liganded HPV E2 structure, and the surprising behavior of the Roche IL-2 inhibitor. It is particularly important to be able to ascertain whether potential binding sites are of an appropriate size for small-molecule ligands, and whether affinity sufficient for biological activity can be derived from them, or if additional contact points, if they exist, need to be accessed. While other methods can be of help in answering these questions, obtaining structures of complexes is of course optimal. Additionally, structure-based drug design approaches can be particularly helpful when tackling a target protein that can offer a number of different surface presentations.

It is of note that for IL-2 and HPV E2, the endogenous ligands do not greatly alter the apoprotein surface conformations, though the bound inhibitors do. In contrast, both MDM2 and Bcl-xL/Bcl-2 small-molecule inhibitors recapitulate the primary interactions of the endogenous ligands, which do induce changes in the apoprotein surfaces. Based on these examples, then, it will not be certain as to whether a given endogenous protein ligand offers clues to small-molecule binding modes.

4 PPIs with Continuous Peptide Epitopes

Though discussions of PPIs almost invariably center on the hydrophobic interactions that are their primary characteristic, many PPIs possess dominant interactions that in part resemble some canonical enzyme-substrate interactions, with 3–4 residue recognition elements constituting binding epitopes. Lacking catalytic active sites, affinity sufficient for biological activity must be generated solely from interactions among the recognition elements. This usually involves a number of polar interactions, including one dominant interacting unit on the peptide ligand which usually makes a salt bridge, a dense cluster of hydrogen bonds, or both, with the protein surface. Additional hydrogen bonds near this main interaction often serve to help anchor the ligand in a rigid conformation, directing individual hydrophobic amino acid side chains into small subpockets. The need to satisfy these structural requirements results in more predictable binding modes than those seen for the class of interactions described in the previous section. For these PPIs, “hot spot” residues correspond not to spatially separated amino acids whose side chains interact with hydrophobic areas, but to the few consecutive residues that form the binding epitope.

There are very few X-ray structures of any of these proteins or domains complexed with complete protein ligands. In those cases where structures are available, the main binding site may be part of a much larger interaction, but is

usually on the periphery of, or almost completely isolated from, a larger interaction surface. These additional surface interactions are sometimes of questionable importance, in terms of their contributions to both binding affinity and biological mechanism. Many proteins with this type of binding motif, such as 14-3-3 proteins, or those proteins acting through SH2, SH3, WW, PTB, and PDZ domains, are involved in recruitment and assembly of proteins into signaling complexes [184]. It has been postulated that these proteins, many of which contain multiple domains of these families, require smaller binding epitopes in order to simultaneously bind and organize two or more target proteins into larger complexes. Also, as many of these PPIs define large protein families, selectivity between family members is often another major concern for the medicinal chemist.

4.1 Integrins

Perhaps the earliest and longest-running effort to find small-molecule inhibitors of PPIs is the search for integrin antagonists [185, 186]. Integrins are adhesion molecules mediating attachment of cells with surrounding tissues. Integrins operate in a diverse array of interactions, and have been targeted for applications in cancer, cardiovascular health, and a number of inflammatory conditions [187]. Members of the integrin family are heterodimers composed of one of 18 α subunits and one of eight β subunits.

Two of the most commonly targeted members of this family are the αIIbβ3 [188] and αvβ3 integrins [189]. The αIIbβ3 integrin is involved in platelet aggregation, and the αvβ3 integrin is implicated in osteoporosis, angiogenesis, and other disease processes. Both recognize the specific zwitterionic tripeptide sequence Arg-Gly-Asp (RGD) of their natural ligands fibrinogen, fibronectin, and vitronectin. The αIIbβ3 cyclic peptide antagonist eptifibatide and the parenterally delivered nonpeptide antagonist tirofiban, both derived from snake venom, have been approved as anti-platelet aggregation therapies [185, 186]. These compounds, administered as an IV bolus and/or a continuous infusion, are employed only in acute situations. A great deal of subsequent effort has gone into finding orally bioavailable, long-acting αIIbβ3 antagonists. Programs typically began from a peptide-like structure or previously discovered peptidomimetic, and maintained the basic-linker-acidic motif with the central scaffolding of molecules becoming increasingly rigid over time, as exemplified by orbofiban and sibrafiban, both of which reached Phase III studies. Compounds from several research groups achieved low-nanomolar or sub-nanomolar affinities, and low double-digit nanomolar in vitro IC_{50} values for platelet aggregation inhibition. To improve pharmacokinetics, single and double prodrugs were often chosen for development. Clinical results were poor, with compounds showing minimal benefit. Difficulties were due to several factors; among them poor bioavailability and an unacceptable variation in drug levels, leading to bleeding or a lack of sustained efficacy [190].

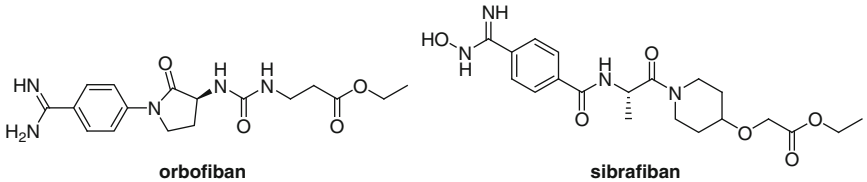

With regard to αvβ3 antagonists, a number of linear and cyclic peptides have been disclosed, including compounds derived from αIIbβ3 antagonists through modification of the N-terminal basic group. Many compounds, echoing the history of αIIbβ3 work, also display a number of constraints on the central linking group. In general, it has been found that small changes to the intramolecular distance between acidic and basic groups, and an appropriate choice of N-terminal basic group, can facilitate the isolation of αIIbβ3-selective, αvβ3-selective, or dual inhibitors. In spite of numerous publications describing highly potent compounds, few αvβ3 antagonists have progressed to the clinic. As with the αIIbβ3 inhibitors, a central difficulty with these compounds has been the challenge of combining good oral bioavailability with an extended, zwitterionic structure [189, 191].

The broad effort to find integrin antagonists has been plagued by a lack of solid structural guidance. Despite an enormous amount of effort, high-resolution crystal structures of bound integrin inhibitors were for many years nonexistent. Membrane proteins are difficult to purify, and integrins are also extremely complex and heavily glycosylated. As a substitute, a variety of techniques including electron microscopy, ultracentrifugation, NMR, fragment crystallography, and computer modeling have been used to evolve structural models [186]. X-ray crystal structures were ultimately obtained for the complete extracellular region of the αvβ3 integrin [192], both unbound and bound to a small ligand containing the RGD-sequence, the cyclic pentapeptide drug cilengitide [193]. Additional structures have subsequently been reported but remain exceedingly rare [194], and most programs rely on homology models for structural support.

The complexed and uncomplexed αvβ3 X-ray structures are extremely similar to one another, with the presence of the ligand causing no alterations of the local structure. The complexed structure reveals binding of the peptide into a gap between the αv and β3 subunits, with the RGD residues contacting the protein, the phenylalanine contacting the β3 surface, and the N-methylvaline pointing into solvent (Fig. 7). The Arg and Asp side chains are fully extended in opposite directions. The Arg guanidine forms salt bridges to Asp218 and Asp150 of the αv subunit, while one Asp side chain oxygen contacts the β3 subunit through hydrogen bonds with backbone amides of Tyr122 and Asn215, and the other contacts a Mn^{+2} ion. Behind the molecule runs a cleft that medicinal chemists have been able to access with hydrophobic groups to gain additional affinity. The complex array of polar interactions surrounding the Arg and Asp side chains attests to the importance of maintaining charged groups in antagonists directed towards αIIbβ3 and αvβ3.

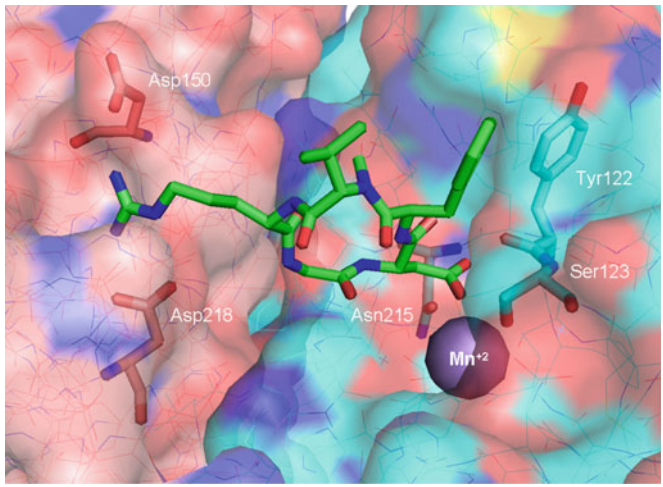

Fig. 7 Crystal structure of cilengitide bound to αvβ3 integrin. The αv subunit is in *red*, and the β3 subunit is in *light blue*. Hydrogen bonding residues are *highlighted* (pdb 1l5g)

The α4β1 integrin, also known as very late antigen-4 (VLA-4), mediates lymphocyte activity in inflammatory processes, and has been validated as a target for inflammatory diseases through the activity of the α4-directed antibody natalizumab [195, 196]. VLA-4 recognizes an EILDVPST epitope of VCAM-1 and a Leu-Asp-Val sequence of fibronectin. Many VLA-4 inhibitors have progressed into clinical trials for asthma, multiple sclerosis, and other indications [197, 198]. Compounds such as **7** and IVL745 were derived from LDV peptidomimetics. Additionally, work on N-acylphenylalanines has spawned a huge number of papers and patents, and reports on this class of inhibitors continue to appear. Several of these, such as valategrast and firategrast, have also progressed into the clinic. Early inhibitors, while potent, suffered from poor absorption and high clearance. Though this continues to plague many structural series, several compounds have displayed good pharmacokinetics, and in general, the single charge required of VLA-4 inhibitors has resulted in a better balance of hydrophobic and polar interactions, and has made this target much more amenable to small-molecule modulation than β3 integrins. If sufficient clinical efficacy is obtained, small-molecule α4β1 antagonists may ultimately offer a more flexible dosing alternative to natalizumab.

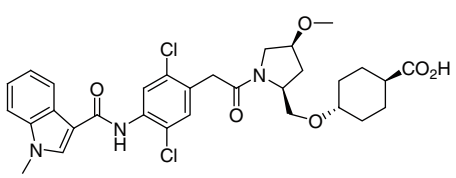

7

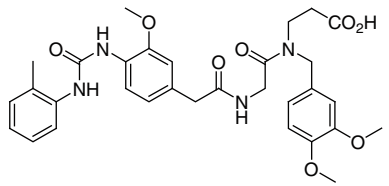

IVL745

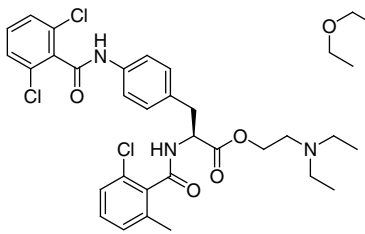

valategrast

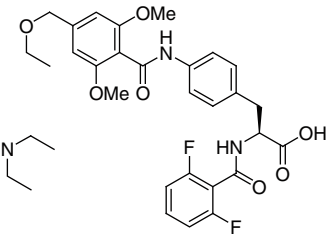

firategrast

LFA-1 is the αLβ2 integrin, and is involved in recruitment of leukocytes and proliferation of T-lymphocytes in inflammatory disease states. The interaction of LFA-1 with its ligand, intercellular adhesion molecule-1 (ICAM-1), has been shown to be important to a number of autoimmune conditions [185–187]. Like some other integrins, LFA-1 contains an inserted, or I-domain, in its αL module, which contains the binding site for ICAM-1. LFA-1 normally has very low affinity for ICAM-1, but conversion of this site from a closed to an open conformation can occur via inside-out signaling [185, 199, 200]. Two separate allosteric sites for locking LFA-1 into the closed form have been accessed by small-molecule inhibitors [201]. Most allosteric LFA-1 inhibitors bind to a hydrophobic cleft on the I-domain [202]. Lovastatin was found to be a micromolar inhibitor acting at this site [203], and subsequently many other statins or statin-derived compounds have demonstrated excellent affinity for the hydrophobic site. Several other potent series directed to this site have also been described [15, 186]. A second class of allosteric inhibitors was discovered by attempting to make ligands for the ICAM-1 binding site. Various experiments showed, however, that these potent compounds actually bound at a site on the β2 subunit [204, 205]. Allosteric inhibitors have also been found for the α2β1 integrin, which appear to bind to the β1 I-like domain [206, 207].

As the phenomenon of allosteric inhibition is in broad outline the same for PPIs as for enzymes or receptors, and does not provide meaningful comparison to the other PPI targets presented here, inhibitors of the LFA-1/ICAM-1 interaction will not be discussed further. This example is noteworthy, however, in illustrating that the complexity of the mechanism of integrin activation in general, and that of LFA-1 in particular, was not fully appreciated at the outset of work on these challenging targets, and has greatly added to the difficulty of deriving small-molecule drugs for them. This, combined with the paucity of structural support

available to aid in drug discovery efforts, has hindered the eventual discovery of clinical candidates for several integrins.

4.2 SH2 Domains

Src homology 2 (SH2) domains are structurally conserved domains found in many intracellular signal transduction proteins [208]. These small domains contain about 100 amino acids and are formed from two α-helices and seven β-strands. The domains bind a short peptide sequence containing a phosphorylated Tyr (pTyr) residue [209]. SH2 domains have been classified in various ways according to their selectivity profiles [209–213]. Some proteins contain SH2 domains along with SH3 domains, which recognize proline-rich sequences; the dual domains often act in tandem in order to bring together signaling proteins.

Src is a nonreceptor tyrosine kinase, and has attracted attention for its role in cancer. The Src SH2 domain has been targeted in an attempt to block binding to client proteins. The recognition motif for the main pocket is pTyr-A-A-B, where *A* varies widely and *B* is hydrophobic. The main interactions are carried by the pTyr and *B* residues, the latter of which resides in a subpocket distant from the pTyr binding site. The backbone of the tetrapeptide makes a right turn at the pTyr+1 residue, and the *B* residue extends its hydrophobic side chain in the direction of that end of the peptide. Accessing both pockets is generally required for good potency, but results in a large molecule. Most reported SH2 inhibitors are peptidic or peptidomimetic [214–216].

Ariad identified antagonists of the Src SH2 domain as inhibitors of osteoclast function [217, 218]. While the negative charge of inhibitors made membrane permeability problematic, targeting to sites of bone resorption seemed possible [219]. Emphasis on rigidification at the pTyr+1 turn, replacement of C-terminal residues with various hydrophobic rings, and phosphotyrosine surrogates led to AP22408, which showed activity in cell assays and an animal model of bone resorption. An X-ray structure using a mutant Lck SH2 domain confirmed modeling-based predictions of binding, with the rigid bicyclic core placing the diphosphonophenyl group in the pTyr position, and the cyclohexyl group in the pTyr+3 pocket. Hydrogen bonds involving the pTyr+1 and pTyr+3 amide groups rigidify the conformation of the small molecule (Fig. 8).

Researchers at Aventis used crystallography-based fragment screening to find pTyr mimetics, and then substituted them for a phosphotyrosine on an optimized semi-peptidic inhibitor [220]. Among the most potent analogs was **8** with an IC_{50} of 10 nM. The Aventis work illustrated a high degree of flexibility in the conformations of residues forming the pTyr-binding pocket, which allowed for a broad range of pTyr mimickry.

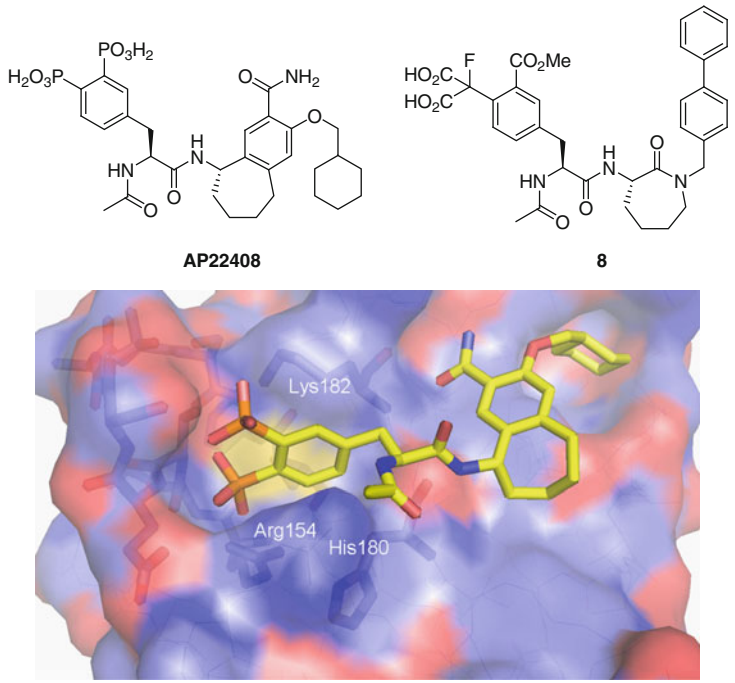

Fig. 8 Crystal structure of AP22408 complexed to Lck SH2 domain. The flexible pTyr-binding loop containing several Ser and Thr residues is *highlighted*. Arg154 is shown below the 4-phosphonate, and Lys182 is shown behind the 3-phosphonate. Lys182 and His180 make hydrogen bonds to the aryl amide carbonyl and pTyr+1 amide NH, respectively (pdb 1fbz)

Grb2 is part of the Ras signal transduction pathway, and has consequently attracted attention as a possible target for cancer. Grb2 acts via its SH2 domain on activated growth factor receptors, upstream of the mitogen-activated protein (MAP) kinase cascade that is crucial for cellular differentiation and proliferation. Scientists at Novartis began their search for a Grb2 inhibitor from a 7-mer pTyr-containing peptide [221], and through separate optimization of residue positions arrived at **9**, with sub-nanomolar affinity [222]. Related compounds with activity in cellular assays include **10** [223]. The Burke laboratory developed a number of phosphate isosteres [224], and the bis-acid **11** was active in cellular assays [225]. The Burke study, like the Aventis work above, noted the ability of various charged groups to induce conformational changes in the pTyr pocket.

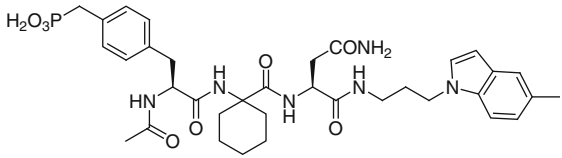

9

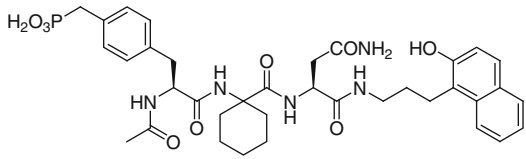

10

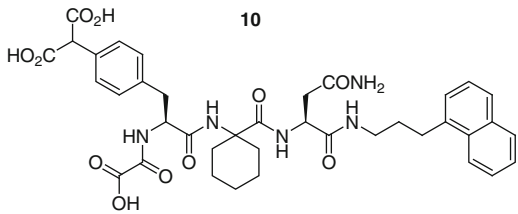

11

Small micromolar inhibitors of the Stat3 and Lck SH2 domain have also been published [226, 227], though little work has been reported in recent years. It has proved possible to make potent SH2 inhibitors, but the extended nature of the ligands and the importance of the end hydrophobic interaction have kept inhibitors large, and the hydrogen bonding of amides has kept them substantially peptide-like. Additionally, though many compounds have shown activity in cellular assays or in vivo, issues associated with phosphotyrosine mimicry, and the resulting necessity of highly charged inhibitors, have not been fully overcome.

4.3 PDZ Domains

PDZ domains are important to a range of signaling processes. Like SH2 domains, PDZ domains are often part of multidomain scaffolding proteins, involved in transport and assembly of various supramolecular signaling complexes [228, 229]. Since their discovery in the early 1990s, over 250 PDZ domains have been identified, and multiple copies are often found in proteins. Individual PDZ domains are usually optimized for specific interactions, but some domains have more than one biological target, and individual domains tolerate some variance in recognition sequences [230, 231].

PDZ domains are very small, and are comprised of two α-helices and six β-sheets. There are over 100 X-ray structures of PDZ domains, and many more

structures obtained by other methods. An extended groove between the β2-strand and α2-helix binds C-terminal tetrapeptide ends of interacting proteins in most cases. The ligand exists in a fully extended, β-sheet-like conformation, making extensive hydrogen bond contacts with the antiparallel β2 strand. This structural motif normally both precludes flexibility among pocket-forming residues, and enforces a peptide-like periodicity of inhibitor structure. A carboxylate-binding loop comprised of a GLGF sequence forms a pocket that sequesters the terminal acidic group, which hydrogen bonds to backbone amides of the LGF residues [232]. A conserved arginine residue near the carboxylate stabilizes the charge. The C-terminal residue is often aliphatic, and a hydrophobic pocket exists for its side chain. The third, or "-2" residue, like the C-terminal residue, points into the bottom of the binding groove, and often governs specificity. For this reason, several classification schemes for PDZ domains have been primarily based on the identity of this residue [230, 233]. The second and fourth ("-1" and "-3") residues vary considerably, as do those further upstream, with their interactions often contributing to affinity. Several small-molecule peptide inhibitors have been reported, with affinities in the micromolar range, commensurate with measurements of native interactions [228]. Bivalent inhibitors recognizing dimeric or oligomeric PDZ domains in some proteins, and conformationally restricted peptidomimetics have also been described. A few groups have also reported small-molecule inhibitors of various PDZ domains [234].

The dishevelled (Dvl) proteins have attracted interest in recent years as a possible site of intervention into the Wnt signaling pathway, which has been shown to play a role in the development of some cancers. The dishevelled PDZ domain interacts with cell-surface Frizzled receptors through recognition of an internal, not a C-terminal, peptide sequence [235]. Additionally, it was demonstrated that among C-terminal peptides, the three highly conserved human Dvl PDZ domains recognize different sequences than most other PDZ domains [230]. More recently, a study using internal peptide ligands found through extensive X-ray crystallography that the Dvl PDZ domain is particularly flexible, and can recognize a number of different peptide sequences, both internal and C-terminal, with K_i values of ~1 μM as determined by FPA [236]. The domain possesses a longer β2 strand and α2 helix than is usual, and the larger cleft between the two can accommodate up to seven residues. In some structures, the β-sheet-like conformation of the peptides is substantially broken, and "incorrect" or multiple residues occupy canonical C-terminal, -1, or -2 positions, such as the Gly-Tyr residues both occupying the -2 site in Fig. 9b, c, and the nominal -2 Trp residue in Fig. 9d in the C-terminal position. Structures have little in common other than interactions between acid functionalities and the carboxylate-binding loops. These new peptide ligand conformations are accompanied by profound changes to the Dvl PDZ surface deriving from side chain movements and displacement of the α2-helices. An arginine on the α2-helix allows for varying conformations to retain the ability to hydrogen bond to different peptide backbone carbonyl groups.

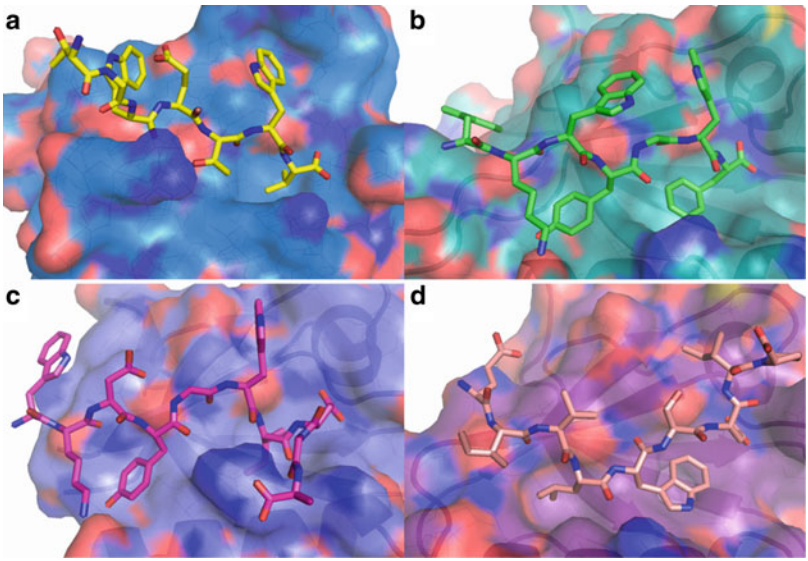

Fig. 9 Comparison of identically oriented PDZ domain crystal structures with bound peptide ligands. (**a**) Erbin PDZ complexed with WETWV peptide. (**b**–**d**) Dvl PDZ complexed with WKWYGWF, and internal peptides WKDYGWIDGK and EIVLWSDIP, respectively. The *blue patch* at the *bottom* of PDZ domains in **b**–**d** corresponds to the arginine residue hydrogen bonding to peptide carbonyl groups (pdb 1n7t, 3cbx, 3cby, 3cc0)

The enhanced capacity for hydrophobic contacts of the Dvl PDZ binding site may allow for the generation of less peptide-like small-molecule inhibitors for this target. Small molecules that bind to the Dvl PDZ domain in the low micromolar range have recently been reported, among them the NSAID sulindac [237–239]. With a relaxed emphasis on a rigid hydrogen bonding template directing a crucial salt bridge interaction, the slightly different structure of the Dvl PDZ domain may turn out to be sufficient to modify its character to that of a discontinuous epitope-binding PPI.

4.4 XIAP/Smac

The inhibitors of apoptosis (IAP) protein family inhibits programmed cell death through direct binding to caspases, which are important players in the execution of apoptosis. IAPs have many other biological functions [240], but they have been targeted by pharma due to their importance in cancer progression. All IAPs contain one to three baculovirus IAP repeats (BIR domains 1–3), a 70-amino acid domain that possess a small peptide binding site. X-linked IAP (XIAP) inhibits caspase-9 activity by binding to a caspase-9N-terminal ATPF sequence through a

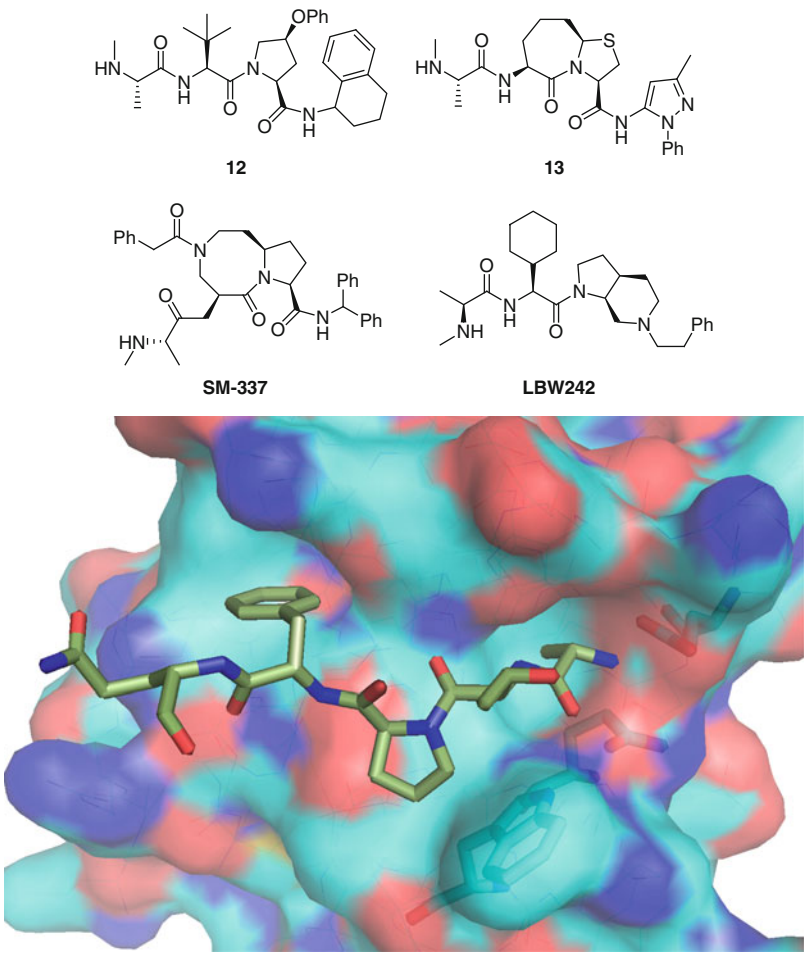

Fig. 10 Crystal structure of ATPF unit of caspase-9 bound to XIAP BIR3, with Glu314, Gln319, and Trp323 *highlighted* (pdb 1nw9)

well-defined cleft on the XIAP BIR3 domain, and through a larger interaction with the surface of caspase-9 that is involved in homodimerization [241, 242]. Caspase-9 requires homodimerization in order to trigger a conformational change that produces a catalytic pocket for caspase processing. XIAP inhibits caspase-3 and caspase-7 through its BIR2 domain and the BIR1–BIR2 linker.

The natural inhibitor of IAPs, Smac (also called DIABLO) [243, 244] blocks IAP binding of caspases. NMR and X-ray structures of the XIAP/Smac complex showed that the first four residues (AVPI) of the N-terminal domain of Smac bind to the same surface groove on XIAP BIR3 that recognizes the N-terminus of caspase-9 (Fig. 10) [245–247]. The terminal alanine methyl group fits into a small pocket,

with the amino group forming three strong hydrogen bonds to Glu314 and Gln319, and the carbonyl interacts with Gln319 and Trp323. Val2 makes two hydrogen bonds and has no real van der Waals interactions, while the Pro3 and Ile4 residues primarily make hydrophobic contacts. The peptide interaction surface covers 892 $Å^2$, and the excised peptide binds to XIAP BIR3 with a K_d of 400 nM.

The interactions of Smac and caspase-9 with XIAP BIR3 are more straightforward and better understood than other interactions involving IAPs, and the XIAP BIR3-Smac interaction has served as the touchstone for drug discovery efforts. The Smac peptide itself and peptide-based mimetics have low cellular activity and poor stability, but the Smac peptide has usefully served as a starting point for the design of small-molecule IAP inhibitors. Early peptide modification established broad requirements for each amino acid position [248]. Subsequent work by several groups has resulted in cell-permeable mimetics that maintain the hydrogen bonding interactions of the peptides, and more effectively fill hydrophobic subsites. Many compounds such as **12** and **13**, from Abbott and Genentech, SM-337 from the Wang group at Michigan, and LBW242 from Novartis, possess sub-micromolar affinities [249–255].

Dissociation constants for complexes of BIR domains with caspases are on the order of 1 nM, while Smac or Smac peptide binding is micromolar or just below. However, Smac binds to a version of XIAP with both BIR2 and BIR3 domains much more strongly [256]. Additionally, Smac forms a 2:1 complex with XIAP, suggesting that Smac interacts with BIR2 and BIR3 simultaneously via a homodimer [256]. In response to this, inhibitors combining two AVPI mimetics into one larger molecule have been produced [257–260]. SM-164 and **14** have been shown to bind two BIR3-only XIAP molecules, but in the presence of an XIAP version with both BIR2 and BIR3 domains, one molecule interacts with both domains [259, 260]. These compounds are 100 and 200 times more potent than the corresponding monovalent compounds.

Many of the monovalent and divalent compounds, such as AEG40730 [258], also bind with high affinity to cIAP1 and cIAP2. Several compounds of both classes have shown efficacy in preclinical cancer models as both single agents and as potentiators of other therapies. Six compounds have entered clinical trials in the last few years. Though divalent inhibitors are expected to be intravenously delivered, two presumably monovalent compounds were dosed orally in Phase I trials.

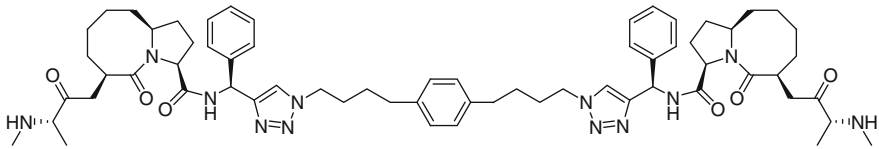

SM-164

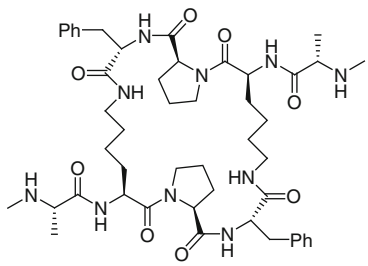

14

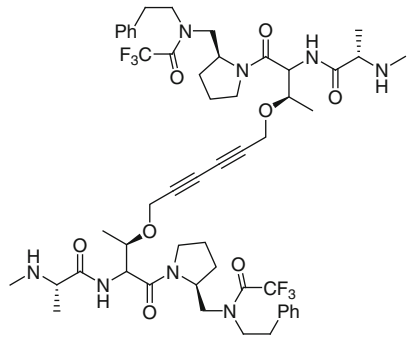

AEG40730

The history of the Smac mimetic field illustrates the highly complex nature of some PPIs, requiring an enormous amount of structural and biological experimentation in order to correctly define mechanisms of interaction and the structural basis of biological activity. Of particular relevance to the effort to discover IAP inhibitors are the interactions of XIAP with caspase-9, and with Smac. The XIAP/caspase-9 X-ray structure exhibits an interaction surface spanning 2,200 $Å^2$, with the ATPF-recognizing groove separated from the rest of the interaction surface. The majority of the surface is comprised of hydrophobic interactions and hydrogen bonds, with BIR3 covering the homodimerization surface of caspase-9 [242]. Mutation of some residues in this part of the interface results in a loss of inhibition of caspase-9 by XIAP. The BIR3 domain still binds to the caspase-9 tetrapeptide, but this no longer prevents homodimerization. Thus, a portion of the interaction surface outside of the N-terminal peptide-binding region is important for biological activity. However, as groove binding by caspase-9 is necessary but not sufficient to block caspase activity, small-molecule blockade of the peptide-binding groove alone is still sufficient to disrupt XIAP inhibition. An X-ray structure of a 2:2 XIAP BIR3/Smac complex also involves interactions over a large surface area beyond the N-terminal peptide-binding groove, but this interaction covers a different part of XIAP BIR3, features poorer shape complementarity, and is of uncertain biological relevance [246].

Importantly, both structures show the peptide binding groove to be essentially unchanged from apo-BIR3 [261]. Various structures of bound inhibitors present a similar binding mode, and the standard evolution of peptidic molecules into more rigid compounds further illustrates that the main binding site for IAP interactions shares much in common with the binding pockets of other continuous epitope-binding proteins. The relative success of efforts directed to Smac mimetics can be

assigned to a number of factors, foremost among them the possible acceptability of intravenous delivery. Additionally, the XIAP BIR3 pocket is relatively deep and hydrophobic for members of this class of PPIs, and the anchoring hydrogen bonding unit is an amino group, which can be modified to a methylamino group with little penalty, in contrast to acidic, bis-acidic, or acidic plus basic groups found in some other PPIs. These factors allow for a more rigid, cell-permeable inhibitor to be fashioned, and the multiple compounds reaching clinical trials testify to the druggability of this target.

4.5 Summary

For most continuous-epitope PPIs, the relative consistency of interaction modes stands in stark contrast to those in the previous section, and probably renders homology modeling sufficient for most applications. However, the example of the dishevelled PDZ domain shows that even this group of interactions can offer surprises that would benefit from a more thorough level of structural surveillance. The XIAP story also highlights the structural complexity of some of the endogenous interactions of PPIs.

The overall pattern of continuous epitope interactions has precipitated a reliance on endogenous peptide substrates as leads for PPI targets of this type. It may be possible to find nonpeptidic leads through various screening methods, but in practice short peptides have uniformly served as starting points for these targets. This has enabled access to highly potent compounds, and has also brought with it the usual concerns about reducing the peptidic character of compounds, but as seen in the examples above, much more drug-like peptidomimetics have often been discovered. Difficulties in fashioning orally bioavailable compounds for some integrin and SH2 domain targets appear to derive more from the need for those compounds to be highly charged than from peptidomimetic, size, or hydrophobicity issues. Successes in getting to the clinic with antagonists of less highly charged interactions, such as $\alpha 4\beta 1$ integrin inhibitors and Smac mimetics, add to the hope that modulation of other PPIs of this structural type may yet prove to be a viable way to inhibit formation of signaling complexes.

5 PPIs with Unique Modes of Interaction

A few PPIs that have drawn the attention of academic and industrial research groups do not fit so easily into either of the groups surveyed in the above two sections. Evolution tends to converge on certain robust solutions to various problems, so it should come as no surprise that the central binding motifs of many PPIs tend to fall into a small number of categories. Still, there is no a priori reason why an endogenous PPI must take on any specific form. The following

interactions, rather than exhibiting fundamentally new characteristics, instead offer combinations of the prominent structural features common to the two previous groups of PPIs, and illustrate that PPIs need not be easily assignable to a given structural category.

5.1 LEDGF/HIV-1 Integrase

Transcriptional coactivator p75, also known as LEDGF, is a chromatin-associated protein that mediates stress response. LEDGF is also the primary binding partner of HIV-1 integrase (IN) in human cells. A chromatin-binding domain at the N-terminal end of LEDGF, and a C-terminal integrase-binding domain (IBD), are responsible for the chromatin-tethering behavior of LEDGF toward HIV-1 IN. Additionally, the interaction with LEDGF protects HIV-1 IN from ubiquitination and proteasome degradation.

The LEDGF IBD is a small five-helix bundle, with two hairpins formed by helices α1–α2 and α4–α5 connected by a short α3 helix crossing the bundle at the opposite end from the two hairpin loops [262]. An X-ray structure of the interacting domains demonstrates that LEDGF interacts with HIV-1 IN through residues on both hairpin loops (Fig. 11a) [263]. Residues Ile365 and Asp366 make deep contact with a small gap at the interface of an HIV-1 IN catalytic core domain (CCD) dimer. The buried anionic Asp366 makes hydrogen bonds to Glu170 and His171 of one monomer of the CCD dimer, while the backbone amide of Ile365 hydrogen bonds to Gln168 of the same monomer, and contacts several other residues from both monomers. Three water molecules are also buried in the interface, one of which mediates a hydrogen bond between Ile365 and the IN surface. The Ile365 side chain is buried, and residues Phe406 and Val408 of the second hairpin loop of LEDGF also make hydrophobic interactions, contacting Trp131 of HIV-1 IN, which situates its indole group toward solvent in the bound structure. Mutation of Ile365, Asp366, or Phe406 abolished binding to HIV-1 IN, while mutation of Val408 significantly reduced binding [262]. The total buried surface area is 1,280 $Å^2$, but the contact area between full-length proteins is probably greater. It has been demonstrated that the N-terminal domain of HIV-1 integrase also contributes, though to a lesser extent than the CCD, to binding of LEDGF [264].

Recently an academic group found a series of quinoline acetic acids that bind to the LEDGF/IN interface [265]. From a virtual screening program, 25 compounds were selected for biological testing. One of these showed moderate inhibition of the LEDGF/HIV-1 IN interaction using an AlphaScreen assay. Testing of several analogs followed by targeted synthesis led to CX04328, with an $IC_{50} = 1.37$ μM, and $EC_{50} = 2.35$ μM in a standard anti-HIV activity cellular assay. A later compound was reported to be threefold better in both assays. Compound CX04328 only weakly affected the catalytic activity of integrase, and did not inhibit DNA binding. Multiple experiments confirmed that the compound inhibits DNA replication via interference with the formation of the LEDGF/integrase complex.

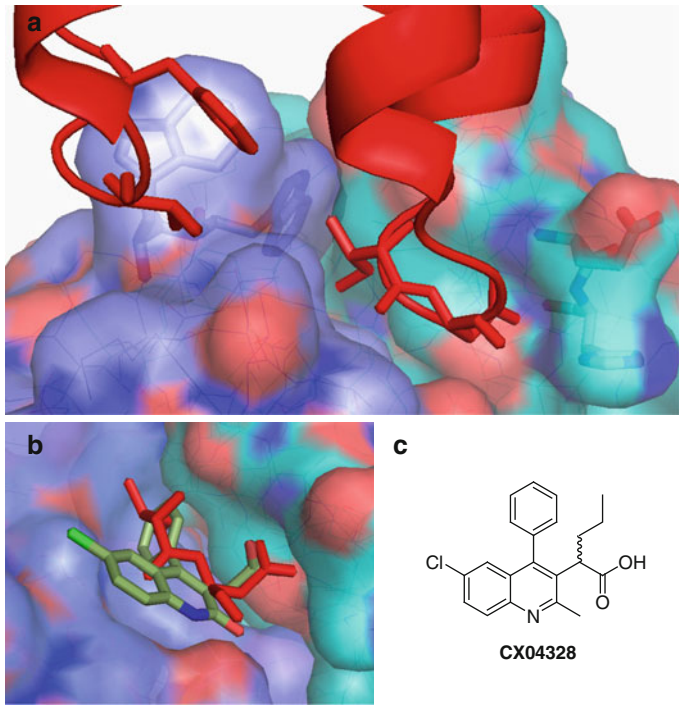

Fig. 11 (**a**) Crystal structure of the IBD of LEDGF (*red*) bound to HIV-1 IN dimer (*light* and *dark blue*). Ile365 and Asp366 penetrate between monomers and hydrogen bond to Glu170 and His171, while Phe406 and Val408 form a hydrophobic face interacting with Trp131. Trp132, forming part of the Ile365 pocket and dimer interface, is also *highlighted*. (**b**) Crystal structure of CX04328 (**c**) bound to HIV-1 integrase monomer, overlaid with LEDGF Ile365 and Asp366 (pdb 2b4j)

Crystal structures of CX04328 and an earlier compound confirm that the compounds bind in the Ile365/Asp366 pocket, with the acid groups making the same hydrogen bonds to IN Glu170 and His171 as the LEDGF Asp366 carboxylate (Fig. 11b).

The LEDGF/HIV-1 IN interaction has characteristics of both discontinuous and continuous epitope-binding interactions. The importance of Asp366, and the relatively high-energy interactions it makes, along with the hydrogen bond made by the backbone amide of Ile365, are typical of anchoring polar interactions. Also, binding of both LEDGF and CX04328 involved no alteration of the HIV-1 IN structure. However, the binding epitope is fundamentally different than those discussed in Sect. 4, with the interactions carried by two separate, distinct loops. The second hairpin loop is also clearly important to the overall complex, and acts solely through hydrophobic contacts. This latter interaction appears to be one where both proteins are roughly equal in their degree of penetration into the other surface. To date, all compounds found to inhibit the LEDGF/HIV-1 IN interaction, including those just discussed and others that have also appeared recently [266–268], only mimic one of

the two hairpin loop interactions. From a drug discovery standpoint, it may prove possible to design sufficiently tight-binding bioactive compounds that mimic only the interaction of the first hairpin loop of LEDGF, but it also may be the case that multiple aspects of this interaction are needed to provide binding energy sufficient for robust biological activity, and mimicry of only one may prove inadequate from a drug discovery standpoint.

5.2 Bromodomains

Bromodomain-containing proteins have attracted interest as modulators of gene expression. Among this broad class of over 40 proteins, the bromodomain and extra-terminal (BET) family has recently been the subject of several papers exploring the viability of small-molecule inhibitors of their behavior. BET proteins recruit transcriptional regulators as part of multiprotein complexes, through recognition of epigenetic markers, specifically, N-acetylated lysine residues on histone tails [269–271]. The BET family of proteins consists of BRD2, BRD3, BRD4, and BRDT; all of these have a common structure with two highly conserved N-terminal bromodomains, and a C-terminal recruitment domain that varies between proteins.

Bromodomains consist of a left-handed four-helix bundle with varying loop regions that contribute to selectivity. Solution NMR and crystal structures of BRD4 bromodomains have been solved [272, 273]. A long, 35-residue loop, containing two short helices, runs between the first two main helices. The AcLys recognition surface is situated in a crevice between this loop and the surface formed by the latter two main helices of the four-helix bundle and their short connecting loop. The ligand sits in a hydrophobic cavity that has a hydrogen-bond-donating residue, usually an asparagine, embedded in the cavity wall. A ring of water molecules surrounds the N-acetyl group at the bottom of the cavity. K_d values for binding of BRD4 bromodomains to acetylated histone peptides were obtained from the NMR study. These and other published values center around a value of 1 mM, though ITC measurements produced values up to tenfold better [273]. However, dimeric bromodomains bind to bisacetylated peptides with affinities in the micromolar range.

A recent patent from Mitsubishi Pharma noted that some thienodiazepines that emerged from an anti-inflammatory program possessed binding activity to BRD4 [274]. A group of academic researchers subsequently designed a related ligand, (+)-JQ1. In contrast to the relatively weak association of AcLys-containing peptides, (+)-JQ1 was found to bind to BRD3 and BRD4 bromodomains with K_d values of 50–90 nM, while affinity to BRDT and BRD2 was roughly threefold weaker. (+)-JQ1 was also effective in competitive binding experiments with an acetylated histone H4 peptide, displaced BRD4 from chromatin in cells, and showed efficacy in a squamous carcinoma xenograft model [275]. Later studies showed that (+)-JQ1 suppresses MYC gene transcription, and has antitumor activity in xenograft models of lymphoma and leukemia [276, 277]. More recently,

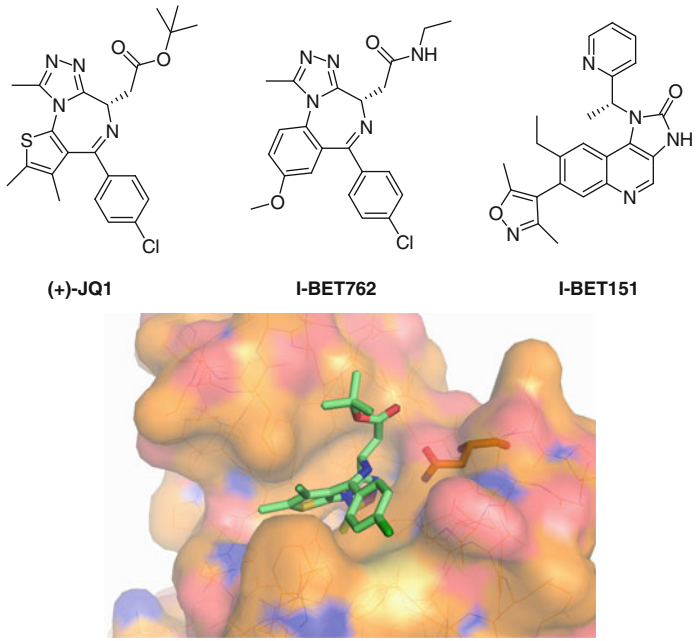

Fig. 12 Crystal structure of (+)-JQ1 in BRD4 BD1 binding pocket. Asn140 residue hydrogen bonding to triazole is *highlighted* (pdb 3mxf)

GlaxoSmithKline reported on a related compound, I-BET762 [278, 279]. A compound from a different series, I-BET151, has shown efficacy against mixed lineage leukemia (MLL) cell lines in vitro and in vivo [280].

X-ray structures of (+)-JQ1 and I-BET762 show much more comprehensive interactions with the BRD4 BD1 surface than the AcLys peptides (Fig. 12). While both compounds place a methyl group in roughly the same position as the acetyl methyl of AcLys, and have hydrogen bond-accepting groups in position to interact with the conserved Asp140, they also much more fully fill the hydrophobic AcLys pocket, and also fit tightly over the lip of the cavity. Further support for the tightness of fit in the case of (+)-JQ1 comes from molecular dynamics simulations, which show much less flexibility of the main loop of BRD4 when binding the small molecule [275]. I-BET151 also places its oxazole in the hydrophobic pocket with one methyl group in the same position as those from the triazoles of (+)-JQ1 and I-BET762. None of the bound structures show any variation in the structure of the bromodomains upon ligand binding.

The puzzle of BET protein binding to its endogenous ligands is not yet definitively understood. The low binding constants for isolated acetylated peptides suggest involvement of multiple binding sites [281]. Indeed, full-length BRD4 not only binds much more strongly to bisacetylated peptides, but association of BRD4 to mitotic chromosomes does not tolerate single bromodomain deletion [269]. It also appears likely that association with other proteins involved in transcription enhances

BRD4 binding to chromatin [270, 271], presumably through additional surface contacts. At any rate, it seems clear that a single AcLys-centered interaction is not sufficient for biological activity of BRD4. It is rather stunning, then, that the structures of bromodomain binding pockets allow for the design of small, high-affinity ligands, and may allow for the possibility of blocking BRD4 activity by binding to only one of two bromodomain AcLys-binding sites. The ability of bromodomains to bind small molecules is further illustrated by the relative ease with which groups have found several low-micromolar hits for a number of bromodomain-containing proteins, such as PCAF and CREBBP, through fragment screening methods [282, 283].

As the BRD4 binding site shows no capacity for flexibility, and anchors its primary ligand with a hydrogen bond, it bears some resemblance to continuous epitope PPIs. However, the single amino acid recognition element results in a notable lack of additional hydrogen bonding contacts that can further lock in a ligand conformation. Additionally, small-molecule binding almost solely involves hydrophobic contacts, and additional, distant interactions with histone tails are necessary for biological activity; so, this PPI again has important differences with continuous epitope interactions.

6 Conclusions

The most important decision in the drug discovery process is the first one – deciding which target to work on. The ideal drug target has well-understood and well-validated biology, and is also amenable to modulation with a small molecule possessing physicochemical properties commensurate with oral dosing. Assays and in vivo models are known, or there is a clear path for their development. Structures of target-inhibitor complexes, or at least reliable models, are available to facilitate structure-based design.

In practice, not all of these qualities are likely to be present in any one target. PPIs are no different than more conventional drug targets in this regard, and the prospects for developing small-molecule PPI modulators depend on a number of factors. In particular, their druggability is highly variable and from protein to protein can be dependent on different structural features. Furthermore, the concept of druggability must not be assumed to be permanently grounded in prior art. Also, because our understanding of protein-ligand and protein-small-molecule interactions are in some cases inadequate, and because many PPIs are unrelated to any previous drug targets, it is usually of the utmost value to have a full appreciation of structural aspects of binding events. Finally, application of various methodologies have gone a long way in educating us on how to better identify binding sites, estimate the possibility of discovering a small-molecule PPI modulator for a particular target, and find chemical matter.

In spite of the obstacles posed by PPIs to drug discovery programs, several potent, orally bioavailable PPI antagonists have entered the clinic in the last

several years. While it is always of the highest importance to choose good targets, the advances made in understanding and solving the problems endemic to small-molecule PPI inhibition over the last 20 years have taught us a great deal, and rendered them much more approachable than in the past. As biologists continue to make strides in understanding signaling pathways, and uncover structural details of important interactions, new and compelling drug targets will continue to be brought forward. Armed with the experience of the last two decades, drug discovery scientists should be much more confident of being able to tackle the next set of PPI drug targets.

Acknowledgments The author is grateful to Kent Stewart for reading and offering comments on the manuscript.

References

1. Hopkins AL, Groom CR (2002) The druggable genome. Nat Rev Drug Discov 1:727–730
2. Russ AP, Lampel S (2006) The druggable genome: an update. Drug Disc Today 10:1607–1610
3. Overington JP, Al-Lazikani B, Hopkins AL (2008) How many drug targets are there? Nat Rev Drug Discov 5:993–996
4. Grant A, Lee D, Orengo C (2004) Progress towards mapping the universe of protein folds. Genome Biol 5:107
5. Kunin V, Cases I, Enrigh E, de Lorenzo V, Ouzounis CA (2003) Myriads of protein families, and still counting. Genome Biol 4:401
6. Vitkup D, Melamud E, Moult J, Sander C (2001) Completeness in structural genomics. Nat Struct Biol 8:559–566
7. Stumpf M, Thorne T, de Silva ERS et al (2008) Estimating the size of the human interactome. Proc Natl Acad Sci USA 105:6959–6964
8. Ideker T, Sharan R (2008) Protein networks in disease. Genome Res 18:644–652
9. Strong M, Eisenberg D (2007) The protein network as a tool for finding novel drug targets. Prog Drug Res 64:191–215
10. Komurov K, White M (2007) Revealing static and dynamic modular architecture of the eukaryotic protein interaction network. Mol Syst Biol 3:110
11. Aggarwal S (2009) What's fueling the biotech engine – 2008. Nat Rev Immunol 11:987–993
12. Toogood PL (2002) Inhibition of protein-protein association by small-molecules: approaches and progress. J Med Chem 45:1543–1558
13. Chene P (2006) Drugs targeting protein-protein interactions. ChemMedChem 1:400–411
14. Whitty A, Kumaravel G (2006) Between a rock and a hard place? Nat Chem Biol 2:112–118
15. Arkin MR, Wells JA (2004) Small-molecule inhibitors of protein-protein interactions: progressing towards the dream. Nat Rev Drug Discov 3:301–317
16. Wells JA, McClendon CL (2007) Reaching for high-hanging fruit in drug discovery at protein-protein interfaces. Nature 450:1001–1009
17. Fischer PM (2005) Protein-protein interactions in drug discovery. Drug Des Rev Online 2:179–207
18. Berg T (2008) Small-molecule inhibitors of protein-protein interactions. Curr Opin Drug Discov Dev 11:666–674
19. Fry DC (2008) Drug-like inhibitors of protein-protein interactions: a structural examination of effective protein mimicry. Curr Protein Pept Sci 9:240–247

20. Stites WE (1997) Protein-protein interactions: interface structure, binding thermodynamics, and mutational analysis. Chem Rev 97:1233–1250
21. Bogan AA, Thorn KS (1998) Anatomy of hot spots in protein interfaces. J Mol Biol 280:1–14
22. Young L, Jernigan RL, Covell DG (1994) A role for surface hydrophobicity in protein-protein recognition. Protein Sci 3:717–729
23. Lo Conte L, Chothia C, Janin J (1999) The atomic structure of protein-protein recognition sites. J Mol Biol 285:2177–219824
24. Archakov AI, Govorun VM, Dubanov AV et al (2003) Protein-protein interactions as a target for drugs in proteomics. Proteomics 3:380–391
25. Keskin O, Gursoy A, Ma B, Nussinov R (2008) Principles of protein-protein interactions: what are the preferred ways for proteins to interact? Chem Rev 108:1225–1244
26. Tsai CJ, Lin SL, Wolfson HJ, Nissinov R (1997) Studies of protein-protein interfaces: a statistical analysis of the hydrophobic effect. Protein Sci 6:53–64
27. Jones S, Thornton JM (1996) Principles of protein-protein interactions. Proc Natl Acad Sci USA 93:13–20
28. Jones S, Thornton JM (1997) Analysis of protein-protein interaction sites using surface patches. J Mol Biol 272:121–132
29. Argos P (1988) An investigation of protein subunit and domain interfaces. Protein Eng 2:101–113
30. Janin J, Miller S, Chothia C (1988) Surface, subunit interfaces and interior of oligomeric proteins. J Mol Biol 204:155–164
31. Bordner AJ, Abagyan R (2005) Statistical analysis and prediction of protein-protein interfaces. Proteins 60:353–366
32. Kufareva I, Budagyan L, Raush E et al (2007) PIER: protein interface recognition for structural proteomics. Proteins 67:400–417
33. Hu Z, Ma B, Wolfson H, Nussinov R (2000) Conservation of polar residues as hot spots at protein interfaces. Proteins 39:331–342
34. Fauchere JL, Pliska VE (1983) Hydrophobic parameters of amino-acid side-chains from the partitioning of N-acetyl-amino-acid amide. Eur J Med Chem 18:369–375
35. Radzicka A, Wolfenden R (1988) Comparing the polarities of the amino acids: side-chain distribution coefficients between the vapor phase, cyclohexane, 1-octanol, and neutral aqueous solution. Biochemistry 27:1664–1670
36. Takano K, Yutani K (2001) A new scale for side-chain contribution to protein stability based on the empirical stability analysis of mutant proteins. Protein Eng 14:525–528
37. Clackson T, Wells JA (1995) A hot spot of binding energy in a hormone-receptor interface. Science 267:383–386
38. Wells JA (1991) Systematic mutational analyses of protein-protein interfaces. Methods Enzymol 202:390–411
39. Atwell S, Ultsch M, de Vos AM, Wells JA (1997) Structural plasticity in a remodeled protein-protein interface. Science 278:1125–1128
40. Jonsson Z, Podust V, Podust L, Hubscher U (1995) Tyrosine 114 is essential for the trimeric structure and the functional activities of human proliferating cell nuclear antigen. EMBO J 14:5745–5751
41. Sattler M, Liang H, Nettesheim D et al (1997) Structure of Bcl-xL-Bak peptide complex: recognition between regulators of apoptosis. Science 275:983–986
42. Hajduk PJ, Huth JR, Fesik SW (2005) Druggability indices for protein targets derived from NMR-based screening data. J Med Chem 48:2518–2525
43. Kozakov D, Hall DR, Chuang G et al (2011) Structural conservation of druggable hot spots in protein–protein interfaces. Proc Natl Acad Sci USA 108:13528–13535
44. DeLano WL (2002) Unraveling hot spots in binding interfaces: progress and challenges. Curr Opin Struct Biol 12:14–20

45. Ma B, Elkayam T, Wolfson H, Nussinov R (2003) Protein-protein interactions: structurally conserved residues distinguish between protein binding sites and exposed protein surfaces. Proc Natl Acad Sci USA 100:5772–5777
46. Sundberg EJ, Mariuzza RA (2000) Luxury accommodations: the expanding role of structural plasticity in protein-protein interactions. Structure 8:R137–R142
47. Morrison KL, Weiss GA (2001) Combinatorial alanine scanning. Curr Opin Chem Biol 5:302–307
48. Sidhu SS, Fairbrother WJ, Deshayes K (2003) Exploring protein-protein interactions with phage display: discovery of peptidic antagonists of IGF-1 function. Chembiochem 4:14–25
49. Deshayes K (2005) Exploring protein-protein interactions using peptide libraries displayed on phage. In: Sidhu SS (ed) Phage display in biotechnology and drug discovery. CRC Press, Boca Raton
50. Hajduk PJ, Huth JR, Tse C (2005) Predicting protein druggability. Drug Discov Today 10:1675–1682
51. Burgoyne MJ, Jackson RM (2006) Predicting protein interaction sites: binding hot-spots in protein-protein and protein-ligand interfaces. Bioinformatics 22:1335–1342
52. Sugaya N, Furuya T (2011) Dr. PIAS: an integrative system for assessing the druggability of protein-protein interactions. BMC Bioinformatics 12:50
53. Perot S, Sperandio O, Miteva MA, Camproux AC, Villoutriex BO (2010) Druggable pockets and binding site centric chemical space: a paradigm shift in drug discovery. Drug Discov Today 15:656–667
54. Fuller JC, Burgoyne MJ, Jackson RM (2009) Predicting druggable binding sites at the protein-protein interface. Drug Discov Today 14:155–161
55. Hopkins A, Groom C, Alex A (2004) Ligand efficiency: a useful metric for lead selection. Drug Discov Today 9:430–431
56. Abad-Zapatero C, Metz JT (2005) Ligand efficiency indices as guideposts for drug discovery. Drug Discov Today 10:464–469
57. Higuerelo AP, Schreyer A, Bickerton GRJ et al (2009) Atomic interactions and profile of small-molecules disrupting protein-protein interfaces: the TIMBAL database. Chem Biol Drug Des 74:457–467
58. Lipinski C, Lombardo F, Dominy BW, Feeney PJ (1997) Experimental and computational approaches to estimate solubility and permeability in drug discovery and development settings. Adv Drug Deliv Rev 23:3–25
59. Clark DE (1999) Rapid calculation of polar molecular surface area and its application to the prediction of transport phenomena. 1. Prediction of intestinal absorption. J Pharm Sci 88:807–814
60. Johnson TW, Dress KR, Edwards M (2009) Using the Golden Triangle to optimize clearance and oral absorption. Bioorg Med Chem Lett 19:5560–5564
61. Morelli X, Bourgeas R, Roche P (2011) Chemical and structural lessons from recent successes in protein-protein interaction inhibition (2P2I). Curr Opin Chem Biol 15:475–481
62. Reynès C, Host H, Camproux A et al (2010) Designing focused chemical libraries enriched in protein-protein interaction inhibitors using machine-learning methods. PLoS Comput Biol 6: e1000695
63. Neugebauer A, Hartmann RW, Klein CD (2007) Prediction of protein-protein interaction inhibitors by chemoinformatics and machine learning methods. J Med Chem 50:4665–4668
64. Oprea TI, Davis AM, Teague SJ, Leeson PD (2001) Is there a difference between leads and drugs? A historical perspective. J Chem Inf Model 41:1308–1315
65. Rishton GM (2003) Nonleadlikeness and leadlikeness in biochemical screening. Drug Discov Today 8:86–96
66. Teague SJ, Davis AM, Leeson PD, Oprea TI (1999) The design of leadlike combinatorial libraries. Angew Chem Int Ed Engl 38:3743–3748
67. Veber DF, Johnson SR, Cheng H-Y et al (2002) Molecular properties that influence the oral bioavailability of drug candidates. J Med Chem 45:2615–2623

68. Bergström CAS, Strafford M, Lazarova L et al (2003) Absorption classification of oral drugs based on molecular surface properties. J Med Chem 46:558–570
69. Hou TJ, Wang JM, Zhang W et al (2006) Recent advances in computational prediction of drug absorption and permeability in drug discovery. Curr Med Chem 13:2653–2667
70. Hou T, Wang J, Zhang W, Xu X (2007) ADME evaluation in drug discovery. 6. Can oral bioavailability in humans be effectively predicted by simple molecular property-based rules? J Chem Inf Model 47:460–463
71. Alex A, Millan DS, Perez M et al (2011) Intramolecular hydrogen bonding to improve membrane permeability and absorption in beyond rule of five chemical space. MedChemComm 2:669–674
72. Paolini GV, van Shepland RHB, Hoorn WP et al (2006) Global mapping of pharmacological space. Nat Biotechnol 24:805–815
73. Leeson PD, Springthorpe B (2007) The influence of drug-like concepts on decision-making in medicinal chemistry. Nat Rev Drug Discov 6:881–890
74. Wenlock MC, Austin RP, Barton P et al (2003) A comparison of physiochemical property profiles of development and marketed oral drugs. J Med Chem 46:1250–1256
75. Walters WP, Green J, Weiss JR, Murcko MA (2011) What do medicinal chemists actually make? A 50-year retrospective. J Med Chem 54:6405–6416
76. Leeson PD, Davis AM (2004) Time-related differences in the physical property profiles of oral drugs. J Med Chem 47:6338–6348
77. Proudfoot JR (2005) The evolution of synthetic oral drug properties. Bioorg Med Chem Lett 15:1087–1090
78. Blake JF (2005) Identification and evaluation of molecular properties related to preclinical optimization and clinical fate. Med Chem 1:649–655
79. Gill AL, Verdonk M, Boyle RG, Taylor R (2007) A comparison of physicochemical property profiles of marketed oral drugs and orally bioavailable anti-cancer protein kinase inhibitors in clinical development. Curr Top Med Chem 7:1408–1422
80. Bergström CAS, Wassvik CM, Johansson K, Hubatsch I (2007) Poorly soluble marketed drugs display solvation limited solubility. J Med Chem 50:5858–5862
81. Hawkins MJ, Soon-Shiong P, Desai N (2008) Protein nanoparticles as drug carriers in clinical medicine. Adv Drug Deliv Rev 60:1000–1017
82. Vintinoiu A, Leroux JC (2008) Organogels and their use in drug delivery: a review. J Control Release 125:179–192
83. Gupta S, Moulik SP (2008) Biocompatible microemulsions and their prospective uses in drug delivery. J Pharm Sci 97:22–45
84. Cheng Y, Xu Z, Ma M, Xu T (2008) Dendrimers as drug carriers: applications in different routes of drug administration. J Pharm Sci 97:123–143
85. Drummond DC, Noble CO, Hayes ME et al (2008) Pharmacokinetics and in vivo drug release rates in liposomal nanocarrier development. J Pharm Sci 97:4696–4740
86. Breitenbach J (2002) Melt extrusion: from process to drug delivery technology. Eur J Pharm Biopharm 54:107–117
87. DeLano WL, Ultsch MH, deVos AM, Wells JA (2000) Convergent solutions to binding at a protein-protein interface. Science 287:1279–1283
88. Eyrisch S, Helms V (2007) Transient pockets on protein surfaces involved in protein-protein interaction. J Med Chem 50:3457–3464
89. Ma B, Shatsky M, Wolfson HJ, Nussinov R (2002) Multiple diverse ligands binding at a single protein site: a matter of preexisting populations. Protein Sci 11:184–197
90. Teague S (2003) Implications of protein flexibility for drug discovery. Nat Rev Drug Discov 2:527–541
91. Kortemme T, Kim DE, Baker D (2004) Computational alanine scanning of protein-protein interfaces. Sci Signal 219:l2
92. McGovern SL, Caselli E, Grigorieff N, Shoichet BK (2002) A common mechanism underlying promiscuous inhibitors from virtual and high-throughput screening. J Med Chem 45:1712–1722

93. Seidler J, McGovern SL, Dornan TL, Shoichet BK (2003) Identification and prediction of promiscuous aggregating inhibitors among known drugs. J Med Chem 46:4477–4786
94. Lebowicz J, Lewis MS, Schuck P (2009) Modern analytical ultracentrifugation in protein science: a tutorial review. Protein Sci 11:2067–2079
95. Arkin M, Lear JD (2001) A new data analysis method to determine binding constants of small-molecules to proteins using equilibrium analytical ultracentrifugation with absorption optics. Anal Biochem 299:98–107
96. Philo JS (2000) Sedimentation equilibrium analysis of mixed associations using numerical constraints to impose mass or signal conservation. Methods Enzymol 321:100–120
97. Leavitt S, Freire E (2001) Direct measurement of protein binding energetics by isothermal titration calorimetry. Curr Opin Struct Biol 11:560–566
98. Lewis EA, Murphy KP (2005) Isothermal titration calorimetry. Methods Mol Biol 305:1–15
99. Pattnaik P (2000) Surface plasmon resonance. Applications in understanding receptor-ligand interaction. Appl Biochem Biotechol 126:79–92
100. Cooper M, Mayr LM, Rich RL, Myszka DG (2011) The revolution of real-time, label-free biosensor applications. In: Cooper M, Mayr LM (eds) Label-free technologies for drug discovery. Wiley, New York
101. Shuker SB, Hajduk PJ, Meadows RP, Fesik SW (1996) Discovering high-affinity ligands for proteins: SAR by NMR. Science 274:1531–1534
102. Hajduk PJ, Greer J (2007) A decade of fragment-based drug design: strategic advances and lessons learned. Nat Rev Drug Discov 6:211–219
103. Congreve M, Chessari G, Tisi D, Woodhead AJ (2008) Recent developments in fragment-based drug discovery. J Med Chem 51:3661–3680
104. Sun C, Petros AM, Hajduk PJ (2011) Fragment-based lead discovery: challenges and opportunities. J Comput Aided Mol Des 25:607–610
105. Coyne AG, Scott DE, Abell C (2010) Drugging challenging targets using fragment-based approaches. Curr Opin Chem Biol 14:299–307
106. Hämäläinen MD, Zhukov A, Ivarsson M et al (2008) Label-free primary screening and affinity ranking of fragment libraries using parallel analysis of protein panels. J Biomol Screen 13:202–209
107. Pellecchia M, Bertini I, Cowburn D et al (2008) Perspectives on NMR in drug discovery: a technique comes of age. Nat Rev Drug Discov 7:738–745
108. Navratilova I, Hopkins AL (2010) Fragment screening by surface plasmon resonance. ACS Med Chem Lett 1:44–48
109. Neumann T, Junker HD, Schmidt K, Sekul R (2007) SPR-based fragment screening: advantages and applications. Curr Top Med Chem 7:1630–1642
110. Nienaber VL, Richardson PL, Klighofer V et al (2000) Discovering novel ligands for macromolecules using X-ray crystallographic screening. Nat Biotechnol 18:1105–1108
111. Davies DR, Begley DW, Hartley RC et al (2011) Predicting the success of fragment screening by X-ray crystallography. Methods Enzymol 493:91–114
112. Jhoti H, Cleasby A, Verdonk M, Williams G (2008) Fragment-based screening using X-ray crystallography and NMR spectroscopy. Curr Opin Chem Biol 11:485–493
113. Hajduk PK, Gerfin T, Boehlen JM et al (1999) High-throughput nuclear magnetic resonance-based screening. J Med Chem 42:2315–2317
114. Dalvit C, Flocco M, Knapp S et al (2002) High-throughput NMR-based screening with competition binding experiments. J Am Chem Soc 124:7702–7709
115. Hajduk PJ, Burns DJ (2002) Integration of NMR and high-throughput screening. Comb Chem High Throughput Screen 6:613–621
116. Blundell TL, Jhoti H, Abell C (2002) High-throughput crystallography for lead discovery in drug design. Nat Rev Drug Discov 1:45–54
117. Blundell TL, Patel S (2004) High-throughput X-ray crystallography for drug discovery. Curr Opin Pharmacol 4:490–496

118. Köppen H (2009) Virtual screening – what does it give us? Curr Opin Drug Discov Dev 12:397–407
119. Cavasotto CN, Orry AJW (2007) Ligand docking and structure-based virtual screening in drug discovery. Curr Opin Med Chem 7:1006–1014
120. Betzi S, Restouin A, Opi S et al (2007) Protein–protein interaction inhibition (2P2I) combining high throughput and virtual screening: application to the HIV-1 Nef protein. Proc Natl Acad Sci USA 104:19256–19261
121. Casey FP, Pihan E, Shields DC (2009) Discovery of small-molecule inhibitors of protein-protein interactions using combined ligand and target score normalization. J Med Chem 49:2708–2717
122. Sandrini S (2005) Use of IL-2 receptor antagonists to reduce delayed graft function following renal transplantation: a review. Clin Transplant 19:705–710
123. Brandhuber BJ, Boone T, Kenney WC, McKay DB (1987) Three-dimensional structure of interleukin-2. Science 238:1707–1709
124. Sauve K, Nachman M, Spence C et al (1991) Localization in human interleukin 2 of the binding site to the α chain (p55) of the interleukin 2 receptor. Proc Natl Acad Sci USA 88:4636–4640
125. Tilley JW, Chen L, Fry DC et al (1997) Identification of a small-molecule inhibitor of the IL-2/IL-2Rα receptor interaction which binds to IL-2. J Am Chem Soc 119:7589–7590
126. Erlanson DA, Wells JA, Braisted AC (2004) Tethering: fragment-based drug discovery. Annu Rev Biophys 33:199–223
127. Hyde J, Braisted AC, Randal M, Arkin MR (2003) Discovery and characterization of cooperative ligand binding in the adaptive region of interleukin-2. Biochemistry 42:6475–6483
128. Raimundo BC, Oslob JD, Braisted AC et al (2004) Integrating fragment assembly and biophysical methods in the chemical advancement of small-molecule antagonists of IL-2: an approach for inhibiting protein-protein interactions. J Med Chem 47:3111–3130
129. Thanos CD, DeLano WL, Wells JA (2006) Hot-spot mimicry of a cytokine receptor by a small-molecule. Proc Natl Acad Sci USA 103:15422–15427
130. Rickert M, Wang X, Boulanger MJ et al (2005) The structure of interleukin-2 complexed with its alpha receptor. Science 308:1477–1480
131. Arkin MR, Randal M, DeLano WL et al (2003) Binding of small-molecules to an adaptive protein-protein interface. Proc Natl Acad Sci USA 100:1603–1608
132. Siddiqui MA, Perry CM (2006) Human papillomavirus quadrivalent (types 6, 11, 16, 18) recombinant vaccine (Gardasil). Drugs 66:1263–1271
133. Monie A, Hung CF, Roden R, Wu TC (2008) Cervarix: a vaccine for the prevention of HPV 16, 18-associated cervical cancer. Biologics 2:97–105
134. Hebner CM, Laimins LA (2006) Human papillomaviruses: basic mechanisms of pathogenesis and oncogenicity. Rev Med Virol 16:83–97
135. White PW, Faucher AM, Goudreau N (2011) Small-molecule inhibitors of the human papillomavirus E1–E2 interaction. Curr Top Microbiol Immunol 348:61–88
136. Yoakim C, Ogilvie WW, Goudreau N et al (2003) Discovery of the first series of inhibitors of human papilloma virus type 11: inhibition of the assembly of the E1-E2 Origin DNA complex. Bioorg Med Chem Lett 13:2539–2541
137. White PW, Titolo S, Brault K et al (2003) Inhibition of human papillomavirus DNA replication by small-molecule antagonists of the E1-E1 protein interaction. J Biol Chem 278:26765–26772
138. Wang Y, Coulombe R, Cameron DR et al (2004) Crystal structure of the E2 transactivation domain of human papillomavirus type 11 bound to a protein interaction inhibitor. J Biol Chem 279:6976–6985
139. Goudreau N, Cameron DR, Deziel R et al (2007) Optimization and determination of the absolute configuration of a series of potent inhibitors of human papillomavirus type-11 E1-E2 protein-protein interaction: a combined medicinal chemistry, NMR and computational chemistry approach. Bioorg Med Chem 15:2690–2700

140. White PW, Faucher AM, Goudreau N (2011) Small-molecule inhibitors of the human papillomavirus E1-E2 interaction. In: Vassilev L, Fry D (eds) Small-molecule inhibitors of protein-protein interactions. Springer, Berlin
141. Antson AA, Burns JE, Moroz OV et al (2000) Structure of the intact transactivation domain of the human papillomavirus E2 protein. Nature 403:805–809
142. Harris SF, Botchan MR (1999) Crystal structure of the human papillomavirus type 18 E2 activation domain. Science 284:1673–1677
143. Abbate E, Berger JM, Botchan MR (2004) The X-ray structure of the papillomavirus helicase in complex with its molecular matchmaker E2. Genes Dev 18:1981–1996
144. Mosyak L, Zhang Y, Glasfeld E et al (2000) The bacterial cell-division protein ZipA and its interaction with an FtsZ fragment revealed by X-ray crystallography. EMBO J 19:3179–3191
145. Tsao DHH, Sutherland AG, Jennings LD et al (2006) Discovery of novel inhibitors of the ZipA/FtsZ complex by NMR fragment screening coupled with structure-based design. Bioorg Med Chem 14:7953–7961
146. Jennings LD, Foreman KW, Rush TS et al (2004) Combinatorial synthesis of substituted 3-(2-indolyl)piperidines and 2-phenyl indoles as inhibitors of ZipA-FtsZ interaction. Bioorg Med Chem 12:5115–5131
147. Kenny CH, Ding W, Kelleher K et al (2003) Development of a fluorescence polarization assay to screen for inhibitors of the FtsZ/ZipA interaction. Anal Biochem 323:224–233
148. Rush TS, Grant JA, Mosyak L, Nicholls A (2005) A shape-based 3-D scaffold hopping method and its application to a bacterial protein-protein interaction. J Med Chem 48:1489–1495
149. Shangary S, Wang S (2009) Small-molecule inhibitors of the MDM2-p53 protein-protein interaction to reactivate p53 function: a novel approach for cancer therapy. Annu Rev Pharmacol Toxicol 49:223–241
150. Kussie PH, Gorina S, Marechal V et al (1996) Structure of the MDM2 oncoprotein bound to the p53 tumor suppressor transactivation domain. Science 274:948–953
151. Lin J, Chen J, Elenbaas B, Levine AJ (1994) Several hydrophobic amino acids in the p53 amino-terminal domain are required for transcriptional activation, binding to mdm-2 and the adenovirus 5 E1B 55-kD protein. Genes Dev 8:1235–1246
152. Picksley SM, Vojtesek B, Sparks A, Lane DP (1994) Immunochemical analysis of the interaction of p53 with MDM2-fine mapping of the MDM2 binding site on p53 using synthetic peptides. Oncogene 9:2523–2529
153. Vassilev LT, Vu BT, Graves B et al (2004) In vivo activation of the p53 pathway by small-molecule antagonists of MDM2. Science 303:844–848
154. Grasberger BL, Lu T, Schubert C et al (2005) Discovery and cocrystal structure of benzodiazapinedione HDM2 antagonists that activate p53 in cells. J Med Chem 48:909–912
155. Allen JG, Bourbeau MP, Wohlhieter GE et al (2009) Discovery and optimization of chromenotriazolopyrimidines as potent inhibitors of the mouse double minute 2-tumor protein 53 protein-protein interaction. J Med Chem 52:7044–7053
156. Demma M, Maxwell E, Ramos R et al (2010) SCH529074, a small-molecule activator of mutant p53, which binds p53 DNA binding domain (DBD), restores growth-suppressive function to mutant p53 and interrupts HDM2-mediated ubiquitination of wild type p53. J Biol Chem 285:10198–10212
157. Yin H, Lee GI, Park HS et al (2005) Terphenyl-based helical mimetics that disrupt the p53/HDM2 interaction. Angew Chem Int Ed Engl 44:2704–2707
158. Stoll R, Renner C, Hansen S et al (2001) Chalcone derivatives antagonize interactions between the human oncoprotein MDM2 and p53. Biochemistry 40:336–344
159. Lu Y, Nikolovska-Coleska Z, Fang X et al (2006) Discovery of a nanomolar inhibitor of the human murine double minute 2 (MDM2)-p53 interaction through an integrated, virtual database screening strategy. J Med Chem 49:3759–3762
160. Bowman AL, Nikolovska-Coleska Z, Zhong H et al (2007) Small-molecule inhibitors of the MDM2-p53 interaction discovered by ensemble-based receptor models. J Am Chem Soc 129:12809–12814

161. Rothweiler U, Czarna A, Krajewski M et al (2008) Isoquinolin-1-one inhibitors of the MDM2-p53 interaction. ChemMedChem 3:1118–1128
162. Fry DC, Graves B, Vassilev LT (2005) Development of E3-substrate (MDM2-p53)-binding inhibitors: structural aspects. Methods Enzymol 399:622–633
163. Ding K, Lu Y, Nikolovska-Coleska Z et al (2006) Structure-based design of spire-oxindoles as potent, specific small-molecule inhibitors of the MDM2-p53 interaction. J Med Chem 49:3432–3435
164. Boettcher A, Buschmann N, Furet P et al (2008) 3-Imidazolylindoles for treatment of proliferative diseases and their preparation. PCT Int Appl WO2008119741
165. Popowicz GM, Czarna A, Wolf S et al (2010) Structures of low molecular weight inhibitors bound to MDMX and MDM2 reveal new approaches for p53-MDMX/MDM2 antagonist drug discovery. Cell Cycle 9:1104–1111
166. Popowicz GM, Domling A, Holak TA (2011) The structure-based design of Mdm2-p53 inhibitors gets serious. Angew Chem Int Ed Engl 50:2680–2688
167. Uhrinova S, Uhrin D, Powers H et al (2005) Structure of free MDM2 N-terminal domain reveals conformational adjustments that accompany p53-binding. J Mol Biol 350:587–598
168. Tovar C, Rosinski J, Filipovic Z et al (2006) Small-molecule MDM2 antagonists reveal aberrant p53 signaling in cancer: implications for therapy. Proc Natl Acad Sci USA 103:1888–1893
169. Shangary S, Qin D, McEachern D et al (2008) Temporal activation of p53 by a specific MDM2 inhibitor is selectively toxic to tumors and leads to complete tumor growth inhibition. Proc Natl Acad Sci USA 105:3933–3938
170. Weber L (2010) Patented inhibitors of p53-Mdm2 interaction (2006–2008). Expert Opin Ther Patents 20:179–191
171. Cheok CF, Verma CS, Baselga J, Lane DP (2011) Translating p53 into the clinic. Nat Rev Clin Oncol 8:25–37
172. Youle RJ, Strasser A (2008) The BCL-2 protein family: opposing activities that mediate cell death. Nat Rev Mol Cell Biol 9:47–59
173. Petros AM, Nettesheim DG, Wang Y et al (2000) Rationale for Bcl-x(L)/bad peptide complex formation from structure, mutagenesis, and biophysical studies. Protein Sci 9:2528–2534
174. Oltersdorf T, Elmore SW, Shoemaker AR et al (2005) An inhibitor of Bcl family proteins induces regression of solid tumours. Nature 435:677–681
175. Lee EF, Czabotar PE, Smith BJ et al (2007) Crystal structure of ABT-737 complexed with Bcl-xL: implications for selectivity of antagonists of the Bcl-2 family. Cell Death Differ 14:1711–1713
176. Park C-M, Bruncko M, Adickes J et al (2008) Discovery of an orally bioavailable small-molecule inhibitor of prosurvival B-cell lymphoma 2 proteins. J Med Chem 51:6902–6915
177. Palladino MA, Bahjat FR, Theodorakis EA, Moldawer LL (2003) Anti-TNF-α therapies: the next generation. Nat Rev Drug Discov 2:736–746
178. Eck ME, Sprang SR (1989) The structure of tumor necrosis factor-α at 2.6 Å resolution. J Biol Chem 264:17595–17605
179. He MM, Smith AS, Oslb JD et al (2005) Small-molecule inhibition of TNF-α. Science 310:1022–1025
180. Debnath AK (2006) Prospects and strategies for the discovery and development of small-molecule inhibitors of six-helix bundle formation in class 1 viral fusion proteins. Curr Opin Investig Drugs 7:118–127
181. Debnath A (2006) Progress in identifying peptides and small-molecule inhibitors targeted to gp41 of HIV-1. Expert Opin Investig Drugs 15:465–478
182. Koszalka GW, Meanwell NA (2006) Inhibition of virus entry: an antiviral mechanism of emerging prominence. Curr Opin Investig Drugs 7:106–108
183. Roymans D, De Bondt HL, Arnoult E et al (2010) Binding of a potent small-molecule inhibitor of six-helix bundle formation requires interactions with both heptad-repeats of the RSV fusion protein. Proc Natl Acad Sci USA 107:308–313

184. Pawson T, Scott JD (1997) Signaling through scaffold, anchoring, and adaptor proteins. Science 278:2075–2080
185. Shimaoka M, Springer TA (2003) Therapeutic antagonists and conformational regulation of integrin function. Nat Rev Drug Discov 2:703–716
186. Scarborough RM, Gretler DD (2000) Platelet glycoprotein IIb-IIIa antagonists as prototypical integrin blockers: novel parenteral and potential oral antithrombotic agents. J Med Chem 43:3453–3473
187. Takada Y, Ye X, Simon S (2007) The integrins. Genome Biol 8:215
188. Duggan ME, Hutchinson JH (2000) Ligands to the integrin receptor $\alpha_v\beta_3$. Expert Opin Ther Patents 10:1367–1383
189. Cox D, Brennan M, Moran N (2010) Integrins as therapeutic targets: lessons and opportunities. Nat Rev Drug Discov 9:804–820
190. Cox D (2004) Oral GPIIb/IIIa antagonists: what went wrong? Curr Pharm Des 10:1587–1596
191. Auzzas L, Zanardi F, Battistini L et al (2010) Targeting αvβ3 integrin: design and applications of mono- and multifunctional RGD-based peptides and semipeptides. Curr Med Chem 17:1255–1299
192. Xiong JP, Stehle T, Diefenbach B et al (2001) Crystal structure of the extracellular segment of integrin αvβ3. Science 294:339–345
193. Xiong JP, Stehle T, Zhang R et al (2002) Crystal structure of the extracellular segment of integrin αvβ3 in complex with an arg-gly-asp ligand. Science 296:151–155
194. Springer TA, Zhu J, Xiao T (2008) Structural basis for distinctive recognition of fibrinogen γC peptide by the platelet integrin $\alpha_{IIb}\beta_3$. J Cell Biol 182:791–800
195. Polman CH, O'Connor PW, Havrdova E et al (2006) A randomized, placebo-controlled trial of natalizumab for relapsing multiple sclerosis. New Engl J Med 354:899–910
196. Targan SR, Feagan BG, Fedorak RN et al (2007) Natalizumab for the treatment of active Crohn's disease: results of the ENCORE trial. Gastroenterology 132:1672–1683
197. Tilley JW (2008) Very late antigen-4 integrin antagonists. Expert Opin Ther Patents 18:841–859
198. Muro F, Iimura S, Sugimoto Y et al (2009) Discovery of trans-4-[1-[[2,5-dichloro-4-(1-methyl-3-indolylcarboxamide)phenyl]acetyl]-(4 S)-methoxy-(2 S)-pyrrolidinylmethoxy] cyclo-hexanecarboxylic acid: an orally active, selective very late antigen-4 antagonist. J Med Chem 52:7974–7992
199. Faull RJ, Ginsberg MH (1996) Inside-out signaling through integrins. J Am Soc Nephrol 7:1091–1097
200. Qin J, Vinogradova O, Plow EF (2004) Integrin bidirectional signaling: a molecular view. PLoS Biol 2:0726–0729
201. Liu G (2001) Small-molecule antagonists of the LFA-1/ICAM-1 interaction as potential therapeutic agents. Expert Opin Ther Patents 11:1383–1393
202. Potin D, Launay M, Monatlik F et al (2006) Discovery and development of 5-[(5S,9R)-9-(4-cyanophenyl)-3-(3,5-dichlorophenyl)-1-methyl-2,4-dioxo-1,3,7-triazaspiro[4.4]non-7-ylmethyl]-3-thiophenecarboxylic acid (BMS-587101) – a small-molecule antagonist of leukocyte function associated antigen-1. J Med Chem 49:6946–6949
203. Kallen J, Welzenbach K, Ramage P et al (1999) Structural basis for LFA-1 inhibition upon lovastatin binding to the CD11a I-domain. J Mol Biol 292:1–9
204. Shimaoka M, Salas A, Yang W et al (2003) Small-molecule integrin antagonists that bind to the β2 subunit I-like domain and activate signals in one direction and block them in the other. Immunity 19:391–402
205. Welzenbach K, Hommel U, Weitz-Schmidt G (2002) Small-molecule inhibitors induce conformational changes in the I domain and the I-like domain of lymphocyte function associated antigen-1. Molecular insights into integrin inhibition. J Biol Chem 277:10590–10598
206. Miller MW, Basra S, Kulp DW et al (2009) Small-molecule inhibitors of integrin $\alpha_2\beta_1$ that prevent pathological thrombus formation via an allosteric mechanism. Proc Natl Acad Sci USA 106:719–724

207. Choi S, Vilaire G, Marcinkiewicz C et al (2007) Small-molecule inhibitors of integrin α2β1. J Med Chem 50:5457–5462
208. Russell RB, Breed J, Barton GJ (1992) Conservation analysis and structure prediction of the SH2 family of phosphotyrosine binding domains. FEBS Lett 304:15–20
209. Kasembeli MM, Xu X, Tweardy DJ (2009) SH2 domain binding to phosphopeptide ligands: potential for drug targeting. Front Biosci 14:1010–1022
210. Gan W, Roux B (2009) Binding specificity of SH2 domains: insight from free energy simulations. Proteins 74:996–1007
211. Songyang Z, Shoelson SE, Chaudhuri M et al (1993) Sh2 domains recognize specific phosphopeptide sequences. Cell 72:767–778
212. Songyang Z, Oelson SE, McGlade J et al (1994) Specific motifs recognized by the sh2 domains of csk, 3bp2, fps/fes, grb-2, hcp, shc, syk, and vav. Mol Cell Biol 14:2777–2785
213. Campbell SJ, Jackson RM (2003) Diversity in the SH2 domain family phosphotyrosyl peptide binding site. Protein Eng 16:217–227
214. Sawyer TK, Bohacek RS, Dalgarno DC et al (2002) Src homology-2 inhibitors: peptidomimetic and nonpeptide. Mini Rev Med Chem 2:475–488
215. Lu XL, Cao X, Liu XY, Jiao BH (2010) Recent progress of Src SH2 and SH3 inhibitors as anticancer agents. Curr Med Chem 17:1117–1124
216. Shakespeare WC (2001) SH2 domain inhibition: a problem solved? Curr Opin Chem Biol 5:409–415
217. Violette SM, Guan W, Bartlett C et al (2001) Bone-targeted Src SH2 inhibitors block Src cellular activity and osteoclast-mediated resorption. Bone 28:54–64
218. Shakespeare W, Yang M, Bohacek R (2001) Structure-based design of an osteoclast-selective, nonpeptide Src homology 2 inhibitor with in vivo antiresorptive activity. Proc Natl Acad Sci USA 97:9373–9378
219. Shakespeare WC, Metcalf CA III, Wang Y et al (2003) Novel bone-targeted Src tyrosine kinase inhibitor drug discovery. Curr Opin Drug Discov Dev 6:729–741
220. Lange G, Lesuisse D, Deprez P et al (2003) Requirements for specific binding of low affinity inhibitor fragments to the SH2 domain of pp 60Src are identical to those for high affinity binding of full length inhibitors. J Med Chem 46:5184–5195
221. Garcia-Echeverria C, Furet P, Gay B et al (1998) Potent antagonists of the SH2 domain of Grb2: optimization of the X_{+1} position of 3-amino-Z-Tyr(PO_3H_2)-X_{+1}-Asn-NH_2. J Med Chem 41:1741–1744
222. Schoepfer J, Fretz H, Gay B et al (1999) Highly potent inhibitors of the Grb2-SH2 domain. Bioorg Med Chem Lett 9:221–226
223. Gay B, Suarez S, Caravatti G et al (1999) Selective Grb2 inhibitors as anti-Ras therapy. Cell 83:235–241
224. Yao ZJ, Richter CR, Cao T et al (1999) Potent inhibition of Grb2 SH2 domain binding by non-phosphate-containing ligands. J Med Chem 42:25–35
225. Gao Y, Luo J, Yao ZJ et al (2000) Inhibition of Grb2 SH2 domain binding by non-phosphate-containing ligands. 2. 4-(2-Malonyl)phenylalanine as a potent phosphotyrosyl mimetic. J Med Chem 43:911–920
226. Park IH, Li C (2009) Characterization of molecular recognition of STAT3 SH2 domain inhibitors through molecular simulation. J Mol Recognit 24:254–265
227. Huang N, Nagarsekar A, Xia G et al (2004) Identification of non-phosphate-containing small molecular weight inhibitors of the tyrosine kinase p56 Lck SH2 domain via in silico screening against the pY+3 binding site. J Med Chem 47:3502–3511
228. Hung AY, Sheng M (2002) PDZ domains: structural modules for protein complex assembly. J Biol Chem 277:5699–5702
229. Harris BZ, Lim WA (2001) Mechanism and role of PDZ domains in signaling complex assembly. J Cell Sci 114:3219–3231
230. Tonikian R, Zhang Y, Sazinsky SL et al (2008) A specificity map for the PDZ domain family. PLoS Biol 6:e239

231. Stiffler MA, Chen JR, Grantcharova VP et al (2007) PDZ domain binding selectivity is optimized across the mouse proteome. Science 317:364–369
232. Doyle DA, Lee A, Lewis J et al (1996) Crystal structures of a complexed and peptide-free membrane protein-binding domain: molecular basis of peptide recognition by PDZ. Cell 85:106–1076
233. Kurakin A, Swistowski A, Wu SC, Bredesen DE (2007) The PDZ domain as a complex adaptive system. PLoS One 2:e953
234. Ducki S, Bennett E (2009) Protein-protein interactions: recent progress in the development of selective PDZ inhibitors. Curr Chem Biol 3:146–158
235. Wong HC, Bourdelas A, Krauss A et al (2003) Direct binding of the PDZ domain of dishevelled to a conserved internal sequence in the C-terminal region of Frizzled. Mol Cell 12:1251–1260
236. Zhang Y, Appleton BA, Wiesmann C et al (2009) Inhibition of Wnt signaling by dishevelled PDZ peptides. Nat Chem Biol 5:217–219
237. Fujiu N, You L, Xu Z et al (2007) An antagonist of dishevelled protein-protein interaction suppresses β-catenin-dependent tumor cell growth. Cancer Res 67:573–579
238. Grandy D, Shan J, Zhang X et al (2009) Discovery and characterization of a small-molecule inhibitor of the PDZ domain of dishevelled. J Biol Chem 284:16256–16263
239. Lee HJ, Wang NX, Shi DL, Zheng JJ (2009) Sulindac inhibits canonical Wnt signaling by blocking the PDZ domain of the protein dishevelled. Angew Chem Int Ed Engl 48:6448–6452
240. Gyrd-Hansen M, Meier P (2010) IAPs: from caspase inhibitors to modulators of NF-kB, inflammation and cancer. Nat Rev Cancer 10:561–574
241. Srinivasula SM, Hegde R, Saleh A et al (2001) A conserved XIAP-interaction motif in caspase-9 and Smac/DIABLO regulates caspase activity and apoptosis. Nature 410:112–116
242. Shiozaki EN, Chai J, Rigotti DJ et al (2003) Mechanism of XIAP-mediated inhibition of caspase-9. Mol Cell 11:519–527
243. Du C, Fang M, Li Y et al (2000) Smac, a mitochondrial protein that promotes cytochrome c-dependent caspase activation by eliminating IAP inhibition. Cell 102:33–42
244. Verhagen AM, Ekert PG, Pakusch M et al (2000) Identification of DIABLO, a mammalian protein that promotes apoptosis by binding to and antagonizing IAP proteins. Cell 102:43–53
245. Liu Z, Sun C, Olejniczak ET et al (2000) Structural basis for binding of Smac/DIABLO to the XIAP BIR3 domain. Nature 408:1004–1008
246. Wu G, Chai J, Suber TL et al (2000) Structural basis of IAP recognition by Smac/DIABLO. Nature 408:1008–1012
247. Chai J, Du C, Wu JW et al (2000) Structural and biochemical basis of apoptotic activation by Smac/DIABLO. Nature 406:855–862
248. Kipp RA, Case MA, Wist AD et al (2002) Molecular targeting of inhibitors of apoptosis proteins based on small-molecule mimics of natural binding partners. Biochemistry 41:7344–7349
249. Zobel K, Wang L, Varfolomeev E et al (2006) Design, synthesis, and biological activity of a potent Smac mimetic that sensitizes cancer cells to apoptosis by antagonizing IAPs. ACS Chem Biol 1:525–534
250. Peng Y, Sun H, Nikolovska-Coleska Z et al (2008) Design, synthesis and evaluation of potent and orally bioavailable diazabicyclic smac mimetics. J Med Chem 51:8158–8162
251. Sun H, Stuckey JA, Nikolovska-Coleska Z et al (2008) Structure-based design, synthesis, evaluation and crystallographic studies of conformationally constrained Smac mimetics as inhibitors of the X-linked inhibitor of apoptosis protein (XIAP). J Med Chem 51:7169–7180
252. Oost TK, Sun C, Armstrong RC et al (2004) Discovery of potent antagonists of the antiapoptotic protein XIAP for the treatment of cancer. J Med Chem 47:4417–4426
253. Park CM, Sun C, Olejniczak ET et al (2005) Non-peptidic small-molecule inhibitors of XIAP. Bioorg Med Chem Lett 15:771–775

254. Chauhan D, Neri P, Velankar M et al (2007) Targeting mitochondrial factor Smac/DIABLO as therapy for multiple myeloma (MM). Blood 109:1220–1227
255. Gaither A, Porter D, Yao Y et al (2007) A Smac mimetic rescue screen reveals roles for inhibitor of apoptosis proteins in tumor necrosis factor-alpha signaling. Cancer Res 67:11493–11498
256. Huang Y, Rich RL, Myszka DG, Wu H (2003) Requirement of both the second and third BIR domains for the relief of X-linked inhibitor of apoptosis protein (XIAP)-mediated caspase inhibition by Smac. J Biol Chem 278:49517–49522
257. Li L, Thomas RM, Suzuki H et al (2004) A small-molecule smac mimic potentiates TRAIL- and TNF-α-mediated cell death. Science 305:1471–1474
258. Bertrand MJ, Milutinovic S, Dickson KM et al (2008) cIAP1 and cIAP2 facilitate cancer cell survival by functioning as E3 ligases that promote RIP1 ubiquitination. Mol Cell 30:689–700
259. Sun H, Nikolovska-Coleska Z, Lu J et al (2007) Design, synthesis and characterization of a potent, nonpeptide, cell-permeable, bivalent smac mimetic that concurrently targets both the BIR2 and BIR3 domains in XIAP. J Am Chem Soc 129:15279–15294
260. Nikolovska-Coleska Z, Meagher JL, Jiang S et al (2008) Interaction of a cyclic, bivalent Smac mimetic with the X-linked inhibitor of apoptosis protein. Biochemistry 47:9811–9824
261. Sun C, Cai M, Meadows RP et al (2000) NMR structure and mutagenesis of the third BIR domain of the inhibitor of apoptosis protein XIAP. J Biol Chem 275:33777–33781
262. Cherepanov P, Sun ZYJ, Rahman S et al (2005) Solution structure of the HIV-1 integrase-binding domain in LEDGF/p75. Nat Struct Mol Biol 12:526–532
263. Cherepanov P, Ambrosio ALB, Rahman S et al (2005) Structural basis for the recognition between HIV-1 integrase and transcriptional coactivator p75. Proc Natl Acad Sci USA 102:17308–17313
264. Maertens G, Cherepanov P, Pluymers W et al (2003) LEDGF/p75 is essential for nuclear and chromosomal targeting of HIV-1 integrase in human cells. J Biol Chem 278:33528–33539
265. Christ F, Voet A, Marchand A et al (2010) Rational design of small-molecule inhibitors of the LEDGF/p75-integrase interaction and HIV replication. Nat Chem Biol 6:442–448
266. Du L, Zhao Y, Chen J et al (2008) D77, one benzoic acid derivative, functions as a novel anti-HIV-1 inhibitor targeting the interaction between integrase and cellular LEDGF/p75. Biochem Biophys Res Commun 375:139–144
267. De Luca L, Barreca ML, Ferro S et al (2009) Pharmacophore-based discovery of small-molecule inhibitors of protein-protein interactions between HIV-1 integrase and cellular cofactor LEDGF/p75. ChemMedChem 4:1311–1316
268. De Luca L, Ferro S, Gitto R et al (2010) Small molecules targeting the interaction between HIV-1 integrase and LEDGF/p75 cofactor. Bioorg Med Chem 18:7515–7521
269. Dey A, Chitsaz F, Abbasi A et al (2003) The double bromodomain protein Brd4 binds to acetylated chromatin during interphase and mitosis. Proc Natl Acad Sci USA 100:8758–8763
270. Wu SY, Lee AY, Hou SY et al (2006) Brd4 links chromatin targeting to HPV transcriptional silencing. Genes Dev 20:2383–2396
271. Wu SY, Chiang CM (2007) The double bromodomain-containing chromatin adaptor Brd4 and transcriptional regulation. J Biol Chem 282:13141–13145
272. Liu Y, Wang X, Zhang J et al (2008) Structural basis and binding properties of the second bromodomain of Brd4 with acetylated histone tails. Biochemistry 47:6403–6417
273. Vollmuth F, Blankenfeldt W, Geyer M (2009) Structures of the dual bromodomains of the P-TEFb-activatin protein Brd4 at atomic resolution. J Biol Chem 284:36547–36556
274. Myoshi S, Ooike S, Iwata K et al (2009) Antitumor agent. PCT Int Appl WO2009084693
275. Filippakopoulos P, Qi J, Picaud S et al (2010) Selective inhibition of BET bromodomains. Nature 468:1067–1073
276. Mertz JA, Conery AR, Bryant BM et al (2011) Targeting MYC dependence in cancer by inhibiting BET bromodomains. Proc Natl Acad Sci USA 108:16669–16674
277. Delmore JE, Issa GC, Lemieux ME et al (2011) BET bromodomain inhibition as a therapeutic strategy to target c-myc. Cell 146:904–917

278. Chung C, Coste H, White JH et al (2011) Discovery and characterization of small-molecule inhibitors of the BET family bromodomains. J Med Chem 54:3827–3838
279. Nicodeme E, Jeffrey KL, Schaefer U et al (2010) Suppression of inflammation by a synthetic histone mimic. Nature 468:1119–1123
280. Dawson MA, Prinjha RK, Dittman A et al (2011) Inhibition of BET recruitment to chromatin as an effective treatment for MLL-fusion leukaemia. Nature 478:529–533
281. Muller S, Filippakopoulos P, Knapp S (2011) Bromodomains as therapeutic targets. Expert Rev Mol Med 13:e29
282. Chung C, Witherington J (2011) Progress in the discovery of small-molecule inhibitors of bromodomain-histone interactions. J Biomol Screen 16:1170–1185
283. Chung C, Dean AW, Woolven JM, Bamborough P (2012) Fragment-based discovery of bromodomain inhibitors part 1: inhibitor binding modes and implications for lead discovery. J Med Chem 55:576–586

Top Med Chem 8: 57–80
DOI: 10.1007/978-3-642-28965-1_2

Targeting the MDM2-p53 Protein-Protein Interaction for New Cancer Therapeutics

Shaomeng Wang, Yujun Zhao, Denzil Bernard, Angelo Aguilar, and Sanjeev Kumar

Contents

S. Wang (✉) • Y. Zhao • D. Bernard • A. Aguilar • S. Kumar
Comprehensive Cancer Center and Departments of Internal Medicine, Pharmacology and Medicinal Chemistry, University of Michigan, 1500 E. Medical Center Drive, Ann Arbor, MI 48109, USA
e-mail: shaomeng@umich.edu

Abstract The p53 tumor suppressor protein is a transcriptional factor that plays a key role in regulation of several cellular processes, including the cell cycle, apoptosis, DNA repair, and angiogenesis. The murine double minute 2 (MDM2) protein is the primary cellular inhibitor of p53, functioning through direct interaction with p53. Design of non-peptide, small-molecule inhibitors that block the MDM2-p53 interaction has been sought as an attractive strategy to activate p53 for the treatment of cancer and other human diseases. Major advances have been made in the design of small-molecule inhibitors of the MDM2-p53 interaction in recent years, and several compounds have moved into advanced preclinical development or clinical trials. In this chapter, we will highlight these advances in the design and development of MDM2 inhibitors, and discuss lessons learned from these efforts.

Keywords HDM2 • Inhibitors • MDM2 • Protein-protein interactions

1 Introduction

1.1 The p53 Tumor Suppressor and Its Primary Cellular Inhibitor MDM2 Protein

Tumor suppressor p53 is a transcriptional factor that plays a pivotal role in the regulation of the cell cycle, apoptosis, DNA repair, senescence, angiogenesis, cellular metabolism, and innate immunity [1–3]. The p53 protein was identified in 1979 [4–6], and its gene, called *TP53*, was cloned in 1983 [7]. Consistent with its role as a prominent tumor suppressor, p53 is functionally inactivated by mutation or deletion in nearly 50% of human cancers [8]. In cancers with wild-type p53, its function is effectively inhibited by its primary cellular inhibitor, the murine double minute 2 (MDM2; HDM2 in humans) protein. MDM2 is an oncoprotein that was initially discovered by its overexpression in a spontaneously transformed mouse cell line [8–12]. The cellular levels of p53 and MDM2 are mutually regulated through an autoregulatory feedback loop (Fig. 1). As a transcription factor, p53 binds to the promoter and increases expression of the *Mdm2* gene. In turn, MDM2 protein directly binds to p53 and inhibits the activity of p53 through multiple mechanisms: MDM2 (1) directly inhibits the transactivation function of p53, (2) exports p53 out of the nucleus, and (3) promotes proteosome-mediated degradation of p53 through its E3 ubiquitin ligase activity [13–15]. The physiological relevance of this regulatory loop was demonstrated by the genetic evidence that embryonic lethality of *Mdm2*-null mice can be successfully rescued by the simultaneous deletion of the p53 gene [16, 17].

Deregulation of the MDM2/p53 balance leads to malignant transformation of normal cells. For example, overexpression of MDM2 provides cells a growth advantage, promotes tumorigenesis, and correlates with a worse clinical prognosis and poor response to cancer therapy [18–24]. A variety of mechanisms, such as

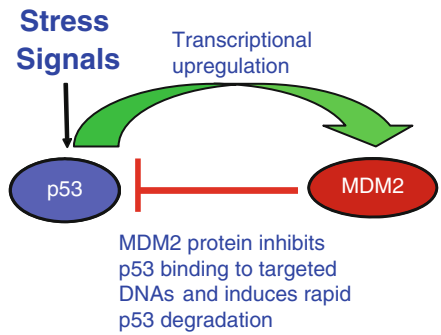

Fig. 1 Autoregulatory loop between p53 and MDM2. Upon activation, p53 transcribes the MDM2 gene and increases the levels of MDM2 protein. In turn, MDM2 protein binds to p53, inhibiting its binding to targeted DNAs and inducing p53 degradation

amplification of the *MDM2* gene, single nucleotide polymorphism at nucleotide 309 (SNP309) in its gene promoter, enhanced transcription, and increased translation account for MDM2 overproduction [18, 24–26]. Genetic studies in mice have revealed that overexpression of MDM2 at an early stage of differentiation neutralizes p53 tumor suppressor function and predisposes mice to tumorigenesis [27]. As with the human inherited cancer predisposition Li-Fraumeni syndrome, mice lacking p53 develop normally, but are predisposed to develop a variety of tumors [28]. Analysis of 28 different types of human cancers in nearly 4,000 human tumor samples showed that MDM2 is amplified in 7% of human cancers and MDM2 overexpression by amplification and p53 mutations are largely mutually exclusive [22]. Collectively, these data support the notion that MDM2 is a chief, though not the only, regulator of p53 function.

1.2 Blocking the Interaction of MDM2 and p53 as a New Cancer Therapeutic Strategy

Because of the critical inhibitory role of MDM2 on p53, blocking the interaction of MDM2 and p53 has been proposed as a potential cancer therapeutic strategy. The MDM2-p53 interaction was mapped to the first ~120 amino acid residues at the N-terminus of MDM2 and to the N-terminus of the transactivation domain of p53 [29, 30]. The high-resolution crystal structures of human and *Xenopus laevis* MDM2 complexed with short p53 peptides (residues 15–29) [31] were solved in 1996, and have provided atomic details of the interaction. These structures show that the MDM2-p53 interaction is mediated by a well-defined hydrophobic surface pocket in MDM2 and three key hydrophobic residues in p53, namely Phe19, Trp23, and Leu26 (Fig. 2). The relatively compact binding pocket in MDM2 makes it appear possible to design non-peptide, drug-like small-molecule inhibitors to block this interaction as a means to reactivate p53 in cells harboring wild-type p53.

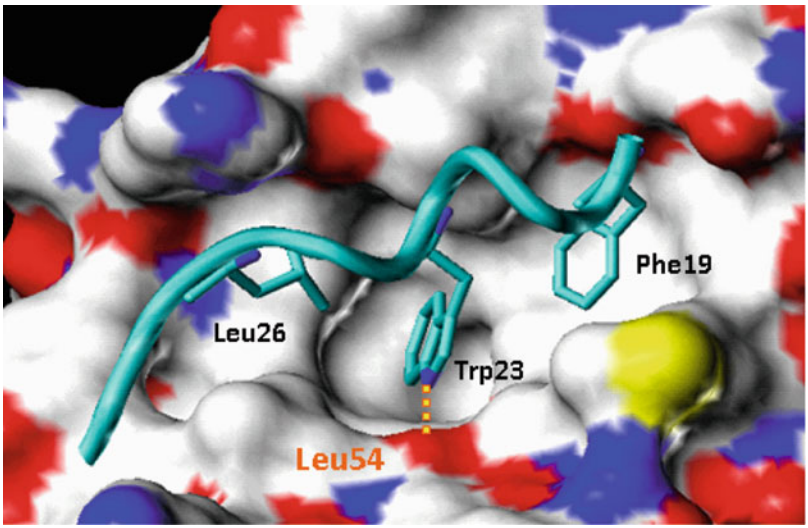

Fig. 2 Crystal structure of MDM2 protein complexed with p53 peptide (residues 13–29)

1.3 Design of High-Affinity Peptide-Based Small-Molecule Inhibitors of the MDM2-p53 Interaction

Wild-type p53 peptides have modest affinity, with K_d values of ~1 μM [31]. To explore whether it was possible to design compounds with much higher binding affinities, extensive modifications have been made on p53 peptides using natural and unnatural amino acids. These efforts led to the discovery of peptidomimetics that bind to MDM2 with K_d values of 1 nM, 1,000-fold more potent than wild-type p53 peptides [32]. The data have provided direct evidence that the MDM2 binding pocket is indeed a feasible target for the design of high-affinity small-molecule inhibitors. Furthermore, the structure-activity relationships obtained from peptidomimetics have proven to be useful in guiding the design of non-peptide, small-molecule inhibitors of the MDM2-p53 interaction.

Despite their high affinity, these peptide-based compounds were not useful for cellular studies, primarily due to their poor cell permeability. To enhance their permeability, compounds were tethered to carrier peptides, which resulted in compounds that activated p53 function in cells at concentrations of 100–500 μM. Although such weak cellular activity clearly makes them unsuitable as potential therapeutic agents, they nevertheless provided the initial proof-of-concept that blocking the interaction between MDM2 and p53 can indeed be an effective means of activating p53.

2 Different Approaches Toward the Discovery of Non-peptide, Small-Molecule Inhibitors of the MDM2-p53 Interaction

One critical step in the design and development of non-peptide, small-molecule inhibitors of the MDM2-p53 interaction is the discovery of novel lead compounds. Different approaches have been employed to discover such lead compounds. These include experimental screening of chemical libraries, computational three-dimensional (3D) database screening of large chemical libraries, and structure-based *de novo* design. Below we review these different approaches.

2.1 Experimental Screening of Small-Molecule Libraries

The Nutlins, discovered by Vassilev and colleagues at Hoffman-La Roche [33], are probably the first potent and specific MDM2 inhibitors. The Nutlins have a *cis*-imidazoline core structure and the initial lead compound was discovered by experimental screening of a diverse library of synthetic compounds using a Biacore surface plasmon resonance assay, although no details have been provided. Extensive chemical modifications of the initial lead compound have ultimately yielded a class of potent small-molecule MDM2 inhibitors. Nutlin-1 and Nutlin-2 are racemic compounds and Nutlin-3a is an active enantiomer (Fig. 3). Nutlins 1–3 block the MDM2-p53 protein-protein interaction with IC_{50} values of 260, 140, and 90 nM, respectively.

Benzodiazepinedione-based MDM2 inhibitors were discovered in a high throughput screening of 338,000 compounds from combinatorial libraries using ThermoFluor microcalorimetry technology [34]. Initial screening led to identification of 1,216 compounds, including 116 benzodiazepinediones, that bound to MDM2. The affinity of selected compounds was further evaluated in an FP-based p53 peptide-displacement MDM2 binding assay. The benzodiazepinedione **1** had a K_i of 80 nM in the FP-based assay. Two additional studies have also reported the discovery and characterization of benzodiazepinedione compounds as fairly potent MDM2 inhibitors using the same technique.

A homogeneous time-resolved fluorescence (HTRF) high throughput screening of ~1.4 million internal library compounds was performed by scientists at Amgen [35]. One compound, the chromenotriazolopyrimidine **2**, was found to have an IC_{50} value of 1.2 μM in the HTRF assay. Subsequent optimization has yielded a class of fairly potent MDM2 inhibitors.

Terphenyl compounds have been put forward as bearing a scaffold capable of mimicking one face of α-helical peptides [36]. The side chains in the designed terphenyl compounds are projected in a similar way to i, $i + 4$, and $i + 7$ residues in α-helical peptides. Since the interaction between p53 and MDM2 is mediated by a short α-helix from p53, it was expected that certain terphenyl compounds may also bind to MDM2. A FP-based competitive binding assay was used to evaluate the

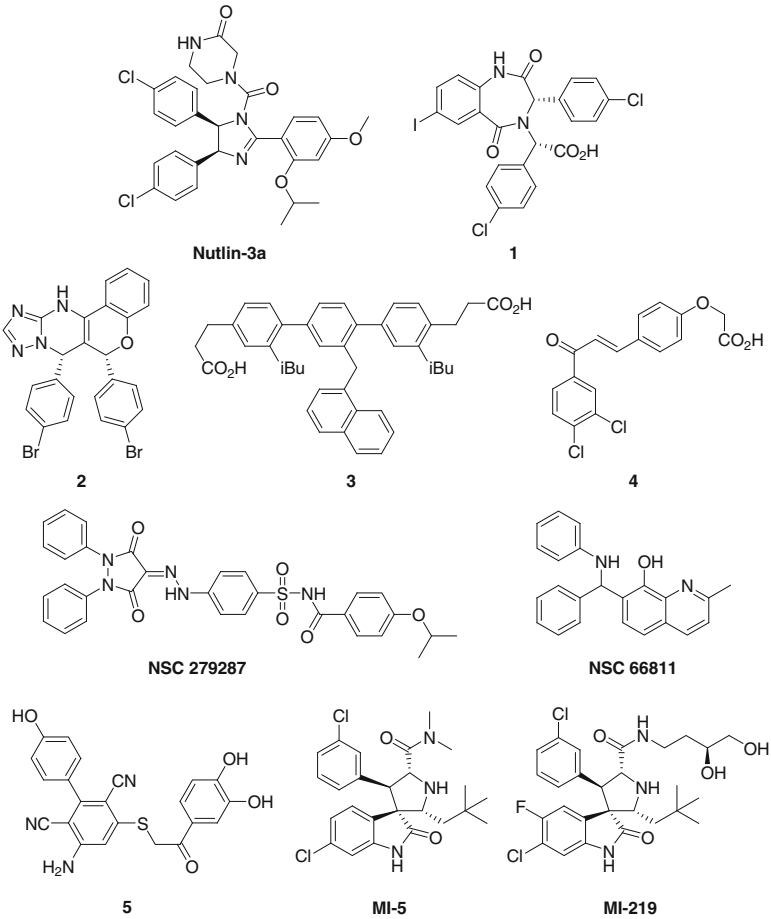

Fig. 3 Representative MDM2 inhibitors discovered using different approaches

binding affinities of 21 designed terphenyl compounds to MDM2. One such compound **3**, (Fig. 3) was found to bind to MDM2 with a K_i of 182 nM [37]. ^{15}N Heteronuclear single quantum correlation (HSQC) NMR spectroscopy further showed that this terphenyl targets the same surface area in MDM2 where p53 binds. Its specificity was evaluated for its binding to Bcl-2 and Bcl-xL proteins since Bcl-2 and Bcl-xL also bind to α-helical peptides. This terphenyl displays 82- and 14-fold selectivity over Bcl-2 and Bcl-xL, respectively, suggesting that although terphenyl compounds are general mimics of helical peptides, some can display certain selectivity for MDM2 over other proteins.

Stoll et al. [38] screened a library of 16 chalcones, which are broadly known to have anticancer properties [39], to identify compounds for disrupting the MDM2-p53 interaction. The most potent compound found, **4**, had an IC_{50} value of 49 μM.

2.2 Computational Structure-Based Screening

Galatin and Abraham were the first to employ a computational pharmacophore searching strategy to discover small-molecule inhibitors of the MDM2-p53 interaction [40]. The hydropathic interactions (HINT) program was used to generate noncovalent interaction measurements between reported p53-based peptide inhibitors and MDM2, which led to the development of a pharmacophore model [41]. Various permutations of this MDM2-binding pharmacophore model were entered as searches to obtain hit compounds from the National Cancer Institute (NCI) database [42]. These candidate compounds were tested in an in vitro MDM2-p53 protein-protein interaction assay. One compound, NSC279287 (Fig. 3), was found to disrupt the interaction between full-length MDM2 and p53 proteins with an IC_{50} value of 31.8 μM. When evaluated in a p53 reporter gene assay, only a 20% increase in p53 transcriptional function after treatment with 100 μM of the compound was observed [40]. Despite the weak affinity, this study nevertheless demonstrated that computational pharmacophore searching can be used to successfully identify small-molecule inhibitors of the MDM2-p53 interaction. No chemical modifications were reported for this class of compounds.

Subsequently, Lu et al. employed an approach combining pharmacophore and structure-based screening to search for small-molecule inhibitors of the MDM2-p53 interaction in an NCI database of 150,000 compounds [42]. A number of filters were used to remove approximately 40,000 non-druglike molecules, providing a working database of 110,000 compounds. A 3D-pharmacophore model was derived from the X-ray crystal structure of the p53 peptide complexed with MDM2, and with several known small-molecule inhibitors. The pharmacophore model consisted of three elements that mimic the three key hydrophobic binding residues in p53 (Phe19, Trp23, Leu26), together with three associated distance constraints. Pharmacophore searching of the 110,000 compounds yielded 2,599 hits. Computational docking was performed using the GOLD program [43, 44] to dock each hit to the p53-binding site in MDM2. Their binding affinities were ranked using Chemscore [45] and *X*-score [46], and the top 200 ranked compounds from each scoring function were combined, yielding 354 non-redundant compounds. A total of 67 compounds were obtained from the NCI and tested in a competitive FP-based MDM2 binding assay. Ten compounds were found to have K_i values of <10 μM. NSC66811 was the most potent compound with a K_i of 120 nM. NSC66811 activated p53 in the LNCaP prostate cancer cell line with wild-type p53 in a dose-dependent manner, providing evidence for its cellular mechanism of action. No chemical modifications were reported for any of these compounds.

Another computational search was performed using a pharmacophore model based on the crystal structure of MDM2 with incorporation of protein flexibility assessed using molecular dynamics simulation [47]. Pharmacophore searching was performed on a database of 35,000 synthetic compounds, followed by evaluation of 24 hits in a fluorescence-polarization MDM2 binding assay that led to the discovery of five non-peptidic, small-molecule MDM2 inhibitors with new scaffolds.

The most potent compound, **5** (Fig. 3), had a K_i of 110 nM to MDM2. Their cellular activity and mechanism of action have not been reported.

2.3 Structure-Based De Novo Design

Computational and experimental screening aim at identification of lead compounds from small-molecule libraries of compounds which have been synthesized previously and have been shown to be effective in the discovery of novel lead compounds as MDM2 inhibitors. However, these screening approaches have the limitation that leads are confined within existing chemical space. To overcome this limitation, the Wang laboratory at the University of Michigan employed a structure-based *de novo* design strategy to design new classes of small-molecule inhibitors to target the MDM2-p53 interaction [48, 49].

Analysis of the crystal structure of p53 complexed with MDM2 showed that the indole ring of the Trp23 residue of p53 is buried deeply inside a hydrophobic cavity in MDM2 and its NH group forms a hydrogen bond with the backbone carbonyl in MDM2. Hence, Trp 23 represents the most critical residue for binding of p53 to MDM2. In searching for a chemical moiety that can mimic the interaction between the indole group and MDM2, the oxindole ring system was found to perfectly mimic the hydrophobic and hydrogen-bonding interactions of the indole. Since many anticancer drugs are natural products or derivatives of natural products, substructure searching was performed to identify natural products that contain an oxindole ring. A number of natural alkaloids such as spirotryprostatin A and alstonisine were found to contain a spirooxindole core structure. However, computational docking of these natural alkaloids suggested that none of them could effectively interact with the MDM2 binding pocket due to steric hindrance. However, the spiro(oxindole-3,3′-pyrrolidine) core structure (hereafter called spirooxindole) emerged as the starting point for the design of a new class of MDM2 inhibitors. In the design, the oxindole closely mimics the Trp23 side chain in p53 in both hydrogen-bonding and hydrophobic interactions with MDM2. Two additional hydrophobic groups were installed on the rigid spiropyrrolidine ring to mimic the side chain of Phe19 and Leu26. Initial compounds were designed with different hydrophobic groups with different stereochemistry and docked into the MDM2 binding cleft using the GOLD program [43, 44]. Docking studies showed that one such compound (MI-5, Fig. 3) closely mimics p53 in its interaction with MDM2. An efficient synthetic method featuring a [1,3]-dipolar cycloaddition reaction as the key step was developed for the synthesis of the designed compound. An FP-based binding assay confirmed that MI-5 binds to MDM2 with a K_i of 8.5 μM. Structure-based optimization of MI-5 ultimately yielded a new class of highly potent, small-molecule inhibitors, such as MI-219 (Fig. 3) [50, 51]. The most potent reported spirooxindole compounds have K_i values of <1 nM to MDM2. This class of compounds also displays exceedingly high specificity over other protein-protein interactions.

3 Representative Classes of Small-Molecule Inhibitors of the MDM2-p53 Interaction

Regardless of how initial lead compounds are discovered, extensive modifications are normally needed to obtain compounds with high affinities to MDM2, high specificity over other proteins, and good physiochemical and pharmacological properties. In this section, we summarize representative classes of potent, non-peptide, small-molecule inhibitors of the MDM2-p53 interaction from different research groups.

To the Nutlins, the first class of potent, non-peptide, small-molecule inhibitors of the MDM2-p53 interaction, extensive modifications have been carried out by scientists from Hoffmann-La Roche. One such compound, RG7112, binds to MDM2 with a K_d of 10.7 nM (Fig. 4) [52] and is the first MDM2 inhibitor to advance into Phase I clinical trials. Daiichi Sankyo has also designed potent MDM2 inhibitors starting from the core structure of Nutlins. The most potent compound **6**, (Fig. 4) disclosed in a patent has an IC_{50} of 1.2 nM [53].

Extensive modifications have been made on spirooxindoles by the Wang group at the University of Michigan [48, 49]. MI-147 is one of the most potent of this class of compounds, with a K_i of 0.6 nM in an FP-based competitive binding assay [51]. Additional modifications yielded new compounds with high affinities to MDM2 and improved pharmacokinetic properties [54]. One such compound in this class, MI-773, has completed IND-enabling studies and is entering clinical trials in 2012.

Starting from spirooxindoles, Hoffmann-La Roche has obtained several classes of potent MDM2 inhibitors through extensive chemical modifications. One class of compounds is structurally closely related to the spirooxindoles reported by the University of Michigan but these compounds differ in their stereochemistry [55, 56]. The most potent compounds disclosed in patents from Hoffmann-La Roche bind to MDM2 with IC_{50} values in the low nanomolar range.

Doemling's group from the University of Pittsburgh has reported a series of MDM2 inhibitors obtained through computational design and multicomponent reaction (MCR) chemistry [57]. One class of compounds contains a pyrazole or imidazole core linked with three hydrophobic groups: one indole ring and two phenyl rings. One of the most potent compounds YH265, (Fig. 4) has a K_i of 20 nM. Independently and simultaneously, Novartis disclosed a similar imidazole-indole family of compounds as inhibitors of MDM2 and MDMX in a patent [58]. The most potent compound has an IC_{50} of 15 nM for MDM2 in an FP binding assay and an IC_{50} of 1.32 μM for the related protein MDMX in a TR-FRET binding assay.

Novartis disclosed tetra-substituted heteroaryl compounds as MDM2 and/or MDMX inhibitors in a patent [59]. One of the most potent compounds in this class (**7**) has an IC_{50} value of 2 nM to MDM2. Interestingly, this compound also binds to MDMX with low micromolar binding affinity. Novartis also reported substituted isoquinolinones and quinazolinones as inhibitors of MDM2 and MDMX in a separate patent [60]. The most potent compound (**8**) has IC_{50} values of 0.8 nM and 2.1 μM for MDM2 and MDMX, respectively.

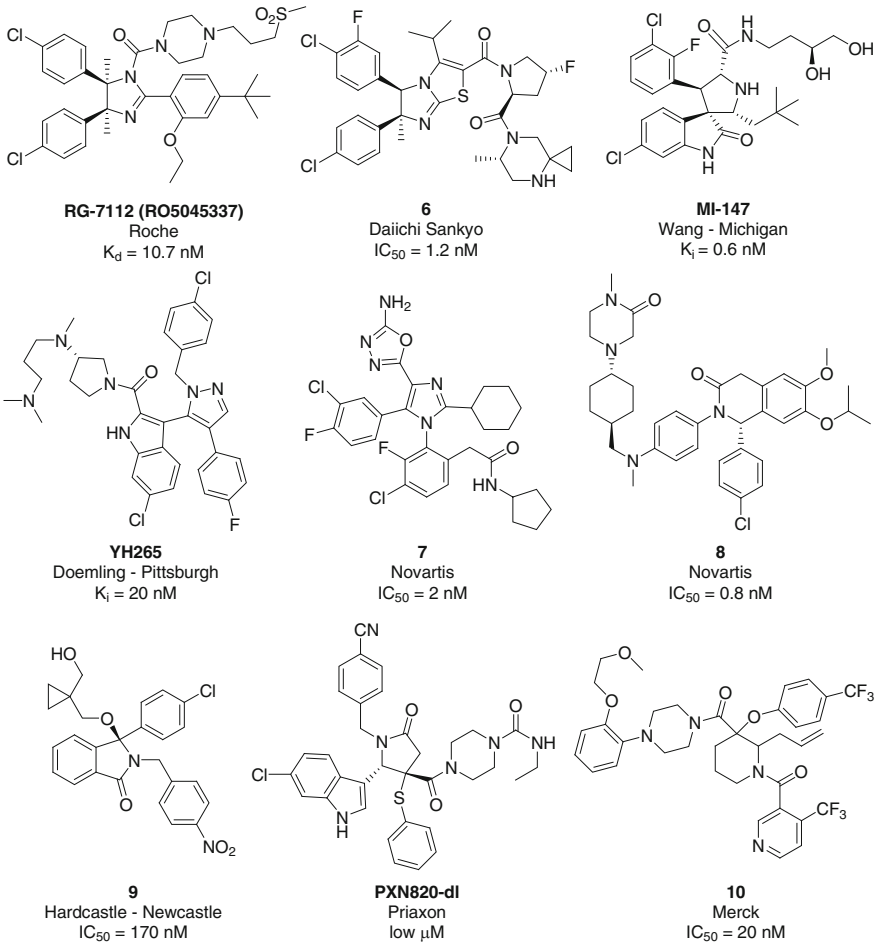

Fig. 4 Chemical structures and binding affinities of representative classes of MDM2 inhibitors

Researchers from Newcastle University reported a series of isoindolinone inhibitors for MDM2, the most potent of which **9**, (Fig. 4) has an IC_{50} value of 170 nM [61]. Priaxon AG Company reported a series of pyrrolidinone compounds as MDM2 inhibitors with IC_{50} values in the low micromolar range, exemplified by PXN820-dl in Fig. 4 [62]. A Merck patent reported highly substituted piperidines as MDM2 inhibitors. The most potent compound in this class, **10**, has an IC_{50} of 20 nM [63].

Since many of these MDM2 inhibitors have only been disclosed in patents, little is known about their cellular activity, pharmacological properties, and mechanism of action. Nevertheless, the successful discovery of these structurally diverse and potent small-molecule MDM2 inhibitors has clearly demonstrated that it is indeed possible to target the MDM2-p53 protein-protein interaction using non-peptide

small-molecule inhibitors. Although the binding affinities of these compounds have not been directly compared to each other under the same assay conditions, it is clear that the most potent, non-peptide, small-molecule MDM2 inhibitors discovered to date are >1,000-times more potent than wild-type p53 peptides.

4 Structural Basis of Binding of Small-Molecule Inhibitors to MDM2

A number of X-ray crystal structures of MDM2 complexed with potent small-molecule inhibitors of the MDM2-p53 interaction have been determined, providing structural insights for their high-affinity binding to MDM2. The first crystal structure of MDM2 complexed with a small molecule, Nutlin-2 [33], shows that Nutlin-2 mimics the interactions of the p53 peptide (Fig. 5a). One bromophenyl moiety in Nutlin-2 fills the Trp23 pocket, the other occupies the Leu26 pocket, and the ethyl ether side chain targets the Phe19 pocket. This crystal structure thus demonstrated that by mimicking the three key hydrophobic residues in p53, non-peptide, small-molecule inhibitors can achieve high affinities to MDM2. Interestingly, while Nutlin-2 mimics the three key hydrophobic interactions, it does not form a hydrogen bond like the one between the Trp23 indole NH group in p53 and the carbonyl group of Leu54 in MDM2.

A crystal structure of MDM2 complexed with a spirooxindole compound was determined (Fig. 5b). This compound is an analogue of MI-219, but differs in its stereochemistry [64]. Consistent with the initial design of this class of compounds, the oxindole inserts into the binding cavity occupied by Trp23 in p53 and nicely mimics both the hydrophobic and hydrogen-bonding interactions of the Trp23 indole. Interestingly, the halogen-substituted phenyl group in the MI-219 analogue binds to the hydrophobic pocket occupied by Leu26 in p53 and the aliphatic hydrophobic group mimics the hydrophobic side chain of Phe19. Additionally, π–π stacking takes place between the halogen-substituted phenyl group and the aromatic His96 in MDM2 and the compound also forms a hydrogen bond with His96, neither of which are observed in interactions between p53 peptides and MDM2.

The crystal structure of a benzodiazepine compound in complex with MDM2 shows that this compound uses three phenyl groups to mimic the three hydrophobic residues in p53 (Fig. 5c) [34]. No hydrogen bonding is observed between the inhibitor and MDM2. Similarly, the crystal structure of WK23, a potent inhibitor from Novartis, reveals that this compound also employs three aromatic groups to mimic the three hydrophobic residues in p53 (Fig. 5d) [64]. A hydrogen bond is formed between the indole NH group of Trp23 and the carbonyl group of Leu54 in MDM2.

Taken together, these high-resolution crystal structures have established a common interaction motif whereby all of the potent inhibitors mimic the three key residues (Phe19, Trp23 and Leu26) for hydrophobic interactions with MDM2. Interestingly, some classes of compounds such as the Nutlins and benzodiazepines

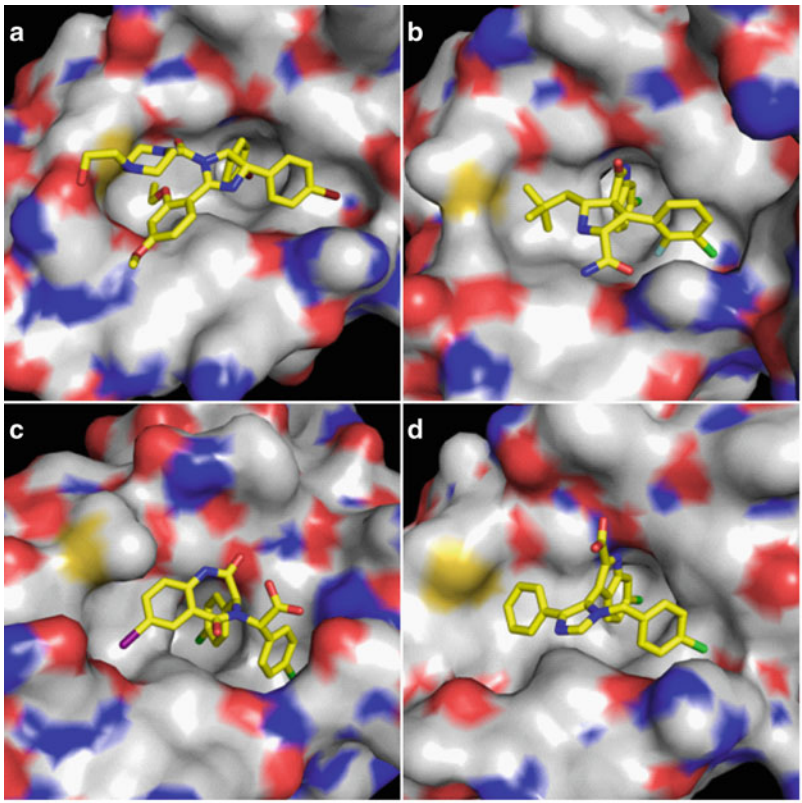

Fig. 5 Crystal structures of MDM2 complexed with several classes of inhibitors. (**a**) Nutlin-2; (**b**) MI-219 analogue; (**c**) benzodiazepine; (**d**) WK23 (PDB codes 1RV1, 3LBL, 1T4E and 3LBK, respectively)

lack the hydrogen bond formed between the indole NH group of Trp23 in p53 and the carbonyl group of Leu54 in MDM2.

5 Biological Aspects of MDM2 Inhibition

5.1 Molecular Mechanism of p53 Activation by MDM2 Inhibitors

Potent and specific MDM2 inhibitors such as Nutlin-3 [33] and MI-219 [50, 51] have provided an opportunity to examine the details of their cellular mechanism of p53 activation. Consistent with in vitro biochemical binding assays, potent MDM2 inhibitors are capable of blocking the MDM2-p53 protein-protein interaction in cells. They induce accumulation of p53 protein but do not increase the transcription

of the p53 gene in either tumor or normal cells with wild-type p53. Instead, they induce transcription of the p53-targeted genes for p21 and MDM2, increasing their protein levels. As compared to conventional genotoxic anticancer agents and radiation, activation of p53 by MDM2 inhibitors does not require phosphorylation of p53. Furthermore, it has been demonstrated that certain proteins, such as the pro-apoptotic Puma, are selectively induced in tumor cells but not in normal cells [50]. Therefore, although p53 is activated by MDM2 inhibitors in both normal and tumor cells with wild-type p53, the genes transcribed by p53 activation in these two settings are not identical, which may translate into different cell fates and have a significant implication for the potential applications of MDM2 inhibitors as new anticancer agents.

5.2 Activity and Selectivity of Small-Molecule MDM2 Inhibitors in Tumor and Normal Cells

Since MDM2 inhibitors activate p53 in both tumor and normal cells with wild-type p53, they can elicit a wide variety of cellular responses attributable to p53 activation. A number of investigations using Nutlin-3, MI-219, and other highly potent MDM2 inhibitors have demonstrated that MDM2 inhibitors result in both common and different cellular responses in normal and tumor cells [33, 50]. In normal cells, activation of p53 by MDM2 inhibitors induces cell cycle arrest but not cell death. In some but not all tumor cells, activation of p53 by MDM2 inhibitors induces both cell cycle arrest and cell death [33, 50, 65]. For example, Nutlin-3 and MI-219 induce robust cell death in SJSA-1 osteosarcoma and RS4;11 acute lymphoblastic leukemia (ALL) cell lines. In contrast, Nutlin-3 and MI-219 have minimal effect on cell death induction in HCT-116 colon, 22Rv1 prostate, and MCF-7 breast cancer cell lines, highlighting that p53 wild-type status in cancer cells is necessary but not sufficient for induction of cell death by MDM2 inhibitors [65]. Both cell-death induction and cell cycle arrest in tumor cells depend upon p53, since knockdown or knockout of p53 abrogates these cellular effects by Nutlin-3 and MI-219 [50, 66]. In addition to human cancer cell lines, cell death induction by MI-63 and Nutlin-3 were extensively evaluated using purified primary human chronic lymphocytic leukemia (CLL) cells [67] and acute myelogenous leukemia (AML) cells [68] from patients. Interestingly, while these MDM2 inhibitors effectively induce cell death in essentially all CLL cells with wild-type p53 status, they selectively kill some but not all AML cells harboring wild-type p53. Detailed genetic analysis revealed that 80% of AML cells with wild-type p53 and FLT-3 internal tandem duplication (FLT-3/ITD) mutation are highly sensitive to apoptosis via MDM2 inhibitors [68].

5.3 Antitumor Activity of MDM2 Inhibitors in Animal Models

A number of potent MDM2 inhibitors have been evaluated in animal models of human cancer for their antitumor activity. In pharmacodynamic experiments, a single oral dose of Nutlin-3 or MI-219 is capable of activating p53 in xenograft tumor tissues of human cancer cell lines with wild-type p53, as revealed by accumulation of p53 and upregulation of p21 [50, 65]. Both Nutlin-3 [33, 65, 69] and MI-219 [50] show strong antitumor activity in some but not all xenograft models of human cancer with wild-type p53. For example, while Nutlin-3 and MI-219 are capable of completely inhibiting tumor growth against SJSA-1 osteosarcoma xenografts, even causing some partial tumor regression, both compounds show minimal antitumor activity against HCT-116 colon cancer xenografts. These in vivo data are consistent with the in vitro robust cell-death induction by Nutlin-3 and MI-219 in the SJSA-1 cell line but not in HCT-116 cells. Immunohistochemical (IHC) analysis showed that MI-219 induced both cell cycle arrest and apoptosis in SJSA-1 xenograft tumor tissues. Significantly, the antitumor activity of these potent MDM2 inhibitors is achieved at dose schedules which cause no visible signs of toxicity in the animals, as assessed by necropsy studies and body weight loss [33, 50, 65, 69].

Although Nutlin-3 and MI-219 failed to achieve complete tumor regression in any of the tumor models tested, subsequent studies have shown that potent MDM2 inhibitors with optimized pharmacological properties can do so. For example, RG7112 achieved either a maintained complete response (MCR) or a complete response (CR) for a medulloblastoma and an alveolar rhabdomyosarcoma, respectively, and partial responses (PR) for a Wilms tumor, rhabdoid tumor, and Ewing tumor xenograft [70]. RG7112 was also highly effective against ALL xenografts: among 13 ALL xenografts, there were 11 CRs, one MCR, and one partial response [70]. In vivo studies on two compounds from the spirooxindole class also achieved rapid and complete tumor regression in SJSA-1 osterosarcoma and ALL RS4;11 xenograft models when dosed daily for 14 days [54]. In fact, a single dose of one such compound is capable of achieving complete tumor regression in the SJSA-1 xenograft model. Taken together, these preclinical data have provided compelling evidence that potent and highly optimized MDM2 inhibitors can achieve impressive antitumor activity in animal models of human cancers.

5.4 Potential Toxicity of MDM2 Inhibitors to Normal Tissues

The potential toxicity of p53 activation by an MDM2 inhibitor in normal tissues is of paramount importance for therapeutic development. Certain tissues such as bone marrow, small-intestine crypts, and thymus are highly susceptible to p53-induced apoptosis [71, 72]. Furthermore, activation of p53 by a genetic approach in the absence of *MDM2* results in severe pathological damage to p53-sensitive mouse

tissues and death of all animals within days [73], raising the possibility that MDM2 inhibitors could be highly toxic to some normal tissues through activation of p53.

To address this issue, a detailed examination of the toxicity of MI-219 in normal tissues was conducted [50]. While both γ-radiation and irinotecan chemotherapy induce robust apoptosis in small-intestine crypts and thymus, MI-219, in either single or repeated doses, did not cause apoptosis or damage in either radio-sensitive or radio-resistant normal mouse tissues. One reason for the lack of toxicity of MDM2 inhibitors in normal mouse tissues is that activation of p53 in the presence of MDM2 is transient; when the concentrations of MDM2 inhibitors decrease from tissues due to pharmacokinetics, MDM2 protein can bind to p53 and rapidly reduce the levels of p53. Furthermore, in the presence of MDM2, p53 action is always under the control of MDM2, in contrast to activation of p53 in the absence of MDM2 in genetic models. While the data in mice provide encouraging evidence for the therapeutic index of MDM2 inhibitors, the ultimate answer will need to come from human clinical trials.

5.5 MDMX Is a Modulator of the Activity of Selective MDM2 Inhibitors

MDMX is a homolog of MDM2. Similarly to MDM2, MDMX also binds directly to p53 and inhibits its transcriptional activity. But unlike MDM2, MDMX does not induce p53 degradation [74].

Crystal structures of MDM2 and MDMX reveal that these two proteins have very similar p53 binding pockets. However, most of the reported MDM2 inhibitors are highly selective for MDM2 over MDMX. For example, although Nutlin-3 still binds to MDMX, its affinity is >100-fold less than that toward MDM2. MI-219 binds to MDM2 with a low nanomolar affinity, but is >1,000-fold weaker to MDMX [50]. When MDMX is overexpressed in tumor cells, selective MDM2 inhibitors may not be able to fully activate p53. Indeed, ectopic expression of MDMX and/or its downregulation by RNAi show that MDMX attenuates the p53 activation by selective MDM2 inhibitors and reduces the cellular activity of MDM2 inhibitors [50, 66, 75, 76]. Interestingly, in some cancer cell lines, MDM2 inhibitors can induce MDMX degradation, presumably mediated though p53-dependent up-regulation of MDM2 [50, 66, 76], which is known to ubiquitinate and degrade MDMX during DNA damage [77]. Such cancer cell lines are more susceptible to Nutlin-3 than those in which Nutlin-3 fails to induce MDMX degradation. Though it is unclear why MDM2 inhibitors can induce MDMX in some cancer cell lines but fail to do so in other cancer cell lines, MDMX has nevertheless emerged as an important modulator for the activity of selective MDM2 inhibitors, which provides an impetus for the design of dual small molecule inhibitors targeting both MDM2 and MDMX.

5.6 p53-Independent Effects of MDM2 Inhibitors

In addition to p53, MDM2 also binds to other proteins such as p73, E2F-1, HIF-1α, and Numb [78–81] using the same binding site. Therefore, small-molecule MDM2 inhibitors that bind to the p53-binding site in MDM2 should also interfere with the binding of MDM2 to these proteins. Using in vitro cell line models, it has been shown that Nutlin-3 disrupts the interaction of MDM2 with p73 [78], E2F-1 [79] and HIF-1α [80]. However, higher concentrations of Nutlin-3 (for a p73-dependent effect) or a DNA damage signal (for an E2F-1-dependent effect) were required for p53-independent effects to be observed. Further studies are needed to determine the contributions of both p53-dependent and p53-indepdenent effects for the overall cellular activity of MDM2 inhibitors.

5.7 MDM2 Inhibitors as Potential Anti-angiogenic Agents

In addition to having a direct effect on tumor cells, MDM2 inhibitors may inhibit angiogenesis through activation of p53 in endothelial cells [82, 83]. Activation of p53 can upregulate several anti-angiogenic factors, including thrombospondin-1 (TSP-1) and brain-specific angiogenesis inhibitor 1 (BAI1), and down-regulate several pro-angiogenic factors, such as vascular endothelial growth factor (VEGF), basic fibroblast growth factor (bFGF), basic fibroblast growth factor binding protein (bFGF-BP), and cyclooxygenase-2 (COX-2) [1]. The in vitro and in vivo anti-angiogenic activity of MDM2 inhibitors has been demonstrated using Nutlin-3 [82]. By inhibiting angiogenesis, MDM2 inhibitors may have an application for the treatment of tumors lacking functional p53.

5.8 Predictors of Response to MDM2 Inhibitors

In tumor cells harboring wild-type p53, activation of p53 by MDM2 inhibitors can induce cell cycle arrest and/or apoptosis. Extensive studies have shown that while MDM2 inhibitors induce cell cycle arrest in all tumor cells with wild-type p53, they induce apoptosis/cell-death only in some tumor cells harboring wild-type p53 [33, 50, 66, 84]. Hence, p53 wild-type status is necessary but not sufficient for apoptosis induction by MDM2 inhibitors. Therefore, it is critical to identify biomarkers for predicting the antitumor activity of MDM2 inhibitors.

The SJSA-1 osterosarcoma cell line has an amplified *MDM2* gene and very high levels of MDM2 protein. Nutlin-3 and MI-219 are very effective in inhibition of cell growth and induction of apoptosis in the SJSA-1 cell line in vitro and both compounds achieve strong antitumor activity against SJSA-1 xenograft tumors in mice. Therefore, tumors with MDM2 amplification may be highly sensitive to

MDM2 inhibitors. MDM2 amplification occurs in approximately 7% of human tumors. Different tumor types have widely varying degrees of MDM2 amplification, such as liposarcoma (50–90%), osteosarcomas (16%), esophageal carcinomas (13%), and colon cancer (9%). Furthermore, MDM2 amplification and p53 mutation are essentially mutually exclusive [22]. Therefore, MDM2 amplification could be a very useful biomarker for predicting the clinical response of an MDM2 inhibitor.

Studies using AML blasts from 109 patients have shown that all AML cases with mutated p53 were resistant to apoptosis induction by MI-219 [68]. Approximately 30% of AML cases with unmutated p53 showed primary resistance to MI-219. Analysis of potential mechanisms associated with MI-219 resistance in AML blasts with wild-type p53 uncovered a number of distinct molecular defects, including low or absent p53 protein induction after MDM2 inhibitor treatment. For a separate subset of resistant blasts, robust p53 protein induction after MI-219 treatment was observed, indicative of defective p53 protein function or defects in the apoptotic p53 network. Interestingly, 80% of AML blasts with mutated Flt3 status (Flt3-ITD) and wild-type p53 are highly sensitive to apoptosis induction by MI-219. Therefore, MDM2 inhibitors could be particularly useful for the treatment of AML with mutated Flt3 status, which constitutes a clinically high-risk group of AML. Since a number of MDM2 inhibitors have now entered human clinical trials, it is expected that analysis of clinical efficacy data and human tumor samples will shed new light on potential biomarkers for the anti-tumor activity of MDM2 inhibitors.

5.9 MDM2 Inhibitors in Combination with Other Anticancer Drugs

A number of studies have demonstrated that MDM2 inhibitors may be used not just as single agents but also in combination with other anticancer drugs to achieve better antitumor activity than single agents. For example, ex vivo experiments using patient tumor samples have shown that Nutlin-3 synergizes with doxorubicin, chlorambucil, and fludarabine in B-CLL [85–87]; with doxorubicin and cytosine arabinoside in AML [88, 89]; and with doxorubicin in Hodgkin and Reed-Sternberg (HRS) cells [90]. Significantly, in these experiments Nutlin-3 as a single agent or in combination was non-toxic towards normal hematopoietic cells. Combination of Nutlin-3 with velcade, a proteasome inhibitor approved for the treatment of multiple myeloma, showed a synergistic activity in multiple myeloma cells harboring wild-type p53 [91]. MI-147, a potent member of the spirooxindole class of MDM2 inhibitor, enhanced the antitumor activity of irinotecan against SJSA-1 xenografts in mice [51]. These studies have provided evidence that MDM2 inhibitors can be developed in combination with other types of anticancer drugs.

5.10 Acquired Resistance to MDM2 Inhibitors

Since p53 activation is critical for the antitumor activity of MDM2 inhibitors, persistent exposure to MDM2 inhibitors may select for tumors that are defective in p53 function. Indeed, a recent study demonstrated that Nutlin treatment in SJSA-1 cells leads to the acquisition of somatic mutations in p53 and selects for p53-mutated cells. Such cells are unable to undergo cell cycle arrest or apoptosis when treated with Nutlins [92]. Since tumor cells can acquire resistance to MDM2 inhibitors through p53 mutation, the combination of MDM2 antagonists with agents that can target p53-mutated cells might potentially limit the impact of selecting for p53-mutated tumors through treatment with MDM2 inhibitors.

5.11 MDM2 Inhibitors in Clinical Development

The first MDM2 inhibitor that entered clinical development is RG7112 (RO5045337, Fig. 4) from Hoffmann-La Roche (clinicaltrials.gov identifiers: NCT01164033, NCT01143740, NCT00623870, and NCT00559533). Four Phase I clinical trials have been conducted to date in patients with advanced solid tumors, hematologic neoplasms, or liposarcomas prior to debulking surgery. Preliminary clinical data indicated that RG7112 appears to be well tolerated in patients and shows initial evidence of clinical activity and a mechanism of action consistent with targeting of the MDM2-p53 interaction [93–95].

Another MDM2 inhibitor from Hoffmann-La Roche, RO5503781, whose structure has not been disclosed, entered into Phase I clinical trials at the end of 2011 (clinicaltrials.gov identifier: NCT01462175). A spirooxindole class of MDM2 inhibitor discovered at the University of Michigan has completed IND-enabling studies by Sanofi and Phase I clinical trials are expected to begin in 2012.

6 Conclusions

Because of the powerful tumor suppressor function of p53, reactivation of p53 has been long sought as a potentially novel cancer therapeutic strategy. In tumors harboring wild-type p53, MDM2 is the primary cellular inhibitor of p53 activity. Since MDM2 was found to inhibit p53 through a direct protein-protein interaction, blocking this interaction using small molecules was pursued in several academic and industrial pharmaceutical laboratories in the last decade.

High-resolution crystal structures of MDM2 complexed with p53 peptides defined the interaction in detail, revealing that the MDM2-p53 interface has a well-defined, relatively compact binding pocket in MDM2, which suggested that for this particular

protein-protein interaction, it may be feasible to design potent, non-peptide, druglike small-molecule inhibitors to block the p53-MDM2 interaction.

A variety of approaches have been employed to identify initial non-peptide lead compounds, including experimental screening of small and large chemical libraries, computational structure-based screening of large chemical libraries, followed by experimental testing and computational structure-based *de novo* design. Extensive chemical modifications have been performed on several classes of compounds, including the Nutlins from Roche and the spirooxindole class from the Wang laboratory at the University of Michigan. These efforts have led to the discovery of several classes of highly potent and specific small-molecule inhibitors of the MDM2-p53 interaction, with suitable physiochemical and pharmacological properties for clinical development. To date, at least three compounds have been advanced into early clinical development, including two compounds from Roche and one compound from the University of Michigan. The first clinical compound, RG7112, from Roche has demonstrated good tolerability and initial evidence of clinical activity in patients with advanced solid tumors and leukemia. Hence, these MDM2 inhibitors may prove to be a class of completely novel anticancer therapy for the treatment of many different types of human cancer.

Acknowledgements Funding from the National Cancer Institute/National Institutes of Health, the Prostate Cancer Foundation, the Leukemia and Lymphoma Society, Ascenta Therapeutics and Sanofi is greatly appreciated.

References

1. Teodoro JG, Evans SK, Green MR (2007) Inhibition of tumor angiogenesis by p53: a new role for the guardian of the genome. J Mol Med 85:1175–1186
2. Fridman JS (2003) Lowe SW (2003) control of apoptosis by p53. Oncogene 22:9030–9040
3. Vousden KH, Lu X (2002) Live or let die: the cell's response to p53. Nat Rev Cancer 2:594–604
4. Lane DP, Crawford LV (1979) T antigen is bound to a host protein in SV40-transformed cells. Nature 278:261–263
5. DeLeo AB, Jay G, Appella E et al (1979) Detection of a transformation-related antigen in chemically induced sarcomas and other transformed cells of the mouse. Proc Natl Acad Sci USA 76:2420–2424
6. Linzer DI, Levine AJ (1979) Characterization of a 54 K Dalton cellular SV40 tumor antigen present in SV40-transformed cells and uninfected embryonal carcinoma cells. Cell 17:43–52
7. Oren M, Levine AJ (1983) Molecular cloning of a cDNA specific for the murine p53 cellular tumor antigen. Proc Natl Acad Sci USA 80:56–59
8. Feki A, Irminger-Finger I (2004) Mutational spectrum of p53 mutations in primary breast and ovarian tumors. Crit Rev Oncol Hematol 52:103–116
9. Momand J, Zambetti GP, Olson DC et al (1992) The mdm-2 oncogene product forms a complex with the p53 protein and inhibits p53-mediated transactivation. Cell 69:1237–1245
10. Fakharzadeh SS, Trusko SP, George DL (1991) Tumorigenic potential associated with enhanced expression of a gene that is amplified in a mouse tumor cell line. EMBO J 10:1565–1569

11. Fakharzadeh SS, Rosenblum-Vos L, Murphy M et al (1993) Structure and organization of amplified DNA on double minutes containing the mdm2 oncogene. Genomics 15:283–290
12. Hainaut P, Hollstein M (2000) p53 and human cancer: the first ten thousand mutations. Adv Cancer Res 77:81–137
13. Freedman DA, Wu L, Levine AJ (1999) Functions of the MDM2 oncoprotein. Cell Mol Life Sci 55:96–107
14. Juven-Gershon T, Oren M (1999) Mdm2: the ups and downs. Mol Med 5:71–83
15. Wu X, Bayle JH, Olson D, Levine AJ (1993) The p53-mdm-2 autoregulatory feedback loop. Genes Dev 7:1126–1132
16. Jones SN, Roe AE, Donehower LA, Bradley A (1995) Rescue of embryonic lethality in Mdm2-deficient mice by absence of p53. Nature 378:206–208
17. de Oca M, Luna R, Wagner DS, Lozano G (1995) Rescue of early embryonic lethality in mdm2-deficient mice by deletion of p53. Nature 378:203–206
18. Bond GL, Hu W, Bond EE et al (2004) A single nucleotide polymorphism in the MDM2 promoter attenuates the p53 tumor suppressor pathway and accelerates tumor formation in humans. Cell 119:591–602
19. Oliner JD, Kinzler KW, Meltzer PS et al (1992) Amplification of a gene encoding a p53-associated protein in human sarcomas. Nature 358:80–83
20. Zhou M, Gu L, Abshire TC et al (2000) Incidence and prognostic significance of MDM2 oncoprotein overexpression in relapsed childhood acute lymphoblastic leukemia. Leukemia 14:61–67
21. Rayburn E, Zhang R, He J, Wang H (2005) MDM2 and human malignancies: expression, clinical pathology, prognostic markers, and implications for chemotherapy. Curr Cancer Drug Targets 5:27–41
22. Momand J, Jung D, Wilczynski S, Niland J (1998) The MDM2 gene amplification database. Nucleic Acids Res 26:3453–3459
23. Gunther T, Schneider-Stock R, Hackel C et al (2000) Mdm2 gene amplification in gastric cancer correlation with expression of Mdm2 protein and p53 alterations. Mod Pathol 13:621–626
24. Bond GL, Hu W, Levine AJ (2005) MDM2 is a central node in the p53 pathway: 12 years and counting. Curr Cancer Drug Targets 5:3–8
25. Capoulade C, Bressac-de Paillerets B, Lefrere I et al (1998) Overexpression of MDM2, due to enhanced translation, results in inactivation of wild-type p53 in Burkitt's lymphoma cells. Oncogene 16:1603–1610
26. Momand J, Wu HH, Dasgupta G (2000) MDM2 – master regulator of the p53 tumor suppressor protein. Gene 242:15–29
27. Ganguli G, Abecassis J, Wasylyk B (2000) MDM2 induces hyperplasia and premalignant lesions when expressed in the basal layer of the epidermis. EMBO J 19:5135–5147
28. Kemp CJ, Donehower LA, BradleyA BA (1993) Reduction of p53 gene dosage does not increase initiation or promotion but enhances malignant progression of chemically induced skin tumors. Cell 74:813–822
29. Chen J, Marechal V, Levine AJ (1993) Mapping of the p53 and mdm-2 interaction domains. Mol Cell Biol 13:4107–4114
30. Picksley SM, Vojtesek B, Sparks A, Lane DP (1994) Immunochemical analysis of the interaction of p53 with MDM2; fine mapping of the MDM2 binding site on p53 using synthetic peptides. Oncogene 9:2523–2529
31. Kussie PH, Gorina S, Marechal V et al (1996) Structure of the MDM2 oncoprotein bound to the p53 tumor suppressor transactivation domain. Science 274:948–953
32. Garcia-Echeverria C, Chene P, Blommers MJ, Furet P (2000) Discovery of potent antagonists of the interaction between human double minute 2 and tumor suppressor p53. J Med Chem 43:3205–3208
33. Vassilev LT, Vu BT, Graves B et al (2004) In vivo activation of the p53 pathway by small-molecule antagonists of MDM2. Science 303:844–848

34. Grasberger BL, Lu T, Schubert C et al (2005) Discovery and cocrystal structure of benzodiazepinedione HDM2 antagonists that activate p53 in cells. J Med Chem 48:909–912
35. Allen JG, Bourbeau MP, Wohlhieter GE et al (2009) Discovery and optimization of chromenotriazolopyrimidines as potent inhibitors of the mouse double minute 2-tumor protein 53 protein-protein interaction. J Med Chem 52:7044–7053
36. Orner BP, Ernst JT, Hamilton AD (2001) Toward proteomimetics: terphenyl derivatives as structural and functional mimics of extended regions of an alpha-helix. J Am Chem Soc 123:5382–5383
37. Yin H, Lee GI, Park HS et al (2005) Terphenyl-based helical mimetics that disrupt the p53/HDM2 interaction. Angew Chem Int Ed Engl 44:2704–2707
38. Stoll R, Renner C, Hansen S et al (2001) Chalcone derivatives antagonize interactions between the human oncoprotein MDM2 and p53. Biochemistry 40:336–344
39. Go ML, Wu X, Liu XL (2005) Chalcones: an update on cytotoxic and chemoprotective properties. Curr Med Chem 12:481–499
40. Galatin PS, Abraham DJ (2004) A nonpeptidic sulfonamide inhibits the p53-mdm2 interaction and activates p53-dependent transcription in mdm2-overexpressing cells. J Med Chem 47:4163–4165
41. Galatin PS, Abraham DJ (2001) QSAR: hydropathic analysis of inhibitors of the p53-mdm2 interaction. Proteins 45:169–175
42. Lu Y, Nikolovska-Coleska Z, Fang X et al (2006) Discovery of a nanomolar inhibitor of the human murine double minute 2 (MDM2)-p53 interaction through an integrated, virtual database screening strategy. J Med Chem 49:3759–3762
43. Jones G, Willett P, Glen RC et al (1997) Development and validation of a genetic algorithm for flexible docking. J Mol Biol 267:727–748
44. Verdonk ML, Cole JC, Hartshorn MJ et al (2003) Improved protein-ligand docking using GOLD. Proteins 52:609–623
45. Eldridge MD, Murray CW, Auton TR et al (1997) Empirical scoring functions: I. The development of a fast empirical scoring function to estimate the binding affinity of ligands in receptor complexes. J Comput Aided Mol Des 11:425–445
46. Wang R, Lai L, Wang W (2002) Further development and validation of empirical scoring functions for structure-based binding affinity prediction. J Comput Aided Mol Des 16:11–26
47. Bowman AL, Nikolovska-Coleska Z, Zhong H et al (2007) Small molecule inhibitors of the MDM2-p53 interaction discovered by ensemble-based receptor models. J Am Chem Soc 129:12809–12814
48. Ding K, Lu Y, Nikolovska-Coleska Z et al (2005) Structure-based design of potent non-peptide MDM2 inhibitors. J Am Chem Soc 127:10130–10131
49. Ding K, Lu Y, Nikolovska-Coleska Z et al (2006) Structure-based design of spiro-oxindoles as potent, specific small-molecule inhibitors of the MDM2-p53 interaction. J Med Chem 49:3432–3435
50. Shangary S, Qin D, McEachern D et al (2008) Temporal activation of p53 by a specific MDM2 inhibitor is selectively toxic to tumors and leads to complete tumor growth inhibition. Proc Natl Acad Sci USA 105:3933–3938
51. Yu S, Qin D, Shangary S et al (2009) Potent and orally active small-molecule inhibitors of the MDM2−p53 interaction. J Med Chem 52:7970–7973
52. Wasserman R (2010) Patient selection strategies for the development of MDM2 inhibitors. http://www.cmod.org/images/CMOD_Presentations_5-28-10/Wasserman%20CMOD%20Ottawa%20May%2017%202010.pdf
53. Uoto K, Kawato H, Sugimoto Y et al (2009) WO 2009/151069, 12 Dec 2009
54. Wang S, Sun W, Yu S et al (2011) Highly potent and optimized small-molecule inhibitors of MDM2 achieve complete tumor regression in animal models of solid tumors and leukemia. Abstract LB-204. AACR 102nd annual meeting, Orlando, FL
55. Bartkovitz D, Chu X-J, Ding Q et al (2011) WO 2011/067185, 9 June 2011
56. Liu J-J, Zhang J, Zhang Z (2011) WO 2011/101297, 25 Aug 2011

57. Czarna A, Beck B, Srivastava S et al (2010) Robust generation of lead compounds for protein-protein interactions by computational and MCR chemistry: p53/Hdm2 antagonists. Angew Chem Int Ed Engl 49:5352–5356
58. Boettcher A, Buschmann N, Furet P et al (2008) WO 2008/119741, 9 Oct 2008
59. Bold G, Furet P, Gessier F et al (2011) WO 2011/023677, 3 Mar 2011
60. Berghausen J, Buschmann N, Furet P et al (2011) WO 2011/076786, 30 June 2011
61. Hardcastle IR, Liu J, Valeur E et al (2011) Isoindolinone inhibitors of the murine double minute 2 (MDM2)-p53 protein-protein interaction: structure-activity studies leading to improved potency. J Med Chem 54:1233–1243
62. Burdack C, Kalinski C, Ross G et al (2010) WO 2010/028862, 18 Mar 2010
63. Ma Y, Lahue BR, Shipps Jr, GW et al (2011) Substituted piperidines that increase P53 activity and the uses thereof. US Patent 7,884,107 B2, 8 Feb 2011
64. Popowicz GM, Czarna A, Wolf S et al (2010) Structures of low molecular weight inhibitors bound to MDMX and MDM2 reveal new approaches for p53-MDMX/MDM2 antagonist drug discovery. Cell Cycle 9:1104–1111
65. Tovar C, Rosinski J, Filipovic Z et al (2006) Small-molecule MDM2 antagonists reveal aberrant p53 signaling in cancer: implications for therapy. Proc Natl Acad Sci USA 103:1888–1893
66. Patton JT, Mayo LD, Singhi AD et al (2006) Levels of HdmX expression dictate the sensitivity of normal and transformed cells to Nutlin-3. Cancer Res 66:3169–3176
67. Saddler C, Ouillette P, Kujawski L et al (2007) Comprehensive biomarker and genomic analysis identifies P53 status as the major determinant of response to MDM2 inhibitors in chronic lymphocytic leukemia. Blood 111:1584–1593
68. Long J, Parkin B, Ouillette P et al (2010) Multiple distinct molecular mechanisms influence sensitivity and resistance to MDM2 inhibitors in adult acute myelogenous leukemia. Blood 116:71–80
69. Sarek G, Kurki S, Enback J et al (2007) Reactivation of the p53 pathway as a treatment modality for KSHV-induced lymphomas. J Clin Invest 117:1019–1028
70. Smith MA, Kang MH, Reynolds CP et al (2011) Pediatric preclinical testing program (PPTP) stage 1 evaluation of the p53-MDM2 antagonist RG7112: early evidence for high activity against MLL-rearranged leukemias. Abstract C103. AACR-NCI-EORTC international conference: molecular targets and cancer therapeutics, San Francisco, CA
71. Lowe SW, Schmitt EM, Smith SW et al (1993) p53 is required for radiation-induced apoptosis in mouse thymocytes. Nature 362:847–849
72. Potten CS, Wilson JW, Booth C (1997) Regulation and significance of apoptosis in the stem cells of the gastrointestinal epithelium. Stem Cells 15:82–93
73. Ringshausen I, O'Shea CC, Finch AJ et al (2006) Mdm2 is critically and continuously required to suppress lethal p53 activity in vivo. Cancer Cell 10:501–514
74. Bottger V, Bottger A, Garcia-Echeverria C et al (1999) Comparative study of the p53-mdm2 and p53-MDMX interfaces. Oncogene 18:189–199
75. Hu B, Gilkes DM, Farooqi B et al (2006) MDMX overexpression prevents p53 activation by the MDM2 inhibitor Nutlin. J Biol Chem 281:33030–33035
76. Wade M, Wong ET, Tang M et al (2006) Hdmx modulates the outcome of p53 activation in human tumor cells. J Biol Chem 281:33036–33044
77. Kawai H, Wiederschain D, Kitao H et al (2003) DNA damage-induced MDMX degradation is mediated by MDM2. J Biol Chem 278:45946–45953
78. Lau LM, Nugent JK, Zhao X, Irwin MS (2008) HDM2 antagonist Nutlin-3 disrupts p73-HDM2 binding and enhances p73 function. Oncogene 27:997–1003
79. Ambrosini G, Sambol EB, Carvajal D et al (2007) Mouse double minute antagonist Nutlin-3a enhances chemotherapy-induced apoptosis in cancer cells with mutant p53 by activating E2F1. Oncogene 26:3473–3481

80. LaRusch GA, Jackson MW, Dunbar JD et al (2007) Nutlin3 blocks vascular endothelial growth factor induction by preventing the interaction between hypoxia inducible factor 1alpha and Hdm2. Cancer Res 67:450–454
81. Colaluca IN, Tosoni D, Nuciforo P et al (2008) NUMB controls p53 tumour suppressor activity. Nature 451:76–80
82. Secchiero P, Corallini F, Gonelli A et al (2007) Antiangiogenic activity of the MDM2 antagonist Nutlin-3. Circ Res 100:61–69
83. Binder BR (2007) A novel application for murine double minute 2 antagonists: the p53 tumor suppressor network also controls angiogenesis. Circ Res 100:13–14
84. Carvajal D, Tovar C, Yang H et al (2005) Activation of p53 by MDM2 antagonists can protect proliferating cells from mitotic inhibitors. Cancer Res 65:1918–1924
85. Secchiero P, Barbarotto E, Tiribelli M et al (2006) Functional integrity of the p53-mediated apoptotic pathway induced by the nongenotoxic agent Nutlin-3 in B-cell chronic lymphocytic leukemia (B-CLL). Blood 107:4122–4129
86. Kojima K, Konopleva M, McQueen T et al (2006) Mdm2 inhibitor Nutlin-3a induces p53-mediated apoptosis by transcription-dependent and transcription-independent mechanisms and may overcome Atm-mediated resistance to fludarabine in chronic lymphocytic leukemia. Blood 108:993–1000
87. Coll-Mulet L, Iglesias-Serret D, Santidrian AF et al (2006) MDM2 antagonists activate p53 and synergize with genotoxic drugs in B-cell chronic lymphocytic leukemia cells. Blood 107:4109–4114
88. Kojima K, Konopleva M, Samudio IJ et al (2005) MDM2 antagonists induce p53-dependent apoptosis in AML: implications for leukemia therapy. Blood 106:3150–3159
89. Secchiero P, Zerbinati C, di Iasio MG et al (2007) Synergistic cytotoxic activity of recombinant TRAIL plus the non-genotoxic activator of the p53 pathway Nutlin-3 in acute myeloid leukemia cells. Curr Drug Metab 8:395–403
90. Drakos E, Thomaides A, Medeiros LJ et al (2007) Inhibition of p53-murine double minute 2 interaction by Nutlin-3A stabilizes p53 and induces cell cycle arrest and apoptosis in Hodgkin lymphoma. Clin Cancer Res 13:3380–3387
91. Saha MN, Jiang H, Jayakar J et al (2010) MDM2 antagonist Nutlin plus proteasome inhibitor velcade combination displays a synergistic anti-myeloma activity. Cancer Biol Ther 9:936–944
92. Aziz MH, Shen H, Maki CG (2011) Acquisition of p53 mutations in response to the non-genotoxic p53 activator Nutlin-3. Oncogene 30:4678–4686
93. Andreeff M, Kojima K, Padmanabhan S et al (2010) A multi-center, open-label, phase I study of single agent RG7112, a first in class p53-MDM2 antagonist, in patients with relapsed/refractory acute myeloid and lymphoid leukemias (AML/ALL) and refractory chronic lymphocytic leukemia/small cell lymphocytic lymphomas (CLL/SCLL). Abstract 657. ASH 53rd annual meeting 2001, Anaheim, CA
94. Ray-Coquard IL, Blay J, Italiano A et al (2011) Neoadjuvant MDM2 antagonist RG7112 for well-differentiated and dedifferentiated liposarcomas (WD/DD LPS): a pharmacodynamic (PD) biomarker study. Abstract 10007b. 2011 ASCO annual meeting, Chicago, IL
95. Beryozkina A, Nichols GL, Reckner M et al (2011) Pharmacokinetics (PK) and pharmacodynamics (PD) of RG7112, an oral murine double minute 2 (MDM2) antagonist, in patients with leukemias and solid tumors. Abstract 3039. 2011 ASCO annual meeting, Chicago, IL

Top Med Chem 8: 81–104
DOI: 10.1007/978-3-642-28965-1_3

The Development of Small-Molecule IAP Antagonists for the Treatment of Cancer

Kurt Deshayes, Jeremy Murray, and Domagoj Vucic

Contents

Abstract Apoptosis is a genetically regulated process of cell death that is critical for cellular homeostasis. Dysregulation of apoptosis can lead to the absence of normal cell death and contribute to cancer development and progression. The Inhibitor of Apoptosis (IAP) proteins contain up to three baculovirus IAP repeat (BIR) domains that interact with members of the caspase family of proteases, thereby blocking apoptosis. Select BIR domains of IAP proteins contain a defined protein-protein interaction region with the N-terminal amino acid residues of the

K. Deshayes (✉) • D. Vucic
Department of Early Discovery Biochemistry, Genentech Inc., South San Francisco, CA 94080, USA
e-mail: deshayes.kurt@gene.com

J. Murray
Department of Structural Biology, Genentech Inc., South San Francisco, CA 94080, USA

natural IAP antagonist protein, SMAC. Antagonizing this interaction formed the basis of all drug discovery efforts and has yielded promising drug candidates. One member of the IAP family, XIAP, can inhibit caspases 3 and 7 through its BIR2 domain and caspase-9 with its BIR3 domain. The c-IAPs play a key role in the regulation of the NF-κB pathways, which is manipulated by the IAP antagonists to yield single agent activity. SMAC mimicking IAP antagonists can be monovalent, representing an equivalent of four amino acid residues from the processed SMAC, or bivalent – having two units connected through a chemical linker. In addition, antagonists specific for a particular IAP protein or a group of IAPs have been reported. So far, six molecules have entered clinical trials with early results showing no dose limiting toxicities and suggesting that IAP proteins can be targeted by small molecules.

Keywords Apoptosis • Cancer • Drug discovery • IAP protein • Peptidiomemetics • Protein-protein interactions • Rational design • TNF signaling

1 Introduction: Biological Rationale

1.1 The IAP Family of Anti-Apoptotic Proteins

One of the major strategies that cancer cells employ to ensure their survival is inhibition of cell death triggered by the immune system and various anti-cancer therapies [1]. The group of proteins that belong to the family of Inhibitors of Apoptosis (IAP) consist of structurally related molecules that possess a broad spectrum of activities required for inhibition of cell death and promotion of survival signaling pathways [2]. IAPs were initially discovered in baculoviruses, and were subsequently found in all multicellular organisms. Eight mammalian IAP proteins are known: neuronal apoptosis inhibitory protein (NAIP/BIRC1); cellular IAP1 (c-IAP1/BIRC2/HIAP2); cellular IAP2 (c-IAP2/BIRC3/HIAP1); X chromosome-linked IAP (XIAP/BIRC4/hILP-1); survivin (BIRC5); BIR-containing ubiquitin conjugating enzyme (BRUCE/BIRC6/Apollon); melanoma IAP (ML-IAP/BIRC7/Livin); and testis-specific IAP (Ts-IAP/BIRC8/hILP-2) [2, 3]. All IAP molecules contain one to three baculovirus IAP repeat (BIR) domains, a signature domain for this group of proteins [3]. BIR domains of IAP proteins are approximately 80-amino acid zinc-binding modules with a conserved alpha/beta fold [4]. In addition to the BIR domains, several IAP molecules possess a carboxy-terminal ubiquitin ligase RING domain [5, 6]. Some IAP proteins also contain a centrally located ubiquitin-associated (UBA) domain and a caspase-recruitment domain (CARD) [7–9] (Fig. 1). There are few additional protein domains that are unique to particular IAPs [3] (Fig. 1). Although they are structurally similar, IAP proteins exhibit diverse functions and contribute to cancer biology in a multitude of ways. XIAP, c-IAP1, c-IAP2, and ML-IAP, bind to and inhibit proapoptotic molecules, and c-IAP1 and c-IAP2 also play central roles in the control of NF-kB (nuclear

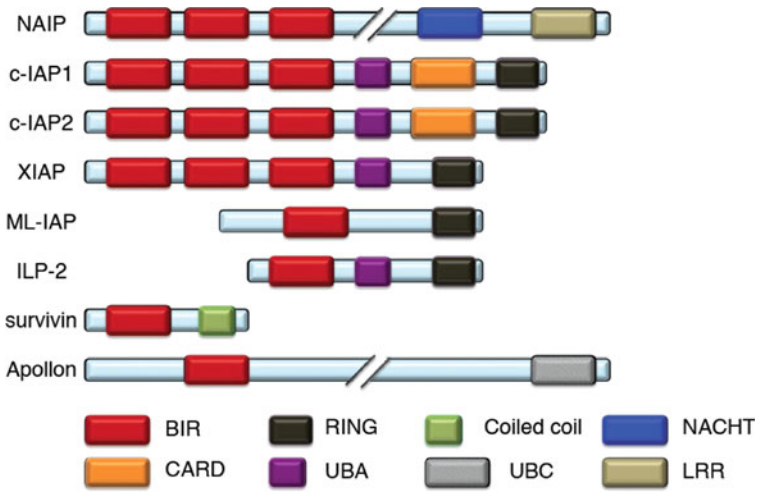

Fig. 1 The human IAP protein family. Human IAP proteins contain one or three baculovirus IAP repeat (BIR) domains. Several IAP family members also have RING (really interesting new gene) and UBA (ubiquitin associated) domains. The c-IAP1 and c-IAP2 proteins each contain a caspase recruitment domain (CARD). Survivin contains a coiled coil domain; NAIP has NACHT (domain present in NAIP, CIITA, HET-E, TP1) and leucine rich repeat (LRR) domains; Apollon possesses a ubiquitin conjugating (UBC) domain

factor-kappaB)-dependent gene induction by regulating the signaling pathways mediated by the members of the tumor necrosis factor (TNF) ligand family [3, 10]. IAP proteins are often associated with advanced stages of various malignancies through their elevated expression, enhanced protein stability, chromosomal translocations, and involvement in survival signaling pathways. On the other hand, the loss of cellular IAP1 and IAP2 potentially contributes to formation of certain types of myelomas [3, 10, 11].

1.2 Role of IAP Proteins in Apoptotic Pathways

The execution of apoptotic cell death is mediated by the intrinsic and extrinsic apoptotic pathways (Fig. 2). Both of these pathways eventually converge, leading to activation of caspases, cysteine-dependent aspartyl-specific proteases that represent the effector arm of apoptotic signaling [12]. The intrinsic or mitochondrial pathway is initiated by developmental cues or cellular stress signals [13]. These signals activate Bcl-2-homology 3 (BH3) proteins leading to neutralization of the anti-apoptotic proteins Bcl-2, Bcl-x_L or Mcl-1, activation of pro-apoptotic proteins, Bax and Bak, and subsequent disruption of mitochondrial membrane potential. Consequent release of cytochrome c from the mitochondria into the cytoplasm leads to Apaf-1-mediated caspase-9 activation, which in turn activates effector

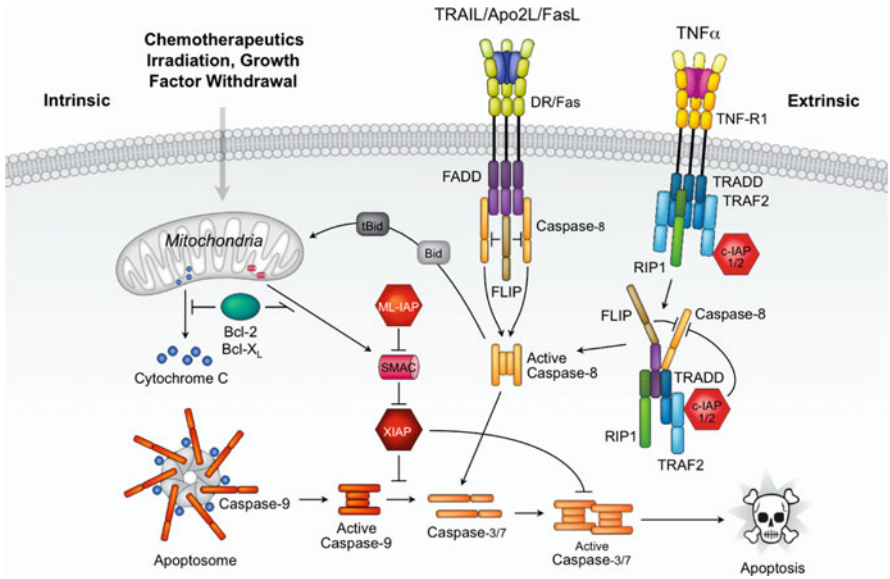

Fig. 2 The intrinsic and extrinsic apoptotic pathways. Programmed cell death is initiated in the intrinsic pathway by irradiation, growth factor withdrawal, or chemotherapeutic agents. BH3-only proteins neutralize anti-apoptotic proteins Bcl-2, Bcl-x_L, and Mcl-1 leading to disruption of the mitochondrial membrane potential, and cytochrome c and SMAC release from the mitochondria into the cytoplasm. This results in activation of caspase-9, subsequent activation of caspases 3 and 7, and ultimately cell death. Apoptotic signaling through the extrinsic pathway is triggered by binding of death ligands, such as TNFα and FasL, to their cognate death receptors, in this case TNFR1 and Fas, respectively, which results in recruitment of the adaptor protein FADD and caspase-8. This leads to the activation of caspase-8, then caspases 3 and 7, and finally apoptosis. XIAP can inhibit caspases 3, 7, and 9; however, SMAC can bind to XIAP and prevent XIAP-mediated inhibition of caspases. ML-IAP, c-IAP1, and c-IAP2 can sequester SMAC away from XIAP, thus blocking its anti-apoptotic activity

caspases 3 and 7, and culminates in cell death. The extrinsic apoptotic pathway is stimulated by binding of FasL, TRAIL/Apo2L or TNF to their respective receptors, resulting in recruitment of the adaptor protein FADD and the apical caspases 8 or 10 [14]. Recruitment of these caspases into the death receptor-associated death-inducing signaling complex (DISC) causes their self-activation and leads to eventual activation of caspases 3 and 7.

IAP proteins represent the ultimate line of defense against cellular suicide by regulating caspase activity and preventing caspase activation [12]. The only physiological endogenous inhibitor of caspases is XIAP as other IAP proteins exhibit weak binding to and inhibition of caspases [15]. XIAP uses the linker region between BIR1 and BIR2 as well as the BIR2 domain for efficient inhibition of caspases 3 and 7 [16–20]. This linker region associates with the substrate-binding groove of activated caspases in a reverse orientation relative to the substrate. At the same time the BIR2 domain interacts with the amino terminus of the small subunit of activated caspases via its peptide-binding groove. For the inhibition of caspase-9,

the peptide-binding groove on the surface of the XIAP BIR3 domain interacts with a conserved four-residue IAP-binding motif (IBM) exposed at the amino terminus of the small subunit of processed caspase-9 [21, 22]. Association of XIAP BIR3 with the caspase-9 homodimerization interface traps caspase-9 in a catalytically inactive conformation and contributes to enzyme inhibition.

SMAC (second mitochondrial activator of caspases)/DIABLO (direct IAP binding protein with low p*I*) is the endogenous antagonist of IAP, which can block XIAP mediated inhibition of caspases [23, 24]. Processed SMAC undergoes release from mitochondria into the cytoplasm upon apoptosis induction [25]. Processing of SMAC exposes an IBM that binds the peptide-binding groove on the surface of the select IAP BIR domains [26, 27]. In case of XIAP, this binding prevents XIAP-mediated interaction with and inhibition of caspases. The conserved four residue IBM of SMAC (A-V-P-I) is critical for its pro-apoptotic activity, and mutations of the amino-terminal alanine residue completely abrogate the IAP-binding and -blocking ability of SMAC [22, 28]. Several IAP proteins bind SMAC with high affinity and some of them, like ML-IAP and probably also c-IAPs and ILP-2, compete with XIAP for SMAC binding, resulting in an increased pool of XIAP molecules available for inhibition of caspases (Fig. 2) [29]. By sequestering SMAC, these IAPs contribute to caspase inhibition and cell survival. Besides SMAC, a number of additional IAP-interacting proteins including HtrA2/Omi, XAF1, and several other proteins with amino-terminal IAP biding motifs have been described [30–32]. By binding to the BIR2 and BIR3 domains of XIAP, many of these proteins are postulated to antagonize XIAP inhibition of caspases and contribute to pro-apoptotic signaling.

1.3 IAP Proteins as E3 Ligases and Mediators of Signaling

c-IAP1 and c-IAP2 are unique amongst IAP proteins for their participation in TNF receptor family signaling complexes [10]. Through their interaction with TNF receptor-associated factor 2 (TRAF2), c-IAP1 and c-IAP2 are recruited to TNFR complexes where they regulate receptor-mediated apoptosis by inhibiting caspase-8 activation (Fig. 3) [10, 33, 34].

Both c-IAP1 and c-IAP2 are E3 ubiquitin ligases that mediate RIP1 and NIK ubiquitination, which represent critical steps in the activation of NF-kB signaling and also in the inhibition of TNFR1-mediated cell death [34–37]. In the NF-kB canonical pathway, c-IAP1 and c-IAP2 promote activation of signaling by their ubiquitination of receptor interacting protein (RIP1) (Fig. 3) [34–36, 38, 39]. However, in noncanonical NF-kB signaling, c-IAP proteins have been identified as the E3 ligases responsible for the ubiquitination and subsequent degradation of NF-kB-inducing kinase (NIK), and thus serve as negative regulators of this signaling pathway [37, 40] (Fig. 3). The absence of c-IAP1 and c-IAP2 eliminates RIP1 ubiquitination and allows association of RIP1 with FADD and caspase-8, leading to induction of apoptosis [35].

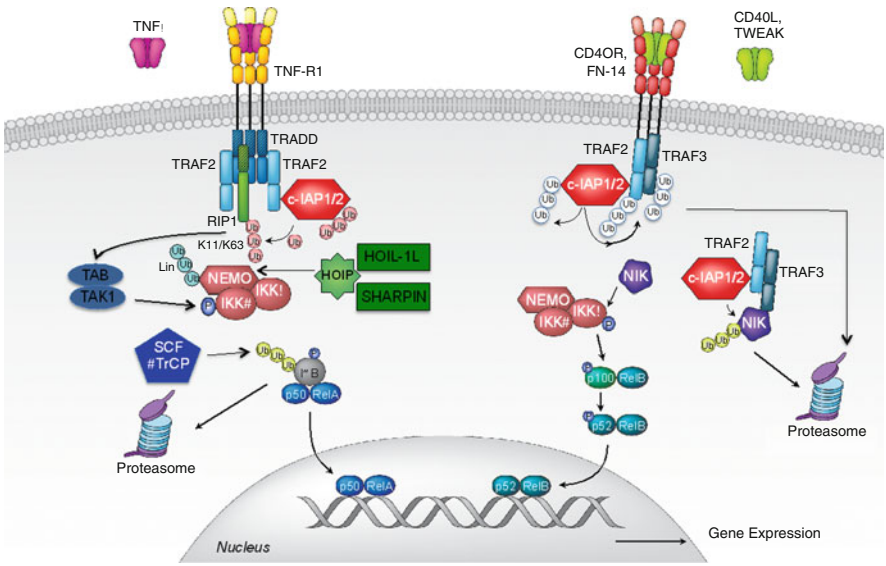

Fig. 3 Canonical and noncanonical NF-κB pathways. NF-κB signaling occurs via canonical and noncanonical pathways. Signaling through the TNFR1 complex activates the canonical pathway; binding of TNFα to TNFR1 triggers recruitment of the adaptor protein TRADD, and subsequent recruitment of TRAF2, RIP1, c-IAP1 and c-IAP2. RIP1 is then ubiquitinated by c-IAP1/2 with a variety of polyubiquitin linkages including K63 and K11 linkages. This modification facilitates assembly of the RIP1-associated kinase complexes, TAK1/TABs, IKK, and LUBAC (HOIP with HIOL-1L and Sharpin) leading to the phosphorylation and proteasomal degradation of IκB that enables NF-κB dimers to translocate to the nucleus and induce gene expression. Other receptors, such as FN14 or CD40R, can activate the noncanonical NF-κB signaling pathway. In this pathway c-IAP1/2 function as E3 ligases to promote K48-linked polyubiquitination and proteasomal degradation of NIK, and thus negatively regulate noncanonical NF-κB signaling

The ubiquitin ligase activity of IAPs can regulate the protein levels of several of their binding partners including other IAPs [5, 6, 10]. Deletion of the XIAP RING domain and elimination of its ubiquitin ligase activity leads to elevated caspase-3 activity, supporting a physiological need for the ubiquitin-ligase activity of XIAP for the inhibition of caspases [41]. SMAC is subject to ubiquitination and proteasomal degradation by XIAP, ML-IAP, and c-IAP1 and c-IAP2 as well [42, 43]. The c-IAP proteins also regulate the ubiquitination and stability of proteins involved in Myc-mediated pathway and TNF receptor signaling. By acting as an ubiquitin ligase for a cellular antagonist of Myc, Max dimerization protein-1 or Mad1, c-IAP1 cooperates with Myc to promote cellular proliferation [44]. Assembly of TNF receptor complexes may lead to c-IAP-mediated ubiquitination of TRAF2 and ASK1, potentially resulting in dampened NF-kB activation, deregulated MAPK signaling, and dampened caspase-8 activation [6]. Several RING domain-containing IAPs can auto-ubiquitinate themselves, and c-IAP1 can also mediate ubiquitination and proteasomal degradation of c-IAP2 and XIAP [5, 10].

1.4 IAP Proteins in Cancer

Numerous studies have clearly implicated IAP proteins in human malignancies [45]. Elevated expression levels of IAP proteins, particularly c-IAP1/2 and XIAP, have been shown in many tumor types and correlated with a poor prognosis [30]. ML-IAP is not expressed in most normal human tissues but is frequently expressed at high levels in melanomas, bladder, and kidney cancers [46–50]. Expression of ML-IAP in melanomas is regulated by the lineage survival oncogene microphthalmia-associated transcription factor (MITF), suggesting that the anti-apoptotic activity of ML-IAP contributes to the pro-survival properties of MITF in melanoma progression [51]. In addition, a number of animal and *in vitro* studies have further explored and illuminated the oncogenic potential of IAP proteins. Down-regulation of XIAP expression in tumor cells, either by RNA interference or antisense oligonucleotides, results in stimulation of apoptosis and sensitization to gamma-irradiation- and chemotherapeutic-induced apoptosis, both *in vitro* and *in vivo* [52–55]. In a similar fashion, down-regulation of c-IAP1, ML-IAP, or survivin causes activation of apoptotic pathways and increased sensitivity to cell death stimuli, such as chemotherapeutic agents and death receptors [30, 56].

Finally, there is direct genetic data that establishes c-IAP1 and c-IAP 2 as potential pro-oncogenes. 11q21-q23 chromosomal region containing c-IAP1 and c-IAP2 is amplified in esophageal squamous cell carcinomas, renal cell carcinomas, glioblastomas, gastric carcinomas, non-small cell lung carcinomas, and other tumor types [30, 57]. In murine tumors, the syntenic region encompassing the c-IAP1 and c–IAP2 genes is amplified as well, and ectopic overexpression of c-IAP1 in mouse models has been demonstrated to lead to tumor growth and hepatoma formation [58]. Additional genetic evidence comes from studies of an extranodal non-Hodgkin lymphoma, termed MALT lymphoma, where in around 50% of the cases surveyed the t(11, 18)(q21;q21) translocation leads to a fusion of the BIR domains of c-IAP2 with the carboxy terminus of the paracaspase/MALT1 (mucosa-associated lymphoid tissue protein) [59–62]. The resultant c-IAP2:MALT1 fusion protein promotes constitutive activation of the NF-kB pathway, leading to increased pro-survival and inflammatory pathway signaling, and greater resistance to chemotherapeutic anti-tumor agents [63–65].

2 Pre-Clinical Studies

2.1 Peptides Based on SMAC

Although crucial, biological rationale alone is not sufficient evidence on which to build a small-molecule drug discovery program. Data supporting the utility of molecular intervention with the target is also highly desirable. The first evidence suggesting the druggability of the IAP proteins was reported in 2002 in two studies

that demonstrated the efficacy of SMAC derived peptides *in vitro* and *in vivo*. We demonstrated [28] that peptides containing the N-terminus of SMAC fused with a cell penetrating antennapedia sequence blocked the anti-apoptotic activity of XIAP and ML-IAP in transiently transfected 293 cells. This was the first reported *in vitro* evidence that blocking the interaction between IAP proteins and caspases using SMAC-derived peptides promotes apoptosis. In a seminal study [66], the Fulda group demonstrated that SMAC peptides fused to antennapedia enhanced the anti-tumor activity of Apo2L/TRAIL in a mouse glioma *in vivo* model. This work was the first *in vivo* study in which an IAP antagonist improves the efficacy of a pro-apoptotic agent. The initial positive data was quickly confirmed in complementary studies [67] presenting persuasive evidence that small molecule IAP antagonist could be useful anticancer therapeutics.

2.2 *Peptides from Phage Display*

Propelled by the initial positive results, we investigated the binding specificity of the BIR domains of selected IAP proteins in order to determine the prospects for high affinity and selective antagonists. Phage display of linear peptides was used to explore BIR2 and BIR3 domains of XIAP and the BIR domain of ML-IAP [68]. Almost identical results were obtained for the two BIR3 domains after six rounds of sorting: exclusively alanine at the N-terminus (P1), variable residues in second position (P2), 95% occurrence of proline in the third position (P3), and a preference for aromatic residues in the fourth position (P4). Although six- and eight-residue linear libraries were used in the screen, consensus was only observed in the four N-terminal residues. This observation is explained by the crystal structure of a peptide containing the nine N-terminal residues of SMAC, AVPIAQKSE, bound to the ML-IAP BIR domain (Fig. 4a).

The structure indicates that only four residues are making contact with the BIR domain, and only these residues are visible [68], providing all of the affinity and specificity. As shown in Fig. 4, the free amine at the N-terminus forms a salt bridge with E143 of the protein, removal of this interaction alleviates binding. The P1 pocket is just big enough to accommodate the methyl side chain of alanine. The nitrogen of the first amide bound and the oxygen atom of the second amide bound form hydrogen bounds with the BIR domain. The proline in P3 makes a hydrophobic interaction with W147 of the BIR domain while simultaneously aligning the residue in P4 into the adaptive binding pocket.

The sequence with the highest affinity, AVPF, bound tightly both to the ML-IAP BIR domain with a K_i of 160 nM and XIAP BIR3 domain with a K_i of 390 nM. Two important points about the BIR3 domain were immediately apparent: Nanomolar affinity was achievable with a small four amino acid epitope and ML-IAP BIR bound ligands slightly tighter than the XIAP BIR3 domain, a trend that persists for the c-IAP1 BIR3 domain. Further investigation of binding affinity in the P3 position showed that ML-IAP BIR tolerated branched amino acids more readily at this

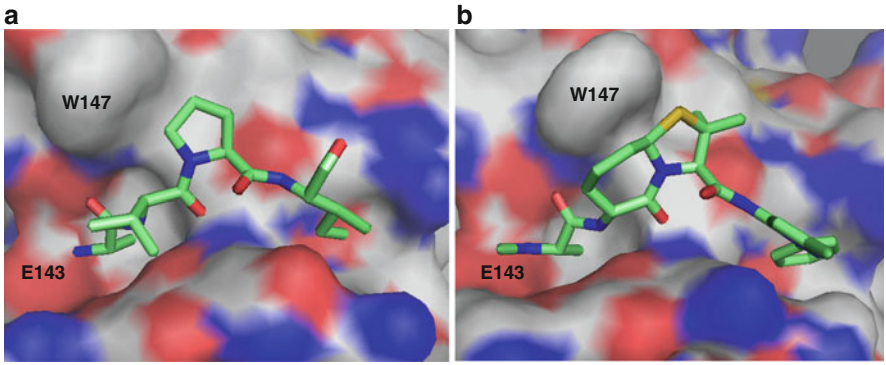

Fig. 4 Structure of peptide and peptidomimetics (**a**) Structure of AVPIAQKSE bound to the BIR domain of ML-IAP, only the four N-terminal residues of the peptide are ordered in the structure (**b**) Structure of [7,5]-bicyclic-γ-thioproline **8** also bound to the BIR domain of ML-IAP. Note the conservation of interactions with between the peptide and the protein

position than XIAP BIR3. This preference is explained by the mutation of a tyrosine in XIAP BIR3 to a phenylalanine in ML-IAP BIR. The peptide AV(3βmethyl)PI was 100-fold selective for ML-IAP, in agreement with our assessment of the role this mutation plays in selectivity at the P3 position. The c-IAP1 BIR3 domain also contains a phenylalanine and shows the same affinity for branched amino acids, a feature that is used to help the create c-IAP selective antagonists discussed in Sect. 2.6.

Aside from the selection of alanine in the P1 position, the results with the XIAP BIR2 domain are quite different than those obtained with the BIR3 domains investigated. Glutamic acid was favored in P2 position with alanine and glycine dominating the selection at the P3 and valine and isoluecine the selection for P4. The tightest binder AEAV is selective for the XIAP BIR2 domain with a K_i of 2.3 μM.

The results from the peptides based studies pointed to the possibility of constructing potent antagonists that are selective for IAP proteins as well as the individual BIR domains. The next step in creating effective antagonists was moving away from peptide scaffolds and towards molecules with better druglike properties. To that end, several groups, including us, undertook efforts to create potent peptidomimetics.

2.3 Peptidomimetics: Pan-Specific Monovalent

From 2004 onward, several reports described interesting approaches for developing potent SMAC peptidomimetics based on the N-terminus of the small subunit of processed Caspase-9 and mature SMAC. These compounds are summarized in Table 1.

Table 1 Monovalent pan-specific IAP antagonists

Compound	Structure	Status	Source	Refs.
2	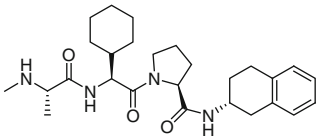	Preclinical	Abbott	[68]
LBW-242	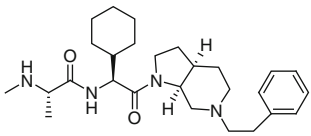	Preclinical	Norvartis	[69]
8	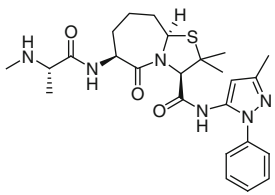	Preclinical	Genentech	[70]
SM-122	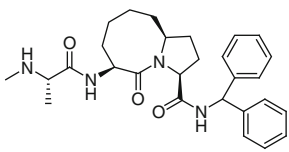	Preclinical	U of Michgan/Ascenta	[71–73]
MV1	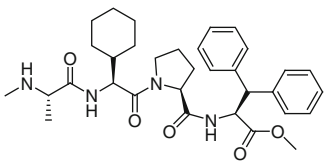	Preclinical	Genentech	[37]
AT-406	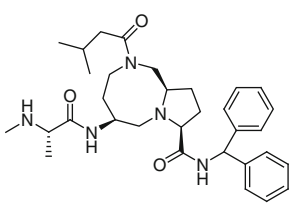	Phase I	Ascenta	[89]

(continued)

Table 1 (continued)

Compound	Structure	Status	Source	Refs.
GDC-0152	NA	Phase I	Genentech	[84]
LCL-161	NA	Phase I	Novartis	[86]
GDC-0917	NA	Phase I	Genentech	[88]

Common features of the most potent molecules are low nanomolar potency, *N*-methyl alanine in P1, proline or a structurally analogous pyrollidines in P3 and an aromatic group in P4. N-Methylation of the N-terminal alanine was found to increase cellular stability without reducing binding affinity. The geometry associated with the pyrollidine moiety in P3 appears to be optimal for placing the aromatic group in P4 into the binding pocket. Subsequent results have confirmed this alignment must be preserved to produce a potent peptidiomimetic against the XIAP or c-IAP BIR3 domains.

The report from Abbott published in 2004, as exemplified by **3** [69], set important precedents in that it identified breast cancer, notably MDA-MB-231 cells, as especially sensitive to IAP antagonists, provided evidence for the importance of having the terminal amine methylated, and demonstrated that IAP antagonists retard tumor growth for extended periods as single agents in animals models with no signs of unmanageable toxicity. Norvatis published the development of LBW-242 in 2007 that used a fused [5, 6] structure in P3 to yield a potent IAP antagonist that also demonstrated potent *in vivo* activity [70].

We published findings with our [7,5]-bicyclic-γ-thioproline scaffolds in 2006 in which we observed that cell death was indeed due to apoptosis with addition of our IAP antagonist enhancing the cytotoxicity of doxorubicin [71] (see Fig. 4b). Compound **8** demonstrated potent single agent efficacy in breast cancer and melanoma cells that closely correlated with binding affinity for c-IAP proteins; this observation will be explained in the context of TNF generation and initiation of the extrinsic pathway in Sect. 2.6. Elegant work by Shaomeng Wang's group at the University of Michigan and Ascenta therapeutics created a series of peptidomimetics such as SM-122 based on a rigid [5, 8] scaffold that yielded tight binding to the XIAP BIR3 domain with potent single agent activity [72–74].

As evidence for the efficacy of the pan-specific monovalent compounds accumulated, parallel studies supported the potential for bivalent molecules with increased potency. However, the two classes have pharmacological properties that must be taken into consideration for clinical development.

2.4 Peptidomimetics: Pan-Specific Bivalent

The BIR2 and BIR3 domains of XIAP are connected via a flexible linker region that allows simultaneous binding of both domains with a bivalent IAP antagonist

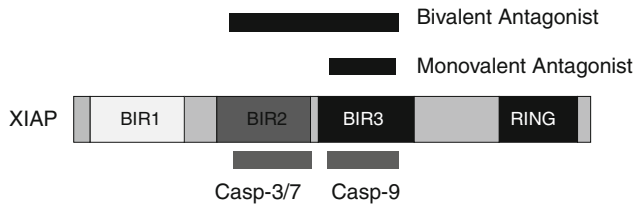

Fig. 5 Difference between monovalent and bivalent IAP antagonists. Monovalent IAP antagonists block binding to the XIAP BIR3 domain, which promotes activation of initiator caspase 9. In contrast, bivalent antagonists simultaneously block binding to both the XIAP BIR2 and BIR3 domains. This promotes activity of caspase 9 as well as effector caspase 3 and 7

molecule that is capable of reaching across the linker. Although IAP antagonists bind XIAP BIR2 domain with micromolar affinity, avidity associated with bivalent molecules that bind simultaneously to both BIR2 and BIR3 domains should significantly increase the potency over the analogous monovalent molecule that only binds to the BIR3 domain. These bivalent antagonists would not only be more potent at blocking XIAP binding to initiator caspase-9, they would also be capable of blocking XIAP binding to effector caspases 3 and 7 since they would directly block BIR2 binding. One would expect that this increased interaction with the apoptotic pathway would increase potency over the monomer class of antagonists (Fig. 5).

The situation is very different for the c-IAP proteins, where only the BIR3 domain displays significant affinity for small molecule ligands. Thus, the only potential new function for bivalent antagonists is the dimerization of c-IAP proteins via the BIR3 domains [37]. The compounds discussed in this section are found in Table 2.

The Wang and Harran groups at UT-Southwestern reported the first potent bivalent IAP inhibitor, JP1010, in 2004, with further development conducted in collaboration with Joyant Pharmaceuticals [75]. The UT bivalent molecule was indeed a more potent activator of caspase-3 than monovalent SMAC mimetics against full length XIAP, most likely due to simultaneous BIR2 and BIR3 binding. The addition of 100 nM to Glioma T98G cells potently sensitized them to apoptosis by Apo2L/TRAIL, thereby demonstrating potent cellular activity. In 2010, studies published with JP2010 and another bivalent Smac mimetic JP1400 demonstrate synergy with standard of care chemotherapeutic agents to promote caspase activation and accelerate cell death [76]. Significant tumor regression was seen using JP1400 in a HCC 461 xenograph tumor model.

In 2007, we published a mechanistic study in which we compared the bivalent IAP antagonist BV6 to its monomer subunit MV1 [37]. Using Biacore and sedimentation equilibrium analysis, we found that BV6 binds XIAP BIR2-BIR3 construct in a two-site model that yielded a 1:1 complex in which one BV6 molecule bound simultaneously to the BIR2 and BIR3 domains of one XIAP molecule. In contrast, the same experiments with c-IAP1 BIR2-BIR3 construct yielded a 2:1 complex in which the BIR3 domain of two c-IAP1 proteins bound to BV6. The BV6

Table 2 Bivalent pan-specific IAP antagonists

Compound	Structure	Status	Source	Refs.
JP1010	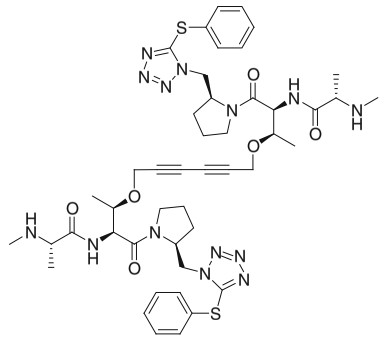	Preclinical	UT-Southwestern/Joyant	[74]
JP1400	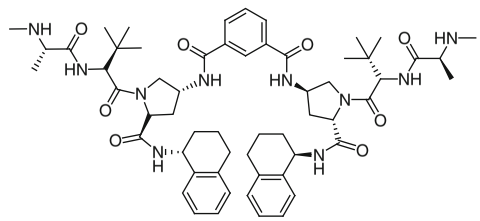	Preclinical	UT-Southwestern/Joyant	[75]
BV6	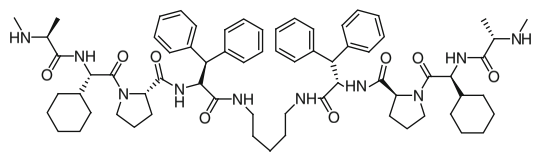	Preclinical	Genentech	[37]

(continued)

Table 2 (continued)

Compound	Structure	Status	Source	Refs.
SM-164	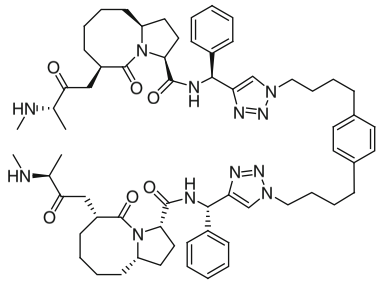	Preclinical	Michigan/Ascenta	[77]
TL32711	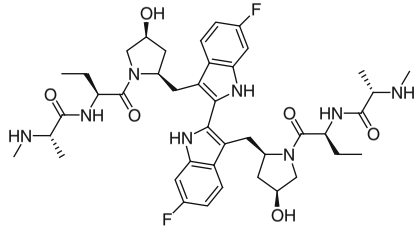	Phase I	Tetralogic	[45, 87]
AEG40826/HGS1029	NA	Phase I	Aegera/HGS	[85]

is approximately 300–400 times more potent than the monomer control MV1 in cellular assays (IC_{50} of 5 μM for MV1 vs. 14 nM for BV6 in EVSA-T cell). In a subsequent study published in 2009, BV6 in combination with a Death Receptor 5 agonist antibody synergistically inhibited tumor growth in a MDA-MB-231 *in vivo* xenograph model [77]. These data demonstrated that although bivalent IAP antagonists such as BV6 are larger than conventional pharmaceuticals, they possess sufficient druglike properties to exert impressive *in vitro* and *in vivo* anti-tumor activity.

In another important publication, Shaomeng Wang's group used gel filtration analysis to definitely demonstrate that bivalent version of their [7,5] bicyclic scaffold, SM-164, bound simultaneously to the BIR2 and BIR3 domains of a XIAP BIR2-BIR3 construct [78]. Mutation of key residues in the BIR2 domain led to a formation a 2:1 complex in which each of the two BIR2-BIR3 constructs bound to bivalent SM-164 via the BIR3 domain. NMR studies with labeled protein also conclusively demonstrated that SM-164 binds concurrently to the BIR2 and BIR3 domains of one XIAP protein. The potency of the bivalent compounds was 300 times more potent than the monomer control with an IC_{50} of 1.39 nM in HL-60 leukemia cells.

These papers along with other studies established that bivalent IAP antagonists are extremely potent in *in vivo* models due to higher binding affinity created by multiple binding contacts between bivalent molecule and protein. Examination of the pre-clinical evidence clearly points to the potential of both monovalent and bivalent Smac peptidiomimetcs as therapeutic agent. In order to develop the best therapeutic agent and drug regiment, we felt that we needed to determine the precise mechanism by which IAP antagonists promote cell death as single-agent compounds.

2.5 Mechanism of Action

We felt the best hope for creating the optimal drug and treatment regiment would be obtained by understanding what was happening to cells upon the introduction of the IAP antagonist. We reasoned that such information should help us identify biomarkers and allow us to make evidence based decisions on when and how to use IAP antagonist based therapeutics.

As discussed earlier, we began our investigation into IAP antagonists thinking IAP antagonists act primarily as XIAP and also ML-IAP antagonists. However, our results, including potent single agent activity, pointed to a more complex situation. Our model for activity changed drastically when, unexpectedly, we and other groups found that small-molecule IAP antagonist-induced apoptosis involves the induction of c-IAP1/2 autoubiquitination and proteasomal degradation. This, in turn, leads to the activation of NF-kB pathways and caspase-8-dependent apoptosis in tumor cells [35, 37, 40, 70, 79, 80]. For several years, it was not clear how

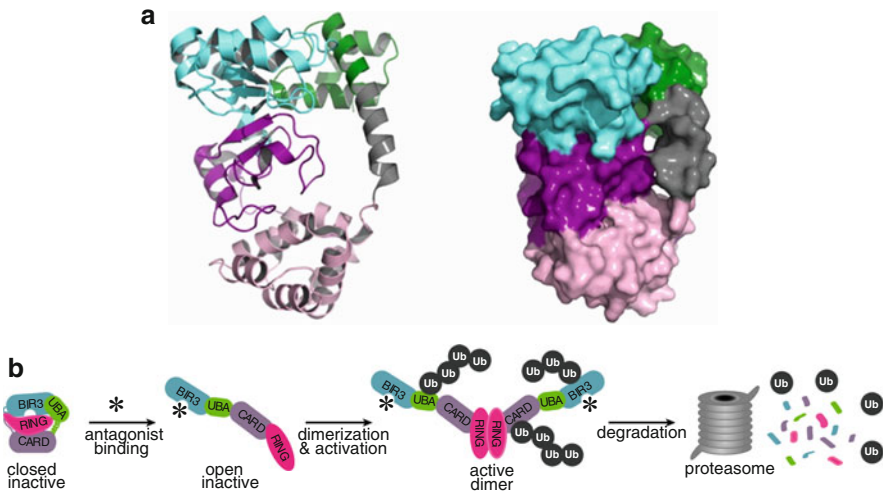

Fig. 6 Ubiquitin ligase activation model for c-IAP1. (**a**) Structure of apo c-IAP1 BIR3-RING. (**b**) Ubiquitin ligase activation model for c-IAP1 in which apo BIR3-RING exists predominantly in a closed, inactive monomer state. Antagonist binding to the BIR3 domain is not compatible with this conformation, and so leads to an open state where the RING domain is exposed and free to dimerize and form an active ubiquitin ligase

binding of IAP antagonists to the BIR3 domain of c-IAP proteins affects the activity of the c-IAP E3 ligase RING domain.

Recently published studies have shown that IAP antagonists promote dimer formation and that RING dimerization is essential for the E3 ligase activity of c-IAP proteins [81, 82]. The final piece of the puzzle was provided when it was demonstrated in an elegant biochemical and structural study that the unliganded, multi-domain c-IAP1 sequesters the RING domain within a compact, monomeric structure that blocks RING dimerization (Fig. 6) [83]. Binding of antagonists to the c-IAP1 BIR3 domain prevents critical BIR3-RING interactions inducing conformational rearrangements that allow RING dimerization and formation of the active E3 ligase (Fig. 6) [83].

IAP antagonist-induced activation of both the canonical and noncanonical NF-kB pathways leads to increased expression of NF-kB responsive gene TNFα. In the absence of c-IAP proteins, TNFa binding to TNFR1 triggers TNFR-mediated signaling, activation of caspase-8, and apoptosis [37, 40, 79] (Fig. 3). The application of TNF-blocking reagents or knockdown of TNFR1 inhibited IAP antagonist-stimulated apoptosis, thus revealing that small-molecule IAP antagonist-induced cell death requires TNF signaling [37, 40, 70, 79]. These studies have conclusively demonstrated that targeting IAP proteins with IAP antagonists results in heightened physiological TNF-receptor apoptotic signaling and apoptosis in tumor cells.

Table 3 c-IAP Selective Antagonist

Compound	Structure	Status	Source	Ref.
CS3	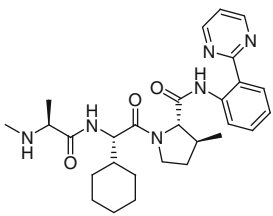 CS3	Preclinical	Genentech	[83]

2.6 *Peptidomimetics: c-IAP-Specific Monovalent*

With conclusive evidence for the role of c-IAP1 and c-IAP2 in the single-agent efficacy of IAP antagonists, we wondered about the necessity of also antagonizing XIAP; i.e., will a similar result be observed with a c-IAP selective molecule? We knew from our initial peptide work discussed in Sect. 2.2 that branched amino acids bound preferentially to c-IAP proteins over XIAP due to a tyrosine to phenylalanine substitution in P3. The addition of a β-methyl to proline in P3 yielded 200-fold selectivity for c-IAP over XIAP due to unfavorable interaction with the tyrosine in P3 of XIAP (see Sect. 2.2 for a more extensive discussion of SAR). The selectivity was increased to >2,000-fold when a c-IAP selective 2-pyrimidinyl group was included in the P4 position, which is speculated to have unfavorable electronic interactions with threonine 308 in the XIAP P4 binding pocket. The most selective compound CS3 is shown in Table 3 [84].

We found that although CS3 had single-agent activity, it was tenfold less efficacious than pan IAP-specific molecule with comparable binding affinity for c-IAP1, PS1. We believe this indicates that, in addition to NF-KB pathway activation and TNF production, more complete activation of caspases 3, 7, and 9 is required for the effective induction of apoptosis. For this reason, a pan-specific molecule is probably the best choice for the broadest range of efficacy.

3 Clinical Programs

An abundance of positive pre-clinical results has led to investigations of both monovalent and bivalent IAP antagonist in clinical studies [45]. By late 2011, six small molecule IAP antagonists were known to have begun Phase I clinical trials. The first molecule, Genentech's monovalent GDC-0152 entered the clinic in June 2007 [85], followed by the bivalent antagonist AEG40826/HGS-1029 co-developed by Human Genome Sciences and Aegera [86], and the monovalent

LCL-161 developed by Norvatis [87]. Soon after, Tetralogic entered Phase I trials with their bivalent antagonist TL3271 [88] and Genentech began clinical trials with another small molecule antagonist GDC-0917 [89], while Ascenta announced the initiation of Phase I trials with their diazabicycle monomer AT-406 in the spring of 2011 [90]. All of these molecules are believed to be pan-specific; so, it will activate the NF-κB pathway as well as promote caspase 9, 3 and 7 activation.

One difference between the monovalent and bivalent antagonists in the clinical setting is that bivalent antagonists are larger molecules and not orally bioavailable; therefore, this class of antagonists will most probably need to be intravenously administered no more than weekly. In contrast, monovalent antagonists can be administered orally and therefore dosing can be much more flexible. Whether the increased potency of the bivalent antagonist demonstrated in pre-clinical models [35, 37] is therapeutically preferable to the more flexibly dosed monovalent molecules is a question that can only be answered in a clinical setting. Another fundamental question pertains to combinations of IAP antagonists with other anti-tumor agents: death receptor agonists, standard of care chemotherapies, or targeted agents. This is a complex problem that will require a combination of clinical and pre-clinical data to establish the best therapeutic approach for distinct indications.

Importantly for the future prospects of small molecule IAP antagonists, the early results are promising. Norvartis reported that LCL161, a monovalent and orally bioavailable antagonist, is well-tolerated with no dose-limiting toxicities [87]. LCL161 evidenced IAP antagonism by causing c-IAP1 protein degradation as well as up regulation of NF-κB regulated cytokines IL-8 and MCP-1 [87]. Aegera/Human Genome Sciences and Tetralogic announced similar findings with their bivalent antagonists HGS1029 and TL32711 [45, 86, 88]. Both bivalent compounds were well tolerated with grade 2 transient lymphoma neutrophilia observed in some patients. As with the Norvartis compound, c-IAP1 levels decreased and MCP1 levels increased. Interestingly, serum processed caspase-3/7 levels were observed to increase at the highest cohort doses. The evidence to this point suggests that the pre-clinical models are valid and the expected biological response to IAP antagonism is occurring.

In order to select the optimal patient population, it will be important to identify predictive biomarkers. It is reasonable to believe c-IAP1 degradation could serve as an indicator of IAP activity, but not as a predictive marker. An increase in caspase 3 and 7 processing may be a valuable indicator of IAP protein antagonist efficacy, while TNFα levels could be the best measure of single-agent activity. It is also possible that other NF-κB regulated cytokines may prove to be useful biomarkers.

4 Conclusion

The biological rationale, preclinical evidence, and early clinical results demonstrate the potential for small-molecule IAP protein antagonists in the treatment of cancer. It has been gratifying for us to participate in an effort that has taken a program from

idea to clinical trial in under a decade. Challenges remain in the development of effective therapeutic combinations and regiments that will ultimately show sufficient benefit to patients so that small-molecule IAP antagonists will become an important agent in battling cancer. The identification of biomarkers that identify patients likely to respond to treatment, and select the most effective therapeutic regiment for that patient, would allow physicians to administer a personalized medicine approach for treatment. This approach has the greatest potential for consistent positive outcome for patients and could serve as a model for future approaches for the treatment of cancer.

References

1. Reed JC (2002) Apoptosis-based therapies. Nat Rev Drug Discov 1(2):111–121
2. Salvesen GS, Duckett CS (2002) IAP proteins: blocking the road to death's door. Nat Rev Mol Cell Biol 3(6):401–410
3. Varfolomeev E, Vucic D (2011) Inhibitor of apoptosis proteins: fascinating biology leads to attractive tumor therapeutic targets. Future Oncol 7(5):633–648
4. Miller LK (1999) An exegesis of IAPs: salvation and surprises from BIR motifs. Trends Cell Biol 9(8):323–328
5. Vaux DL, Silke J (2005) IAPs, RINGs and ubiquitylation. Nat Rev Mol Cell Biol 6(4):287–297
6. Vucic D, Dixit VM, Wertz IE (2011) Ubiquitylation in apoptosis: a post-translational modification at the edge of life and death. Nat Rev Mol Cell Biol 12(7):439–452
7. Blankenship JW, Varfolomeev E, Goncharov T et al (2009) Ubiquitin binding modulates IAP antagonist-stimulated proteasomal degradation of c-IAP1 and c-IAP2(1). Biochem J 417(1):149–160
8. Gyrd-Hansen M, Darding M, Miasari M et al (2008) IAPs contain an evolutionarily conserved ubiquitin-binding domain that regulates NF-kappaB as well as cell survival and oncogenesis. Nat Cell Biol 10(11):1309–1317
9. Hofmann K, Bucher P, Tschopp J (1997) The CARD domain: a new apoptotic signalling motif. Trends Biochem Sci 22(5):155–156
10. Varfolomeev E, Vucic D (2008) (Un)expected roles of c-IAPs in apoptotic and NF-κB signaling pathways. Cell Cycle 7(11):1511–1521
11. Hunter AM, LaCasse EC, Korneluk RG (2007) The inhibitors of apoptosis (IAPs) as cancer targets. Apoptosis 12(9):1543–1568
12. Salvesen GS, Abrams JM (2004) Caspase activation – stepping on the gas or releasing the brakes? Lessons from humans and flies. Oncogene 23(16):2774–2784
13. Kaufmann SH, Vaux DL (2003) Alterations in the apoptotic machinery and their potential role in anticancer drug resistance. Oncogene 22(47):7414–7430
14. Ashkenazi A, Dixit VM (1998) Death receptors: signaling and modulation. Science 281 (5381):1305–1308
15. Eckelman BP, Salvesen GS, Scott FL (2006) Human inhibitor of apoptosis proteins: why XIAP is the black sheep of the family. EMBO Rep 7(10):988–994
16. Chai J, Shiozaki E, Srinivasula SM et al (2001) Structural basis of caspase-7 inhibition by XIAP. Cell 104(5):769–780
17. Huang Y, Park YC, Rich RL et al (2001) Structural basis of caspase inhibition by XIAP: differential roles of the linker versus the BIR domain. Cell 104(5):781–790
18. Riedl SJ, Renatus M, Schwarzenbacher R et al (2001) Structural basis for the inhibition of caspase-3 by XIAP. Cell 104(5):791–800

19. Scott FL, Denault JB, Riedl SJ et al (2005) XIAP inhibits caspase-3 and -7 using two binding sites: evolutionarily conserved mechanism of IAPs. EMBO J 24(3):645–655
20. Suzuki Y, Nakabayashi Y, Nakata K et al (2001) X-linked inhibitor of apoptosis protein (XIAP) inhibits caspase-3 and -7 in distinct modes. J Biol Chem 276(29):27058–27063
21. Shiozaki EN, Chai J, Rigotti DJ et al (2003) Mechanism of XIAP-mediated inhibition of caspase-9. Mol Cell 11(2):519–527
22. Srinivasula SM, Hegde R, Saleh A et al (2001) A conserved XIAP-interaction motif in caspase-9 and Smac/DIABLO regulates caspase activity and apoptosis. Nature 410(6824):112–116
23. Du C, Fang M, Li Y et al (2000) Smac, a mitochondrial protein that promotes cytochrome c-dependent caspase activation by eliminating IAP inhibition. Cell 102(1):33–42
24. Verhagen AM, Ekert PG, Pakusch M et al (2000) Identification of DIABLO, a mammalian protein that promotes apoptosis by binding to and antagonizing IAP proteins. Cell 102(1):43–53
25. Burri L, Strahm Y, Hawkins CJ et al (2005) Mature DIABLO/Smac is produced by the IMP protease complex on the mitochondrial inner membrane. Mol Biol Cell 16(6):2926–2933
26. Liu Z, Sun C, Olejniczak ET et al (2000) Structural basis for binding of Smac/DIABLO to the XIAP BIR3 domain. Nature 408(6815):1004–1008
27. Wu G, Chai J, Suber TL et al (2000) Structural basis of IAP recognition by Smac/DIABLO. Nature 408(6815):1008–1012
28. Vucic D, Deshayes K, Ackerly H et al (2002) SMAC negatively regulates the anti-apoptotic activity of Melanoma Inhibitor of Apoptosis (ML-IAP). J Biol Chem 277(14):12275–12279
29. Vucic D, Fairbrother WJ (2007) The inhibitor of apoptosis proteins as therapeutic targets in cancer. Clin Cancer Res 13(20):5995–6000
30. Vucic D (2008) Targeting IAP (inhibitor of apoptosis) proteins for therapeutic intervention in tumors. Curr Cancer Drug Targets 8(2):110–117
31. Verhagen AM, Kratina TK, Hawkins CJ et al (2007) Identification of mammalian mitochondrial proteins that interact with IAPs via N-terminal IAP binding motifs. Cell Death Differ 14(2):348–357
32. Liston P, Fong WG, Kelly NL et al (2001) Identification of XAF1 as an antagonist of XIAP anti-caspase activity. Nat Cell Biol 3(2):128–133
33. Chen G, Goeddel DV (2002) TNF-R1 signaling: a beautiful pathway. Science 296(5573):1634–1635
34. Varfolomeev E, Goncharov T, Fedorova AV et al (2008) c-IAP1 and c-IAP2 are critical mediators of Tumor Necrosis Factor alpha (TNFα)-induced NF-κB activation. J Biol Chem 283(36):24295–24299
35. Bertrand MJ, Milutinovic S, Dickson KM et al (2008) cIAP1 and cIAP2 facilitate cancer cell survival by functioning as E3 ligases that promote RIP1 ubiquitination. Mol Cell 30(6):689–700
36. Dynek JN, Goncharov T, Dueber EC et al (2010) c-IAP1 and UbcH5 promote K11-linked polyubiquitination of RIP1 in TNF signalling. EMBO J 29(24):4198–4209
37. Varfolomeev E, Blankenship JW, Wayson SM et al (2007) IAP antagonists induce autoubiquitination of c-IAPs, NF-κB activation, and TNFα-dependent apoptosis. Cell 131(4):669–681
38. Mahoney DJ, Cheung HH, Mrad RL et al (2008) Both cIAP1 and cIAP2 regulate TNFalpha-mediated NF-kappaB activation. Proc Natl Acad Sci USA 105(33):11778–11783
39. Haas TL, Emmerich CH, Gerlach B et al (2009) Recruitment of the linear ubiquitin chain assembly complex stabilizes the TNF-R1 signaling complex and is required for TNF-mediated gene induction. Mol Cell 36(5):831–844
40. Vince JE, Wong WW, Khan N et al (2007) IAP antagonists target cIAP1 to induce TNFalpha-dependent apoptosis. Cell 131(4):682–693
41. Schile AJ, Garcia-Fernandez M, Steller H (2008) Regulation of apoptosis by XIAP ubiquitin-ligase activity. Genes Dev 22(16):2256–2266

42. Hu S, Yang X (2003) Cellular inhibitor of apoptosis 1 and 2 are ubiquitin ligases for the apoptosis inducer Smac/DIABLO. J Biol Chem 278(12):10055–10060
43. MacFarlane M, Merrison W, Bratton SB et al (2002) Proteasome-mediated degradation of Smac during apoptosis: XIAP promotes Smac ubiquitination in vitro. J Biol Chem 277(39):36611–36616
44. Wright CW, Duckett CS (2008) New insights into the function of IAP proteins: modulation of the MYC/MAX/MAD network. Dev Cell 14(1):3–4
45. Fulda S, Vucic D (2012) Targeting IAP proteins for therapeutic intervention in cancer. Nat Rev Drug Discov 11:109–124
46. Vucic D, Stennicke HR, Pisabarro MT et al (2000) ML-IAP, a novel inhibitor of apoptosis that is preferentially expressed in human melanomas. Curr Biol 10(21):1359–1366
47. Gong J, Chen N, Zhou Q et al (2005) Melanoma inhibitor of apoptosis protein is expressed differentially in melanoma and melanocytic naevus, but similarly in primary and metastatic melanomas. J Clin Pathol 58(10):1081–1085
48. Gazzaniga P, Gradilone A, Giuliani L et al (2003) Expression and prognostic significance of LIVIN, SURVIVIN and other apoptosis-related genes in the progression of superficial bladder cancer. Ann Oncol 14(1):85–90
49. Kempkensteffen C, Hinz S, Christoph F et al (2007) Expression of the apoptosis inhibitor livin in renal cell carcinomas: correlations with pathology and outcome. Tumour Biol 28(3):132–138
50. Crnkovic-Mertens I, Wagener N, Semzow J et al (2007) Targeted inhibition of Livin resensitizes renal cancer cells towards apoptosis. Cell Mol Life Sci 64(9):1137–1144
51. Dynek JN, Chan SM, Liu J et al (2008) Microphthalmia-associated transcription factor is a critical transcriptional regulator of melanoma inhibitor of apoptosis in melanomas. Cancer Res 68(9):3124–3132
52. Hu Y, Cherton-Horvat G, Dragowska V et al (2003) Antisense oligonucleotides targeting XIAP induce apoptosis and enhance chemotherapeutic activity against human lung cancer cells in vitro and in vivo. Clin Cancer Res 9(7):2826–2836
53. Sasaki H, Sheng Y, Kotsuji F et al (2000) Down-regulation of X-linked inhibitor of apoptosis protein induces apoptosis in chemoresistant human ovarian cancer cells. Cancer Res 60(20):5659–5666
54. Bilim V, Kasahara T, Hara N et al (2003) Role of XIAP in the malignant phenotype of transitional cell cancer (TCC) and therapeutic activity of XIAP antisense oligonucleotides against multidrug-resistant TCC in vitro. Int J Cancer 103(1):29–37
55. McManus DC, Lefebvre CA, Cherton-Horvat G et al (2004) Loss of XIAP protein expression by RNAi and antisense approaches sensitizes cancer cells to functionally diverse chemotherapeutics. Oncogene 23(49):8105–8117
56. Ryan BM, O'Donovan N, Duffy MJ (2009) Survivin: a new target for anti-cancer therapy. Cancer Treat Rev 35(7):553–562
57. LaCasse EC, Mahoney DJ, Cheung HH et al (2008) IAP-targeted therapies for cancer. Oncogene 27(48):6252–6275
58. Zender L, Spector MS, Xue W et al (2006) Identification and validation of oncogenes in liver cancer using an integrative oncogenomic approach. Cell 125(7):1253–1267
59. Akagi T, Motegi M, Tamura A et al (1999) A novel gene, MALT1 at 18q21, is involved in t(11;18) (q21;q21) found in low-grade B-cell lymphoma of mucosa-associated lymphoid tissue. Oncogene 18(42):5785–5794
60. Dierlamm J, Baens M, Stefanova-Ouzounova M et al (2000) Detection of t(11;18)(q21;q21) by interphase fluorescence in situ hybridization using API2 and MLT specific probes. Blood 96(6):2215–2218
61. Dierlamm J, Baens M, Wlodarska I et al (1999) The apoptosis inhibitor gene API2 and a novel 18q gene, MLT, are recurrently rearranged in the t(11;18)(q21;q21)p6ssociated with mucosa-associated lymphoid tissue lymphomas. Blood 93(11):3601–3609

62. Morgan JA, Yin Y, Borowsky AD et al (1999) Breakpoints of the t(11;18)(q21;q21) in mucosa-associated lymphoid tissue (MALT) lymphoma lie within or near the previously undescribed gene MALT1 in chromosome 18. Cancer Res 59(24):6205–6213
63. Imoto I, Yang ZQ, Pimkhaokham A et al (2001) Identification of cIAP1 as a candidate target gene within an amplicon at 11q22 in esophageal squamous cell carcinomas. Cancer Res 61(18):6629–6634
64. Imoto I, Tsuda H, Hirasawa A et al (2002) Expression of cIAP1, a target for 11q22 amplification, correlates with resistance of cervical cancers to radiotherapy. Cancer Res 62(17):4860–4866
65. Isaacson PG (2005) Update on MALT lymphomas. Best Pract Res Clin Haematol 18(1):57–68
66. Fulda S, Wick W, Weller M et al (2002) Smac agonists sensitize for Apo2L/TRAIL- or anticancer drug-induced apoptosis and induce regression of malignant glioma in vivo. Nat Med 8(8):808–815
67. Arnt CR, Chiorean MV, Heldebrant MP et al (2002) Synthetic Smac/DIABLO peptides enhance the effects of chemotherapeutic agents by binding XIAP and cIAP1 in situ. J Biol Chem 277(46):44236–44243
68. Franklin MC, Kadkhodayan S, Ackerly H et al (2003) Structure and function analysis of peptide antagonists of melanoma inhibitor of apoptosis (ML-IAP). Biochemistry 42(27):8223–8231
69. Oost TK, Sun C, Armstrong RC et al (2004) Discovery of potent antagonists of the antiapoptotic protein XIAP for the treatment of cancer. J Med Chem 47(18):4417–4426
70. Gaither A, Porter D, Yao Y et al (2007) A Smac mimetic rescue screen reveals roles for inhibitor of apoptosis proteins in tumor necrosis factor-alpha signaling. Cancer Res 67(24):11493–11498
71. Zobel K, Wang L, Varfolomeev E et al (2006) Design, synthesis, and biological activity of a potent Smac mimetic that sensitizes cancer cells to apoptosis by antagonizing IAPs. ACS Chem Biol 1(8):525–533
72. Sun H, Nikolovska-Coleska Z, Lu J et al (2006) Design, synthesis, and evaluation of a potent, cell-permeable, conformationally constrained second mitochondria derived activator of caspase (Smac) mimetic. J Med Chem 49(26):7916–7920
73. Sun H, Nikolovska-Coleska Z, Yang CY et al (2004) Structure-based design of potent, conformationally constrained Smac mimetics. J Am Chem Soc 126(51):16686–16687
74. Sun H, Nikolovska-Coleska Z, Yang CY et al (2008) Design of small-molecule peptidic and nonpeptidic Smac mimetics. Acc Chem Res 41(10):1264–1277
75. Li L, Thomas RM, Suzuki H et al (2004) A small molecule Smac mimic potentiates TRAIL- and TNFα-mediated cell death. Science 305(5689):1471–1474
76. Probst BL, Liu L, Ramesh V, Li L, Sun H, Minna JD, Wang L (2010) Smac mimetics increase cancer cell response to chemotherapeutics in a TNF-α-dependent manner. Cell Death Differ 17(10):9
77. Varfolomeev E, Alicke B, Elliott JM et al (2009) X chromosome-linked inhibitor of apoptosis regulates cell death induction by proapoptotic receptor agonists. J Biol Chem 284 (50):34553–34560
78. Sun H, Nikolovska-Coleska Z, Lu J et al (2007) Design, synthesis, and characterization of a potent, nonpeptide, cell-permeable, bivalent Smac mimetic that concurrently targets both the BIR2 and BIR3 domains in XIAP. J Am Chem Soc 129(49):15279–15294
79. Petersen SL, Wang L, Yalcin-Chin A et al (2007) Autocrine TNFalpha signaling renders human cancer cells susceptible to smac-mimetic-induced apoptosis. Cancer Cell 12(5):445–456
80. Wang L, Du F, Wang X (2008) TNF-alpha induces two distinct caspase-8 activation pathways. Cell 133(4):693–703
81. Feltham R, Bettjeman B, Budhidarmo R et al (2011) Smac mimetics activate the E3 ligase activity of cIAP1 protein by promoting RING domain dimerization. J Biol Chem 286(19):17015–17028

82. Mace PD, Linke K, Feltham R et al (2008) Structures of the cIAP2 RING domain reveal conformational changes associated with ubiquitin-conjugating enzyme (E2) recruitment. J Biol Chem 283(46):31633–31640
83. Wertz IE, Kusam S, Lam C et al (2011) Sensitivity to antitubulin chemotherapeutics is regulated by MCL1 and FBW7. Nature 471(7336):110–114
84. Ndubaku C, Varfolomeev E, Wang L et al (2009) Antagonism of c-IAP and XIAP proteins is required for efficient induction of cell death by small-molecule IAP antagonists. ACS Chem Biol 4(7):557–566
85. Genentech (2007) A study of the safety and pharmacokinetics of GDC-0152, administered intravenously to patients with locally advanced or metastatic malignancies. http://clinicaltrialsfeeds.org/clinical-trials/show/NCT00977067.
86. Sikic BI, Eckhardt SG, Gallant G, et al (2011) Safety, pharmacokinetics (PK), and pharmacodynamics (PD) of HGS1029, an inhibitor of apoptosis protein (IAP) inhibitor, in patients (Pts) with advanced solid tumors: results of a phase I study. In: 2011 annual ASCO meeting, Chicago, IL
87. Infante JR, Dees EC, Burris HA III, et al (2010) A phase I study of LCL-161, an oral IAP inhibitor, in patients with advanced cancer. In: The annual meeting of the American Association for Cancer Research, Washington, DC
88. Amaravadi RK, Schilder RJ, Dy GK, et al (2011) Phase 1 study of the smac mimetic TL32711 in adult subjects with advanced solid tumors & lymphoma to evaluate safety, pharmacokinetics, pharmacodynamics and anti-tumor activity. In: 2011 annual AACR conference, Orlando, FL
89. Genentech (2010) I. A study evaluating the safety, tolerability and pharmacokinetics of GDC-0917 administered to patients with refractory solid tumors or lymphoma. http://clinicaltrialsfeeds.org/clinical-trials/show/NCT01226277.
90. Cai Q, Sun H, Peng Y et al (2011) A potent and orally active antagonist (SM-406/AT-406) of multiple inhibitor of apoptosis proteins (IAPs) in clinical development for cancer treatment. J Med Chem 54(8):2714–2726

Top Med Chem 8: 105–166
DOI: 10.1007/978-3-642-28965-1_4

Protein-Protein Interaction Targets to Inhibit HIV-1 Infection

John F. Kadow, David R. Langley, Nicholas A. Meanwell, Richard Pracitto, Michael A. Walker, and Kap-Sun Yeung

Contents

J.F. Kadow (✉) • N.A. Meanwell • R. Pracitto • M.A. Walker • K.-S. Yeung
Department of Medicinal Chemistry, Bristol-Myers Squibb Research and Development, 5 Research Parkway, Wallingford, CT 06492, USA
e-mail: john.kadow@bms.com; Nicholas.Meanwell@bms.com

D.R. Langley
Department of Computer-Aided Drug Design, Bristol-Myers Squibb Research and Development, 5 Research Parkway, Wallingford, CT 06492, USA

Abstract Efforts to interfere with four key protein-protein interactions in the HIV-1 lifecycle with the goal of achieving clinically-relevant, orally administered HIV-1 therapies are reviewed. These four targets: the HIV-1 gp120/human CD4 interaction, the HIV-1 gp41 six-helix bundle formation, the human LEDGF/p75-integrase interaction, and HIV-1 protease dimerization each present unique challenges to the discovery of viable small molecule inhibitors. Background information from the literature is provided. A class of inhibitors which target gp120 from which an orally dosed member has been advanced into Phase II clinical studies as well as other small molecule approaches to disrupt the gp120/CD4 interaction are discussed. The unrealized efforts to find a small-molecule inhibitor of gp41 six-helix bundle formation that is suitable for clinical studies are described, including a summary of the work on effective, peptidic inhibitors that lack the properties needed for oral use. An overview of the progress to identify small molecule inhibitors of the LEDGF/HIV-1 p75-integrase interaction and the dimerization of the HIV-1 protease enzyme describes the preclinical compounds of greatest interest and discusses the rationale behind their design/activity.

Keywords CD4 • Entry inhibitor • gp41 • gp120 • HIV-1 • LEDGF • Protease • Protein-protein interaction

1 Introduction

The human immunodeficiency virus-1 (HIV-1) causes depletion of $CD4^+$-lymphocytes in infected individuals which ultimately leads to acquired immunodeficiency syndrome (AIDS) in the absence of highly active antiretroviral therapy (HAART) [1]. Considerable progress has been made in effectively controlling viremia in HIV-1-infected patients using oral combination antiretroviral therapy; however, efforts to realize a cure for this disease remain unrealized [2, 3]. There is an increasing population of patients, even among those characterized as responders, whose medical needs are not completely satisfied by current therapy [4]. Mechanistically distinct, non cross-resistant drugs are still needed to address the increasing occurrence of drug-resistant strains and the emergence of comorbidities associated with long-term HAART [3]. Antiviral agents and oral fixed-dose combinations that span six mechanistic classes are now available for use in the treatment of HIV-1 infection, so many of the targets that are the most obviously amenable to small molecule drug discovery efforts have been explored [5–7]. However, a number of opportunities for realizing mechanistically novel agents remain. Four of these possibilities that do not yet have small molecule inhibitors approved for clinical use would require the disruption of protein-protein interactions (PPIs) to achieve inhibition of HIV-1 infection. The current status of research aimed at exploiting these targets and their particular challenges with an emphasis on attaining small molecules for oral use are described in this chapter.

2 HIV gp120-CD4

2.1 Background and Mechanism

HIV-1 gains entry into cells via a multistep process, each of which is dependent on protein-protein interactions [8, 9]. Presumably in order to better evade host immune responses, HIV-1 has developed additional structural features, an exacting choreography, and the presence of additional steps when compared to other viruses in order to effect viral entry [10]. The virus protein gp160 is encoded by the env gene and is cleaved post-translationally to gp120 and gp41 [11]. A small-molecule inhibitor of this processing with low single digit μM EC_{50}s was reported in 2007 [12], but this mode of intervention has received little additional attention.

Viral spikes on the surface of the HIV-1 virion are used by the virus to gain entry into human cells [13]. These spikes are composed of three gp120 envelope glycoproteins non-covalently bound to three gp41 transmembrane, fusion proteins in a trimeric topology. Several protein crystal structures of truncated/modified gp120 bound to a D1D2 fragment of CD4 and an antibody have been obtained [13–16]. A crystal structure of unliganded and fully glycosylated simian immunodeficiency virus gp120 has also been published [17, 18]. Sequence analysis of HIV-1 isolates has determined that gp120 contains five highly glycosylated variable regions, designated V1–V5, interspersed with five conserved regions, C1–C5. Intramolecular disulfide bonding in V1–V4 results in loop formation and C1–C5 fold to form the gp120 core. The gp120 proteins reside completely outside of the viral membrane while gp41 contains a cytoplasmic domain, a membrane-spanning domain, and an extracellular domain that is used to effect the conformational changes that lead to host cell-virus membrane fusion [11]. The majority of the exposed surfaces of the viral spike consist of the variable regions of gp120 or of carbohydrates covalently attached to gp120, the so-called glycan shield. In addition, gp120 is a highly flexible protein and studies have shown that a large number, possibly up to 50%, of unstructured residues are present in unliganded gp120 [19]. In the initial step of viral entry, the gp120 viral envelope binds in a specific manner to the human CD4 protein which is expressed to differing degrees on human T-lymphocytes, monocytes, dendritic cells, and brain microglia, which appear to be the main target cells of primate immunodeficiency viruses [10]. As a result of binding to CD4, the conformation of bound gp120 changes significantly and up to 130 residues in the gp120 become structured [19]. This conformational change assembles and organizes a co-receptor binding region on gp120 (the top and an area around the base of the V3 loop) and many of the newly structured residues of gp120 are in this region [20]. The more structured co-receptor binding region can then engage a co-receptor on the surface of the host cell with significantly enhanced affinity. This conformation of gp120 is frequently referred to as the CD4-bound conformation. The cell surface proteins of lymphocytes most often used as co-receptors are the G-protein coupled chemokine receptors CCR5 and CXCR4. Co-receptor binding leads to further conformational changes

and causes gp41 to rearrange into a trimeric coiled-coil that allows the hydrophobic gp41 amino terminus (the fusion protein) to insert into the cell membrane and initiate viral envelope-cell fusion which ultimately leads to delivery of the viral core to the cytoplasm of the host lymphocyte. Agents which are able to prevent successful execution of any of these steps are collectively characterized as HIV-1 entry inhibitors and a plethora of reviews have appeared on the subject, of which only a few are cited here [8, 9, 21–29]. At the time of writing, no approved drug exists which acts by inhibiting the initial attachment step of the entry process. An approved CCR5 co-receptor antagonist maraviroc (marketed as SELZENTRY®) and a fusion inhibitor enfuvirtide (marketed as FUZEON®) are available to patients [5, 8, 9].

To avoid the host humoral immune response, it is believed that HIV-1 gp120 has evolved to acquire a high level of glycosylation on exposed surfaces, present surface-exposed variable loops, possess significant conformational flexibility, and locate conserved regions in recessed surfaces [30, 31]. In addition, other strategies by which gp120 may reduce the effectiveness of antibody-mediated immune activation have been proposed [32]. CD4 consists of an extracellular region of 370 amino acid residues organized into four domains (D1–D4), with the HIV-1 binding site of CD4 being localized to D1, centered around residues 40–48. Bound CD4 binds into a recessed region on gp120 and the majority of the affinity is due to electrostatic interactions. In contrast to gp120, the conformation of CD4 changes little after binding.

The gp120/CD4 interface has been estimated to bury 802 $Å^2$ from gp120 and 742 $Å^2$ from CD4 [14]. The size of this interaction might suggest that it would be difficult to inhibit with a small molecule; however, the numbers are somewhat misleading since the surfaces are highly irregular and mismatched over much of that area. There are direct interatomic contacts between 22 CD4 and 26 gp120 amino acid residues that are distributed over the length of gp120. Protein crystal structures of ternary complexes of CD4 bound to truncated gp120 and antibodies along with mutational studies have identified Phe43 and Arg59 as key elements on CD4 that bind to gp120 [11, 14]. Phe43, located on a beta turn of CD4, binds into the opening of a pocket formed from conserved regions of gp120 in a manner that can be visualized as a lid and which is surrounded by the inner core domain, the variable outer domain and a bridging β-sheet. In the CD4-bound conformation, this Phe43 pocket, as it is commonly referred to, extends about 10 Å into the interior of gp120 and has a volume of about 153 $Å^3$, and is positioned critically at a site where all three regions of gp120 meet. In addition, this binding pocket is connected to a water-filled channel that extends to the gp120 surface. Arg59 of CD4 binds electrostatically to Asp368 on an adjacent α-helix and while it has been shown to be important to the interaction, fully 23% of the binding interactions between the two proteins is attributed to interactions between the CD4 Phe43 and residues on gp120 (Glu370, Ile371, Asn425, Met426, Trp427,

Gly473, and Asp368). The conserved CD4 Phe43 binding pocket of gp120 has frequently been proposed as a potential target for inhibitor binding by either macromolecules or small molecule inhibitors [33]. The binding of CD4 has been determined to be an enthalpy-driven process which overcomes the high entropy cost incurred by the significant structural rearrangement and considerable restriction of the conformational entropy of gp120 upon association with CD4 [34]. Isothermal titration calorimetry measurements shows the favorable enthalpy and unfavorable entropy changes to be $\Delta H = 63$ kcal/mol and $T\Delta S = 52$ kcal/mol, respectively. It may seem somewhat surprising that such a small interaction could be a key driver of a highly enthalpic driven process which overcomes significant entropy since these values would be more typical of an interaction covering $10{,}000 \pm 2{,}000$ Å^2, but the gp120 protein has evolved to be poised to adopt a conformation close to the CD4-bound conformation and considerable intramolecular interactions are formed during conformational rearrangement [34].

Occupation of the Phe43 binding pocket can trigger conformational changes. For example, mutation of Ser375, a key residue lining the pocket, to a tryptophan results in the Trp375 occupying some of the volume of the pocket. This gp120 mutant exists in a conformation highly similar to that of the gp120-CD4 bound conformation [35]. Without occupation of the Phe43 binding pocket, free gp120 has been estimated to sample a CD4-binding conformation only about 12–15% of the time [36], which agrees with the observation that transmission of HIV-1 without CD4 binding is extremely rare. However, a larger CD4-mimetic protein with a Phe43 mutation was still able to induce a conformation that could be used by CCR5, albeit with reduced affinity [37]. This propensity to switch conformations is highly evolved and delicately balanced. Support for this observation comes from some laboratory viruses that have been produced which exist in a conformation similar to the CD4-bound state and are able to infect CD4-negative cell lines. Mutation of a single residue, H66N, in HIV-1 viruses able to infect CD4-deficient cells results in a gp120 that adopts a CD4-bound conformation less frequently and reverts the virus to a CD4-dependent phenotype [38]. In addition, this same mutation in the context of a CD4-dependent virus reduces susceptibility to small molecule compounds (*vide infra*) that act by eliciting a CD4-bound conformation. Interestingly, this mutation has only a minimal effect on the binding potency of CD4 itself. Clearly, there is a range in the degree of difficulty associated with the inhibition of protein-protein interactions but, because gp120 has evolved to exist in a conformation poised to be triggered by a binding event that occurs in a relatively small, concentrated, and conserved area of the protein that is located at the point where the three main regions come together, this protein-protein interaction appears to be vulnerable to intervention by small-molecule inhibitors. If the interactions were a simple lock-and-key-type between two proteins over a large area, it would likely not be as susceptible to inhibition.

2.2 *Small-Molecule Inhibitors of HIV gp120/CD4 Targeting gp120*

A series of ketopiperazinamide-based small molecule inhibitors that bind to gp120 and capture a conformation that interferes with its ability to productively interact with CD4 have been discovered and, to date, represent the most progress made towards realizing an orally bioavailable compound that blocks viral entry at the initial attachment stage [39–41]. Detailed accounts reviewing the discovery and progression of these attachment inhibitors (AIs) have appeared so this review will concentrate on describing the key events and strategic decisions made in the history of the progression of these small molecule inhibitors [26–29].

A mechanistically unbiased, cell-based screen using infectious HIV-1 was used to interrogate a collection of >100,000 compounds at Bristol-Myers Squibb. Hits were triaged based on cytotoxicity, selectivity for inhibition of HIV-1 vs. other viruses, potency, and mode of action. A number of non-nucleoside reverse transcriptase inhibitors (NNRTIs) were discarded, leaving one compound of interest, obtained from a commercially available library, which displayed a novel profile. Indole **1** displayed an EC_{50} of 153 nM in a pseudotyped virus assay and was not overtly cytotoxic to eight cell lines. The compound inhibited both M- and T-cell HIV-1 infection independent of co-receptor usage. Activity was determined to be exerted early in the virus life cycle prior to reverse transcription. The compound was shown to inhibit infection by virions packaged with the HIV-1 envelope and not those expressing an envelope from vesicular stomatitis virus (VSV). Encouraged by these and other mechanistic studies, an early discovery chemistry effort was initiated.

Initial studies systematically surveyed changes in single regions of the molecule while the remainder of the structure was held constant. Combinatorial chemistry was employed where feasible, especially in the early stages of SAR development. Indole substitution, piperazine modifications, and benzamide substitution were extensively explored [42–44]. These initial SAR studies established that a significant increase in potency could be realized by substitution at the indole 4-position with halogens, particularly fluorine, or a methoxy group, while larger substituents were detrimental. Changes in other regions of the molecule in these initial studies did not immediately provide significant benefit. Fluoroindole **2** proved to be a potent HIV-1 inhibitor with a low, single digit EC_{50} value in a pseudotype assay which represented a potency enhancement of about 64-fold from the addition of the single fluorine atom to **1** [42, 43]. The reason for this remarkable enhancement in potency is still not clear at a molecular level but illustrates the significant effects that can be gleaned by subtle changes in substitution. Poor solubility properties precluded advancement of **2** beyond initial pharmacokinetic studies and greater metabolic stability was deemed desirable. The four possible azaindole regioisomers **4**–**7** were prepared in the context of a common, unsubstituted core background and compared to the corresponding indole analog **3** (Scheme 1) [45]. The 5-azaindole **5** lost considerable potency, the 6-azindole **6** showed a modest five-fold loss in potency, and both

the 4-azaindole **4** and the 7-azaindole **7** appeared equipotent when compared to the parent indole in pseudotype virus assays. All of the azaindoles displayed improved profiles in assays that assessed drug-like properties, including solubility and metabolic stability. The commercial availability of 7-azaindole accelerated the optimization of this regioisomeric series which initially progressed most rapidly.

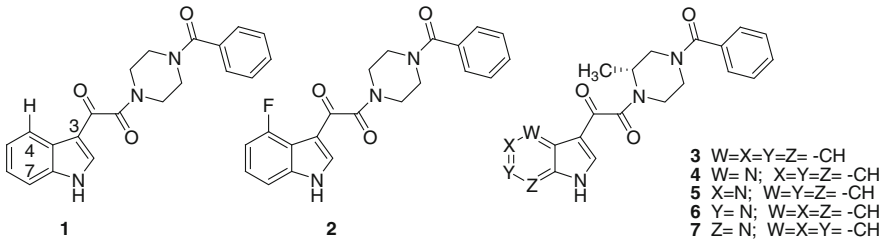

Using the SAR established in the indole series, the optimized 7-azaindole **8** (BMS-378806) was identified and the preclinical profile was determined to have the potential to explore proof-of-concept for this novel class of inhibitors in the clinic [46, 47]. Following pre-IND safety studies, the molecule was advanced to clinical trials in healthy volunteers but, unfortunately, the exposure of the compound was deemed insufficient to justify additional studies and development was discontinued [47, 48]. Efforts to improve on **8** were initiated prior to the availability of clinical feedback and focused on improving Caco-2 permeability, which was a modest 51 nm/s for BMS-378806 (**8**), and in vitro microsomal half-life, which predicted for intermediate clearance in humans [49]. Caco-2 permeability, tested at a drug concentration of 200 μM, was placed at the front of the preclinical evaluation tier along with rat and human liver microsomal half-life screens. These assays allowed the program to rapidly identify compounds with the potential for high absorption and low clearance, respectively, and to quickly eliminate all others from consideration. Among the avenues explored, optimization of the 6-azaindole core was pursued since the five-fold reduced potency seen in the comparison to the corresponding indole was believed to be small enough to be overcome by proper substitution during optimization. From the initial assays, BMS-488043 (**9**) emerged as a lead, with an improved Caco-2 permeability of 178 nm/s and a microsomal half-life predictive of a low clearance (4 mL/min/kg) in humans. In vivo, PK data conformed to predictions of the in vitro assays and was promising. The oral bioavailability of **9** in rats, dogs, and monkeys was 90%, 57%, and 60%, respectively. The clearance was low in all species, with terminal half-lives ranging from 2.4 to 4.7 h. BMS-488043 (**9**) displayed a 6–12-fold improvement in oral exposure in rats and monkeys compared to the prototype **8**. Predictions of the human pharmacokinetic profile suggested that after a 100 mg dose, the oral bioavailability would be 60% and that the AUC of **9** would be 5.1 μg/mL which were ~10-fold higher than from a similar dose projection done for **8**. As noted below, the human oral exposure of **9** actually proved to be >15-fold higher than that of **8**. Compound **9** was found to have modestly enhanced potency vs. a panel of B clade viruses while physicochemical properties, including measured pK_as and log D, were

very similar when compared to **8**. However, the improved permeability and metabolic stability of **9** came at a cost, as the compound displayed reduced aqueous solubility (0.40 mg/mL vs. 0.17 mg/mL for **8** at pH 6.5) and a higher protein binding in human plasma, 95.1% for **9** vs. 73% for **8**. The compound was advanced to clinical trials following successful pre-IND safety studies.

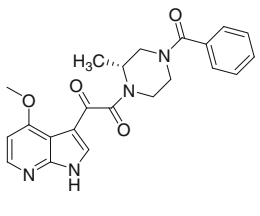

8
EC_{50} = 0.75 nM
EC_{50} Panel of B Clade Clin. Isolates = 61.5 nM

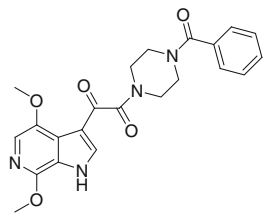

9
EC_{50} = 0.76 nM
EC_{50} Panel of B Clade Clin. Isolates = 36.5 nM

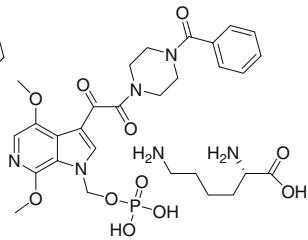

10

The antiviral activity, safety, and tolerability of BMS-488043 (**9**) were evaluated in a multiple ascending dose study conducted in 30 HIV-1-infected adult subjects. Doses of 800 and 1,800 mg or placebo control (4:1, respectively) were administered orally twice daily in combination with a high fat meal for 8 days, with daily viral load (VL) monitoring for up to 14 days [50, 51]. Placebo-treated subjects, as might be anticipated, showed little change, with all displaying a VL reduction of <0.4 $\log_{10}$. However, at the 1,800 mg dose of **9**, 67% (8/12) of subjects experienced a VL decline of >1.0 $\log_{10}$ with 42% (5/12) having a VL decline >1.5 $\log_{10}$. There were no serious adverse events, no discontinuations from the study, and overall the compound was well tolerated. Analysis of the results showed that a lower baseline, 50% effective concentration (EC_{50}) of **9** in the non-placebo subjects was predictive of a greater antiviral response. Trough concentration (C_{trough}), adjusted by the baseline EC_{50} (C_{trough}/EC_{50}), was associated with antiviral activity even though absolute levels of drug alone did not associate with activity. Assessment of virus sensitivity to **9** was performed at baseline and post-dosing on day 8 [52]. These analyses revealed that baseline EC_{50}s were high in four subjects (>200 nM) and phenotypic resistance had emerged during treatment in four of subjects (a 50% effective concentration [EC_{50}] shift of >10-fold greater than from the baseline value). Resistance to **9** was associated with five mutations in gp120 at four residues, V68A, L116I, S375I/N, and M426L, which were detected by population sequencing and sequence determination of cloned envelope genes [52]. The most common mutation, identified in 5/8 subjects at day 8, was at amino acid 375, which is located near the CD4 binding pocket.

An additional subject from the 800 mg cohort treated with BMS-488043 (**9**) did not display an antiviral response and EC_{50}s for the baseline and day 8 samples from this subject in the phenotyping assay were 66 and 358 nM, respectively, which did not meet the criteria for emergent or preexisting resistance mentioned above. This patient was infected with an HIV-1 strain that contained S375N at both the baseline and day 8 assay points, and this was attributed to be the most likely reason for the

poor antiviral response in the absence of no other plausible causes. Reverse genetics studies in which the mutations were placed into functional envelopes, confirmed that all five mutations decreased sensitivity to the drug. Additional analyses revealed that other classes of HIV-1 entry inhibitors effectively inhibited viruses containing these substitutions. The observed >10-fold reductions in viral susceptibility to **9** observed in four subjects during the course of dosing suggested that the compound was indeed acting directly against the virus. It was concluded that the observed efficacy and other data from this initial study in infected subjects provided clinical proof-of-concept for this inhibitor class and the data have encouraged additional efforts to realize a more effective attachment inhibitor drug [51, 52].

Mechanistic studies with the AIs BMS-378806 (**8**) and BMS-488043 (**9**) showed that they bind to gp120 and stabilize a conformation that is not competent for CD4 binding and downstream entry events [39–41]. Studies in other laboratories have concluded that a gp120-CD4-AI ternary complex is formed that acted to inhibit entry events downstream of attachment [53, 54]. A plausible explanation for the differences in these mechanistic conclusions has been published and suggests that the latter results arise from the specialized virus system and experimental conditions (such as very high levels of soluble CD4) employed [28]. Overall, this class of AI appears to function primarily by binding to gp120 and stabilizing a conformation that prevents CD4 binding and the subsequent rearrangements that facilitate co-receptor engagement [19, 28, 52]. A visual explanation of the proposed mechanism is shown in Fig. 1.

A binding model for BMS-488043 (**9**) in gp120 was proposed based on the anticipation that the key resistance mutations were likely to be in close proximity to the drug [52]. The locations of the key mutations are shown in Fig. 2 and a view of the proposed model is shown in Fig. 3. The S375N/I signature substitutions obtained from the clinical study, along with the M475I mutation selected in vitro are all located near the CD4 binding pocket and, not surprisingly, a model in which the drug docks deep within this cavity best fit all of the accumulated data. Consistent with the experimental data that showed that AIs reduced soluble CD4 binding to the envelope, in the model, **9** binds to the pre-CD4-bound conformation of gp120 and stabilizes it such that it adopts a conformation that does not allow productive binding to CD4. S375 is predicted to hydrogen-bond to the piperazine carbonyl of the oxamide moiety and M475 is proposed to pack against the benzamide ring of **9**. In the model, M426 packs against W427, which stacks with the azaindole ring of **9**. Mutations that are outside of the proposed binding site, including L116, M434, and S440 (selected in vitro [55]), would be predicted to exert indirect effects on compound binding. Interestingly, the V68A mutation is outside of the model which begins at amino acid 83. As mentioned earlier, previous studies have demonstrated that a tryptophan substitution for Ser375 occupies the Phe43 cavity and predisposes gp120 to assume a CD4-bound conformation. In viruses with either the HXBc2 or theYU2 HIV-1 envelope glycoprotein, the S375W change resulted in very high levels of resistance to AI **8** [54].

The most prevalent amino acid changes in the eight subjects with resistant viruses were at position 375, which in four subjects changed from Ser to Asn and

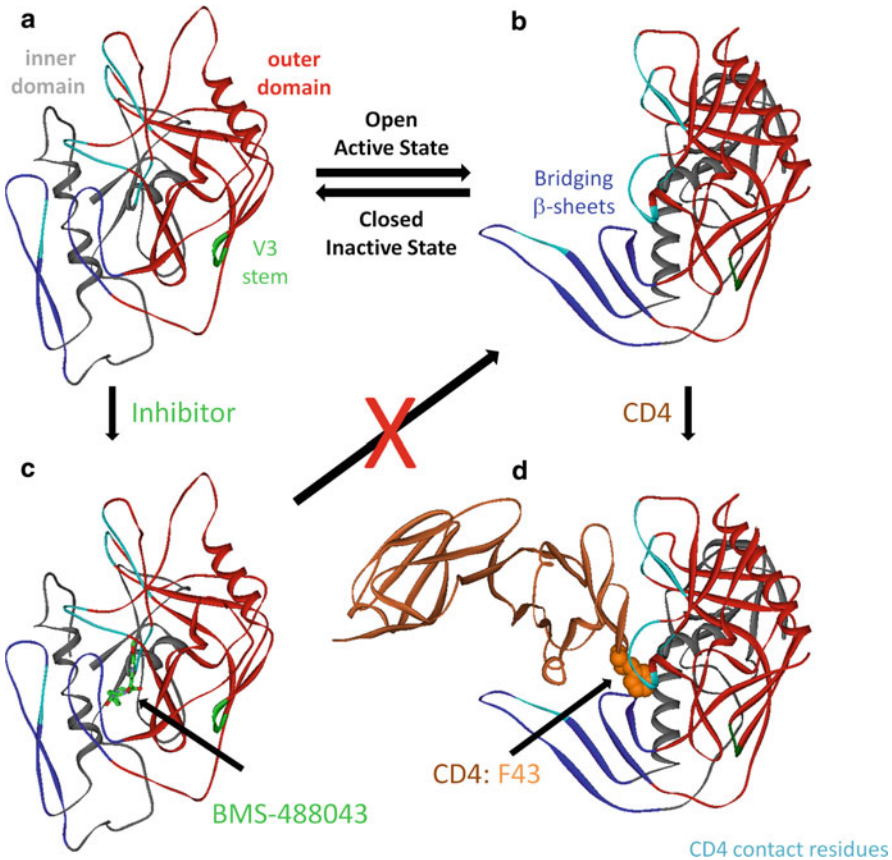

Fig. 1 Proposed mechanism of action for attachment inhibitors (**a, b**) Depiction of representatives of the closed and open (CD4-bound) states of gp120, respectively, existing in dynamic equilibrium (**c**) Attachment inhibitors bind to and shift the equilibrium to the closed state thereby blocking formation of the open state (**d**) CD4 binds to and stabilizes the open state, promoting additional conformational changes in the gp120 open state to facilitate co-receptor engagement

to Ile in another subject. In the published binding model discussed above, BMS-488043 (**9**) binds within a region of the outer domain that makes up part of the Phe43 binding cavity (Fig. 4) and S375 would make direct contact with the inhibitor. A change to Asn or Ile could directly affect AI-gp120 binding characteristics, as well as dynamic equilibrium of gp120 and thus, the resistant mutations at 375 observed in the clinical study are consistent with the previously proposed mechanism of these inhibitors. At position 426, the M426L mutation conferred resistance and this was explained in the proposed docking model by the fact that amino acid 426 packs against W427 and the modification could affect the way in which W427 interacts with **9**. L116 is outside of the ligand binding pocket and this mutation would likely only have an indirect effect on the binding of **9**,

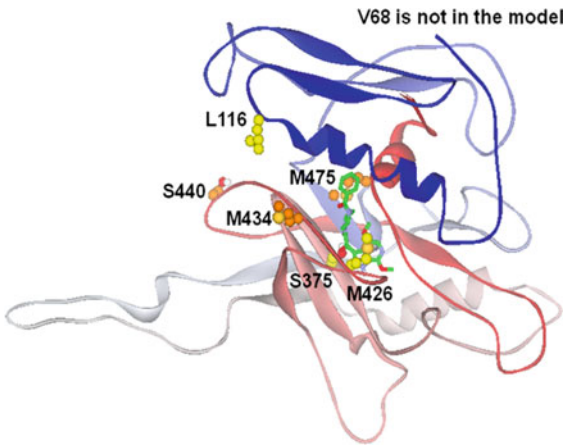

Fig. 2 Location of mutations in gp120 that confer resistance to AIs

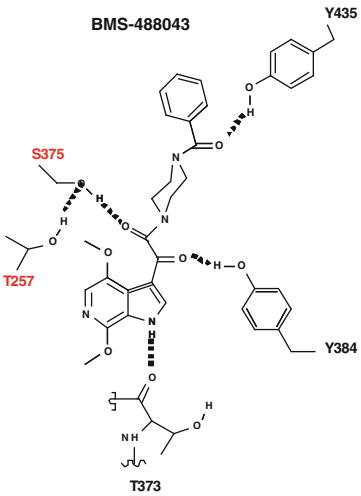

HIV gp120 Within 3 Å (contact distance)	HIV gp120 Between 3-6Å
H105, I108, I109, W112, S256, T257, Q363, T373, S375, Y384, I424, W427, Y435, G471, G472, G473, D474, M475, R476	M104, E106, I109, F223, T248, G250, I251, V255, Q258, K362, S264, I371, V372, H374, F376, N377, F382, F383, C385, K421, N425, M426, Q428, A433, M434, L453, T455, P470, W479

Fig. 3 Amino acid residues in gp120 predicted by modeling to be near (**9**) and related attachment inhibitors. *Dotted line* represents a hydrogen bond between HIV-1 gp120 and the inhibitor. *Red* amino acids (when appropriately mutated) reduce the binding affinity of one or more of the BMS inhibitors with HIV gp120 (resistance mutations)

which agrees with the reduced effects this mutation has on drug potency. It is believed that the L116 mutations may affect the positioning of the V1/V2 loop since it is located near the base of the loops, and this may affect the drug binding site. Only two of five resistant mutations selected in in vitro (V68A and M426L) were identified in the clinical trial, which could potentially be attributed to differences in

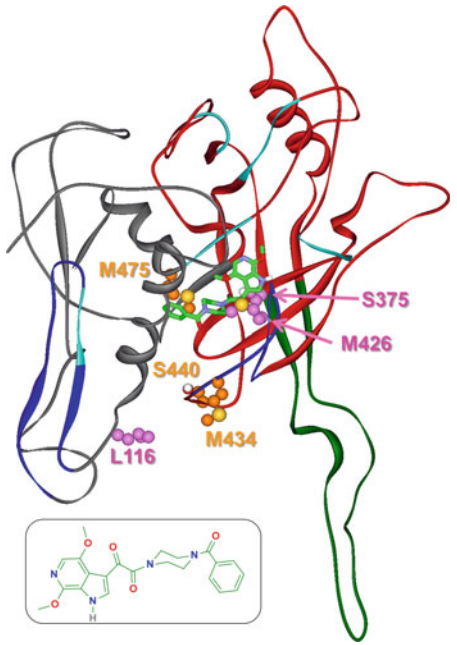

Fig. 4 The homology model of the BMS-488043 (**9**)/pre-CD4 bound gp120 complex. Carbon atoms for amino acid changes observed in clinical studies that induce resistance to **9** (L116, S375, M426) are pictured in *mauve* while changes observed during in vitro selection (M434, S440, M475) are in *orange*. The gp120 inner domain is in *gray* and the outer domain is *red*. The V3 loop is in *dark green*, the bridging β-sheets are in *dark blue*, and the CD4 contact residues are *light blue*. **9** (*inset*) when bound into pre-CD4 bound gp120 structure blocks the formation of the CD4 binding site

the viral envelope sequences, the fact that clinical viruses utilized CCR5 rather than the CCXCR4 receptor used in the in vitro laboratory viruses, or pressures from the human immune system in vivo. The frequency of pre-existing insensitive strains seems to correlate with the observed frequency of resistance mutations in the sequence databases (4 out of 30 in this study) while the emergence of resistance in the clinical study can likely be attributed to the suboptimal nature of the compound or low concentrations achieved. Since the rate of resistance development for early attachment inhibitors in vitro has been described to be similar to the NNRTI nevirapine, there is a reasonable expectation that resistance development during treatment would be suppressed in an appropriate combination regimen [28]. In summary, BMS-488043 (**9**) is believed to bind to a conserved region of gp120 and the clinical data suggest that the majority of the mutations that cause the most resistance occurred in close proximity to the drug rather than at distal positions and, thus, identification of improved analogs with even greater affinity in the binding site should be able to improve upon the utility of this class of HIV-1 inhibitor.

BMS-488043 (**9**) is a BCS class II molecule by virtue of its low solubility and high intrinsic membrane permeability [56]. The clinical study data showed that the

absorption of the compound in HIV-1 infected subjects was limited by poor dissolution and/or poor solubility. In the clinical study, the area under the concentration-time curve (AUC) plateaued at a dose of 800 mg with fasting. Two-fold greater exposure was realized from a single 200 mg solution dose than that obtained from an equivalent dose of a clinical capsule without a concomitant high fat meal (capsule containing wet milled crystalline active pharmaceutical ingredient (API) (95% <23 μm, surface area (SA) = 0.8 m^2/g)). To achieve proof of concept, a high dose (800 or 1,800 mg BID) was administered concomitantly with a high fat meal in order to maximize drug exposure. Both the high fat meal and the excessive pill burden necessitated by these dosing regimens were considered to be unacceptable liabilities for a useful HIV-1-inhibiting drug. The team evaluated the potential of two courses to address these issues. In one path, formulation and prodrug approaches were evaluated, and in a second path, molecules with ten-fold improvements in both potency and exposure from pharmacokinetics were sought. Ultimately, the fruits of both of these efforts were combined into what has emerged as currently the best molecule.

Nanosizing and amorphous formulation approaches were examined with some success, providing approximately five- and nine-fold enhancements in exposure in dogs, respectively, compared to the formulation used in the clinical capsule [57]. These data, along with the data from solution dosing, provided evidence that addressing dissolution-limited absorption had the potential to improve plasma exposure of BMS-488043 (**9**) following oral administration.

The phosphonooxymethyl prodrug of BMS-488043 (**9**) was synthesized as the lysine salt **10** and the physical and pharmaceutical characteristics confirmed that this prodrug possessed significantly improved solubility and sufficient chemical stability in both the solid state and solution to be viable as a development candidate [58, 59]. The prodrug **10** crystallized as an off-white powder containing a small amount of amorphous material. The aqueous solubility at room temperature of the crystalline parent compound **9** was determined to be approximately 0.04 mg/mL in the pH range of 4–8, 0.9 mg/mL at pH 1.5, and 0.25 mg/mL at pH 10.0, while the solubility under similar conditions for the prodrug increased from 0.22 mg/mL at pH 1.4 to >12 mg/mL at pH 5.4 and pH 8.9. The potential of the prodrug to remedy the high dose and solubility-limited absorption observed with the parent compound was assessed preclinically as a prelude to clinical studies [58, 59]. Preclinical profiling showed that, like other successful oral phosphate prodrugs, the compound was hydrolyzed by alkaline phosphatase(s) and this hydrolysis would be expected to occur at the intestinal brush border membrane just prior to absorption of the parent molecule. Concentrations of >100 mg/mL were achieved in water for dosing solutions used in preclinical in vivo studies. In rats, the difference between exposure after oral dosing of the parent and prodrug were minimal at low doses; however, the exposure advantages afforded by the prodrug increased with dose and, for example, at ~200 mg/kg equivalent of **9**, the prodrug **10** provided ~threefold higher C_{max} and ~twofold higher AUC of **9** in rats than a suspension formulation of parent drug. In healthy human volunteers, the prodrug significantly increased both the C_{max} and AUC and reduced T_{max}. At the highest dose of **10** evaluated, 800 mg

equivalents of **9**, the prodrug provided an AUC increase of more than threefold from dosing of 800 mg of the parent drug concomitant with the high fat meal. The prodrug methodology succeeded in significantly improving the overall exposure of the molecule and provided plasma concentrations that increased more proportionally with dose than the parent molecule. Unfortunately, the rapid absorption of the parent molecule after dosing of the prodrug revealed that the intrinsic pharmacokinetic properties of **9** in humans were less than ideal, as evidenced by a short $T_{1/2}$ in plasma. The C_{12} of parent at the 800 mg dose of prodrug **10** was 150 ± 32 ng/mL, which was too low to support a twice daily dosing regimen. It was less than the protein binding-adjusted EC_{50} for **9**, determined in vitro vs. a panel of HIV-1 subtype B clinical virus isolates to be 156 ng/mL (370 nM). The C_{12} of the drug in humans falls below the targeted protein binding-adjusted EC_{50} measured in vitro that would give confidence that this compound could be developed as a twice daily dosing regimen. Importantly, the prodrug methodology had demonstrated that it could provide enhanced exposure, but further development of the compound was not pursued in favor of candidates with improved pharmacokinetic and antiviral properties [60–65].

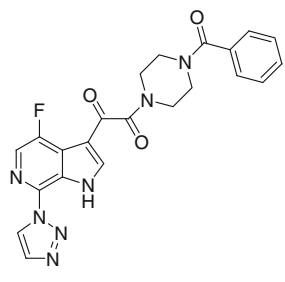

11

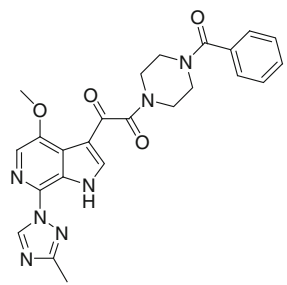

12

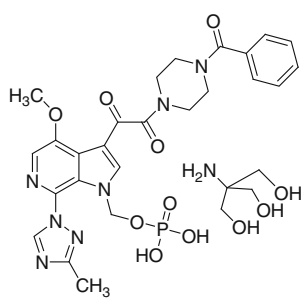

13

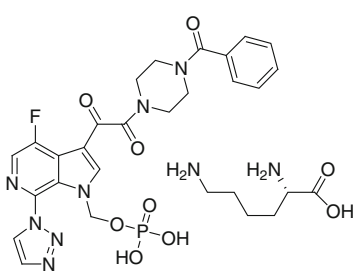

14

Optimization efforts with the goal of obtaining a minimum ten-fold improvement in both the virology and PK profiles over BMS-488043 (**9**) ultimately identified the C-7 position in the 6-azaindole series as the optimal position to achieve the intended goals. Certain C-7 amides and heteroaryl compounds provided enhanced potency and ultimately led to the development of coherent SAR [62, 63,

Table 1 Rat PK parameters of optimized AIs

	F (%)	PO AUC 24 h (μg·h/mL)	$T_{1/2}$ i.v. (h)	IV CL (mL/min/kg)
9	90	6.3 ± 2.7	2.4 ± 0.33	13 ± 4.0
11	64	32 ± 12	5.9 ± 4.9	1.6 ± 0.2
12	82	52 ± 12	4.3 ± 1.1	1.3 ± 0.19

66–68]. The development of suitable synthetic methodology was necessary to fully explore the SAR at an acceptable pace and both C and N-linked heteroaryls were explored. Ultimately, two promising compounds with improved virology and PK profiles, BMS-585248 (**11**) and BMS-626529 (**12**), emerged from preclinical research and both displayed an approximate ten-fold enhancement in potency in preliminary assessments of antiviral activity. Both molecules showed enhanced PK profiles compared to **9**, as exemplified by the increased AUC and reduced clearance in rat PK data compiled in Table 1. Initial analyses predicted both to be capable of covering a trough concentration of ten times the EC_{50} at 12 h after dosing without the need for a high fat meal adjuvant and a dose that was lower than utilized for **9** in POC studies. In rats, as shown below, the exposure after oral dosing was considerably improved for both compounds with respect to **9**. Overall, the preclinical PK profile, which included chimp data, suggested that the compounds were predicted to be suitable for twice daily dosing in man at a reasonable dose and without the need for a high fat meal. When compared directly, fluoro-azaindole **11** showed a slightly lower clearance in chimp studies while the methoxy-azaindole **12** was predicted to have a slightly lower clearance in humans based on in vitro studies in hepatocytes and liver microsomes. Both parent molecules were advanced to clinical studies, but in order to maximize coverage of viral spectrum, the prodrug methodology described previously for **9** (BMS-488043) was also applied to both molecules. The crystalline solubility of **11** was 0.007 mg/mL, while for **12** it was 0.022 mg/mL, roughly twofold lower than for **9**. In pre-IND studies, the exposure and safety associated with BMS-663068 (**13**), the prodrug of **12**, was superior to that of **14**, the prodrug of **11**. Some of this was attributed to the fact that a relatively more insoluble molecule **11** was being delivered rapidly in high local concentrations upon prodrug unmasking and release of parent.

Similar to earlier members of the class, the parent azaindole **12** binds directly to gp120 and inhibits the binding of soluble CD4 to gp120, with an IC_{50} of 14 nM. The displacement of [^{3}H]-**12** from gp120 by excess soluble CD4 was studied [64, 65]. The time required for complete liberation of compound in this assay was ~8 h, which amounts to an off-rate that was ~16-fold longer than that observed with **9**. Methyl triazole **12** is active against both R5 and X4 viruses and exhibits a spectrum of activity against clinical isolates of HIV-1 within and between subtypes. The EC_{50} for envelopes from clinical isolates ranged from 67 pM to >0.1 μM in the PhenoSense® assay. Between 93% and 94% of viruses from both subtypes exhibited an EC_{50} of less than 10 nM, with 73% of the clade B and 42% of the clade C viruses exhibiting EC_{50}'s of less than 1 nM in a screen of 157 subtype B and 36 C viruses. Similar ranges were observed with clades A, AG, BF, F, and F1

(although with fewer samples). However, **12** was inactive against all subtype AE viruses examined, was inactive against HIV-2, and was non-cytotoxic in multiple human cell lines. Inhibitor **12** showed synergistic or additive antiviral effects in all assays when employed in combination with 24 marketed and investigational anti-HIV agents, including other entry inhibitors. The favorable antiviral and preclinical profile of **12** represented a significant improvement over **9** and thus encouraged development of its oral prodrug, BMS-663068 (**13**).

In order to maximize the exposure and thus the viral spectrum of **12** in the clinic, the highly water soluble Tris salt (aqueous solubility >10 mg/mL) of prodrug **13** was selected for advancement. To reduce the relatively high peak to trough ratio observed after oral dosing with this class of molecules, a slow release formulation was developed and was shown to facilitate absorption from the entire GI tract [69].

Twice daily doses of 600–1,200 mg of the prodrug **13** plus 100 mg of ritonavir or 1,200 mg of drug without ritonavir, or a single daily dose of 1,200 mg plus ritonavir produced mean maximal reductions in viral RNA of >1 $\log_{10}$. Prodrug **13** was generally well tolerated and the PK profile supports once or twice daily dosing, with or without ritonavir, and the potential for lower doses will be examined in future studies [60, 61]. Longer term clinical trials of **13** as part of a combination of an antiretroviral agent regimen are in progress.

The potential of these inhibitors to provide therapeutic effects beyond a typical antiviral response will need to be determined in the clinic, but preclinical studies have provided data to suggest the potential for several additional benefits. Mutations identified by in vitro resistance selection resulted in viruses that were less sensitive to both AI **9** and earlier analogs, but were more sensitive to neutralization by certain broadly neutralizing antibodies [70]. Nanomolar concentrations of attachment inhibitors **8**, **9**, and **11** prevented HIV-1 envelope-mediated toxicity toward two neuronal cell lines while enfuvirtide and two CCR5 co-receptor antagonists had no effect [71]. HIV-1 envelope binding induces pro-apoptotic signals in CD4+ T-cells, even in the absence of infection. Because defective virus particles represent the majority of HIV-1 and typically contain a functional Env protein, this interaction could be a significant cause of CD4+-T-cell depletion. The AIs **8** and **9** displayed low-nanomolar anti-apoptotic potency and prevented CD4+-T-cell depletion from mixed lymphocyte cultures [72]. The anti-apoptotic effects were eliminated by amino acid changes in the envelope protein that provided resistance to the antiviral effects of the compounds.

A series of related gp120-CD4 inhibitors that incorporate a sulfonamide moiety as an isostere for the ketoamide group has been disclosed from which analog **15** exhibits potency similar to **8**, with an IC_{50} of 6 nM in a pseudotype virus assay, suggesting that this isostere is associated with intrinsically lower potency [51, 73]. An SAR study of analogs inspired by **8** produced inhibitors in which the azaindole was replaced by a heterobiaryl group which was proposed, based on the SAR, to be accommodated by a crevice in the HIV-1 gp120 protein [74]. The methylated isoxazole **16** was highlighted as a key compound that displayed an IC_{50} of ~5 nM in a pseudotyped viral assay, and potency similar to **8** towards a panel of clinical isolates.

Independent molecular modeling studies of HIV-1 gp120 inhibitors have appeared. The synthetic bivalent inhibitor **17**, constructed from two molecules of **8** tethered at the C-4 positions, was reported [75]. However, the potency of this compound was not significantly enhanced when compared to **8** although it was more potent than a monomer core with the linker attached.

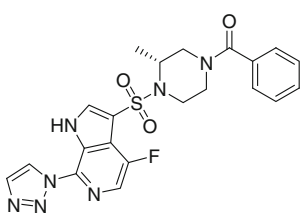

15

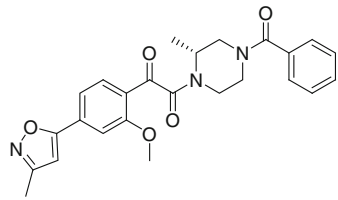

16

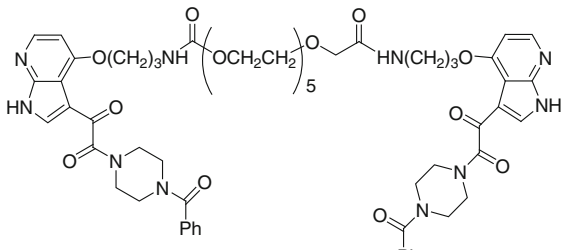

17

In an alternative approach, novel inhibitors of the gp120–CD4 interaction were sought by starting from ketoamides **8** and **9** and replacing what was hypothesized might be a potentially reactive and metabolically vulnerable carbonyl moiety [76]. In actuality, no metabolic or reactive liabilities have been reported for these ketones, presumably due to the fact that they behave more like a vinylogous amide due to conjugation with the indole moiety; however, the premise to seek replacements for this moiety did lead to a new isosteric series of inhibitors. A plate-based coupling of acids to the 2-methyl 4-benzoyl piperazine unit designed to prepare analogs containing a range of potential ketoamide replacements, led to the identification of **18**, which was a 3 μM inhibitor in a high throughput cell fusion assay. Optimization efforts, initially guided by the desire to generate compounds which fell within Lipinski's rule-of-five, led to amide **19** which displayed an IC_{50} of 17 nM in a JRFL-derived envelope cell-cell fusion assay. The compound also displayed excellent antiviral activity with an IC_{50} of 2 nM in an assay designed to measure protection of infection of HeLa-P4 cells by a laboratory-adapted HIV NL4-3 virus. Efforts to improve the physicochemical properties led to pyridine **20** which retained the potency of **19** in the fusion ($IC_{50} = 11$ nM) and antiviral ($IC_{50} = 2$ nM) assays and displayed considerably improved metabolic stability. While **19** demonstrated moderate oral bioavailability (rat bioavailability = 48%; clearance (CL) = 75 mL/mg/kg; $T_{1/2} = 0.7$ h), the full pharmacokinetic profile of **20** was superior and showed that the compound possessed improved clearance and oral bioavailability

($F = 65\%$; CL = 18 mL/mg/kg; $T_{1/2} = 1$ h). A projection of the human pharmacokinetics of **20** predicted an oral bioavailability of greater than 90% and a half-life of ~5 h. Compound **20** showed encouraging antiviral potency against a number of laboratory-adapted strains and primary isolates in human peripheral blood mononuclear cells (PBMCs). Additionally, 70% of a panel of 25 clade B virus isolates were inhibited with an IC_{90} below a C_{min} of 500 nM, which modeling suggested could be achieved with a twice-daily dose of 200 mg of **20**; so, antiviral coverage of many relevant isolates was predicted to be feasible. Based on these data and further profiling, **20** was selected for clinical development. Further optimization in an effort to identify a backup compound was carried out and led to the identification of analog **21** which was, as expected, active toward R5-, X4-, and dual-tropic viruses [77]. Significantly, when evaluated against a panel of B clade viruses, **21** was active toward all 25 isolates tested, displayed subnanomolar levels of potency against several clade B isolates, and had an improved spectrum profile compared to **20**. Human PK predictions and antiviral spectrum data suggested that a 100 mg bid dose of **21** could give a C_{min} of 50 nM in humans, covering 70% of clade B viruses at the EC_{90}. Assuming a linear pharmacokinetic profile across the dose range, 600 mg bid had a predicted C_{min} of 300 nM, which would cover 96% of clade B at the EC_{90}. Despite the fact **21** had an inferior pharmacokinetic profile ($F = 21\%$; CL = 48 mL/mg/kg; $T_{1/2} = 0.5$ h) compared to **20**, its superior potency provided increased antiviral spectrum coverage. The article states that further studies conducted on **20** showed that cross-clade inhibition would be very difficult with this chemical class; so, additional resistance studies would be required in order to further progress **21**. Compound **20** was advanced to clinical studies in humans [78]. Due to the evidence of dose-related increases in heart rate and blood pressure in preclinical studies in dogs, the initial human study was a limited, well-monitored safety trial. The compound was safe and well-tolerated at the low doses studied. However, the propensity to cause increases in heart rate and blood pressure was found to correlate well between dogs and humans. Modeling of the PK/PD relationship based on the low dose human PK data predicted that a dose of 1,300 mg would be required to realize a 1.5 $\log_{10}$ viral load reduction in infected subjects; consequently, an efficacy study was not pursued and development of the compound was terminated.

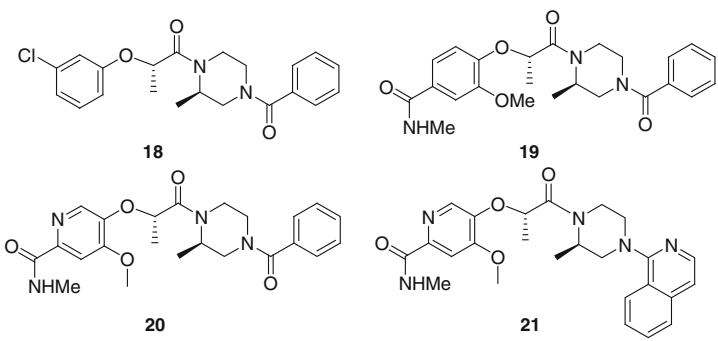

Both NBD-556 (**22**) and NBD-557 (**23**) are small molecule entry inhibitors that were discovered by screening and shown to block gp120-CD4 interactions [79]. These (*N*-phenyl-*N*′-(2,2,6,6-tetramethyl-piperidin-4-yl))-oxalamide analogs were initially demonstrated to bind to unliganded gp120 but not to the cellular CD4 receptor and inhibited some HIV-1 laboratory strains with μM potency. They exhibit minimal cytotoxicity and the activity of these compounds is co-receptor independent and does not interfere with gp41 six-helix bundle formation. Structurally, the NBD series chemotype was viewed as being constructed from three elements which are the *para*-substituted phenyl ring, the oxalamide linker, and the tetramethylpiperidine moiety. SAR studies from these three regions based on computational approaches have demonstrated their importance for activity [80, 81]. While these studies demonstrated that potency can easily be lost, they did lead to the identification of two analogs, **24** and **25**, which contain halogen groups at the *para*-position and at one of the *meta*-positions of the phenyl ring, that exhibited a very limited potency improvement [80]. The binding K_d of **22** in one system was 3.7 μM, vs. 0.76 μM for **24**, and 1.3 μM for **25**. The antiviral EC_{50} in one system was just slightly over 100 μM for **22** vs. WT HIV-1 YU2, which compared to 54.4 μM for **24** and 13.6 μM for **25**.

Both **22** and **23** bind to gp120 and elicit changes that resemble those produced by the binding of CD4. Binding elicits a large, favorable enthalpy and unfavorable entropy change, and produces a conformation that resembles that produced by binding of CD4 itself as structuring of the co-receptor-binding site and affinity for the CCR5 co-receptor is enhanced [19, 80]. The remarkably large change in conformation elicited by these small molecules has been estimated to result in the structuring of approximately 67 gp120 residues, which is smaller than the number observed for soluble CD4 (sCD4), but is nevertheless sufficient to provide some of the same effects. The thermodynamic signature produced by these compounds contrasted with that of **8**, which binds to gp120 in a mostly entropy-driven process and elicits only a small enthalpy change. One potentially undesirable effect of the mechanism of action of this class of compound is that as a result of their ability to enhance co-receptor binding, they have been shown to facilitate virus entry into CD4-negative, CCR5-expressing cells [80]. In contrast, the previously described AIs such as **8** do not exhibit this ability to increase infection in CD4-deficient cell lines. While the effect of **22** and related analogs on binding of gp120 to CCR5 is qualitatively similar to the effect observed for CD4, the antiviral mechanism of the compounds may not be completely due to simple competition with CD4 for binding [82]. In another study, **24** or sCD4 were used to further investigate the mechanism of inhibition and inhibitor-induced changes in the conformation and functional competence of the HIV-1 envelope glycoproteins in relation to time. Both sCD4 and **24** efficiently activated the envelope glycoproteins to mediate infection of cells lacking CD4, in a manner dependent on co-receptor affinity and density. This activated state was, however, short-lived and was followed by spontaneous and what appeared to be irreversible changes in conformation and loss of functional competence. The longevity of the activated intermediate was essentially the same for sCD4 and **24**, but was

sensitive to differences in temperature and HIV-1 strain. In contrast, the activated intermediate induced by cell-surface CD4 was relatively long-lived. The class of inhibitors was exemplified by **22**–**24** predominantly affects cell-free virus, whereas virus that was prebound to the target cell surface was mainly activated and was able to infect the cells even in the presence of high concentrations of the analogs. These results demonstrate the ability of soluble CD4 mimics to inactivate HIV-1 by prematurely triggering active but transient intermediate states of the envelope glycoproteins. It was proposed that this novel strategy for inhibition may be generally applicable to high potential energy viral entry machines that are normally activated by receptor binding.

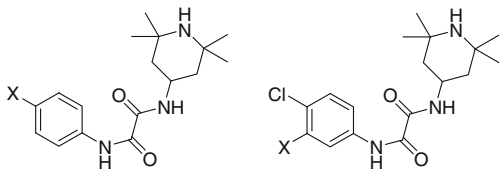

22 (NBD-556) X = Cl **24** X = F

23 (NBD-557) X = Br **25** X = Cl

Compounds from this class are believed to bind in the Phe43 cavity. SAR, molecular modeling, and viral mutagenicity studies in which changes in this region confer resistance to **22** all support this hypothesis. A model in which **22** binds within the same Phe43 cavity as previously described attachment inhibitors such as **9**, has been developed. Inhibitors such as **22** are proposed to project the phenyl ring into the Phe43 pocket more deeply than does Phe43 of CD4 itself. However, the class of molecules represented by **22** are ~1,000-fold less potent than the early AI **8**. Initially, the low molecular weight and simple structure of **22** suggested high potential for further optimization but despite considerable effort to date, this potential has not been realized and a good lead molecule with $<$100 nM potency has not yet been reported [81]. The difficulty in increasing potency with this class may perhaps be explained by the observation that the increases in enthalpy of binding were much larger, up to 24.5 kcal/mol, than predicted from the binding of compound to target alone, which was considered consistent with the formation of a network of interactions within gp120 initiated by compound binding. Furthermore, compounds with similar binding affinity displayed enthalpy differences of $>$10 kcal/mol, suggesting that formation of favorable interactions within gp120 were major contributors to the binding affinity of **22** and related analogs [82]. In addition, analogs with similar binding affinity displayed differing abilities to elicit viral entry in CD4-negative cells and, thus, formation of the CCR5 or CXCR4 binding pocket was said to be a function of both binding affinity and entropy changes. Consequently, optimization of this class of inhibitors may be more difficult because of the affinity of the compounds for the receptor, and efficacy is not due to a simple lock and key-type binding interaction but is dependent on remote interactions within gp120. It remains to be seen if a breakthrough in the SAR can be realized in the future.

The betulinic acid derivatives **26** and **27** inhibited primary HIV-1 isolates from A, B, and C clades of virus with average EC_{50}s in the sub-μM range, although there was a considerable range of potency [83]. Based on resistance mutations and mechanistic studies, these inhibitors were proposed to bind to the end of the V3 loop, and to function by preventing the gp120-CD4 complex from engaging the co-receptor which in these studies was CCR5 or, in one example, CXCR4. The small cyclic peptide **28** has been reported to bind to the Phe43 binding pocket using a benzyl group as a Phe surrogate and to display 80% inhibition of viral entry at μM concentrations [84]. The compound had 10% oral bioavailability in rat.

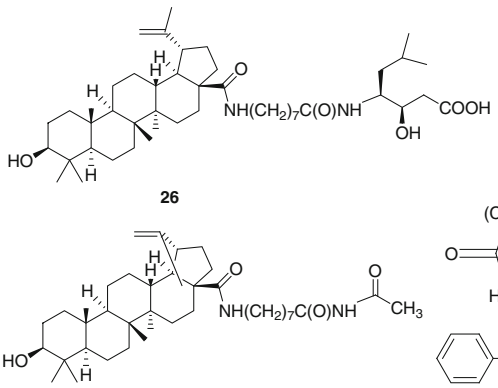

2.3 Other Inhibitors

In previous and recent reviews of inhibitors that target gp120/CD4 interaction, the actions of macromolecules that target gp120, including various polysulfated polysaccharide, derivatives and the parent bacterial polypeptide cyanovirin, and the CD4-IgG fusion protein PRO-542 have been described [8, 9, 21, 22, 25, 27, 28]. Although PRO-542 entered clinical trials, there appears to be no published update on its progression in the last five years. To date, small molecule approaches to inhibit the interaction by targeting CD4 have realized even less progress in the last five years, but some of the small molecule and macromolecule approaches have also been reviewed [8, 9, 21, 25, 28].

2.4 Conclusions

In summary, progress over the last several years toward realizing a HIV-1 entry inhibitor that acts on the first step of viral entry by inhibiting a protein-protein interaction between gp120 and CD4 has been made, but has come only as a result of

significant effort. A number of avenues that have been pursued have yet to realize advances that demonstrate a path forward to a clinically useful entity, and some of these have been abandoned. The fact that unbound gp120 is poised in a high-energy state waiting to be triggered toward a new conformation by CD4 has allowed small molecules that bind to gp120 in a conserved CD4 binding pocket to exploit this propensity and achieve inhibition. However, the fact that the binding interactions can be governed by reordering of residues in other regions of gp120, the conformational flexibility of gp120, the genetic diversity of HIV-1 that is responsible for a wide spectrum of potency even for compounds binding in a highly conserved region, and the physical properties of the compounds required to maintain maximum potency have all contributed to the hurdles encountered in inhibiting this protein-protein interaction. Other factors that could add to this challenge include variations in receptor density on the viral or host cell surfaces and the presence of large amounts of non-functional viral particles or unassociated gp120 that has been shed. In order to provide a molecule that could effectively inhibit infection by a significant portion of the HIV-1 strains encountered in a clinical setting, the highest levels of potency and exposure attainable were necessary, leaving the medicinal chemist little room to maneuver. These requirements necessitated advancement of compounds that required the use of phosphate prodrug methodology and the development of extended release formulations, but have ultimately provided a compound that, at the time of writing, is being evaluated in Phase II clinical studies in combination with other HIV-1 inhibitors.

3 Inhibitors of HIV gp41

3.1 Peptides and Peptide-Based Compounds

The discovery that peptides derived from the N- and C-termini of gp41 were potent and effective inhibitors of virus replication in cell culture paved the way not only for the discovery of the 36-residue peptide enfuvirtide (**29**, T-20) as the first marketed HIV-1 entry inhibitor but also provided key tool molecules that contributed significantly to developing an understanding of aspects of virus fusion mechanism that was more broadly applicable to a range of viruses [85–90]. The initial experimental observation of HIV-1 entry inhibition was with a 38-residue peptide designated DP107 (T-21) (**30**) that was derived from the amino terminal heptad repeat (HR-1 or HR-N) segment of HIV-1 gp41 and which adopted a α-helical conformation in solution [85]. DP107 (**30**) potently inhibited HIV-1 infection in cell culture with an EC_{50} of ~250 nM while an analogue in which Ile573 was replaced by proline failed to adopt a helical conformation and was inactive as an antiviral agent [85]. A contemporaneous study with the peptide SJ-2176 (**31**), comprised of residues 637–666 derived from the carboxy terminus heptad repeat region of gp41 (HR-2 or HR-C), inhibited replication of the IIIB strain of HIV-1 in cell culture with an EC_{50} of 101 nM when gag p24 production was measured and prevented HIV-1 envelope-

mediated cell-cell fusion with an EC_{50} of 156 nM [86, 87]. This observation was confirmed with the synthesis and evaluation of the 36-residue peptide enfuvirtide (**29**) which was significantly more active in cell culture and fusion assays, with EC_{50}'s ranging from 1.8 to 853 ng/mL [91–94]. The striking antiviral activity of enfuvirtide (**29**) presented both a unique and significantly challenging opportunity to develop a novel HIV-1 drug [88, 89, 95, 96]. The molecule is prepared synthetically on an industrial scale by assembling three separate fragments using solid phase methodology that are subsequently united in solution followed by a global deprotection [95, 96]. The development enterprise was successful, with accelerated approval for the marketing of enfuvirtide (**29**) based on 24 weeks of clinical data granted on March 14, 2003 and traditional, full approval based on 48 weeks of clinical experience occurring on October 15, 2004 [97, 98]. Enfuvirtide dosing in these trials was 90 mg twice daily administered parenterally by subcutaneous injection into the upper arm, abdomen, or thigh. Despite good efficacy in combination with other antiretroviral agents and a generally acceptable safety profile, the parenteral route of administration, and high cost associated with therapy have largely restricted enfuvirtide (**29**) use to salvage therapy [99–101].

$Ac\text{-}_{638}$YTSLIHSLIEESQNQQEKNEQELLELDKWASLWNWF$_{673}$-NH_2

29 (enfuvirtide, T-20)

$Ac\text{-}_{553}$NNLLRAIEAQQHLLQLTVWGIKQLQARILAVERYLKDQ$_{590}$-NH_2

30 (DP-107, T-21)

EWDREINNYTSLIHSLIEESQNQQEKNEQE*GGC*

31 (SJ-2176)

The successful development of enfuvirtide (**29**) has stimulated considerable effort directed towards understanding the mode of action of this class of HIV-1 inhibitor, identifying improved peptide-based drug candidates and seeking small molecule inhibitors of gp41 function [102]. The six-helix bundle structure of the key elements of HR-1 and HR-2 of gp41 in the post-fusion conformation was solved simultaneously by three groups and provided a structural basis not only to understand the antiviral activity of enfuvirtide (**29**) but also to design improved inhibitors of gp41-mediated virus fusion [102–108]. Basic mechanistic aspects of the carefully choreographed process of HIV-1 entry have been elucidated with the binding of HIV-1 gp120 to the host cell glycoprotein CD4 the initiating event that triggers a conformational change in gp120 to expose binding sites for co-receptors CCR5 or CXR4. The engagement of the co-receptor by gp120 catalyzes a more substantial change in the structure of gp120 that releases it from its role of constraining gp41. This allows the smaller protein, which exists in a metastable state, to undergo a significant conformational rearrangement. This structural reorganization exposes the hydrophobic fusion peptide (FP) at the amino terminus of gp41, a 23-residue, glycine-rich sequence comprised of lipophilic amino acids (Fig. 5) and projects it into the host cell membrane and away from the virus membrane [109]. The functional elements of gp41 are also depicted in Fig. 5,

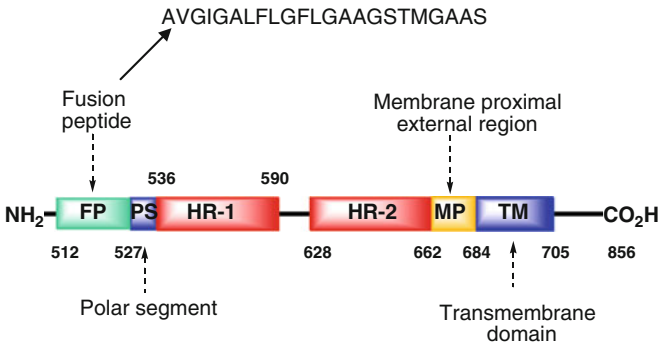

Fig. 5 The structure of HIV-1 gp41 with sequence of HIV-1 fusion peptide

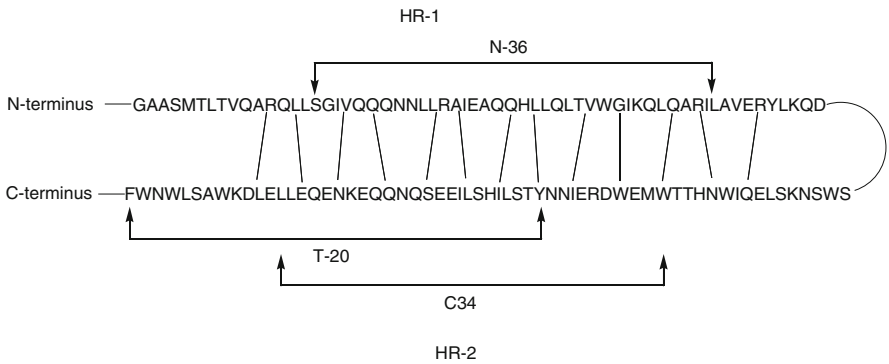

Fig. 6 The key interacting elements of HR-N and HR-C of HIV-1 gp41

which identifies the topological relationships between the fusion peptide (FP) at the amino terminus, the polar segment that intervenes between FP, and the amino terminal heptad repeats (HR-1, residues 536–590). A flexible loop region separates HR-1 from the carboxy terminal heptad repeats (HR-2, residues 628–684) and this is followed by the membrane proximal region (MP), the transmembrane domain (TM) and the cytosolic carboxy terminus.

The conformational rearrangement of gp41 allows the HR-1 element to assemble into a symmetrical, trimeric, coiled-coil arrangement that creates three identical binding grooves recognizing HR-2. The HR-2 elements associate with the HR-1 trimer in an anti-parallel fashion to form a six-helix bundle structure that induces a hairpin configuration in the flexible loop region of gp41, thereby drawing the host and virus membranes into proximity and initiating the final steps of membrane-membrane fusion [108, 110–113]. The topology of the association of HR-2 with HR-1 is depicted in Fig. 6 in which the key interacting residues are identified and for HR-2, are shown more explicitly in Fig. 7 [104, 111, 113].

Enfuvirtide (**29**) and related carboxy terminus-derived peptides bind to the HR-1 trimer, successfully competing with the intramolecular association of HR-2 with the

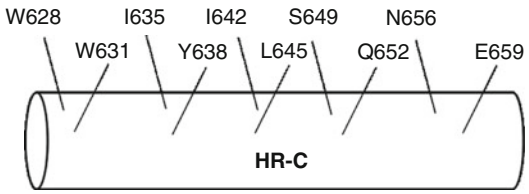

Fig. 7 Key residues of HR-2 that project into the pockets formed by association of the HR-1 segments into a trimeric bundle

SGIVQQQNNLLRAIEAQQHLLQLTVWGIKQLQARIL-CO_2H

N36

IEAQQHLLQLTVWGIKQLQARIL-CO_2H

N23

LLQLTVWGIKQLQARIL-CO_2H

N17

Ac-RMKQIEDKIEEIESKQKKIENEIARIKKLI

IQ

Ac-IKKEIEAIKKEQEAIKKKIEAIEKEL

IZ

Fig. 8 The structures of peptide elements derived from HR-1 and HR-2 of HIV-1 gp41

complex, thereby interfering with the formation of the natural six-helix bundle and the hairpin configuration of gp41 [90, 112–116]. Peptides derived from the C-terminus HR-2 region are generally more potent inhibitors of HIV-1 infection than peptides derived from the amino terminus heptad repeat HR-1 reflecting differences in the mode of action. The HR-1-derived peptides are thought to function either by interfering with the formation of the HR-1 trimer by a process of intercalation with HR-1, by association into a trimeric species resembling HR-1 that binds to HR-2, or by associating directly with the HR-2 sequence in the pre-fusogenic state [114–116]. The HR-1 based peptides N17, N23, and N36 are poor inhibitors of HIV-1 infectivity with EC_{50}s of 13, 29, and 2 μM, respectively (Fig. 8) [117]. Aggregation of the HR-1 peptide inhibitors under physiological conditions was considered to be an important contributor to their poor antiviral activity, stimulating the design of chimeric peptides that hybridized carefully designed, soluble, trimeric coiled coil-forming peptides, designated IQ and IZ, ligated to the N-terminus of the HR-1 peptide (Fig. 8) [117]. These chimeric peptides were considerably more potent antiviral agents with EC_{50}s of 190, 15, and 88 nM for the IQN17, IQN23, and IQN36 molecules, respectively, and 22, 30, and 26 nM for IZN17, IZN23, and IZN36, respectively [117]. They were considered to function in a dominant-negative fashion by assembling into a structure that resembled the HR-1 trimer and intercepting the HR-2 element during the process of conformational rearrangement,

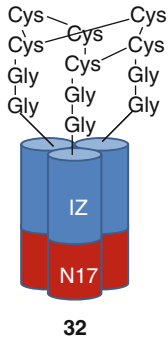

Fig. 9 Covalently assembled construct CCIZN17

interfering with the formation of the six-helix bundle, and reducing the propensity for gp41 to adopt the hairpin configuration [117].

An attempt to improve the potency of the IZN17 chimeric peptide focused on the construction of a covalently assembled construct designed to circumvent the process of self-association of the peptide, accomplished by introducing cysteine residues to the amino terminus that formed interchain disulfide bonds [118] (Fig. 9). The resulting construct, designated CCIZN17 (**32**), demonstrated high thermodynamic stability and inhibited HIV-1 replication in cell culture with EC_{50}s of 40–380 pM toward the HXB2, NL4-3 and MN-1 strains and was similarly potent in a cell-cell fusion assay, with an $IC_{50} = 260$ pM [118]. In a phenotypic assay, CCIZN17 (**32**) was active against a panel of 22 HIV-1 isolates with EC_{50}s ranging from 3.9 to 202 nM and interacted synergistically when used in combination with enfuvirtide (**29**), a logical experiment based on the latter not binding to the hydrophobic pocket created by the N17 segment [118, 119]. An alternative approach to prevent unstructured aggregation of HR-1-based peptides fused N36 or N28 to the N terminus of Foldon (Fd), the trimerization domain from T4 bacteriophage fibritin [120]. These constructs, designated N36Fd and N28Fd, were shown to be stable trimers that bound to a HR-2 derived peptide to from a soluble complex and N28Fd inhibited HIV-1_{IIIB}-mediated cell-cell fusion with an EC_{50} of 21 nM, markedly more potent than N36Fd, with an $EC_{50} = 1.23$ μM [120].

The effect of intercalation of exogenous HR-1 peptides on the association of HR-1 into the trimeric species was explored in the context of two structurally modified versions of the N36 peptide [121]. By replacing nine residues that mediate self association, $N36^{Mut(a,d)}$ was constructed while $N36^{Mut(e,g)}$ incorporated changes to residues that are intimately involved in the interaction with the HR-2 region. $N36^{Mut(a,d)}$ existed in monomeric form in solution and exhibited no demonstrable antiviral activity, indicative of the requirement for the formation of a trimeric coiled-coil structure to interact with the HR-2 peptide elements. In contrast, $N36^{Mut(e,g)}$ was a potent inhibitor of HIV envelope-mediated cell-cell fusion, $IC_{50} = 308$ nM, a 50-fold improvement on the native N36 peptide [121]. $N36^{Mut(e,g)}$ was

hypothesized to function by interfering with the formation of HR-1 trimeric species by successfully competing with the self-association process.

A more sophisticated construct grafted N35 onto the amino terminus of a peptide comprised of N34 attached by a six-residue linker to C28 derived from HR-2 (N34-SGGRGG-C28) which adopts a stable, trimeric hairpin configuration in solution [122]. This peptide, designated N_{CCG}-gp41, presents the N35 moiety in trimeric form and is a potent inhibitor of HIV-1 envelope-mediated cell-cell fusion, with an $IC_{50} = 16.1$ nM [122].

The higher intrinsic antiviral potency associated with peptides derived from HR-2 and the successful development of enfuvirtide (**29**) has focused considerable attention on further optimizing this class of HIV-1 fusion inhibitor to improve both the antiviral and pharmacokinetic profiles. T-1249 (**33**) and sifuvirtide (**34**) are longer HR-C-based peptides, 39 and 36 residues respectively, that incorporate two tryptophan residues proximal to the amino terminus that complement the hydrophobic cavity that is formed by the N17 region of HR-1, an interaction that enfuvirtide (**29**) does not exploit [123–132]. Both **33** and **34** are more potent than **29** and express activity toward virus resistant to this prototypical HIV-1 fusion inhibitor. T-1249 (**33**) appears to more readily adopt a helical structure in solution and associates with lipidic areas on the cell surface, which may contribute towards its increased clinical efficacy [133, 134]. Sifuvirtide (**34**) was engineered based on insights gleaned from X-ray structures of the gp41 six-helix bundle and shares only limited structural identity with enfuvirtide (**29**) [128, 129]. Charged amino acids were strategically incorporated to allow the formation of seven ion pairs as a means of stabilizing the helical conformation, a design hypothesis confirmed by the X-ray structure of **34** bound to the HR-1 trimer [135]. However, **34** does not exhibit significant helicity in solution in the absence of HR-1-derived peptides. Interestingly, unlike **29**, **34** formed a stable six-helix bundle with the HR-1 peptide N36, suggestive of some differences in the precise mode of HIV-1 fusion inhibition. This was further supported by the observation that the two peptides interact synergistically to inhibit virus replication in cell culture [130, 131]. As an individual agent, **34** inhibits HIV-1 envelope-mediated cell-cell fusion with an $IC_{50} = 3.6$ nM, a sixfold potency advantage over **29**, and is active toward enfuvirtide-resistant virus [128, 135]. Both compounds have been evaluated clinically, although development of **33** has not resumed following suspension on January 6, 2004 for the resolution of formulation issues, while **34** has completed Phase II trials in China [135, 136].

Ac-WQEWEQKITALLEQAQIQQEKNEYELQKLDKWASLWEWF-NH_2

33 (T-1249)

Ac-WIEWEREISNYTNQIYEILTESQNQQDRNEKDLLE-OH

34 (sifuvirtide)

Several additional HR-C-based peptides have been designed to take advantage of intramolecular electrostatic interactions that stabilize a helical conformation, including CP32M (**35**), S29EK (**36**), SC34EK (**37**), and T-2635 (**38**) [137–143].

The design principles for these peptides typically rely upon introducing glutamate-lysine pairs in an *i* to *i* + 4 relationship on the solvent-accessible surface of the peptide while optimizing the hydrophobic amino acids that interact with the HR-N trimeric core. These molecules retain activity toward enfuvirtide-resistant virus which maps to mutations at G36, V38, and N43 of HR-1 and the source of resistance has been categorized into four distinct mechanisms [143]. The resistance shown by V38/A/G/S mutations is attributed to reduced contact between HR-1 and enfuvirtide (**29**) while the incorporation of larger residues at this position (*F*, *H*, *M*, *W*, or *Y*) leads to steric repulsion that reduces association of the inhibitor [143]. While smaller residues than valine at position 38 lead to reduced helix bundle stability, that is not the case for the larger amino acids. A third mechanism focuses on electrostatic repulsion in which the valine at position 38 is substituted by an aspartic or glutamic acid which sets up an unfavorable interaction with the glutamic acid at position 146 of HR-2 and which is found in **29** and **33**. Interestingly, T-2635 (**38**) incorporates a glutamic acid at this position but intramolecular ion pairing with the C-terminal arginine, designed to stabilize the helical conformation, neutralizes this residue thereby reducing the electrostatic repulsion with V38D/E [143]. The fourth mechanism of resistance was associated with the introduction of a positive charge at residue 38 of HR-1 in which valine is substituted by arginine or lysine, an observation considered counterintuitive and which was partially explained by reduced stability of the HR-1 helix [143].

Ac-VEWNEMTWMEWEREIENYTKLIYKILEESQEQ-OH

35 (CP32M)

WEEWDKKIEEYTKKIEELIKKSEEQQKKN-OH

36 (S29EK)

W-Nle-EWDRKIEEYTKKIEELIKKSQEQQEKNEKELK-OH

37 (SC34EK)

TTWEAWDRAIAEYAARIEALIRAAQEQQEKNEAALREL

38 (T-2635)

RAWVAWRNR

39 (HL9)

The shortest peptide that has been shown to interact with the HR-N trimer is HL9 (**39**), a nine-residue peptide derived from human lysozyme that potently inhibits HIV-1 syncytia formation in cell culture with an EC_{50} of 50 nM [144, 145]. HL9 (**39**) contains two tryptophan residues separated by two amino acids that complement the hydrophobic pocket formed by the HR-N N17 fragment [142]. However, HL9 (**39**) is not completely specific for HIV-1, since it also exhibits antimicrobial activity [146].

An approach to inducing an α-helical conformation in peptides that is more definitive than relying on salt-bridging interactions involves chemical ligation of side-chain residues using either ring-closing olefin metathesis or Cu-catalyzed azide cycloaddition to an alkyne (click chemistry) [147–153]. This approach,

referred to as stapling, is of emerging importance in peptide design, offering the additional advantage of conferring increased stability toward proteolytic degradation. A series of singly and doubly stapled peptides were designed and prepared based on the HR-2 peptide T-649v (**40**), a 37-mer that was evaluated for both antiviral activity and stability towards chymotrypsin [154]. The sites for stapling were introduced carefully, avoiding interrupting key elements of the HR-2 residue side-chains that interact with the HR-1 trimer, with (*S*)-2-(((9*H*-fluoren-9-yl) methoxy)carbonylamino)-2-methyl-hept-6-enoic acid the key residue incorporated at the *i* and *i* + 4 positions. Ruthenium-catalyzed metathesis then afforded the stapled peptides. While simple peptides related to enfuvirtide (**29**) were rapidly degraded in the presence of chymotrypsin, the singly and doubly stapled peptides were much more stable, with the singly stapled derivatives offering a six- to eightfold increase in half-life, while the doubly stapled peptides exhibited further enhanced stability, with the half-life of SAH-gp41$_{(626–662)}$(A, B) (**41**) measured at 335 min, 24-fold longer than the unmodified peptide [154]. Based on structure-stability studies of the stapled peptides, proteolytic stability was not related to the extent of peptide helicity; rather the presence of the staples was the dominant factor [154]. SAH-gp41$_{(626–662)}$(A, B) (**41**), which demonstrated an intermediate 36% α-helical content, was a potent inhibitor of CXCR4-dependent HIV-1 infection in cell culture (EC_{50} = 2.5 nM, compared to an EC_{50} of 2.9 nM for T-649v (**40**)), while the figures for inhibiting CCR-5-dependent HIV-1 infectivity were EC_{50} = 87 and >3,000 nM, respectively. Intravenous administration of **40** and **41** to mice revealed significant differences in pharmacokinetic properties with the doubly stapled peptide exhibiting 4-to-23-fold higher blood levels at all time points measured between 5 and 240 min post-dosing. The total body clearance of **40** was ten-fold higher than for **41**, reflecting the increased stability towards proteolysis. Remarkably, detectable plasma levels of **41** were measured following oral administration to mice and exposure was dose-dependent although plasma concentrations were modest [154].

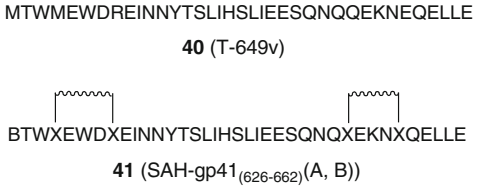

40 (T-649v)

41 (SAH-gp41$_{(626-662)}$(A, B))

An alternate approach to the design of peptide derivatives with enhanced stability towards proteolytic degradation has focused on the discovery of D-peptide derivatives [155–157]. The identification of lead inhibitors relied upon the use of a mirror image of the gp41 HR-1 trimeric species, synthesized using D-amino acids, to screen for peptides using phage display technology that bound to this structure. Potent molecules emerging from this approach were then synthesized as the

D-isomers and studied for inhibition of HR-1 and HR-C association in the natural L-peptide series [155–157]. The culmination of this process was the identification of a series of D-amino acid based pocket-specific inhibitors of entry (PIE) of which PIE7 (**42**) was modestly potent while the larger PIE12 (**43**) represented a significant improvement with EC_{50}s of 37 and 580 nM against the HXB2 and JRFL strains of HIV-1, respectively, in virus infectivity assays [157]. Further increases in potency were derived by taking advantage of the potential for polyvalent interactions in which two or three molecules of PIE12 (**43**) were assembled using polyethylene glycol-based diacids to acylate the amino terminal lysine residues. The constructs were optimized by varying the linker length between five and nine glycol units, and were markedly more potent, with EC_{50}s of 0.1–1.9 nM against the HXB2 virus and 2.8–2,300 nM towards the JRFL strain [157]. X-ray crystallographic analysis revealed the binding modes in the N17 hydrophobic pocket with improved complementarity rather than the establishment of additional interactions responsible for the enhanced potency compared to earlier sequences [157].

AcKGACDYPEWQWLCAA

42 (PIE7)

AcHPDYPEWQWLCELGK

43 (PIE12)

The association of HR-2-derived peptides with albumin has also been explored as a means of enhancing potency and/or pharmacokinetic properties [158–162]. Conjugation of HR-2-based peptides to albumin by introducing a maleimide moiety that reacts with the thiol of Cys34 of the plasma protein affords conjugates that, remarkably, retain potent antiviral activity despite the covalent attachment to a large macromolecule [158, 159]. FB006M (**44**), in which the conjugating element is incorporated in the middle of the peptide, inhibits a panel of HIV-1 viruses in cell culture with EC_{50}s of 0.5–5 nM [158]. The maleimide moiety in PC1505 (**45**) is attached at the amino terminus of the peptide, a topology also compatible with potent antiviral activity, $EC_{50} = 1.8$ nM [159]. Both compounds exhibited improved pharmacokinetic properties in mice and exhibited sustained antiviral activity in SCID mouse models of infection and PC1505 (**45**) is an effective microbicide in SCID-hu Thy/Liv mice with a single 200 mg dose 24 h prior to inoculation with HIV-1 reducing viral load by 3.3 $\log_{10}$ compared to control [158–160]. TRI-999 (**46**) explores an alternative approach to association with albumin that does not rely on covalent bond formation but rather takes advantage of lipophilic binding sites in albumin by attaching a C18 fatty acid derivative *via* a linker to the ε-amino moiety of the Lys30 residue [161]. Although TRI-999 (**46**) offered an improved pharmacokinetic profile in preclinical species and exhibited good potency towards wild-type and enfuvirtide-resistant virus, the compound was not developed because it failed to meet all of the targeted criteria [161].

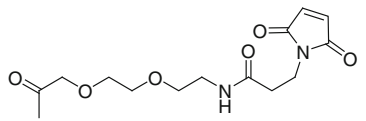

Ac-WEEWDREINNYYTKLIHELIEESQNQQEKNEQELL-NH_2

44 (FB006M)

HSA-Cys34-MPA-AEEA-WMEWDREINNYTSLIHSLIEESQNQQEKNEQELL-NH_2

45 (PC1505)

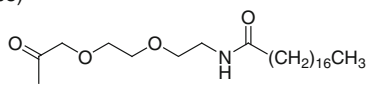

Ac-LTWQEWDREI NNYTSLIHSL IEESQNQQEKNEQELL-NH_2

46 (TRI-999)

Conjugation of C-34 with cholesterol was conceived as a means of localizing the peptide to the host cell membrane, in essence targeting the compound to the site of action [162]. Cholesterol was installed at both the amino- and carboxy- termini using thioether-based chemistry, but only C34-Chol (**47**) exhibited potent HIV-1 inhibitory activity in a single cycle assay where the EC_{50} was 4 pM, which compared to an EC_{50} of 9.5 nM for the alternate topology and 205 pM for the undecorated C34 peptide. This result reflected binding of **47** to the host cell membrane and the antiparallel association with the HR-1 trimer, as depicted in Fig. 10. The antiviral activity of **47** was not dependent simply on lipophilicity since replacing cholesterol with palmitic acid gave a markedly weaker inhibitor, EC_{50} = 713 pM [162, 163]. However, this approach does offer advantage over the simple parent peptide and the four lipophilic residues, WNWF, at the C-terminus of enfuvirtide (**29**) may play a similar role since they do not appear to affect interactions with the HR-1 trimer but are, nevertheless, critically important to antiviral activity [162–165]. C34-Chol (**47**) was similarly active toward a range of HIV-1 strains, including primary isolates, and demonstrated persistent exposure in the plasma of mice following sub-cutaneous administration with compound still detectable 24 h post-dose at a concentration >300-fold above the in vitro EC_{90} of 80–360 pM [162].

3.2 Small-Molecule gp41 Antagonists

Not surprisingly, small-molecule inhibitors of the HR-1-HR-2 interaction have been sought since the elucidation of the formation of the hairpin gp41 structure with the view to developing effective drugs with more convenient dosing regimens than the parenteral route required for enfuvirtide (**29**) [102, 166]. However, the identification of small-molecule inhibitors of gp41 fusion has presented a significant challenge, in contrast to the successful discovery and characterization of a range of chemotypes that interfere with six-helix bundle function in respiratory syncytial virus (RSV) entry [167–171 and Chap. 5 of this volume]. The hydrophobic pocket formed by the N17 element of the HIV-1 gp41 HR-1 accommodates the two tryptophans, Trp628

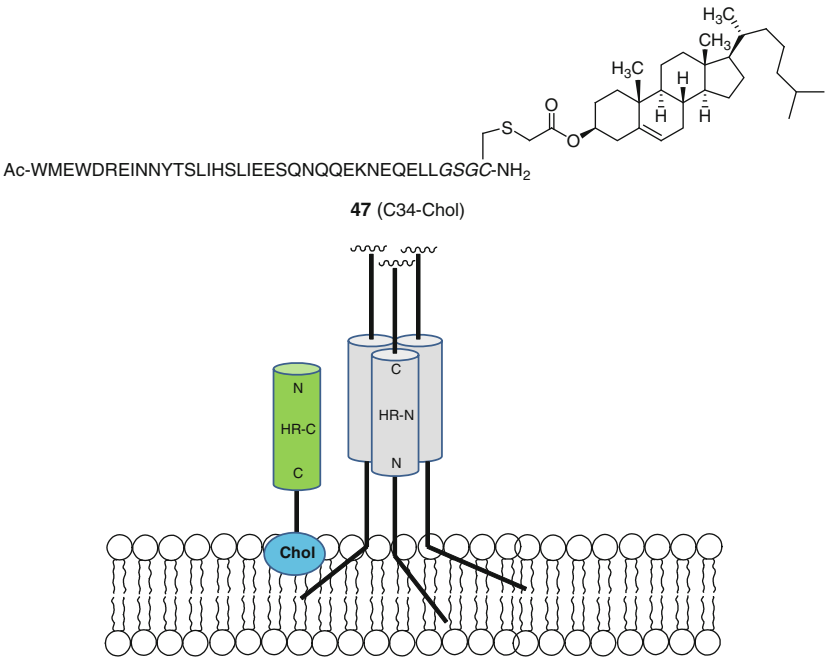

Fig. 10 Proposed binding topology of C34-Chol (**47**) to the HR-1 bundle and the virus membrane

and Trp631, and the isoleucine, Ile635 from the HR-2, analogous to a similar cavity formed in the RSV F protein by the HR-1 trimer which recognizes Phe483 and Phe488 and Ile492 of the HR-2 region [167]. The underlying reason for the difficulty encountered in identifying small-molecule inhibitors of HIV-1 fusion is not understood but may reflect subtle differences in the function of the gp41 six-helix bundle during the entry process compared to the RSV F protein. Nevertheless, a range of strategies have been employed to identify lead molecules and some progress has been made. One approach sought inhibitors of the association of a fluorescein-labeled HR-2 peptide, residues 117–154 and designated C38, with a protein construct comprised of three HR-1 segments interspersed with two HR-1 segments linked by flexible element that allowed the protein to fold into a five-helix bundle that mimics the natural six-helix bundle but with an open groove (Fig. 11) [172]. A screening campaign identified five compounds **48**–**52** that blocked binding of the HR-2 peptide to the five-helix bundle at a concentration of 40 μM of which **48** and **49** exhibited measurable IC_{50}s of 5 and 9 μM, respectively, while the related compound **50** was inactive. Both **48** and **50** interfered with cell-cell fusion at concentrations above 50 μM, limited by poor solubility, and inhibited HIV-1 infectivity in PBMCs with EC_{50}s of 19 (**48**) and 18 μM (**50**), respectively [172]. Additional binding experiments coupled with NMR analyses suggested that these compounds bound to the hydrophobic cavity of the HR-1 trimer [172].

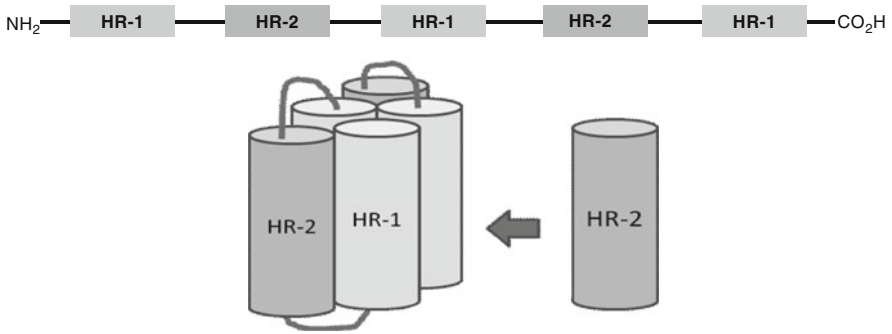

Fig. 11 The structure of a covalently linked five-helix bundle used to screen inhibitors of association with HR-2

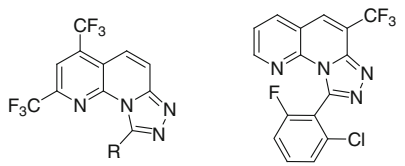

48 R = Ph
49 R = 2-theinyl
50 R = 4-toluyl
51 R = 1-pyrrolyl

52

ADS-J1 (**53**) was selected as a potential inhibitor of gp41 six-helix bundle activity using a docking approach based on the X-ray crystallographic structure [173, 174]. This compound was characterized as an inhibitor of the formation of the gp41 six-helix bundle that exhibited antiviral activity in cell culture but the mode of action of this compound at blocking HIV-1 infectivity in cell culture remains controversial, with some experimental data suggesting that gp120 may be the actual target [173–178].

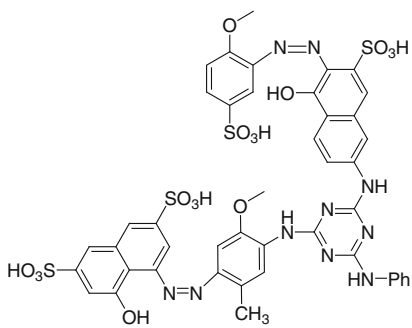

53 (ADS-J1)

NB-2 (**54**) and NB-64 (**55**) were identified as HIV-1 entry inhibitors from a library of over 33,000 molecules using syncytium-forming and gp41 six-helix bundle assembly assays [179]. NB-2 (**54**) and NB-64 (**55**) demonstrated antiviral activity in cell culture with EC_{50}s ranging from 0.89 to 98 μM for NB-2 (**54**) and 2.2 to 39.7 μM for NB-64 (**55**) against a range of HIV strains, while initial SAR studies pointed to the importance of the carboxylic acid moieties for activity, thought to interact with Arg579 or Lys574 to form salt bridges [179, 180]. More recent studies have sought to improve the potency of these leads by exploring the addition of potential binding contacts but with only modest success, represented by structures **56–59** [181–184].

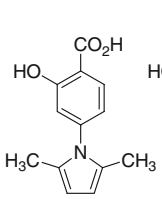

54 (NB-2)

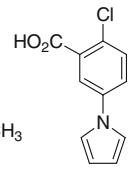

55 (NB-64)

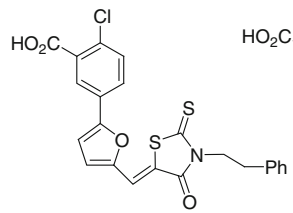

56

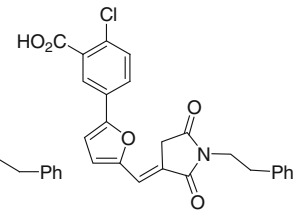

57

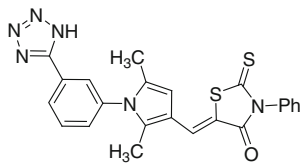

58

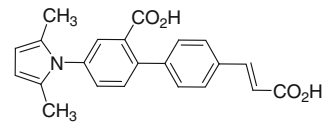

59

An interesting approach to identify gp41 inhibitors relied upon the ability of strategically-substituted terphenyl derivatives to project amino acid side chain moieties with vectors that closely mimic the *i*, *i* + 4, and *i* + 7 elements of an α-helix [185, 186]. The terphenyl derivative **60**, in which the substituents are designed to mimic leucine and isoleucine, disrupted the gp41 six-helix bundle based on circular dichroism analysis and inhibited HIV-1 envelope-mediated cell-cell fusion with an EC_{50} of 15.7 μg/mL [185]. Increasing the size of the hydrophobic substituents to more effectively mimic the tryptophan moieties present in HR-2 and which interact with the hydrophobic N17 pocket gave **61**, which displayed only a modest increase in potency in the six-helix bundle assay [185]. This result presumably reflects differences in the binding mode of **61** compared to the peptide-based inhibitors that may require the application of more careful design principles. However, additional follow-up on this observation by evolving the chemotype has not been reported.

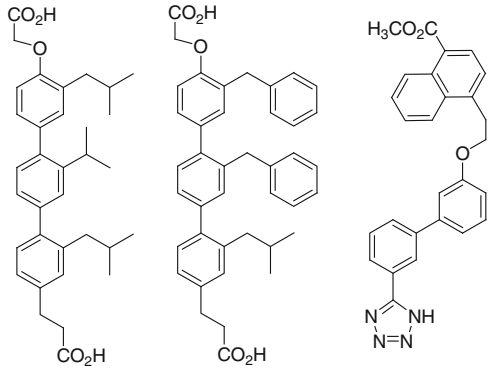

The tetrazole **62** was designed using a computational fragment-based technology that anchored on Lys574 in the HR-1 trimer and focused on exploiting proximal lipophilic pockets [187]. This compound exhibited an IC_{50} of 31 μM for disrupting the gp41 six-helix bundle in a bundle assembly assay but SAR studies were limited to just two close analogues [187].

A survey of compound libraries based on flat and rigid scaffolds that displayed a range of polar and non-polar substituents, some incorporating H-bonding potential, with an assay assessing gp41 six-helix bundle formation identified several inhibitors of which **63** exhibited an IC_{50} of 38 μM [188]. This compound blocked HIV-1-mediated cell-cell fusion with an EC_{50} of 11 μM but with a CC_{50} of 47 μM the therapeutic index was only a modest fourfold.

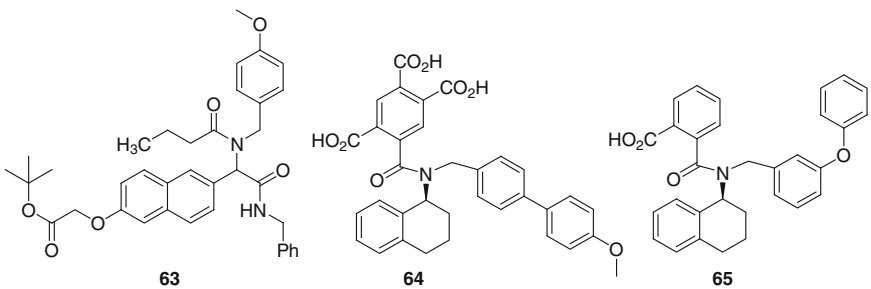

The benzoic acid **65** was optimized from the screening lead **64** identified from an NMR-based assay using an engineered version of the gp41 HR-1 trimer [189]. Acid **65** inhibited HIV-1-mediated cell-cell fusion with an EC_{50} of 3 μM compared to 14 μM for **64** and the NMR data were consistent with **65** binding to the hydrophobic pocket exposed in the construct, with the biphenyl moiety occupying the same region as Trp628 and Trp631 but with the rings orthogonal to the vectors utilized by these amino acid side chains [189].

The bis-indole derivative **66** is a gp41 inhibitor optimized from the benzoic acid **67**, a compound that bound weakly to hydrophobic pocket of gp41 using NMR-based methodology [176, 190–194]. Optimization to **66** relied upon detailed

NMR analysis of the binding modes of predecessor compounds to identify vectors for introducing additional elements designed to establish productive interactions with the pocket. Compound **66** inhibits replication of the HXB2 strain of HIV-1 with an $EC_{50} = 0.8$ μM, with cytotoxicity toward the parental cell line manifested at 20-fold higher concentration [192]. The EC_{50}s for the HIV-1 Ba-L and IIIB strains were 2.38 and 2.80 μM, respectively, in the presence of 10% serum. A correlation was established between HIV-1 inhibition in cell culture and fusion inhibition for this series, with fusion inhibition correlated with binding of the compounds to the hydrophobic pocket. The preferred binding pose places the carboxylic acid moiety of **66** in an electrostatic interaction with Lys574 of gp41 while the methoxyphenyl moiety is proximal to Arg579 [192].

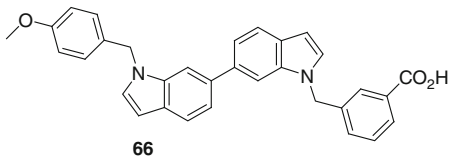

66

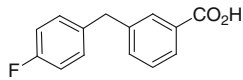

67

The most potent and effective inhibitors of HIV-1 gp41 function described to date are peptide-based derivatives that appear to act by preventing the association of HR-2 with the HR-1 trimer. This contrasts with the situation for RSV where both peptide-based inhibitors and small druglike molecules have been discovered and optimized [167–171, 195]. However, the X-ray crystallographic structure of a small-molecule RSV inhibitor bound to the HR-1/HR-2 six-helix bundle reveals interactions with elements of both HR-1 and HR-2, suggesting that the formation of a binary complex in which the small molecule is trapped in the bundle structure is sufficient to interfere with viral entry [171]. These observations may reflect subtle differences between the function of the RSV F protein and HIV-1 gp41 following the formation of the hairpin configuration. The merging of virus and host membranes via a process involving hemi membrane fusion followed by full membrane fusion as a prelude to the formation of a fusion pore is a poorly understood process and it may be that in the case of RSV, this process exhibits high sensitivity to a deformed six-helix bundle. Although challenging, interfering with HIV-1 gp41 using small molecule inhibitors remains a target of interest to the medicinal chemistry community, but progress has been slow and hard won, reflecting an inadequate understanding of the process of virus entry.

4 Inhibitors of LEDGF/p75 Binding to HIV Integrase

4.1 Background

HIV-1 integrase (IN) is one of three enzymes expressed by the HIV-1 virus and is essential for completion of the viral life cycle [196]. The enzyme carries out two reactions on the viral DNA (vDNA) produced by HIV-reverse transcriptase.

The first is referred to as 3′-processing since the enzyme clips off two nucleotides from both 3′-ends of the vDNA. This is followed by the strand transfer (ST) reaction, wherein the vDNA is inserted into the host DNA. Research has shown that isolated, recombinantely-produced IN can carry out both steps in vitro without the aid of additional protein co-factors.

During infection, integrase carries out its function in the context of a polyprotein complex, referred to as the pre-integration complex (PIC) consisting of both HIV and host proteins. This ensemble of proteins is needed to orchestrate the replication and integration events and aid in transportation of integrase into the nucleus. One of the binding partners of HIV-1 IN has been identified as Lens Epithelial Derived Growth Factor (LEDGF). The LEDGF-IN protein-protein interaction was initially observed in 293T and HeLa cells [197, 198]. In addition, a yeast two-hybrid screen also established LEDGF as a binding partner to IN [199]. LEDGF had been previously discovered as a transcription regulator and was later characterized as being involved in cell survival and autoimmunity [200, 201]. There are two splice variants of this protein, LEDGF/p75 and LEDGF/p52, the former being the one which binds to HIV-1 integrase.

4.2 The Role of LEDGF/p75 in HIV-1 Infection and Viral Integration

Protein knockdown [202, 203] and gene knockout [204] studies showed significant reduction in HIV-1 infection in the absence of, or at very reduced levels of LEDGF/p75. Importantly, these studies showed that replication was inhibited at the point of integration, which more precisely showed that the LEDGF/p75-IN interaction and presumably its role in integration was essential for viral replication.

The mechanism of LEDGF/p75-dependent HIV-1 integration is related to its endogenous role as a nuclear-located protein which displays tight binding to host chromatin. Therefore, LEDGF/p75 mediates binding of the PIC to host DNA, enabling viral integration. The LEDGF/p75-mediated association of IN to host chromatin has been demonstrated in cell culture. For example, fluorescently labeled IN accumulates in the cell nucleus, co-localizing with labeled LEDGF/p75 bound to chromatin. Furthermore, labeled-IN remains bound throughout the cellular lifecycle [197]. In contrast, when LEDGF/p75 is knocked down, localization to nuclear DNA is not observed [205]. Not only does LEDGF/p75 tether IN to host chromatin, it directs the enzyme towards integration into active genes [206].

4.3 Structure of LEDGF/p75 IBD Bound to the HIV CCD

LEDGF/p75 is a 530 amino acid protein consisting of two major functional domains (Fig. 12). The first ~300 amino acids make up the chromatin binding portion of the protein which includes a PWWP chromatin recognition sequence,

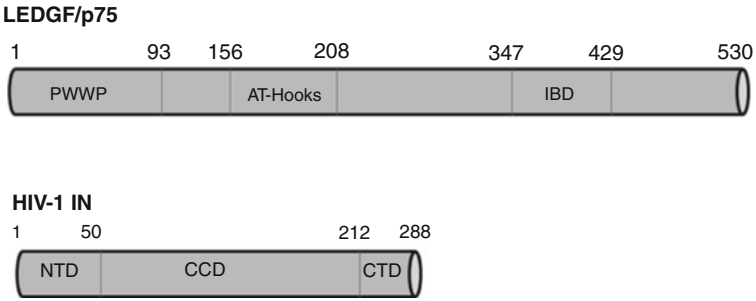

Fig. 12 Domain organization of LEDGF/p75 and HIV-1 IN

two AT-hook DNA binding units, a nuclear localization sequence (NLS), and three charged regions (not shown). The C-terminus functions as the protein recognition portion of LEDGF/p75. A subdomain of the C-terminus (347–429) is referred to as the integrase binding domain (IBD) [207, 208]. LEDGF/p52 lacks the IBD domain and thus does not bind to IN. Site-directed mutational analysis showed that the IBD residues most critical for binding are Ile365, Asp366, Phe406, and Val408 [204, 206, 209]. For integrase, the critical residues are Trp131, Ile161, Gln168, Glu170, and Arg166 in the catalytic core domain (CCD) domain as well some residues in the N-terminal domain (NTD) [207, 210, 211]. The structural details of the interaction of the IBD with the integrase CCD and NTD have recently been elucidated via X-ray crystallography including the structure of HIV-1 INT_{CCD} (50–212) [212], HIV-$2_{NTD\text{-}CCD}$ (1–209) [213], and maedi-visna virus NTD-CCD (1–219) [214] bound to the LEDGF/p75 IBD.

The binding of the IBD to the HIV-1 IN-CCD is depicted in Fig. 13a showing two IBDs bound to the interface of a single dimer of the CCD, yielding a nearly symmetrical structure [212]. The IBD is composed of a five-helix bundle, consistent with the earlier-described NMR solution structure [209]. Binding to integrase occurs via the α1-to-α2 (loop 1) and α4-to-α5 (loop 2) interhelical loops. Loop 1 projects into a crevice at the CCD dimer interface and interacts with both CCD monomers. In contrast, loop 2 interacts exclusively with only one monomer. A total of 1,280 $Å^2$ of protein surface area is buried at the IBD-CCD union. It should be noted that an additional 200–300 $Å^2$ of buried surface area also comes from the interaction of the IBD with the NTD.

A close-up view of the IDB-CCD interface (Fig. 13b) shows the key amino acids participating in the binding. A particularly interesting interaction is the hydrogen bonding of the side chain carboxylate of Asp366 located on loop 1, to the backbone amide NHs of Glu170 and His171. This interaction is set up, in part, by the unusual conformation of the CCD loop connecting the α4- and α5-helices. In addition to this, Asp366 can form an H-bond to the side chain of Thr174. Also located on loop 1 and binding to the CCD-dimer interface is Ile365, which is surrounded by a number of hydrophobic residues that are contributed by both monomers, including Ala128 and Trp132. Additional residues making up the hydrophobic pocket, but which are not shown in Fig. 13B, are Trp131, Thr174, Met178, Phe181, and Ile182.

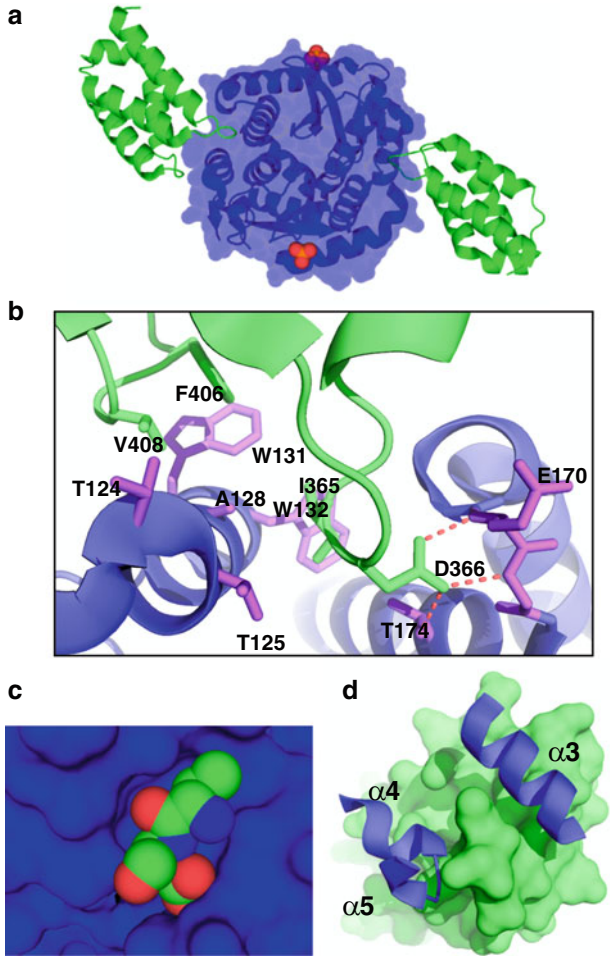

Fig. 13 Binding of the LEDGF/p75-IBD to the CCD of HIV-1 integrase (pdb2BJ4) (**a**) Integrase CCD dimer (*blue*) bound to two IBD units (*green*). Phosphate ions (*orange*) are bound at the CCD-active site (**b**) Close-up of the IBD-CCD interface with labeled residues. The *hashed red line* shows the H-bonding interactions between Asp366 with the Glu170-His171 backbone NHs and Thr174 (**c**) Truncated Ile365-Asp366 bound in the CCD-dimer cleft (**d**) Intergrase α-helices 3, 4 and 5 (*blue*) binding to the IBD (*green*)

The interaction of IBD-loop 2 with the α3-helix of the CCD is also intriguing. Phe406 of the IBD forms an edge-to-face π-π interaction with Tyr131 of the CCD, which is flanked by Val408.

Figure 13c illustrates the binding of the Ile365-Asp366 portion of loop 1 at the dimer interface, suggesting that this is a potential hot spot for inhibitor design. The interaction is shown from a different perspective in Fig. 13d. Here, the IN α3-helix and the IN α4-α5 interhelical loop appear to grasp the Ile365-Asp366 tip of IBD loop

1. This implies that a significant amount of binding energy and specificity is concentrated into a relatively small region of the interface. This clearly demonstrates that this site could serve as a potential hot spot for a small molecule inhibitor.

Transdominant inhibition of LEDGF/p75 binding to IN in cell culture via overexpression of the truncated IBD validated the LEDGF/p75-IN interaction as an antiviral target [215]. The rationale behind this experiment was that truncated IBD should compete with endogenous full-length LEDGF/p75 for binding to integrase in the cell. However, since the truncated IBD lacks a chromatin binding domain, the resulting IBD-IN complex will not bind to host chromatin and therefore will not undergo integration. This was demonstrated in HeLaP4 cells which were engineered to stably overexpress the truncated IBD. Under these conditions, viral replication (HIV NL3.4) was suppressed. As a control, cells expressing a non-IN binding IBD-mutant (D366A) remained susceptible to infection. As with the knockdown and knockout studies described above, replication was blocked at the integration step. Furthermore, virus which was resistant to active-site-directed diketoacid IN-inhibitors was sensitive to transdominant inhibition. Finally, virus selected for resistance to IBD-transdominant inhibition showed mutations at A128T and E170G located in the IBD-binding domain of IN proving that antiviral target was the IBD-IN interaction.

4.4 Retrospective Analysis of Small-Molecule Interactions with the LEDGF/p75 Binding Domain

The CCD dimeric interface encompassing the IDB binding domain demonstrates affinity towards the binding of small molecules. Reports of compounds capable of targeting the CCD dimer interface appeared prior to, or concurrently with, the discovery of LEDGF/p75 as an HIV integrase cofactor. The earliest example comes from an X-ray structure of tetraphenyl arsonium chloride (Ph_4AsCl) bound to the integrase catalytic core domain [216]. As illustrated in Fig. 14a, the Ph_4As^+ group occupies the hydrophobic region which normally accommodates Ile365 of the IBD, with the phenyl groups interacting with Trp131 and Trp132. In addition, the position of the Cl^- counterion appears to mimic the side chain CO_2^- of Asp366 in that it lies within H-bonding distance (3–4 Å) to the Glu170-His171 backbone NH groups and the Thr174 hydroxyl. Taken together, $Ph_4As^+Cl^-$ occupies the same footprint as the Ile365-Asp366 dipeptide moiety and is oriented in an analogous manner with respect to the hydrophobic and electrostatic interactions. In a separate study, the site of action of certain coumarin [217] based inhibitors was determined to be located here based on covalent labeling studies.

The structural information provided by X-ray crystallography proved useful in developing a pharmacophore that could be used for virtual screening and rational drug design. Compound **68** was discovered as an inhibitor of the LEDGF/p75-IN interaction (35% inhibition at 100 μM) out of set of 200,000

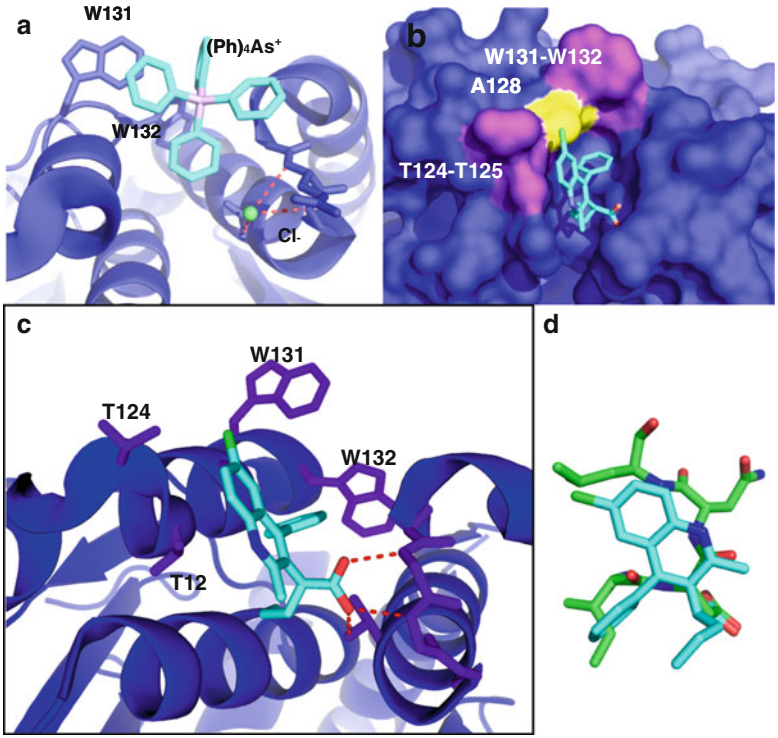

Fig. 14 Structures of IN-CCD and small organic compounds bound to the interface of the IN-CCD dimer (**a**) $Ph_4As^+Cl^-$ (pdb1HYV) (**b,c**) CX0438 (**71**) (pdb3LPU) (**d**) overlay of **71** with the truncated Ile365-Asp366 segment of the IBD from pdb2BJ4

Table 2 Activity of quinoline-based inhibitors of LEDGF binding to integrase and antiviral activity in cell culture

	IC_{50} (μM)	EC_{50} (μM)
68	100 (36%)	ND
69	12.2 ± 3.4	41.9 ± 1.1
70	9.24 ± 0.79	10.8 ± 1.1
71	1.37 ± 0.36	2.35 ± 0.28

commercially-available compounds [218]. As shown in Table 2, further optimization of this series led to improved activity with **69** and **70** eventually providing 2(quinolin-3-yl)acetic acid derivative CX0438 (**71**) [219]. In addition to blocking the binding of LEDGF/p75 to integrase in vitro, **71** is also effective at inhibiting HIV replication in cell culture, with an $EC_{50} = 2.35$ μM. An X-ray crystal structure of CX0438 (**71**) bound to integrase provide detail of how the compounds interact with integrase.

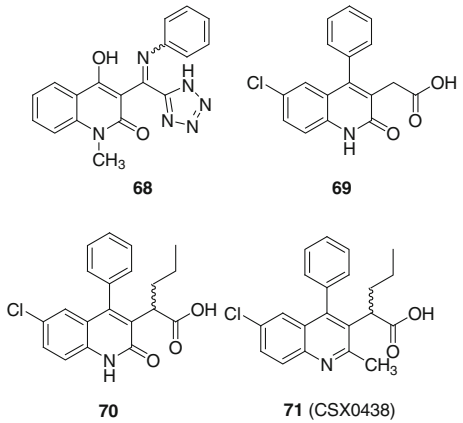

Figure 14b shows that CX0438 (**71**) is significantly buried in the IBD-IN binding pocket at the CCD dimer interface and is oriented such that the carboxylic acid is located at exactly the same position of the corresponding carboxylate group of Asp366 of the IBD, while the C4-phenyl group is located in the hydrophobic portion of the pocket. The fused benzene ring of the quinoline heterocycle projects out of the pocket, but is hydrophobically associated with Thr124–125 and Ala128. Further analysis of the interaction (Fig. 14c) indicates that the carboxylate group of **71** displays the same H-bonding interactions as Asp366 of the IDB to Glu170-His171 backbone NH groups and the Thr174 side-chain of IN. As illustrated by Fig. 14d, the inhibitor overlays well with the Ile365-Asp366 dipeptide of the IDB and therefore, for the most part lies within the steric boundaries defined by the natural substrate. One exception to this is the n-butyl group attached to the acetyl side chain which projects deeper into the binding cleft than the IBD dipeptide.

The 2-(quinolin-3-yl)acetic acid template appears to be a very promising chemotype for further drug development in that it displays efficient binding to IN. In addition, it takes advantage of the same binding interactions that are required for binding to the IBD and for the most part, its structure lies within the envelope defined by the natural ligand. This might have a favorable effect on the potential barrier to the virus developing resistance [220].

4.5 Other Small-Molecule Inhibitors

A number of other small molecules have been reported as inhibitors of LEDGF/p75 binding to integrase. D77 (**72**) binds to both wild type, full length IN (K_d = 5.81 μM) and the isolated IN-CCD (K_d = 6.83 μM). However, it does not bind to integrase containing mutations at positions 95, 124, 131, and 174 which are located in the LEDGF/p75 binding domain [221]. CHIBA-3002 (**73**) (46% inhibition at a

concentration of 100 μM) was discovered in a virtual screen of the CHIME database in which compounds were scored based on their ability to satisfy the IBD-binding pharmacophore [222]. A rational design approach to improve activity yielded compounds **74** and **75** which inhibited LEDGF/p75 binding with $IC_{50} = 3.5$ and 7.5 μM, respectively [223].

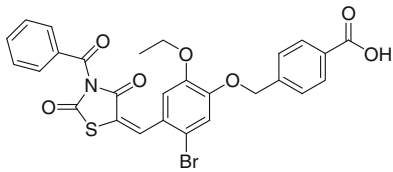

72
D77

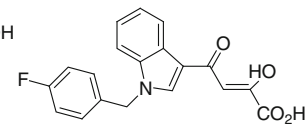

73

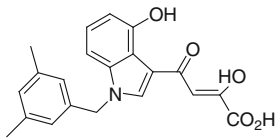

74

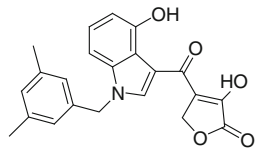

75

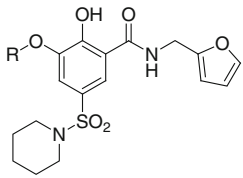

76 R = H
77 R = CH_3

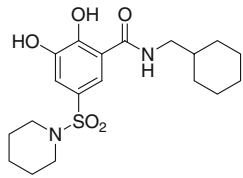

78

Interestingly, CHIBA-3002 (**73**) and the related diketoacids **74** and**75** have previously been shown to bind to the active site of integrase and inhibit strand transfer [224]. Based on this observation, it might be possible to design a dual inhibitor which targets both the LEDGF/p75 binding domain and the active site of integrase [225]. The catechol amide template present in **76** is an isostere of the diketoacid chemotype and yields compounds which are strand transfer inhibitors [226]. Presumably the catechol hydroxyl groups and the amide carbonyl function in the same manner as the diketoacid moiety in binding to the active site Mg^{2+} cofactor. For example, compound **76** is a relatively moderate strand transfer inhibitor ($IC_{50} = 13$ μM) but does not inhibit the binding of LEDGF/p75 to integrase ($IC_{50} > 100$ μM). As might be expected when one of the chelating atoms is blocked, strand transfer-inhibitory activity is lost ($IC_{50} > 100$ μM), but the resulting analogue **77** is a selective LEDGF/p75-IN inhibitor ($IC_{50} = 13$ μM). A favorable balance between strand transfer and LEDGF/p75 inhibition was achieved with compound **78**.

4.6 The LEDGF/p75-Integrase PPI as a Druggable Target

The PPI between LEDGF/p75 and IN represents an ideal antiviral target for a number of reasons. First, the extent of the interaction is smaller than the average PPI as measured by total buried surface area. The nature of the structural motifs making up the interaction yields an interdigitated-type interface wherein the two helix-turn-helix loops of the IBD project into the CCD dimer interface of IN. Structural analysis of this interaction suggests that a large amount of binding energy is concentrated in a pocket about the size of a dipeptide. Within the pocket, there are a diverse set of structural elements available for small-molecule binding, including H-bonding and hydrophobic residues. Most importantly, there are reports emerging in the literature demonstrating antiviral activity for small-molecule inhibitors. One family of inhibitors, the 2-(quinolin-3-yl)acetic acid derivatives, achieves potent inhibition from molecules which lie almost completely within the spatial envelope defined by the natural ligand.

5 HIV-1 Protease Dimerization Inhibitors

5.1 Background and Mechanism

HIV-1 protease is a homodimeric aspartyl protease comprised of two monomers each containing 99 amino acid residues (Fig. 15). The catalytic site is formed upon dimerization, with each monomer providing one of the two catalytic Asp25 residues, and is located at the base of a cavity within the dimer interface. Dissociation of the functional homodimer to the catalytically inactive monomers therefore results in the loss of enzymatic activity. Below the catalytic cavity, a four-stranded anti-parallel β-sheet accounts for 50% of the hydrogen bonds along the dimer interface and appears to be highly conserved among HIV-1 isolates. This secondary structure is composed of the residues of both the N- and C-termini of each monomer (i.e., HN-Pro1-Gln2-Ile3-Thr4-Leu5 and Cys95-Thr96-Leu97-Asn98-Phe99-CO_2H, respectively) and arranged in a way that the two C-terminal β-strands are sandwiched between the two N-terminal β-strands (Fig. 16). Thermodynamic analysis of the protease homodimer by differential scanning calorimetry indicated that the dimer is primarily stabilized by this region, which contributes close to 75% of the total Gibbs free energy of stabilization [227]. Studies using truncated constructs lacking residues 1–4 and 96–99 further suggested that the interaction between the residues of the two inner C-terminal β-strands is primarily required for dimerization [228]. In fact, the C-terminal tetrapeptide Ac-Thr-Leu-Asn-Phe-CO_2H was first identified as an inhibitor of the protease enzyme in vitro with a K_i of 45 μM measured at pH 5.0 and 37°C. Its inhibitory mechanism was determined as dissociative in which competitive binding of the peptide to the inactive monomers inhibits their dimerization into the active enzyme [229].

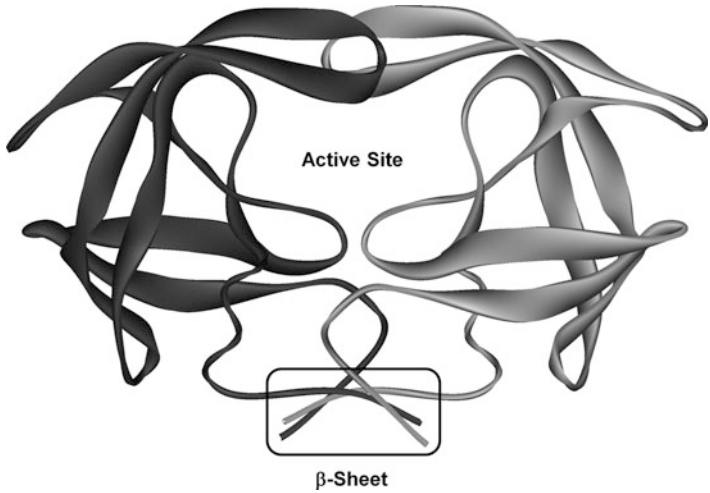

Fig. 15 Structure of the homodimeric HIV-1 protease with the locations of the active site and the four-stranded anti-parallel β-sheet as indicated

5.2 Inhibitors of HIV-1 Protease Dimerization

The main class of compounds that have been reported to inhibit HIV-1 protease dimerization were derived from the residues at the N- and C-termini and designed to mimic the interdigitation of the two termini, although a small number of natural products have been claimed to exhibit micromolar inhibitory potency [230–233]. However, although the peptidic inhibitors displayed potent activity in enzymatic assays, their activity in cell culture systems has not been demonstrated. Dimerization inhibitor **79** is comprised of a peptide sequence derived from the N-terminus of the enzyme cross-linked by a flexible linker to a sequence derived from the C-terminus [233]. The linker with 14 methylene units provides an optimal distance, matching the 10 Å between the backbones of the two interfacial peptides of the protease monomer. A challenge in the development of dimerization inhibitors is the competition between protease monomer/inhibitor complex formation and monomer/monomer dimerization, which has a dissociation constant K_d in the range of 50 nM to 23 pM, depending on the experimental conditions [227, 229], although conceptually, in vivo, the dissociative inhibitor can bind to the polyprotein before auto-cleavage. Due to the nature of concentration-dependence on the stability of the HIV-1 protease dimer, the inhibitory potency of the compounds is decreased at higher protease concentration. For example, the in vitro IC_{50} of **79** was raised from 0.3 to 2 μM when the protease concentration was increased fourfold in the assay. Systematic truncation studies identified **80**, with substitution of Tyr6 by a Phe residue to restore the dimerization inhibition from a poorly characterized competitive inhibition, as

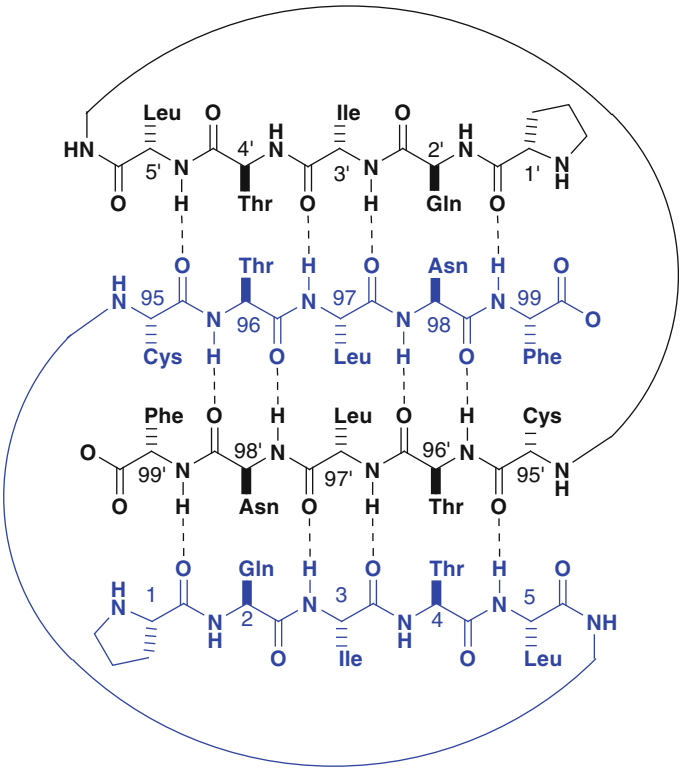

Fig. 16 A four-stranded anti-parallel β-sheet of the HIV-1 protease dimer interface formed by hydrogen-bonding interactions between the residues of the N- and C-termini of each monomer

exhibited by **81** [234]. It has been shown that changes in the residue/side-chain, e.g., removal of Thr4 from **80** [235], or even a small modification, e.g. of the substitution on the phenyl ring of Phe6 [236] will alter the mechanism between dimerization and competitive inhibition. The two peptide subunits of **80** could also be linked through the Thr4 and the Asn98 – based on molecular modeling that suggested the side-chains of these two residues were on the same side of the solvent-exposed face – to provide potent inhibitors that possessed hydrophobic alkyl side chains at the amino termini [237]. Modeling also suggested that the side chain of Phe99 in **80** resided in a hydrophobic pocket, while that of Phe6 was located in an extended hydrophobic area [238] such that larger aromatic side chains would be preferred. This kind of modification coupled with variations in other positions worked synergistically to produce some of the most potent inhibitors, e.g., **82**, of this class [239]. It would appear that an effective protease dimerization inhibitor would rely to a great extent upon precise formation of a hydrogen-bonding network between the inhibitor and the protease β-strands; however, a methylation scan of the backbone amide NH of **80** revealed that the

amide hydrogen atoms were not crucial and only resulted in a twofold loss of potency [240]. These findings led to the design of peptoid inhibitors, such as **83**, that exhibited dimerization inhibition activity comparable to peptide inhibitors [241].

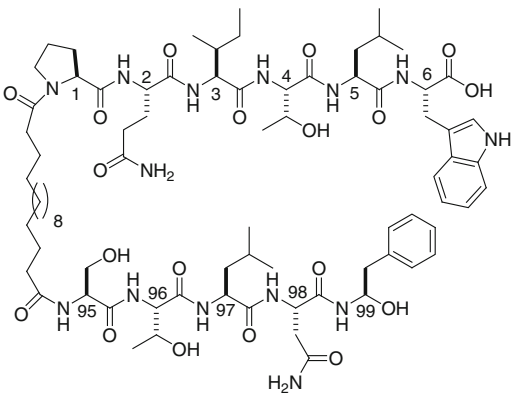

79 K_i = 220 nM
IC_{50} 0.3 μM (25 nM protease)
IC_{50} 2.0 μM (100 nM protease)

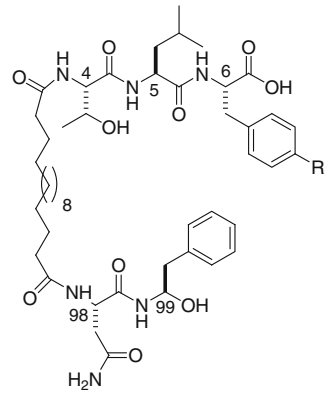

80 Phe6, R= -H, K_i = 3.0 μM
IC_{50} 5.9 μM (25 nM protease)

81 Tyr6, R= -OH, IC_{50} 9.2 μM
(25 nM protease) competitive inhibitor

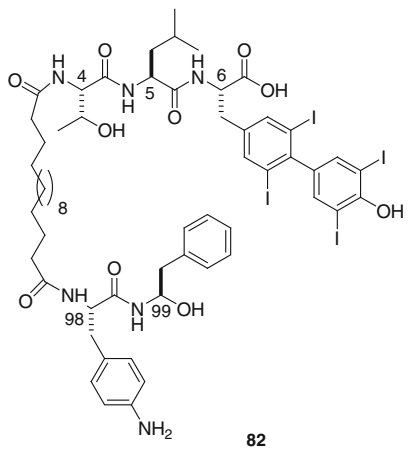

82
K_i = 29.3 nM

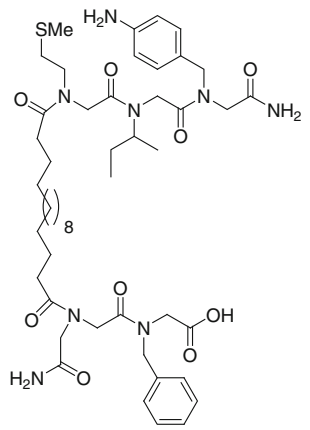

83 K_i = 0.8 μM
IC_{50} 8.8 μM (50 nM protease)

Another class of peptidic HIV-1 protease dimerization inhibitors incorporated a rigid, conformationally restrained template such as the naphthalene moiety in compound **84**, which maintained the desirable 10 Å separation length. A symmetrical inhibitor from this series utilizing the C-terminal fragment, Thr96-Leu97-Asn98-Phe99-CO_2Me, inhibited protease dimerization with an IC_{50} of 4.4 μM at 7.5 nM enzyme concentration and a K_i of 1 μM, while no inhibition was observed at

the solubility limit for the corresponding compound derived from the N-terminal fragment Gln2-Ile3-Thr4-Leu5-CO_2Me [242]. These observations are reasonable because the interaction between the sandwiched C-terminal β-strands is crucial for protease dimerization as described above [243]. Further simplification of the C-terminal inhibitor led to the twofold more active **84**, employing a tripetide Val-Leu-Val-CO_2Me motif. This tripetide sequence could be matched with the C-terminal sequence to produce unsymmetrical inhibitors that displayed similar dimerization inhibitory potency [243]. Peptidomimetic moieties that replaced two amino acids could be incorporated into the carboxylate end of **84** to provide inhibitors (**85**) that preserved the hydrogen-bonding interactions with the protease dimerization interface [244]. The peptidic character of **85** was further reduced by employing mimetic groups at both carboxylate ends, as in **86**, while maintaining potency [245]. However, this type of modification may also introduce a competitive inhibition mechanism to give inhibitors that show a mixed mode of inhibition or solely rely on competitive inhibition.

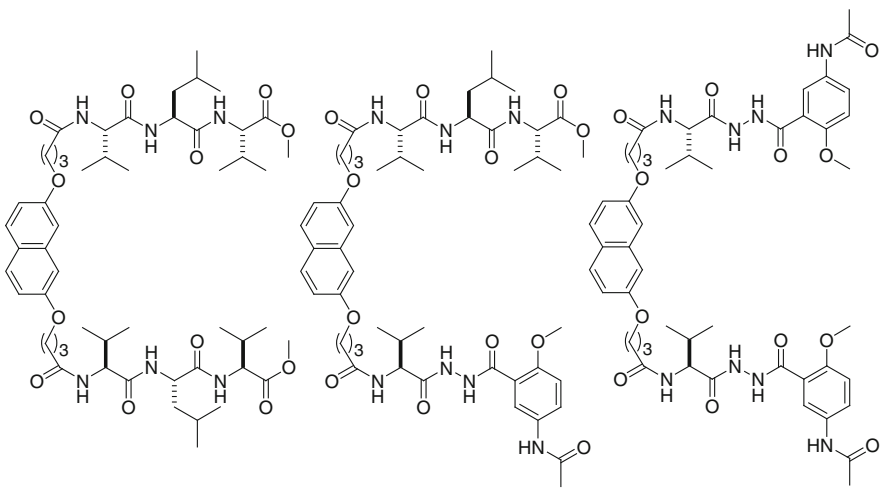

84: K_i = 0.56 μM
IC_{50} 2.0 μM (7.5 nM protease)

85: K_i = 0.2 μM
(dimerization)

86: K_i = 0.22 μM
(dimerization)

Recently, the approved HIV-1 protease inhibitors, darunavir (**87**) and tipranavir (**91**), inhibiting the protease at the catalytic site, have also been shown to disrupt protease dimerization in COS7 cells transfected with a FRET-based HIV-1 expression system that carried cyan and yellow fluorescent protein-tagged protease monomers [246]. Interestingly, none of the other licensed HIV-1 protease inhibitors showed the dual inhibition mechanism. Darunavir (**87**) blocked the dimerization at a concentration of 0.1 μM and above and at a stage before the monomers associated into active dimers. Darunavir analogs with small structural difference, e.g., TMC-126 (**88**), and those with substantial structural changes, e.g., the macrocycle GRL-216 (**89**) [247], also exhibited similar protease dimerization inhibition activity. GRL-0519A (**90**) was, however, about tenfold more active than **87** [248]. Although

the mechanism by which **87** inhibits dimerization remains to be determined, as implicated by the hydrogen-bonding interaction between the tetrahydrofuran of **87** and Asp29, binding of the inhibitor in the active site that disrupts the formation of the hydrogen-bonding network of the key four-stranded anti-parallel β-sheet below the active site that is prerequisite for dimerization may be a possible explanation and represents an interesting example of inhibition of a PPI.

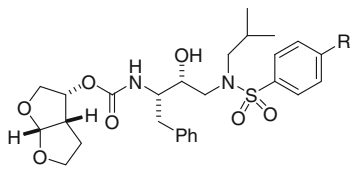

87 R = NH_2 (darunavir)

88 R = OMe (TMC-126)

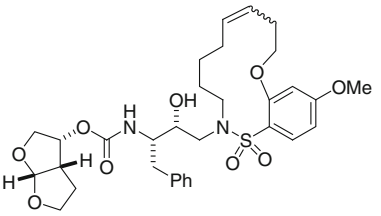

89 (GRL-216)

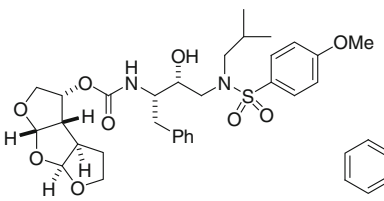

90 (GRL-0519A)

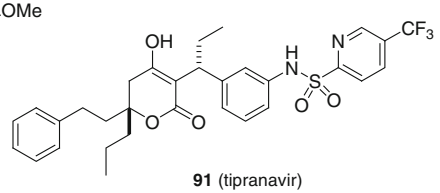

91 (tipranavir)

6 Conclusions

The efforts to attain inhibitors of HIV infection via disruption of protein-protein interactions have been demanding but have provided considerable scientific knowledge. In this chapter, the challenges and progress associated with interfering with four key protein-protein interactions in the HIV-1 lifecycle, gp120/human CD4, HIV-1 gp41 six-helix bundle formation, the human LEDGF/p75-integrase interaction, and dimerization of HIV-1 protease have been reviewed. The first target has realized an orally administered inhibitor that targets HIV-1 gp120 that is currently being actively pursued in Phase II clinical studies. The efforts to target gp41 and protease dimerization using small molecules have also made progress but challenges remain and an oral inhibitor has not yet been advanced to development. The available published literature suggests that the LEDGF/p75 integrase interaction may have the potential to realize an inhibitor; however, this target has been pursued for the shortest time among the four that have been discussed. In conclusion, the medical need for new HIV-1 therapies provides the incentive and justifies future efforts to continue to overcome the challenges that would allow identification of suitable inhibitors of these four PPIs for eventual clinical use.

References

1. Fauci A (2006) Twenty-five years of HIV/AIDS. Science 313:409
2. Hashimoto C, Tanaka T, Narumi T et al (2011) The successes and failures of HIV drug discovery. Exp Opin Drug Disc 10:1067–1090
3. Mehellou Y, De Clercq E (2010) Twenty-six years of anti-HIV drug discovery: where do we stand and where do we go? J Med Chem 53:521–538
4. Taiwo B, Hicks C, Eron J (2010) Unmet therapeutic needs in the new era of combination antiretroviral therapy for HIV-1. J Antimicrob Chemother 65:1100–1107
5. De Clercq E (2009) Anti-HIV drugs: 25 compounds approved within 25 years after the discovery of HIV. Int J Antimicrob Agents 33:307–320
6. Frampton JE, Croom KF (2006) Efavirenz/emtricitabine/tenofovir disoproxil fumarate: triple combination tablet. Drugs 66:1501–1512
7. Killingley B, Pozniak A (2007) The first once-daily single-tablet regimen for the treatment of HIV-infected patients. Drugs Today 43:427–442
8. Tilton JC, Doms RW (2010) Entry inhibitors in the treatment of HIV-1 infection. Antiviral Res 85:91–100
9. Lobritz MA, Ratcliff AN, Arts EJ (2010) HIV-1 entry, inhibitors, and resistance. Viruses 2:1069–1105
10. Wyatt R, Sodroski J (1998) The HIV-1 envelope glycoproteins: fusogens, antigens, and immunogens. Science 280:1884–1888
11. Arrildt KT, Joseph SB, Swanstrom R (2012) The HIV-Env protein. A coat of many colors. Curr HIV/AIDS Rep. doi:10.1007/s11904-011-0107-3
12. Blair WS, Cao J, Jackson L et al (2007) Identification and characterization of UK-201844, a novel inhibitor that interferes with human immunodeficiency virus type 1 gp160 processing. Antimicrob Agents Chemother 51:3554–3561
13. Kwong PD, Wyatt R, Sattentau QJ et al (2000) Oligomeric modeling and electrostatic analysis of the gp120 envelope glycoprotein of human immunodeficiency virus. J Virol 74:1961–1972
14. Kwong PD, Wyatt R, Robinson J et al (1998) Structure of an HIV gp120 envelope glycoprotein in complex with the CD4 receptor and a neutralizing human antibody. Nature 393:648–659
15. Huang C, Tang M, Zhang M-Y et al (2005) Structure of a V3-containing HIV-1 gp120 core. Science 310:1025–1028
16. Kwong PD, Wyatt R, Majeed S et al (2000) Structures of HIV-1 gp120 envelope glycoproteins from laboratory-adapted and primary isolates. Structure 8:1329–1339
17. Chen B, Vogan EM, Gong H (2005) Determining the structure of an unliganded and fully glycosylated SIV gp120 envelope glycoprotein. Structure 13:197–211
18. Chen B, Vogan EM, Gong H et al (2005) Structure of an unliganded simian immunodeficiency virus gp120 core. Nature 433:834–841
19. Schon A, Madani N, Klein JC et al (2006) Thermodynamics of binding of a low-molecular-weight CD4 mimetic to HIV-1 gp120. Biochemistry 45:10973–10980
20. Rizzut CD, Wyatt R, Hernandez-Ramos N et al (1998) A conserved HIV gp120 glycoprotein structure involved in chemokine receptor binding. Science 280:1949–1953
21. Kuritzkes DR (2009) HIV-1 entry inhibitors: an overview. Curr Opin HIV AIDS 4:82–87
22. Caffrey M (2011) HIV envelope: challenges and opportunities for development of entry inhibitors. Trends Microbiol 19:191–197
23. Hertje M, Zhou M, Dietrich U (2010) Inhibition of HIV-1 entry: multiple keys to close the door. ChemMedChem 5:1825–1835
24. Teixeira C, Gomes JR, Gomes P et al (2011) Viral surface glycoproteins, gp120 and gp41, as potential drug targets against HIV-1: brief overview one quarter of a century past the approval of zidovudine, the first anti-retroviral drug. Eur J Med Chem 46:979–992
25. Este JA (2011) Inhibition of HIV entry. Method Prin Med Chem 50:29–50

26. Wang H-g, Kadow J, Lin P-F (2005) HIV gp120 envelope as a therapeutic target. Drugs Future 30:359–367
27. Kadow J, Wang HG, Lin PF (2006) Small-molecule HIV-1 gp120 inhibitors to prevent HIV-1 entry: an emerging opportunity for drug development. Curr Opin Invest Drugs 7:721–726
28. Lin P-F, Kadow J, Alexander L (2007) Inhibitors that target gp120-CD4 interactions, in entry inhibitors. In: Reeves JD, Derdeyn CA (eds) HIV therapy. Birkhäuser Verlag, Basel
29. Kadow JF, Bender J, Regueiro-Ren A et al (2011) Discovery and development of HIV-1 entry inhibitors that target gp120. In: Kazmierski WM (ed) Antiviral drugs: from basic discovery through clinical trials. Wiley, Hoboken
30. Wyatt R, Kwong PD, Desjardins E et al (1998) The antigenic structure of the HIV gp120 envelope glycoprotein. Nature 393:705–711
31. Zhou T, Xu L, Dey B et al (2007) Structural definition of a conserved neutralization epitope on HIV-1 gp120. Nature 445:732–737
32. Chen L, Kwon Y-D, Zhou T et al (2009) Structural basis of immune evasion at the site of CD4 attachment on HIV-1 gp120. Science 326:1123–1127
33. Xie H, Ng D, Savinov SN et al (2007) Structure-activity relationships in the binding of chemically derivatized CD4 to gp120 from human immunodeficiency virus. J Med Chem 50:4898–4908
34. Myszka DG, Sweet RW, Hensley P et al (2000) Energetics of the HIV gp120-CD4 binding reaction. Proc Natl Acad Sci USA 97:9026–9031
35. Xiang S-H, Kwong PD, Gupta R et al (2002) Mutagenic stabilization and/or disruption of a CD4-bound state reveals distinct conformations of the human immunodeficiency virus type 1 gp120 envelope glycoprotein. J Virol 76:9888–9899
36. Yuan W, Bazick J, Sodroski J (2006) Characterization of the multiple conformational states of free monomeric and trimeric human immunodeficiency virus envelope glycoproteins after fixation by cross-linker. J Virol 80:6725–6737
37. Dowd CS, Leavitt S, Babcock G et al (2002) β-turn Phe in HIV-1 env binding site of CD4 and CD4 mimetic miniprotein enhances env binding affinity but is not required for activation of co-receptor/17b site. Biochemistry 41:7038–7046
38. Kassa A, Madani N, Schon A et al (2009) Transitions to and from the CD4-bound conformation are modulated by a single-residue change in the human immunodeficiency virus type 1 gp120 inner domain. J Virol 83:8364–8378
39. Guo Q, Ho H-T, Dicker I et al (2003) Biochemical and genetic characterizations of a novel human immunodeficiency virus type 1 inhibitor that blocks gp120-CD4 interactions. J Virol 77:10528–10536
40. Lin P-F, Blair W, Wang T et al (2003) A small molecule HIV-1 inhibitor that targets the HIV-1 envelope and inhibits CD4 receptor binding. Proc Natl Acad Sci USA 100:11013–11018
41. Ho H-T, Fan L, Nowicka-Sans B et al (2006) Envelope conformational changes induced by human immunodeficiency virus type 1 attachment inhibitors prevent CD4 binding and downstream entry events. J Virol 80:4017–4025
42. Meanwell NA, Wallace OB, Fang H et al (2009) Inhibitors of HIV-1 attachment. Part 2: an initial survey of indole substitution patterns. Bioorg Med Chem Lett 19:1977–1981
43. Meanwell NA, Wallace OB, Wang H et al (2009) Inhibitors of HIV-1 attachment. Part 3: a preliminary survey of the effect of structural variation of the benzamide moiety on antiviral activity. Bioorg Med Chem Lett 19:5136–5139
44. Wang T, Kadow JF, Zhang Z et al (2009) Inhibitors of HIV-1 attachment. Part 4: a study of the effect of piperazine substitution patterns on antiviral potency in the context of indole-based derivatives. Bioorg Med Chem Lett 19:5140–5145
45. Wang T, Yin Z, Zhang Z et al (2009) Inhibitors of human immunodeficiency virus type 1 (HIV-1) attachment. 5. An evolution from indole to azaindoles leading to the discovery of 1-(4-benzoylpiperazin-1-yl)-2-(4,7-dimethoxy-1*H*-pyrrolo[2,3-*c*]pyridin-3-yl)ethane-1,2-dione (BMS-488043), a drug candidate that demonstrates antiviral activity in HIV-1-infected subjects. J Med Chem 52:7778–7787

46. Wang T, Zhang Z, Wallace OB et al (2003) Discovery of 4-benzoyl-1-[(4-methoxy-1H- pyrrolo [2,3-b]pyridin-3-yl)oxoacetyl]-2-(R)-methylpiperazine (BMS-378806): a novel HIV-1 attachment inhibitor that interferes with CD4-gp120 interactions. J Med Chem 46:4236–4239
47. Yang Z, Zadjura L, D'Arienzo C et al (2005) Preclinical pharmacokinetics of a novel HIV-1 attachment inhibitor BMS-378806 and prediction of its human pharmacokinetics. Biopharm Drug Disp 26:387–402
48. Xue Y-J, Yan J-H, Arnold M et al (2007) Quantitative determination of BMS-378806 in human plasma and urine by high-performance liquid chromatography/tandem mass spectrometry. J Sep Sci 30:1267–1275
49. Yang Z, Zadjura LM, Marino AM et al (2010) Utilization of in vitro Caco-2 permeability and liver microsomal half-life screens in discovering BMS-488043, a novel HIV-1 attachment inhibitor with improved pharmacokinetic properties. J Pharm Sci 99:2135–2152
50. Hanna G, Lalezari J, Hellinger J et al (2004) Antiviral activity, safety, and tolerability of a novel, oral small-molecule HIV-1 attachment inhibitor, BMS-488043, in HIV-1 infected subjects. Abstract 141. 11th conference on retroviruses opportunistic infect, San Francisco, CA
51. Hanna GJ, Lalezari J, Hellinger JA et al (2011) Antiviral activity, pharmacokinetics, and safety of BMS-488043, a novel oral small-molecule HIV-1 attachment inhibitor, in HIV-1-infected subjects. Antimicrob Agents Chemother 55:722–728
52. Zhou N, Nowicka-Sans B, Zhang S et al (2011) In vivo patterns of resistance to the HIV attachment inhibitor BMS-488043. Antimicrob Agents Chemother 55:729–737
53. Si Z, Madani N, Cox JM et al (2004) Small-molecule inhibitors of HIV-1 entry block receptor-induced conformational changes in the viral envelope glycoproteins. Proc Natl Acad Sci USA 101:5036–5041
54. Madani N, Perdigoto AL, Srinivasan K et al (2004) Localized changes in the gp120 envelope glycoprotein confer resistance to human immunodeficiency virus entry inhibitors BMS-806 and #155. J Virol 78:3742–3752
55. Lin P-F, Ho HT, Gong YF et al (2004) Characterization of a small molecule HIV-1 attachment inhibitor BMS-488043: virology, resistance, and mechanism of action. Abstract 534. 11th Conference on retroviruses opportunistic infect, San Francisco, CA
56. Dahan A, Miller JM, Amidon GL (2009) Prediction of solubility and permeability class membership: provisional BCS classification of the world's top oral drugs. AAPS J 11:740–746
57. Fakes MG, Vakkalagadda BJ, Qian F et al (2009) Enhancement of oral bioavailability of an HIV-attachment inhibitor by nanosizing and amorphous formulation approaches. Int J Pharm 370:167–174
58. Wang T, Ueda Y, Connolly TP et al (2010) Use of a phosphonoxymethyl prodrug approach to successfully improve the oral delivery of HIV-1 attachment inhibitors: design, preclinical profile, and human exposure. Abstract MEDI-346. 239th ACS national meeting, San Francisco, CA
59. Kadow JF, Ueda Y, Meanwell NA et al (2012) Inhibitors of human immunodeficiency virus type 1 (HIV-1) attachment 6. Preclinical and human pharmacokinetic profiling of BMS-663749, a phosphonooxymethyl prodrug of the HIV-1 attachment Inhibitor 2-(4-benzoyl-1-piperazinyl)-1-(4,7-dimethoxy-1H-pyrrolo[2,3-*c*]pyridin-3-yl)-2-oxoethanone (BMS-488043). J Med Chem 55:2048–2056
60. Nettles R, Schurmann D, Zhu L et al (2011) Pharmacodynamics, safety, and pharmacokinetics of BMS-663068, a potentially first in class oral HIV attachment inhibitor. Paper 49. 18th conference retroviruses opportunistic infections, Boston, MA
61. Nettles R, Schürmann D, Zhu L et al (2012) Pharmacodynamics, safety, and pharmacokinetics of BMS-663068, an oral HIV-1 attachment inhibitor in HIV-1-infected subjects. J Inf Dis (manuscript accepted)
62. Kadow JF, Ueda Y, Connolly TP et al (2011) Discovery of BMS-663068, an HIV attachment inhibitor for the treatment of HIV-1. Abstracts MEDI-29. 241st ACS national meeting, Anaheim, CA

63. Wang T. Inhibitors of Human Immunodeficiency Virus Type 1 (HIV-1) attachment. Part x. SAR of 4-Methoxy 6-Azaindole series of HIV gp120 entry inhibitors and discovery of BMS-626529 and its phosphonoxymethyl prodrug BMS-663068 (Manuscript in preparation)
64. Nowicka-Sans B, Gong Y-f, Ho H-T et al (2011) Antiviral activity of a new small molecule HIV-1 attachment inhibitor, BMS-626529, the parent of BMS-663068. Poster 518. 118th conference retroviruses opportunistic infections, Boston, MA
65. Nowicka-Sans B, Gong Y-F, McAuliffe B et al (2012) In vitro antiviral characteristics of HIV-1 attachment inhibitor BMS-626529, the active component of the prodrug BMS-663068 (Manuscript in preparation)
66. Yeung K-S, Browning MR, Colonno RJ et al (2010) Discovery of indole and azaindole-7-carboxamides as potent and orally bioavailable HIV attachment inhibitors. Abstract MEDI-12. 239th ACS national meeting, San Francisco, CA
67. Regueiro-Ren A, Xue QM, Ueda Y et al (2009) HIV-1 attachment inhibitors: structure-activity relationships leading to the identification of 1-(4-benzoylpiperazin-1-yl)-2-(4-fluoro-7-(1*H*-1,2,3-triazol-1-yl)-1*H*-pyrrolo[2,3-*c*]pyridin-3-yl)ethane-1,2-dione. Abstract MEDI-450. 238th ACS national meeting, Washington, DC
68. Regueiro-Ren A (2012) Inhibitors of Human Immunodeficiency Virus Type (HIV-1) attachment IX. Structure-activity relationships associated with 4-Fluoro-6-azaindole derivatives leading to the identification of 1-(4-Benzoyl-piperazin-1-yl)-2-(4-fluoro-7-[1,2,3]triazol-1-yl-1H-pyrrolo[2,3-c]pyridin-3-yl)-ethane-1,2-dione (BMS-585248) (Manuscript in preparation)
69. Brown JR, Toale H, Dennis AB et al (2010) Stable pharmaceutical composition for optimized delivery of an HIV attachment inhibitor. US Pat Appl Publ 20100056540A1
70. Zhou N, Fan L, Ho H-T et al (2010) Increased sensitivity of HIV variants selected by attachment inhibitors to broadly neutralizing antibodies. Virology 402:256–261
71. Zhang S, Alexander L, Wang T et al (2010) Protection against HIV-envelope-induced neuronal cell destruction by HIV attachment inhibitors. Arch Virol 155:777–781
72. Alexander L, Zhang S, McAuliffe B et al (2009) Inhibition of envelope-mediated CD4+−T-cell depletion by human immunodeficiency virus attachment inhibitors. Antimicrob Agents Chemother 53:4726–4732
73. Lu RJ, Tucker JA, Zinevitch T et al (2007) Design and synthesis of human immunodeficiency virus entry inhibitors: sulfonamide as an isostere for the α-ketoamide group. J Med Chem 50:6535–6544
74. Lu R-J, Tucker JA, Pickens J et al (2009) Heterobiaryl human immunodeficiency virus entry inhibitors. J Med Chem 52:4481–4487
75. Wang J, Le N, Heredia A et al (2005) Modification and structure-activity relationship of a small molecule HIV-1 inhibitor targeting the viral envelope glycoprotein gp120. Org Biomol Chem 3:1781–1786
76. Tran T-D, Adam FM, Calo F et al (2009) Design and optimization of potent gp120-CD4 inhibitors. Bioorg Med Chem Lett 19:5250–5255
77. Williams DH, Adam F, Fenwick DR et al (2009) Discovery of a small molecule inhibitor through interference with the gp120-CD4 interaction. Bioorg Med Chem Lett 19:5246–5249
78. Langdon G, Davis JD, McFadyen LM et al (2010) Translational pharmacokinetic-pharmacodynamic modelling; application to cardiovascular safety data for PF-00821385, a novel HIV agent. Br J Clin Pharmacol 69:336–345
79. Zhao QL, Ma S, Jiang H et al (2005) Identification of N-phenyl-N′-(2,2,6,6-tetramethyl-piperidin-4-yl)-oxalamides as a new class of HIV-1 entry inhibitors that prevent gp120 binding to CD4. Virology 339:213–225
80. Haim H, Si Z, Madani N et al (2009) Soluble CD4 and CD4-mimetic compounds inhibit HIV-1 infection by induction of a short-lived activated state. PLoS Pathog 5:e1000360
81. Madani N, Schoen A, Princiotto AM et al (2008) Small-molecule CD4 mimics interact with a highly conserved pocket on HIV-1 gp120. Structure 16:1689–1701

82. LaLonde JM, Elban MA, Courter JR et al (2011) Design, synthesis and biological evaluation of small molecule inhibitors of CD4-gp120 binding based on virtual screening. Bioorg Med Chem 19:91–101
83. Lai W, Huang L, Ho P et al (2008) Betulinic acid derivatives that target gp120 and inhibit multiple genetic subtypes of human immunodeficiency virus type 1. Antimicrob Agents Chemother 52:128–136
84. Hurevich M, Swed A, Joubran S et al (2010) Rational conversion of noncontinuous active region in proteins into a small orally bioavailable macrocyclic drug-like molecule: the HIV-1 CD4:gp120 paradigm. Bioorg Med Chem 18:5754–5761
85. Wild C, Oas T, McDanal C et al (1992) A synthetic peptide inhibitor of human immunodeficiency virus replication: correlation between solution structure and viral inhibition. Proc Natl Acad Sci USA 89:10537–10541
86. Jiang SB, Lin K, Strick N, Neurath AR (1993) HIV-1 inhibition by a peptide. Nature 365:113
87. Jiang SB, Lin K, Strick N, Neurath AR (1993) Inhibition of HIV-1 infection by a fusion domain binding peptide from the HIV-1 envelope glycoprotein gp41. Biochem Biophys Res Commun 195:533–538
88. Matthews T, Salgo M, Greenberg M et al (2004) Case history: Enfuvirtide: the first therapy to inhibit the entry of HIV-1 into host CD4 lymphocytes. Nat Rev Drug Disc 3:215–225
89. Cooper DA, Lange JMA (2004) Peptide inhibitors of virus-cell fusion: enfuvirtide as a case study in clinical discovery and development. Lancet Infect Dis 4:426–436
90. Eckert DM, Kim PS (2001) Mechanisms of viral membrane fusion and its inhibition. Annu Rev Biochem 70:777–810
91. Wild CT, Shugars DC, Greenwell TK et al (1994) Peptides corresponding to a predictive α-helical domain of human immunodeficiency virus type 1 gp41 are potent inhibitors of virus infection. Proc Natl Acad Sci USA 91:9770–9774
92. Wild C, Greenwell T, Shugars D et al (1995) The inhibitory activity of an HIV type 1 peptide correlates with its ability to interact with a leucine zipper structure. AIDS Res Hum Retrovir 11:323–325
93. Ketas TK, Klasse PJ, Spenlehauer C et al (2003) Entry inhibitors SCH-C, RANTES, and T-20 block HIV type 1 replication in multiple cell types. AIDS Res Hum Retrovir 19:177–186
94. Joly V, Jidar K, Tatay M, Yeni P (2010) Enfuvirtide: from basic investigations to current clinical use. Exp Opin Pharmacother 11:2701–2713
95. Bray BL (2003) Innovation: large-scale manufacture of peptide therapeutics by chemical synthesis. Nat Rev Drug Disc 2:587–593
96. Schneider SE, Bray BL, Mader CJ (2005) Development of HIV fusion inhibitors. J Pept Sci 11:744–753
97. Lalezari J, Henry K, O'Hearn M et al (2003) Enfuvirtide, an HIV-1 fusion inhibitor, for drug-resistant HIV infection in North and South America. New Engl J Med 348:2175–2185
98. Lazzarin A, Clotet B, Cooper D et al (2003) Efficacy of enfuvirtide in patients infected with drug-resistant HIV-1 in Europe and Australia. New Engl J Med 348:2186–2195
99. Oldfield V, Keating GM, Plosker G (2005) Enfuvirtide: a review of its use in the management of HIV infection. Drugs 65:1139–1160
100. Marr P, Walmsley S (2008) Reassessment of enfuvirtide's role in the management of HIV-1 infection. Exp Opin Pharmacother 9:2349–2362
101. Manfredi R, Sabbatani S (2006) A novel antiretroviral class (fusion inhibitors) in the management of HIV infection. Present features and future perspectives of enfuvirtide (T-20). Curr Med Chem 13:2369–2384
102. Gochim M, Zhou G (2011) Amphipathic properties of HIV-1 gp41 fusion inhibitors. Curr Topics Med Chem 11:3022–3023
103. Lu M, Blacklow SC, Kim PS (1995) A trimeric structural domain of the HIV-1 transmembrane glycoprotein. Nat Struct Biol 2:1075–1082
104. Chan DC, Fass D, Berger JM, Kim PS (1997) Core structure of gp41 from the HIV envelope glycoprotein. Cell 89:263–273

105. Weissenhorn W, Dessen A, Harrison SC et al (1997) Atomic structure of the ectodomain from HIV-1 gp41. Nature 387:426–430
106. Tan K, Liu J-H, Wang J-H et al (1997) Atomic structure of a thermostable subdomain of HIV-1 gp41. Proc Natl Acad Sci USA 94:12303–12308
107. Chan DC, Chutkowski CT, Kim PS (1998) Evidence that a prominent cavity in the coiled coil of HIV type 1 gp41 is an attractive drug target. Proc Natl Acad Sci USA 95:15613–15617
108. Peisajovich SG, Shai Y (2002) New insights into the mechanism of virus-induced membrane fusion. Trends Biochem Sci 27:183–190
109. Torres O, Bong D (2011) Determinants of membrane activity from mutational analysis of the HIV fusion peptide. Biochemistry 50:5195–5207
110. Colman PM, Lawrence MC (2003) The structural biology of type I viral membrane fusion. Nat Rev Mol Cell Biol 4:309–319
111. Wexler-Cohen Y, Ashkenazi A, Viard M et al (2010) Virus-cell and cell-cell fusion mediated by the HIV-1 envelope glycoprotein is inhibited by short gp41 N-terminal membrane-anchored peptides lacking the critical pocket domain. FASEB J 24:4196–4202
112. Cai L, Jiang S (2010) Development of peptide and small-molecule HIV-1 fusion inhibitors that target gp41. ChemMedChem 5:1813–1824
113. Qadir MI, Malik SA (2010) HIV fusion inhibitors. Rev Med Virol 20:23–33
114. Chan DC, Kim PS (1998) HIV entry and its inhibition. Cell 93:681–684
115. Debnath AK (2006) Progress in identifying peptides and small-molecule inhibitors targeted to gp41 of HIV-1. Exp Opin Invest Drugs 15:465–478
116. Weng Y, Weiss CD (1998) Mutational analysis of residues in the coiled-coil domain of human immunodeficiency virus type 1 transmembrane protein gp41. J Virol 72:9676–9682
117. Eckert DM, Kim PS (2001) Design of potent inhibitors of HIV-1 entry from the gp41 N-peptide region. Proc Natl Acad Sci USA 98:11187–11192
118. Bianchi E, Finotto M, Ingallinella P et al (2005) Covalent stabilization of coiled coils of the HIV gp41 N region yields extremely potent and broad inhibitors of viral infection. Proc Natl Acad Sci USA 102:12903–12908
119. Izumi K, Watanabe K, Oishi S et al (2011) Potent anti-HIV-1 activity of N-HR-derived peptides including a deep pocket-forming region without antagonistic effects on T-20. Antiviral Chem Chemother 22:51–55
120. Chen X, Lu L, Zhi Q et al (2010) Novel recombinant engineered gp41 N-terminal heptad repeat trimers and their potential as anti-HIV-1 therapeutics and microbicides. J Biol Chem 285:25506–25515
121. Bewley CA, Loius JM, Ghirlando R, Clore GM (2002) Design of a novel peptide inhibitor of HIV fusion that disrupts the internal trimeric coiled-coil of gp41. J Biol Chem 277:14238–14245
122. Louis JM, Bewley CA, Clore GM (2001) Design and properties of N_{CCG}-gp41, a chimeric gp41 molecule with nanomolar fusion inhibitory activity. J Biol Chem 276:29485–29489
123. Conway B (2000) T-1249, Trimeris Inc. Curr Opin Anti-Infect Invest Drugs 2:317–322
124. Eron JJ, Gulick RM, Bartlett JA et al (2004) Short-term safety and antiretroviral activity of T-1249, a second-generation fusion inhibitor of HIV. J Infect Dis 189:1075–1083
125. Lalezari JP, Bellos NC, Sathasivam K et al (2005) T-1249 retains potent antiretroviral activity in patients who had experienced virological failure while on an enfuvirtide-containing treatment regimen. J Infect Dis 191:1155–1163
126. Melby T, Demasi R, Cammack N et al (2007) Evolution of genotypic and phenotypic resistance during chronic treatment with the fusion inhibitor T-1249. AIDS Res Hum Retrovir 23:1366–1373
127. Chinnadurai R, Muench J, Kirchhoff F (2005) Effect of naturally-occurring gp41 HR1 variations on susceptibility of HIV-1 to fusion inhibitors. AIDS 19:1401–1405
128. He Y, Xiao Y, Song H et al (2008) Design and evaluation of sifuvirtide, a novel HIV-1 fusion inhibitor. J Biol Chem 283:11126–11134

129. Wang R-R, Yang L-M, Wang Y-H et al (2009) Sifuvirtide, a potent HIV fusion inhibitor peptide. Biochem Biophys Res Commun 382:540–544
130. Pan C, Lu H, Qi Z, Jiang S (2009) Synergistic efficacy of combination of enfuvirtide and sifuvirtide, the first- and next-generation HIV-fusion inhibitors. AIDS 23:639–641
131. Pan C, Cai L, Lu H et al (2009) Combinations of the first and next generations of human immunodeficiency virus (HIV) fusion inhibitors exhibit a highly potent synergistic effect against enfuvirtide-sensitive and -resistant HIV type 1 strains. J Virol 83:7862–7872
132. Covens K, Megens S, Dekeersmaeker N et al (2010) The rare HIV-1 gp41 mutations 43T and 50V elevate enfuvirtide resistance levels of common enfuvirtide resistance mutations that did not impact susceptibility to sifuvirtide. Antiviral Res 86:253–260
133. Canto AMT Martins do, Carvalho AJP, Ramalho JPP, Loura LMS (2008) T-20 and T-1249 HIV fusion inhibitors' structure and conformation in solution: a molecular dynamics study. J Peptide Sci 14:442–447
134. Veiga AS, Santos NC, Loura LMS et al (2004) HIV fusion inhibitor peptide T-1249 is able to insert or adsorb to lipidic bilayers. Putative correlation with improved efficiency. J Am Chem Soc 126:14758–14763
135. Yao X, Chong H, Zhang C et al (2012) Broad antiviral activity and crystal structure of HIV-1 fusion inhibitor sifuvirtide. J Biol Chem 287:6788–6796
136. Liu Z, Shan M, Li L et al (2011) In vitro selection and characterization of HIV-1 variants with increased resistance to sifuvirtide, a novel HIV-1 fusion inhibitor. J Biol Chem 286:3277–3287
137. Dwyer JJ, Wilson KL, Davison DK et al (2007) Design of helical, oligomeric HIV-1 fusion inhibitor peptides with potent activity against enfuvirtide-resistant virus. Proc Natl Acad Sci USA 104:12772–12777
138. He Y, Cheng J, Lu H et al (2008) Potent HIV fusion inhibitors against enfuvirtide-resistant HIV-1 strains. Proc Natl Acad Sci USA 105:16332–16337
139. Nishikawa H, Nakamura S, Kodama E et al (2009) Electrostatically constrained α-helical peptide inhibits replication of HIV-1 resistant to enfuvirtide. Int J Biochem Cell Biol 41:891–899
140. Naito T, Izumi K, Kodama E et al (2009) SC29EK, a peptide fusion inhibitor with enhanced α -helicity, inhibits replication of human immunodeficiency virus type 1 mutants resistant to enfuvirtide. Antimicrob Agents Chemother 53:1013–1018
141. Shimura K, Nameki D, Kajiwara K et al (2010) Resistance profiles of novel electrostatically constrained HIV-1 fusion inhibitors. J Biol Chem 285:39471–39480
142. Eggink D, Langedijk JPM, Bonvin AMJJ et al (2009) Detailed mechanistic insights into HIV-1 sensitivity to three generations of fusion inhibitors. J Biol Chem 284:26941–26950
143. Oishi S, Ito S, Nishikawa K et al (2008) Design of a novel HIV-1 fusion inhibitor that displays a minimal interface for binding affinity. J Med Chem 51:388–391
144. Lee-Huang S, Maiorov V, Huang PL et al (2005) Structural and functional modeling of human lysozyme reveals a unique nonapeptide, HL9, with anti-HIV activity. Biochemistry 44:4648–4655
145. Hartono YD, Lee AN, Lee-Huang S, Zhang D (2011) Computational study of bindings of HL9, a nonapeptide fragment of human lysozyme, to HIV-1 fusion protein gp41. Bioorg Med Chem Lett 21:1607–1611
146. Gonzalez R, Albericio F, Cascone O, Iannucci NB (2010) Improved antimicrobial activity of h-lysozyme (107–115) by rational Ala substitution. J Peptide Sci 16:424–429
147. Blackwell HE, Grubbs RH (1998) Highly efficient synthesis of covalently cross-linked peptide helices by ring-closing metathesis. Angew Chem Int Ed Engl 37:3281–3284
148. Schafmeister CE, Po J, Verdine GL (2000) An all-hydrocarbon cross-linking system for enhancing the helicity and metabolic stability of peptides. J Am Chem Soc 122:5891–5892
149. Blackwell HE, Sadowsky JD, Howard RJ et al (2001) Ring-closing metathesis of olefinic peptides: design, synthesis, and structural characterization of macrocyclic helical peptides. J Org Chem 66:5291–5302

150. Kim Y-W, Grossmann TN, Verdine GL (2011) Synthesis of all-hydrocarbon stapled α-helical peptides by ring-closing olefin metathesis. Nat Protocol 6:761–771
151. Jacobsen O, Maekawa H, Ge N-H et al (2011) Stapling of a 3_{10}-helix with click chemistry. J Org Chem 76:1228–1238
152. Cantel S, Le Chevalier IA, Scrima M et al (2008) Synthesis and conformational analysis of a cyclic peptide obtained via i to i + 4 intramolecular side-chain to side-chain azide-alkyne 1,3-dipolar cycloaddition. J Org Chem 73:5663–5674
153. Scrima M, Le Chevalier-Isaad A, Rovero P et al (2010) CuI-catalyzed azide-alkyne intramolecular i-to-(i + 4) side-chain-to-side-chain cyclization promotes the formation of helix-like secondary structures. Eur J Org Chem 2010:446–457
154. Bird GH, Madani N, Perry AF et al (2010) Hydrocarbon double-stapling remedies the proteolytic instability of a lengthy peptide therapeutic. Proc Natl Acad Sci USA 107:14093–14098
155. Eckert DM, Malashkevich VN, Hong LH et al (1999) Inhibiting HIV-1 entry: discovery of D-peptide inhibitors that target the gp41 coiled-coil pocket. Cell 99:103–115
156. Welch BD, VanDemark AP, Heroux A et al (2007) Potent D-peptide inhibitors of HIV-1 entry. Proc Natl Acad Sci USA 104:16828–16833
157. Welch BD, Francis JN, Redman JS et al (2010) Design of a potent D-peptide HIV-1 entry inhibitor with a strong barrier to resistance. J Virol 84:11235–11244
158. Xie D, Yao C, Wang L et al (2010) An albumin-conjugated peptide exhibits potent anti-HIV activity and long in vivo half-life. Antimicrob Agents Chemother 54:191–196
159. Stoddart CA, Nault G, Galkina SA et al (2008) Albumin-conjugated C34 peptide HIV-1 fusion inhibitor: equipotent to C34 and T −20 in vitro with sustained activity in SCID-hu Thy/Liv mice. J Biol Chem 283:34045–34052
160. Stoddart CA, Nault G, Galkina SA et al (2012) Preexposure prophylaxis with albumin-conjugated C34 peptide HIV-1 fusion inhibitor in SCID-hu Thy/Liv mice. Antimicrob Agents Chemother. doi:10.1128AAC.05015-11
161. Zhang H, Schneider SE, Bray BL et al (2008) Process evelopment of TRI-999, a fatty-acid-modified HIV fusion inhibitory peptide. Org Proc Res Develop 12:101–110
162. Ingallinella P, Bianchi E, Ladwa NA et al (2009) Addition of a cholesterol group to an HIV-1 peptide fusion inhibitor dramatically increases its antiviral potency. Proc Natl Acad Sci USA 106:5801–5806
163. Peisajovich SG, Gallo SA, Blumenthal R, Shai Y (2003) C-terminal octylation rescues an inactive T-20 mutant: Implications for the mechanism of HIV/simian immunodeficiency virus-induced membrane fusion. J Biol Chem 278:21012–21017
164. Champagne K, Shishido A, Root MJ (2009) Interactions of HIV-1 inhibitory peptide T20 with the gp41 NH-R coiled coil. J Biol Chem 284:3619–3627
165. Liu S, Jing W, Cheung B et al (2007) HIV gp41 C-terminal heptad repeat contains multifunctional domains. Relation to mechanisms of action of anti-HIV peptides. J Biol Chem 282:9612–9620
166. Debnath AK (2006) Prospects and strategies for the discovery and development of small-molecule inhibitors of six-helix bundle formation in class 1 viral fusion proteins. Curr Opin Invest Drugs 7:118–127
167. Meanwell NA, Krystal M (2007) Respiratory syncytial virus – the discovery and optimization of orally bioavailable fusion inhibitors. Drugs Future 32:441–455
168. Douglas JL, Panis ML, Ho E et al (2003) Inhibition of respiratory syncytial virus fusion by the small molecule VP-14637 via specific interactions with F protein. J Virol 77:5054–5064
169. Douglas JL, Panis ML et al (2005) Small molecules VP-14637 and JNJ-2408068 inhibit respiratory syncytial virus fusion by similar mechanisms. Antimicrob Agents Chemother 49:2460–2466
170. Cianci C, Langley DR et al (2004) Targeting a binding pocket within the trimer-of-hairpins: small-molecule inhibition of viral fusion. Proc Natl Acad Sci USA 101:15046–15051

171. Roymans D, De Bondt HL et al (2010) Binding of a potent small-molecule inhibitor of six-helix bundle formation requires interactions with both heptad-repeats of the RSV fusion protein. Proc Natl Acad Sci USA 107:308–313
172. Frey G, Rits-Volloch S, Zhang X-Q et al (2006) Small molecules that bind the inner core of gp41 and inhibit HIV envelope-mediated fusion. Proc Natl Acad Sci USA 103:13938–13943
173. Debnath AK, Radigan L, Jiang S (1999) Structure-based identification of small molecule antiviral compounds targeted to the gp41 core structure of the human immunodeficiency virus type 1. J Med Chem 42:3203–3209
174. Naicker KP, Jiang S, Lu H et al (2004) Synthesis and anti-HIV-1 activity of 4-[4-(4,6-bisphenylamino-triazin-2-ylamino)-5-methoxy-2-methylphenylazo]-5-hydroxynaphthalene-2,7-disulfonic acid and its derivatives. Bioorg Med Chem 12:1215–1220
175. Wang H, Qi Z, Guo A et al (2009) ADS-J1 inhibits human immunodeficiency virus type 1 entry by interacting with the gp41 pocket region and blocking fusion-active gp41 core formation. Antimicrob Agents Chemother 53:4987–4998
176. Cai L, Gochin M (2007) A novel fluorescence intensity screening assay identifies new low-molecular-weight inhibitors of the gp41 coiled-coil domain of human immunodeficiency virus type 1. Antimicrob Agents Chemother 51:2388–2395
177. Armand-Ugon M, Clotet-Codina I, Tintori C et al (2005) The anti-HIV activity of ADS- J1 targets the HIV-1 gp120. Virology 343:141–149
178. Gonzalez-Ortega E, Mena M-P, Permanyer M et al (2010) ADS- J1 inhibits HIV-1 entry by interacting with gp120 and does not block fusion-active gp41 core formation. Antimicrob Agents Chemother 54:4487–4492
179. Jiang S, Lu H, Liu S et al (2004) N-substituted pyrrole derivatives as novel human immunodeficiency virus type 1 entry inhibitors that interfere with the gp41 six-helix bundle formation and block virus fusion. Antimicrob Agents Chemother 48:4349–4359
180. Liu K, Lu H, Hou L et al (2008) Design, synthesis, and biological evaluation of n-carboxyphenylpyrrole derivatives as potent HIV fusion inhibitors targeting gp41. J Med Chem 51:7843–7854
181. Wang Y, Lu H, Zhu Q, Jiang S, Liao Y (2010) Structure-based design, synthesis and biological evaluation of new N-carboxyphenylpyrrole derivatives as HIV fusion inhibitors targeting gp41. Bioorg Med Chem Lett 20:189–192
182. Jiang S, Tala SR, Lu H et al (2011) Design, synthesis, and biological activity of a novel series of 2,5-disubstituted furans/pyrroles as HIV-1 fusion inhibitors targeting gp41. Bioorg Med Chem Lett 21:6895–6898
183. Jiang S, Tala SR, Lu H et al (2011) Design, synthesis, and biological activity of novel 5-((arylfuran/1*H*-pyrrol-2-yl)methylene)-2-thioxo-3-(3-(trifluoromethyl)phenyl)thiazolidin-4-ones as HIV-1 fusion inhibitors targeting gp41. J Med Chem 54:572–579
184. He X-Y, Zou P, Qiu J et al (2011) Design, synthesis and biological evaluation of 3-substituted 2,5-dimethyl-N-(3-(1*H*-tetrazol-5-yl)phenyl)pyrroles as novel potential HIV-1 gp41 inhibitors. Bioorg Med Chem 19:6726–6734
185. Ernst JT, Kutzki O, Debnath AK et al (2002) Design of a protein surface antagonist based on α-helix mimicry: inhibition of gp41 assembly and viral fusion. Angew Chem Int Ed Engl 41:278–281
186. Garner J, Harding MM (2007) Design and synthesis of α-helical peptides and mimetics. Org Biomol Chem 5:3577–3585
187. Liu B, Joseph RW, Dorsey BD et al (2009) Structure-based design of substituted biphenyl ethylene ethers as ligands binding in the hydrophobic pocket of gp41 and blocking the helical bundle formation. Bioorg Med Chem Lett 15:5693–5697
188. Xu Y, Lu H, Kennedy JP et al (2006) Evaluation of "credit card" libraries for inhibition of HIV-1 gp41 fusogenic core formation. J Comb Chem 8:531–539
189. Stewart KD, Huth JR, Ng TI et al (2010) Non-peptide entry inhibitors of HIV-1 that target the gp41 coiled coil pocket. Bioorg Med Chem Lett 20:612–617

190. Balogh E, Wu D, Zhou G, Gochin M (2009) NMR second site screening for structure determination of ligands bound in the hydrophobic pocket of HIV-1 gp41. J Am Chem Soc 131:2821–2823
191. Zhou G, Wu D, Hermel E et al (2010) Design, synthesis, and evaluation of indole compounds as novel inhibitors targeting gp41. Bioorg Med Chem Lett 20:1500–1503
192. Zhou G, Wu D, Snyder B et al (2011) Development of indole compounds as small molecule fusion inhibitors targeting HIV-1 glycoprotein-41. J Med Chem 54:7220–7231
193. Gochin M, Zhou G-Y, Phillips AH (2011) Paramagnetic relaxation assisted docking of a small indole compound in the HIV-1 gp41 hydrophobic pocket. ACS Chem Biol 6:267–274
194. Gochin M, Cai L (2009) The role of amphiphilicity and negative charge in glycoprotein 41 interactions in the hydrophobic pocket. J Med Chem 52:4338–4344
195. Wang E, Sun X, Qian Y et al (2003) Both heptad repeats of human respiratory syncytial virus fusion protein are potent inhibitors of viral fusion. Biochem Biophys Res Commun 302:469–475
196. LaFemina RL, Schneider CL, Robbins HL et al (1992) Requirement of active human immunodeficiency virus type 1 integrase enzyme for productive infection of human T-lymphoid cells. J Virol 66:7414–7419
197. Cherepanov P, Maertens G, Proost P et al (2003) HIV-1 integrase forms stable tetramers and associates with LEDGF/p75 protein in human cells. J Biol Chem 278:372–381
198. Turlure F, Devroe E, Silver PA et al (2004) Human cell proteins and human immunodeficiency virus DNA integration. Front Biosci 9:3187–3208
199. Emiliani S, Mousnier A, Busschots K et al (2005) Integrase mutants defective for interaction with LEDGF/p75 are impaired in chromosome tethering and HIV-1 replication. J Biol Chem 280:25517–25523
200. Ge H, Si Y, Roeder RG (1998) Isolation of cDNAs encoding novel transcription coactivators p52 and p75 reveals an alternate regulatory mechanism of transcriptional activation. EMBO J 17:6723–6729
201. Llano M, Morrison J, Poeschla EM (2009) Virological and cellular roles of the transcriptional coactivator LEDGF/p75. In: Spearman P, Freed EO (eds) HIV interactions with host cell proteins, vol 339, Current topics in microbiology and immunology. Springer, Heidelberg
202. Llano M, Saenz DT, Meehan A et al (2006) An essential role for LEDGF/p75 in HIV integration. Science 314:461–464
203. Vandekerckhove L, Christ F, Van Maele B et al (2006) Transient and stable knockdown of the integrase cofactor LEDGF/p75 reveals its role in the replication cycle of human immunodeficiency virus. J Virol 80:1886–1896
204. Shun M-C, Raghavendra NK, Vandegraaff N et al (2007) LEDGF/p75 functions downstream from preintegration complex formation to effect gene-specific HIV-1 integration. Genes Dev 21:1767–1778
205. Maertens G, Cherepanov P, Pluymers W et al (2003) LEDGF/p75 is essential for nuclear and chromosomal targeting of HIV-1 integrase in human cells. J Biol Chem 278:33528–33539
206. Ciuffi A, Llano M, Poeschla E et al (2005) A role for LEDGF/p75 in targeting HIV DNA integration. Nat Med 11:1287–1289
207. Cherepanov P, Devroe E, Silver PA, Engelman A (2004) Identification of an evolutionarily conserved domain in human lens epithelium-derived growth factor/transcriptional co-activator p75 (LEDGF/p75) that binds HIV-1 integrase. J Biol Chem 279:48883–48892
208. Vanegas M, Llano M, Delgado S et al (2005) Identification of the LEDGF/p75 HIV-1 integrase-interaction domain and NLS reveals NLS-independent chromatin tethering. J Cell Sci 118:1733–1743
209. Cherepanov P, Sun ZY, Rahman S et al (2005) Solution structure of the HIV-1 integrase-binding domain in LEDGF/p75. Nat Struct Mol Biol 12:526–532
210. Busschots K, Voet A, De Maeyer M et al (2007) Identification of the LEDGF/p75 binding site in HIV-1 integrase. J Mol Biol 365:1480–1492

211. Rahman S, Lu R, Vandegraaff N et al (2007) Structure-based mutagenesis of the integrase-LEDGF/p75 interface uncouples a strict correlation between in vitro protein binding and HIV-1 fitness. Virology 357:79–90
212. Cherepanov P, Ambrosio AL, Rahman S et al (2005) Structural basis for the recognition between HIV-1 integrase and transcriptional coactivator p75. Proc Natl Acad Sci USA 102:17308–17313
213. Hare S, Shun MC, Gupta SS et al (2009) A novel co-crystal structure affords the design of gain-of-function lentiviral integrase mutants in the presence of modified PSIP1/LEDGF/p75. PLoS Pathog 5:e1000259
214. Hare S, Di Nunzio F, Labeja A et al (2009) Structural basis for functional tetramerization of lentiviral integrase. PLoS Pathog 5:e1000515
215. De Rijck J, Vandekerckhove L, Gijsbers R et al (2006) Overexpression of the lens epithelium-derived growth factor/p75 integrase binding domain inhibits human immunodeficiency virus replication. J Virol 80:11498–11509
216. Molteni V, Greenwald J, Rhodes D et al (2001) Identification of a small-molecule binding site at the dimer interface of the HIV integrase catalytic domain. Acta Cryst Sect D 57:536–544
217. Al-Mawsawi LQ, Fikkert V, Dayam R et al (2006) Discovery of a small-molecule HIV-1 integrase inhibitor-binding site. Proc Nat Acad Sci USA 103:10080–10085
218. Christ F, Voet A, Marchand A et al (2010) Rational design of small-molecule inhibitors of the LEDGF/p75-integrase interaction and HIV replication. Nat Chem Biol 6:442–448
219. Compound (**27**) had been previously disclosed as an HIV antiviral agent. (2007) WO 2007131350
220. Altman MD, Ali A, Reddy GSKK et al (2008) HIV-1 protease inhibitors from inverse design in the substrate envelope exhibit subnanomolar binding to drug-resistant variants. J Am Chem Soc 130:6099–6113
221. Du L, Zhao Y, Chen J et al (2008) D77, one benzoic acid derivative, functions as a novel anti-HIV-1 inhibitor targeting the interaction between integrase and cellular LEDGF/p75. Biochem Biophys Res Commun 375:139–144
222. De Luca L, Barreca ML, Ferro S et al (2009) Pharmacophore-based discovery of small-molecule inhibitors of protein-protein interactions between HIV-1 integrase and cellular cofactor LEDGF/p75. ChemMedChem 4:1311–1316
223. De Luca L, Ferro S, Gitto R et al (2010) Small molecules targeting the interaction between HIV-1 integrase and LEDGF/p75 cofactor. Bioorg Med Chem 18:7515–7521
224. Barreca ML, Ferro S, Rao A et al (2005) Pharmacophore-based design of HIV-1 integrase strand-transfer inhibitors. J Med Chem 48:7084–7088
225. De Luca L, Gitto R, Christ F et al (2011) 4-[1-(4-Fluorobenzyl)-4-hydroxy-1H-indol-3-yl]-2-hydroxy-4-oxobut-2-enoic acid as a prototype to develop dual inhibitors of HIV-1 integration process. Antiviral Res 92:102–107
226. Zhao XZ, Semenova EA, Vu BC et al (2008) 2,3-Dihydro-6,7-dihydroxy-1*H*-isoindol-1-one-based HIV-1 integrase inhibitors. J Med Chem 51:251–252
227. Todd MJ, Semo M, Freire E (1998) The structural stability of the HIV-1 protease. J Mol Biol 283:475–488
228. Ishima R, Ghirlando R, Tözsér J et al (2001) Folded monomer of HIV-1 protease. J Biol Chem 276:49110–49116
229. Zhang Z-Y, Poorman RA, Maggiora LL et al (1991) Dissociative inhibition of dimeric enzymes. Kinetic characterization of the inhibition of HIV-1 protease by its COOH-terminal tetrapeptide. J Biol Chem 266:15591–15594
230. Bannwarth L, Reboud-Ravaux M (2007) An alternative strategy for inhibiting multidrug-resistant mutants of the dimeric HIV-1 protease by targeting the subunit interface. Biochem Soc Trans 35:551–554
231. Camarasa M-J, Velázquez S, San-Félix A et al (2006) Dimerization inhibitors of HIV-1 reverse transcriptase, protease and integrase: a single mode of inhibition for the three HIV enzymes? Antiviral Res 71:260–267

232. Berg T (2003) Modulation of protein-protein interactions with small organic molecules. Angew Chem Int Ed Engl 42:2462–2481
233. Bowman MJ, Chmielewski J (2002) Novel strategies for targeting the dimerization interface of HIV protease with cross-linked interfacial pep-tides. Biopolym Pept Sci 66:126–133
234. Shultz MD, Bowman MJ, Ham Y-W et al (2000) Small-molecule inhibitors of HIV-1 protease dimerization derived from cross-linked interfacial peptides. Angew Chem Int Ed Engl 39:2710–2713
235. Hwang YS, Chmielewski J (2005) Development of low molecular weight hiv-1 protease dimerization inhibitors. J Med Chem 48:2239–2242
236. Bowman MJ, Byrne S, Chmielewski J (2005) Switching between allosteric and dimerization inhibition of HIV-1 protease. Chem Biol 12:439–444
237. Bowman MJ, Chmielewski J (2009) Sidechain-linked inhibitors of HIV-1 protease dimerization. Bioorg Med Chem 17:967–976
238. Shultz MD, Ham Y-W, Lee S-G et al (2004) Small-molecule dimerization inhibitors of wild-type and mutant HIV pro-tease: a focused library approach. J Am Chem Soc 126:9886–9887
239. Lee S-G, Chmielewski J (2006) Rapid synthesis and in situ screening of potent HIV-1 protease dimerization inhibitors. Chem Biol 13:421–426
240. Bowman MJ, Chmielewski J (2004) Crucial amides for dimerization inhibitors of HIV-1 protease. Bioorg Med Chem Lett 14:1395–1398
241. Lee S-G, Chmielewski J (2010) Cross-linked peptoid-based dimerization inhibitors of HIV-1 protease. Chembiochem 11:1513–1516
242. Bouras A, Boggetto N, Benatalah Z et al (1999) Design, synthesis, and evaluation of conformationally constrained tongs, new inhibitors of hiv-1 protease dimerization. J Med Chem 42:957–962
243. Merabet N, Dumond J, Collinet B et al (2004) New constrained "molecular tongs" designed to dissociate HIV-1 protease dimer. J Med Chem 47:6392–6400
244. Bannwarth L, Kessler A, Pèthe S et al (2006) Molecular tongs containing amino acid mimetic fragments: new inhibitors of wild-type and mutated HIV-1 protease dimerization. J Med Chem 49:4657–4664
245. Vidu A, Dufau L, Bannwarth L et al (2010) Toward the first nonpeptidic molecular tong inhibitor of wild-type and mutated HIV-1 protease dimerization. ChemMedChem 5:1899–1906
246. Koh Y, Matsumi S, Das D et al (2007) Potent inhibition of HIV-1 replication by novel non-peptidyl small molecule inhibitors of protease dimerization. J Biol Chem 282:28709–28720
247. Tojo Y, Koh Y, Amano M et al (2010) Novel protease inhibitors (PIs) containing macrocyclic components and 3(R),3a(S),6a(R)-bis-tetrahydrofuranylurethane that are potent against multi-PI-resistant HIV-1 variants in vitro. Antimicrob Agents Chemother 54:3460–3470
248. Ghosh AK, Xu C-X, Rao KV et al (2010) Probing multidrug-resistance and protein-ligand interactions with oxatricyclic designed ligands in HIV-1 protease inhibitors. ChemMedChem 5:1850–1854

Top Med Chem 8: 167–196
DOI: 10.1007/978-3-642-28965-1_5

Inhibitors of Protein-Protein Interactions in Paramyxovirus Fusion: A Focus on Respiratory Syncytial Virus

Nicholas A. Meanwell and David R. Langley

Contents

Abstract The assembly of the N-terminus heptad repeats of the respiratory syncytial virus (RSV) F protein into a trimeric complex that associates with the C-terminus heptad repeats to form a six-helix bundle is a critical step in the process of virus-host fusion and represents an intramolecular protein-protein interaction. Screening campaigns using replicating virus assays have identified several structurally distinct but mechanistically similar chemotypes that interfere with RSV fusion by disrupting the function of the F protein six-helix bundle. This chapter summarizes structure-activity relationships and mechanistic insights associated with the most prominent RSV fusion inhibitors and the key issues in the development of potential clinical candidates.

Keywords Inhibitors • Protein-protein interaction • Respiratory syncytial virus

N.A. Meanwell (✉)
Department of Medicinal Chemistry, Bristol-Myers Squibb Research and Development, 5 Research Parkway, Wallingford, CT 06492, USA
e-mail: Nicholas.Meanwell@bms.com

D.R. Langley
Department of Computer-Aided Drug Design, Bristol-Myers Squibb Research and Development, 5 Research Parkway, Wallingford, CT 06492, USA

1 Introduction

Fundamental aspects of the mechanics of virus fusion processes have been elucidated by a combination of extensive biochemical studies, experimental observations with inhibitors of fusion and X-ray crystallographic data of fusion proteins in their native and postfusion states [1–7]. A key step in respiratory syncytial virus (RSV) fusion that is common to many viruses involves a significant rearrangement of the fusion protein, a process that unmasks a hydrophobic 10–12 residue fusion peptide from a protected environment within the fusion protein architecture and projects it into the host cell membrane [8]. This is one of the several critical and carefully choreographed steps that ultimately result in virus and host cell membrane fusion, and for which the triggering cues vary depending on the virus. As part of this process, a helical segment in the amino terminus (HR-N) of the fusion protein oligomerizes into a trimeric coiled-coil assembly that subsequently associates with a complementary helical segment in the carboxy terminus region (HR-C) of the fusion protein to form a six-helix bundle (Fig. 1). This process folds the fusion protein into a hairpin configuration that draws virus and host membranes into close association as a prelude to fusion [1–7]. X-ray crystallographic data of six-helix bundle structures from several viruses that possess Class 1 fusion proteins reveal commonalities and, in several cases, identified potential binding sites for small-molecule drugs that might interfere with function [8, 9]. This process represents an intramolecular protein-protein interaction that can be intercepted by pharmacological agents, although for many viruses effective inhibitors have been restricted to large peptides derived from the carboxy terminal heptad repeat segment of the fusion protein that compete effectively with the natural HR-C peptide sequence [10]. This mode of inhibition of virus entry was discovered initially in the context of from HIV-1 in advance of the elucidation of X-ray crystallographic data [9–14]. However, the pursuit of inhibitors of respiratory syncytial virus has provided multiple small-molecule chemotypes that interfere with six-helix bundle formation and/or function, show potent antiviral activity in cell culture and are active in animal models of disease [15–20]. Well-characterized small-molecule fusion inhibitors that act in this fashion are unique to RSV and the key discoveries in this arena will be summarized in this chapter.

2 Respiratory Syncytial Virus: Background

Respiratory syncytial virus is a member of the paramyxovirus family, a genera that includes metapneumovirus, measles and Newcastle disease viruses [21]. The discovery of RSV as a human pathogen began with an outbreak of coryza in chimpanzees, documented in 1956, which was quickly followed by the identification of the virus in infants presenting with bronchiolitis and pneumonia [22–25]. Epidemiological studies have established the patterns of outbreaks of RSV

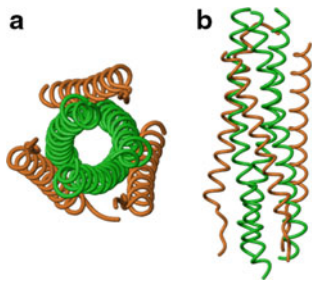

Fig. 1 The structure of the RSV six-helix bundle formed between the N-terminus heptad repeats (HR-N) depicted in *green* and the C-terminus heptad repeats (HR-C) in *brown*. (**a**) View down the axis of the six-helix bundle. (**b**) Side view of the six-helix bundle (Adapted from Ref. [8])

infection which occur on a seasonal basis beginning in the Northern Hemisphere in the late autumn and typically extending for several months before dissipating with the arrival of spring [26–28]. However, there is some evidence that the virus can be present during the summer months [29, 30]. Virus transmission is facile, with infection occurring after exposure to airborne respiratory secretions from infected individuals [31, 32]. Serological studies have revealed that virtually all children are infected within the first two years of life and reinfection is common since the immune response to the virus is of limited durability [33, 34]. For the majority of individuals, RSV manifests as a self-limiting, upper respiratory tract infection that produces influenza-like symptoms, frequently leading to misdiagnosis, and which is not usually associated with clinical complications. However, for some patients the virus can migrate to the lower respiratory tract, leading to a more severe disease that may be associated with more significant morbidity and mortality [35–38]. RSV infection can be particularly problematic for those with underlying cardiopulmonary problems (congenital heart defects, bronchopulmonary dysplasia) or immune deficiency, and for infants born prematurely who have underdeveloped lung function [39–44].

Reinfection with RSV later in life is common, although frequently of lower severity, and the virus has been identified as the principal etiological viral agent in otitis media infections. There is also a rising appreciation of the problems associated with RSV infection in the elderly, where the symptoms are frequently confused with influenza and mortality has been estimated to be 60–80% higher than that for influenza [45–53].

3 Respiratory Syncytial Virus Structure and Function

RSV is an enveloped virus that has been classified into subgroups A and B based on serological differences in the viral surface proteins [21, 54, 55] The genome is comprised of a 15,222 nucleotide, nonsegmented negative strand of RNA that encodes for ten viral proteins, as summarized in Fig. 2. The F (fusion),

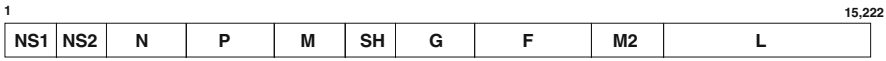

Fig. 2 Organization of the 15,222 nucleotide RSV genome. The relative size of an encoded protein is approximated by the depicted size of the segment of the RNA

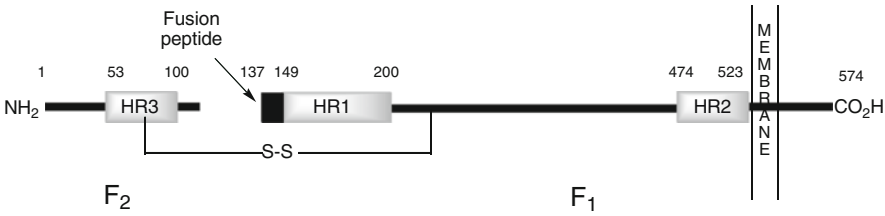

Fig. 3 The structure of the RSV F-protein

G (attachment) and SH (short hydrophobic) proteins are expressed on the surface of the virion and anchored in the lipid envelope, while the M, M2, N (major nucleocapsid), L (viral RNA polymerase) and P (phosphoprotein) proteins are packaged in the virion. The two nonstructural proteins NS1 and NS2 accumulate in the cytoplasm of infected cells where replication occurs and are present in mature virions only at very low levels, while the 11th protein comprising 90 residues and designated as M2-2, has been identified as an additional open reading frame contained within the M2 RNA sequence [56].

The G protein is believed to be deployed on the virus surface as a trimer and is heavily glycosylated and palmitoylated, to the extent that its molecular mass is more than double that predicted by the protein sequence [57]. The G protein mediates attachment of the virus to host cell receptors that remain to be definitively identified although glycosoaminoglycans, the CX3CR1 receptor and annexin II are all implicated in the recognition process [58–60]. However, the G protein is not essential for infectivity since infection can occur in vitro in its absence, although virulence is attenuated in vivo [61–64].

The F protein is synthesized as a single polyprotein (F_0) comprising 574 amino acids that is activated to the fusion-competent form by a host cell endoprotease, which produces a disulfide-linked heterodimer designated F_1 and F_2. The carboxy terminus of F_2 is the site of cleavage, a process that reveals the hydrophobic amino acids at the amino terminus of F_1 as the fusion peptide (Fig. 3) [65, 66]. The processed peptide assembles on the surface of the virion in an oligomeric form, most probably as a trimeric species, and mediates virus-host cell membrane fusion in a fashion that is not dependent on endocytosis. The F protein has also been shown to interact with the cell surface proteins intercellular adhesion molecule-1 (ICAM-1) and nucleolin, which provide potential avenues for virus entry in the absence of the G or SH proteins [67, 68].

The function of the 64-residue, membrane-spanning SH protein is largely unknown although it facilitates fusion and may interfere with TNFα signaling

[69]. The virus polymerase (L protein) is packaged in the virion along with the N and P proteins, with the N protein encapsidating the viral RNA [70, 71]. Although viral polymerases are well-established targets for therapeutic intervention, the RSV L protein is poorly characterized – a function of the inability to fully recapitulate its activity in vitro.

4 Inhibitors of Respiratory Syncytial Virus Replication

To date, the generation of lead small-molecule inhibitors of RSV has generally relied upon a screening approach using a viral replication assay, although specific biochemical assays have been used successfully to screen for inhibitors [72]. Viral replication screens are particularly advantageous since they offer diversity based on the collection of compounds under evaluation and the panoply of viral targets, while a third dimension recognizes the temporal nature of viral protein function, since they may engage in multiple aspects of the virus life cycle and the inhibitors can target a specific activity. Lead inhibitors are characterized further in order to illuminate the mode of action with a chemical genetics-type analysis the most common approach [73]. This is generally a straightforward process for inhibitors of virus replication, accomplished by generating resistant virus and identifying the responsible genetic mutations by demonstrating resistance when individually introduced into the virus, a process referred to as a reverse genetics approach. Resistance mutations can occur across the viral genome but several usually map to sequences coding for the targeted protein and may occur at or close to sites of contact with the inhibitor [72]. This tactic can be augmented by time-of-addition experiments that provide a very useful experimental technique for determining the stage of the virus life cycle at which replication is interrupted. However, rigorous characterization of lead inhibitors is essential in order to determine whether the agents under examination target the virus or host cell proteins [72–74].

Although the nonnucleoside polymerase inhibitor **1** was discovered using a crude RSV ribonucleoprotein complex–catalyzed RNA polymerization screen [75, 76], both YM-53403 (**2**) [77] and the nucleocapsid protein inhibitor RSV-604 (**3**), which is currently in clinical trials [78–81], were discovered using mechanistically unbiased virus replication screens. The sulfated sialyl lipid NMS03 (**4**) has been characterized as an inhibitor of RSV entry that acts by interfering with the binding of the RSV G protein to host cells, potentially providing an example of a protein-protein interaction inhibitor [82–84]. NMS03 (**4**) inhibited the Long strain of RSV infection of HEp-2 cells in culture with an EC_{50} of 200–320 nM, an activity that extended to a range of clinical isolates. The generation and sequencing of virus grown to be resistant to NMS03 (**4**) revealed amino acid changes in the G but not the F protein, confirming time-of-addition and temperature shift experiments that suggested inhibition of RSV binding to HEp-2 cells [81]. NMS03 (**4**) reduced RSV titers in the lungs of cotton rats by over one $\log_{10}$ when administered intraperitoneally daily at a dose of 100 mpk beginning 1 day prior to or 1 h after intranasal

inoculation with the virus [83]. Lower doses of 4 and 20 mpk reduced viral titers by 0.86 and 1.42 $\log_{10}$, respectively, when administered daily for 3 days beginning 1 h after infection. However, NMS03 (**4**) is not a selective inhibitor of RSV since it has also been shown to inhibit human metapneumovirus and HIV-1 replication [85].

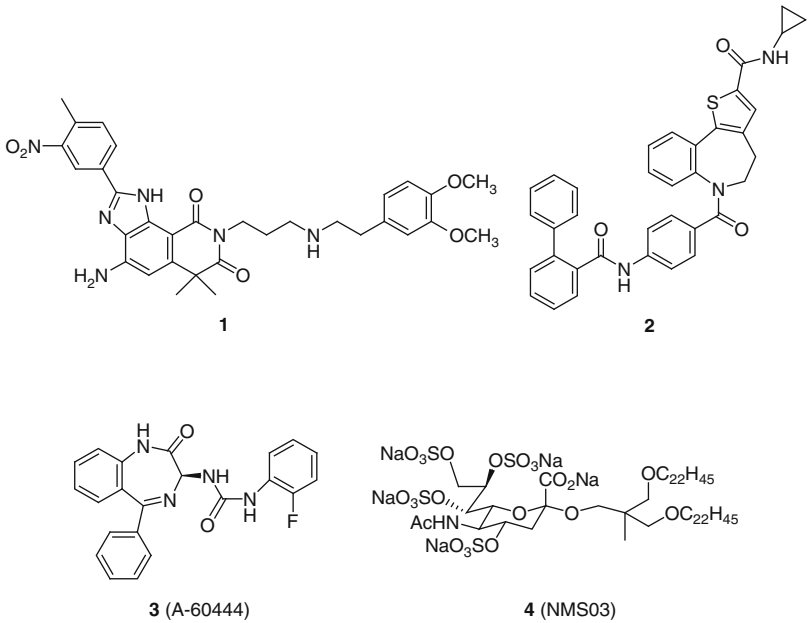

The majority of RSV inhibitors that have emerged from cell-based virus replication assays have been determined to be inhibitors of the virus-host fusion process. The discovery and basic SAR associated with these compounds will be described followed by a discussion of their mode of action that, quite remarkably given the structural diversity, appears to converge on interfering with the formation and/or function of the RSV F protein six-helix bundle complex.

The first RSV fusion inhibitor to be described in the literature was bis-(5-amidino-2-benzimidazolyl)methane (BABIM, **5**), a compound that demonstrates a range of biological activities largely based on its ability to inhibit trypsin-like proteases [86–89]. The initial antiviral profiling of BABIM (**5**) revealed inhibitory potency in the 500–1,000 nM range and although inhibition of F protein proteolysis may contribute to the observed activity, there was no clear correlation between blockade of RSV fusion and inhibition of a range of trypsin-like proteases [89]. However, it is conceivable that the host protease responsible for F protein activation may not have been sampled. From this survey, the structurally simpler amidines 4-((1*H*-indol-1-yl)methyl)benzimidamide (**6**) and 1-methyl-1*H*-indole-5-carboximidamide (**7**) were identified as inhibitors of RSV fusion with potency comparable to BABIM (**5**) but weaker protease inhibitory properties, lending support to the notion that these molecules are direct-acting fusion inhibitors [88]. Further experimental support can be found in more recent experiments that reveal that the antiviral activity of

BABIM (**5**) is sensitive to F protein mutations with a F140I substitution that arises in response to pressure by fusion inhibitors conferring >1,250-fold resistance compared to inhibition of the wild type Long strain of RSV [90]. BABIM (**5**) is active in the cotton rat model of RSV infection, reducing viral titers by 1.27 $\log_{10}$ when administered intraperitoneally at a dose of 25 mpk prior to intratracheal inoculation with virus with subsequent daily dosing for 3 days. When cotton rats rendered immune deficient by treatment with cyclophosphamide were used in this experimental protocol, lung viral titers measured following a 7-day dosing schedule were reduced by 2.47 $\log_{10}$ compared to placebo-treated control animals [91].

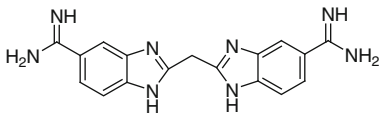

5 (BABIM)

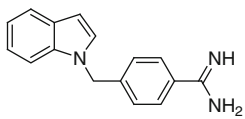

6

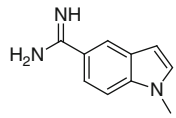

7

CL-387626 (**8**) was identified from a series of symmetrical, dendrimer-like triazine derivatives that originated with a structurally-related screening lead [92–95]. CL-387626 (**8**) exhibits an EC_{50} = 50–80 nM towards RSV with much weaker inhibition of HCMV (EC_{50} = 25 μM) and HSV (EC_{50} = 175 μM). Structure–activity relationships emphasized the importance of the sulfonic acid moieties in the core, the triazine heterocycles since pyrimidines were generally weaker RSV inhibitors, and the requirement for at least three of the peripheral sulfonamide elements [92–96]. However, there was some tolerance for structural variation of the sulfonamide terminus, a survey that led to the discovery of RFI-641 (**9**) as an optimized compound with a slight potency advantage over CL-387626 (**8**) [97]. The mode of action of this class of compound was deduced to be fusion inhibition rather than blockade of virus adsorption to the host cell by temperature shift experiments, which revealed that the compound retained activity after allowing the virus to attach at 4°C and then warming to 37°C to allow fusion to proceed [97–99].

CL-387626 (**8**) was active as a prophylactic agent in the cotton rat when administered as a single intranasal dose of 30 mpk at zero, 4 or 5 days prior to inoculation of the animals with RSV, reducing the viral titers by 1.7–3.6 $\log_{10}$ with the greatest efficacy observed when drug was dosed on day zero [93]. However, CL-387626 (**8**) was inactive in this model when dosed intraperitoneally and was ineffective when given as a therapeutic dosing regimen initiated after virus inoculation.

RFI-641 (**9**) was evaluated more extensively in vivo than CL-387626 (**8**), exhibiting efficacy in mouse, cotton rat and African green monkey models of RSV

infection [96–101]. In mice, a prophylactic regimen of 0.04–2 mpk administered intranasally 2 h before inoculation with virus resulted in 0.63–1.53 $\log_{10}$ reduction in viral titers compared to control while doses of 0.2–10 mpk in the cotton rat showed efficacy with the 10 mpk dose protecting cotton rats against both the A2 and Long RSV strains [100]. In the African green monkey, intranasal doses ranging from 0.24 to 6 mg 2 h prior to infection reduced viral titers in nasal and throat samples by 2.1–3.1 $\log_{10}$ compared to control animals and in bronchoalveolar lavage samples taken at days 6 (1.8–2.3 $\log_{10}$) and 8 (1.6–2.9 $\log_{10}$) postinfection [100–102]. Therapeutic efficacy was also demonstrated in this model in an experiment in which a 12 mg intranasal dose of RFI-641 (**9**) was administered once daily for 12 days beginning 24 h after virus inoculation leading to marked reductions (0.4–1.78 $\log_{10}$) in viral titers in daily nasal and throat samples taken over the course of the experiment [101, 102]. In this model, RFI-641 (**9**) also demonstrated antiviral efficacy when administered by inhalation after nebulization of the drug for a 2 h exposure period with a shorter, 15 min exposure ineffective.

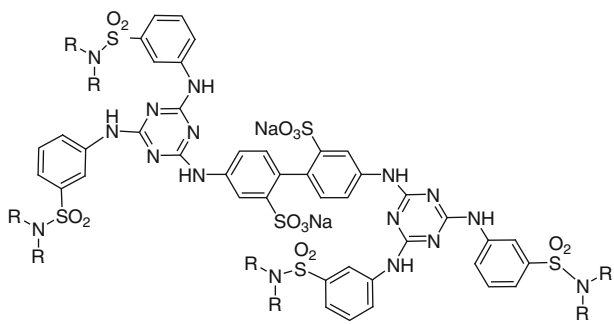

8: R = $CH_2CH_2CONH_2$ (CL-387626)

9: R = CH_2CONH_2 (RFI-641)

The original lead that led to the identification of the RSV fusion inhibitor VP-14637 (**10**) was discovered as an impurity in a sample of (*E*)-4-((5-amino-1*H*-tetrazol-1-ylimino)methyl)phenol (**11**) that had been prepared from 4-hydroxybenzaldehyde and 1,5-diaminotetrazole [15, 103, 104]. The impurity, compound **12**, exhibited an EC_{50} of 1 nM in a RSV replication assay and was thought to have originated from a condensation between three molecules of 4-hydroxybenzaldehyde that then reacted with 1,5-diaminotetrazole. Optimization of **12** established that the phenol moieties on the rings bearing the tetrazoles made a critical contribution to the pharmacophore, although the third phenol element could be methylated without effect on potency, ultimately affording VP-14637 (**10**), which is twofold more potent than **12** [15, 103, 104]. VP-14637 (**10**) inhibits RSV replication in cell culture with an $EC_{50} = 1.4$ nM and is active in a fusion inhibition assay with an $EC_{50} = 5.4$ nM [15, 103–105]. Against a panel of clinical isolates, the EC_{50}s ranged from 0.1 to 80 nM and activity was optimal when drug was added 1 h before initiating infection. However, significant activity was observed when VP-14637 (**10**) was added 1 h postinfection although; this

was significantly diminished if the drug was added 2 h after infection, data indicating that VP-14637 (**10**) interferes with an early step in the virus life cycle [105].

Since VP-14637 (**10**) exhibits poor aqueous solubility and is not orally bioavailable, the drug was administered topically as small droplets aerosolized from a 0.2 mg/mL solution in 85% ethanol, 10% propylene glycol and 5% water in experiments investigating its antiviral efficacy in models of RSV infection [105]. Exposure of cotton rats to aerosolized VP-14637 (**10**) for 60 min a day for 4 days beginning 1 h postinoculation resulted in the maximal 2.3 $TCID_{50}$ log_{10}/g of lung reduction. However, alternate regimens of 60-min exposure beginning 1 h postinoculation followed by 2 × 60-min exposures on the following day or 2 × 60 min at 1 and 4 h postinoculation and 2 × 60-min exposures on the following day or 2 × 60-min exposures on the day following inoculation with virus were equally effective. In a somewhat surprising result, 2 × 60-min exposures to the drug either 1 h before or after inoculation followed by a second 60-min exposure 4 h postinoculation did not result in a significant antiviral effect [105].

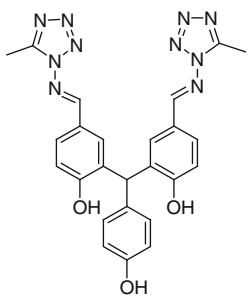

10 (VP-14637)

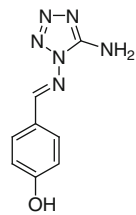

11

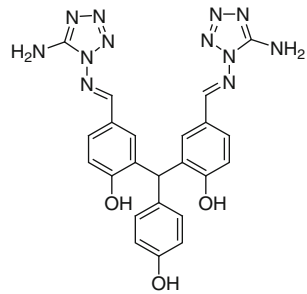

12

The discovery and profile of the potent and orally bioavailable RSV fusion inhibitor BMS-433771 (**13**) has been described in some detail in a series of publications [16, 90, 106–114]. BMS-433771 (**13**) was the first RSV fusion inhibitor to demonstrate antiviral activity in vivo following oral administration and its discovery resulted from optimization of the two isomeric benzotriazole derivatives **14** and **15** that were identified as potent inhibitors of RSV in cell culture in a high throughput screen. These compounds, which had been prepared over 30 years earlier by an Italian academic laboratory for evaluation as potential analgesic and anti-arrhythmic agents, were potent and selective inhibitors of RSV with EC_{50}s of 470 nM for **14** and 220 nM for **15** [115–117]. The initial probe of structure-activity relationships focused on variation of the dialkylaminoethyl benzimidazole substituent in the context of **14** and revealed considerable tolerance for structural variation of the terminal element with amide, carboxylic acid, sulfone, sulfoxide, sulfide, amine, alcohol and alkane moieties generally exhibiting potency similar to or within tenfold of the leads **14** and **15** [107]. A limited survey of analogues of **15**, produced as the minor isomer during synthesis of the core, suggested that this heterocycle topology offered comparable potency to the isomeric series defined by **14**. The only apparent requirement revealed by this survey was that activity was optimal when the terminal moiety and branching were separated from the core by

at least two carbon atoms [107]. However, more recent studies of the original chemotype suggest some latitude with respect to this topological parametric requirement [117].

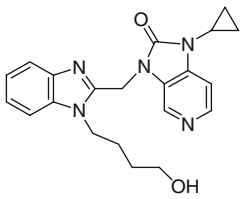

13 (BMS-433771)

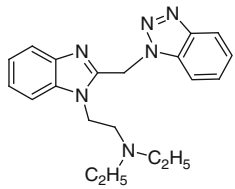

14

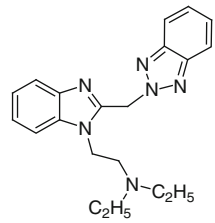

15

Replacement of the benzotriazole heterocycle was examined as a means of probing the effect of introducing substituents to the heterocycle or the aromatic ring element, with the chemically inert isoamyl moiety selected as the side chain appended to the benzimidazole core. The benzimidazol-2-one moiety, a heterocycle readily functionalized in a regiospecific fashion on the second N atom and the fused phenyl ring, was selected as the initial vehicle, a decision that proved propitious since the silhouette was ultimately incorporated into BMS-433771 (**13**) [108]. Variation of the R group in the general structure **16** revealed a broad tolerance for substituent variation based on the extensive range of functionality probed in this phase of the survey. Of particular note, the isopropenyl derivative **17** is an exceptionally potent RSV inhibitor, $EC_{50} = 4$ nM, while the valeric acid derivative **18**, $EC_{50} = 8$ nM, established compatibility between antiviral activity and the incorporation of polar, water-solubilizing elements [108, 109].

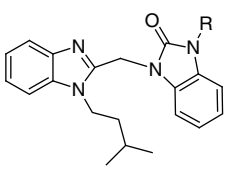

16

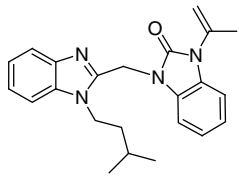

17

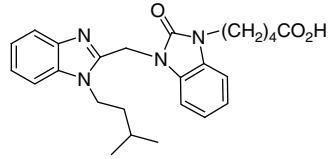

18

The latter was subsequently demonstrated to be of considerable importance in establishing antiviral activity in the cotton rat model of RSV infection using topical administration by small particle aerosol (SPA), a delivery method that optimally requires compounds with sufficient aqueous solubility to allow formulation in the nebulizer [109]. The benzimidazol-2-one moiety provided convenient synthetic access to the 20 g quantities of material required for this study which, in the initial experiments, exposed infected cotton rats to drug for 20 h a day for 4 consecutive days beginning 1 h postinoculation of the animals with virus. The acids **19–21** are potent RSV inhibitors in cell culture, with EC_{50}s = 16, 4 and 6 nM, respectively, while **22**, which incorporates the acidic oxadiazolone moiety, displayed an EC_{50} of 23 nM [109]. These compounds were typically formulated as their sodium salts for

aerosolization and all were soluble at >10 mg/mL in water, while the concentration was varied as a means of modulating exposure levels of the drug. All four compounds significantly reduced viral titers in the lungs of cotton rats measured at sacrifice on day 4 postinoculation, the established peak of viral titers in this model of infection, at concentrations ranging from 0.5 to 2.0 mg/mL in the SPA solution. The oxadiazolone **22** was subsequently evaluated in a BALB/c mouse model of RSV infection, where it was administered subcutaneously at a dose of 120 mpk, beginning 1 h postinfection and reproducibly reduced viral titers in lungs homogenates. This experiment established the potential of this class of RSV inhibitor to interfere with RSV replication in the lung following systemic exposure [109].

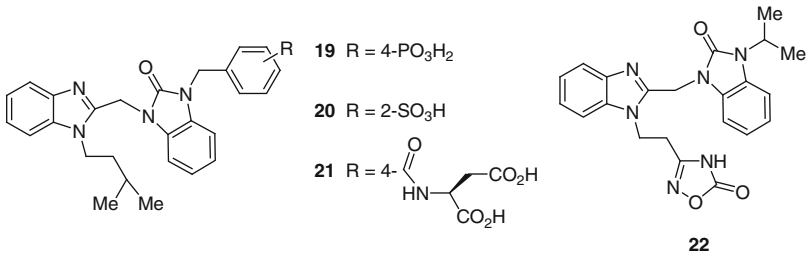

Further optimization of this series of compounds focused on improving pharmacokinetic properties, particularly in reducing the potential for metabolism by CYP 450 enzymes [110]. The aromatic portion of the benzimidazol-2-one ring was identified as a site of hydroxylation, a facile process that was mitigated by reducing the electron density of the ring. Since substituents attached to the benzene ring of the benzimidazol-2-one heterocycle were incompatible with high potency, the focus of this effort was in replacing the phenyl ring with a pyridine. As summarized in Table 1, this facet of SAR was explored in a systematic fashion, an exercise that established that the potency was preserved when an N atom was substituted for C-6 (**25**) or C-7 (**26**) but not for C-4 (**23**) or C-5 (**24**). The C-6 series represented by **25** became the major focus of further study based largely on synthetic accessibility.

Metabolic stability was further enhanced by manipulation of the benzimidazol-2-one N-3 substituent with cyclopropyl, trifluoroethyl or difluoromethyl useful moieties [110]. This process distilled the selection to compounds **13** and **27**–**30** (Table 2), with oral exposure as the final arbiter of decision making, a property that correlated with membrane permeability as measured across a confluent layer of Caco-2 cells.

BMS-433771 (**13**) was selected as the clinical candidate based on its pharmacokinetic properties in rat, dog and cynomolgus monkey that predicted targeted exposure levels in humans based on allometric scaling [16, 90, 106, 114]. BMS-433771 (**13**) exhibited dose-dependent antiviral activity in both the BALB/c mouse and cotton rat models of RSV infection, following oral administration in a prophylactic mode with a single dose of drug given 1 h prior to intranasal virus inoculation [114]. This dosing regimen was as effective as when the drug was administered twice daily for 4 days beginning 1 h prior to infection. In the cotton rat, which is a more permissive model of RSV infection, doses of 25–200 mpk reduced viral titers in the lungs measured at 4 days postinoculation; whereas in the mouse, in which the

Table 1 Structure and antiviral activity of a series of aza-benzimidazol-2-one derivatives

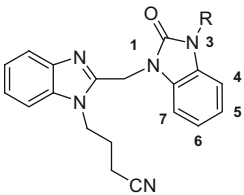

Compound	Position of N	R	EC_{50} (μM)
23	4	*iso*-Propenyl	0.202
24	5	H	5.71
25	6	*iso*-Propenyl	0.006
26	7	*iso*-Propenyl	0.003

Table 2 Structure and antiviral activity of a series of N-substituted aza-benzimidazol-2-one derivatives

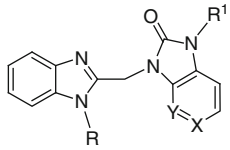

Compound	X	Y	R	R^1	EC_{50} (nM)	CC_{50} (μM)	HLM $t_{1/2}$ (min)	Caco-2 permeability (nm/s)
13	N	CH	$(CH_2)_4OH$	cC_3H_5	10	>218	36	143
27	N	CH	$(CH_2)_3CN$	cC_3H_5	10	236	38	181
28	N	CH	$(CH_2)_3SO_2CH_3$	CH_2CF_3	12	236	87	33
29	N	CH	$(CH_2)_3SO_2CH_2CH_3$	CH_2CF_3	4	236	36	92
30	CH	N	$(CH_2)_3SO_2CH_2CH_3$	CHF_2	6	236	55	59

exposure of the drug was higher, lower doses of 10–100 mpk demonstrated efficacy. BMS-433771 (**13**) was not efficacious in the mouse model when virus with a K394R mutation in the F1 protein that confers resistance was used, confirming that the molecule acts in vivo by interfering with virus-host fusion.

A cell-based virus infection assay conducted in HeLa/M cells using the Long strain of RSV identified JNJ-1789008 (**31**) as a lead inhibitor with promising potency, $EC_{50} = 398$ nM, that was significantly enhanced by structural modification, which afforded JNJ-2408068 (R170591, **32**), $EC_{50} = 0.16$ nM [118]. This compound potently inhibited RSV infection in HEp-2 and A549 cells, was active towards clinical isolates representative of the A and B strains of virus with EC_{50}s ranging from 0.16 to 4.47 nM and also potently inhibited bovine RSV. Time-of-addition experiments indicated that JNJ-2408068 (**32**) acted early in the virus lifecycle with fusion inhibition implicated by allowing virus to adsorb at 4°C and then warming to 37°C in the presence of the compound, circumstances under which inhibition was preserved. Resistance revealed point mutations in the F protein with S398L and D486N conferring >10,000 and 500-fold increases in the EC_{50}, respectively [118].

In the cotton rat model of infection, JNJ-2408068 (**32**) delivered by aerosol provided protection against RSV infection when administered for 15 min both 1 day

prior to and 1 day after virus inoculation compared to control animals [119]. Pharmacokinetic experiments indicated effective lung exposure to JNJ-2408068 (**32**) under these conditions with significant amounts of drug remaining in lung tissue 96 h after dosing, while distribution to the plasma compartment was minimal. The extended tissue retention time observed with JNJ-2408068 (**32**) in the lungs of cotton rats was also seen in rats, dogs and monkeys, providing cause for concern and focusing optimization studies on identifying the compounds with improved profiles. Structure-activity relationships indicated that the aminoethyl piperidine element of JNJ-2408068 (**32**) was responsible for tissue retention, attributed to the highly basic nature of this moiety which contributed significantly to antiviral activity [120, 121]. Extended lung retention times were associated with compounds exhibiting a pKa of >9, providing a strategy for optimization that ultimately identified TMC-353121 (**33**) as a potent RSV inhibitor. The reduced overall basicity of TMC-353121 (**33**) contributes to a $T_{1/2}$ in lung tissue of 25.1 h, which compares to a $T_{1/2}$ of 153 h for JNJ-2408068 (**30**) [120, 121]. TMC-353121 (**33**) exhibits modest oral bioavailability in rats (14%), slow absorption with T_{max} occurring at 4 h, a high volume of distribution (79 L) and a plasma $T_{1/2}$ of 4–24 h after IV dosing [122]. In the cotton rat model, TMC-353121 (**33**) significantly reduced viral titers when administered orally (40 mpk), intravenously (10 mpk) or by aerosol, with the IV experiments determining that drug exposure 1 h prior to virus challenge provided optimal efficacy. Minimal efficacy was observed when the drug was administered 24 h before or 3 h after virus inoculation. TMC-353121 (**33**) is also active in a BALB/c mouse model of infection administered at doses between 0.25 and 10 mpk, significantly reducing viral load and lung histopathologic damage when therapy was initiated within 48 h of virus inoculation, suggesting the potential for therapeutic application of this drug [123].

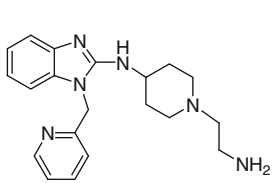

31 (JNJ-1789008)

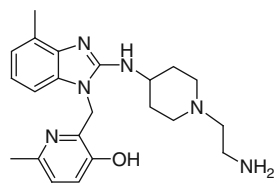

32 (JNJ-2408068)

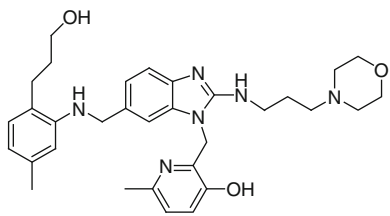

33 (TMC-353121)

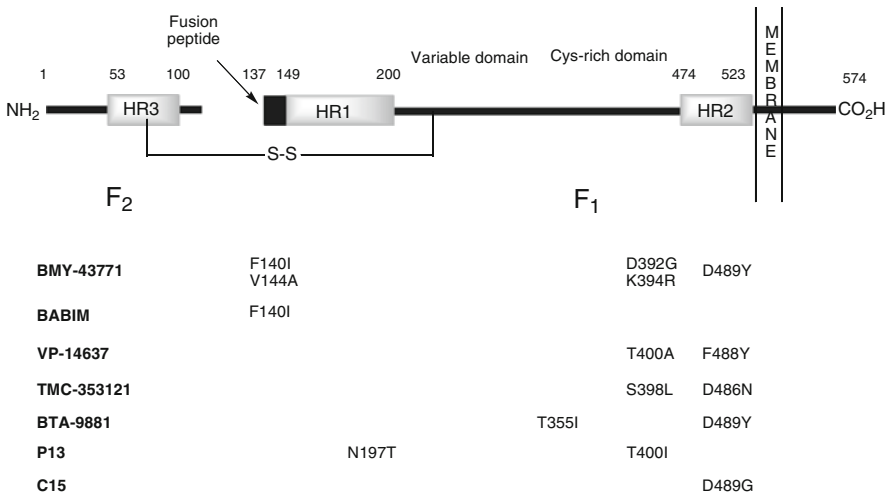

Fig. 4 A map of the RSV F protein and resistance mutations arising in response to selective pressure by fusion inhibitors

A series of imidazo[2,1-*a*]isoindol-5(9*bH*)-one derivatives have been described as RSV fusion inhibitors by Biota with compounds **34**–**37** representative examples [19, 124–126]. Antiviral activity is associated with the (*S*)-enantiomer, exemplified by **34**, which exhibits an EC_{50} of 140 nM in a replication assay in cell culture and is active towards both RSV A and B strains. The pharmacokinetic properties of **34** were improved by introducing a nitrogen atom into the isoindolone ring to afford the pyridine derivative **35** with further enhancement in exposure observed with the N-oxide **36** [19]. In cotton rats, daily 100 mpk oral doses of **35** initiated 2 h prior to inoculation with virus reduced lung viral titers by 96% compared to placebo-treated control animals [18]. Optimization of the 4-fluorophenyl moiety gave compounds with increased potency, exemplified by the substituted thiazole **37** which displays an EC_{50} of 12 nM. These compounds were deduced to function by inhibiting fusion based on the observation of activity in a syncytium-forming assay and the analysis of virus developed to be resistant to **34**. A T335I substitution in the F protein was associated with a 76-fold increase in the EC_{50} value and **34** exhibited cross-resistance to the D489Y mutation that conferred resistance to BMS-433771 (**13**). BTA-9881, the structure of which has not been disclosed, was selected as a candidate for evaluation in Phase I clinical trials, where it demonstrated good exposure and an extended plasma half-life. However, development of BTA-9881 is not being pursued by the sponsors, AstraZeneca/MedImmune, based on an inadequate safety margin in humans, and refined compounds are reportedly being profiled as potential candidates for clinical evaluation [127].

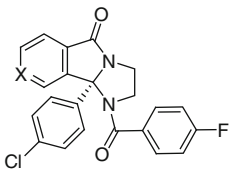

34: X = CH
EC_{50} = 140 nM
35: X = N
EC_{50} = 120 nM
36: X = N^+-O^-
EC_{50} = 190 nM

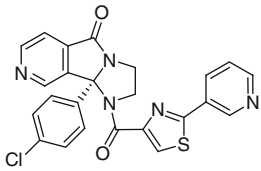

37
EC_{50} = 12 nM

The most recently described RSV fusion inhibitors are P13 (**38**) and C15 (**39**), identified from a screen of 16,671 structurally diverse compounds, that demonstrate EC_{50}s of 110 and 130 nM, respectively [128]. Experiments designed to provide insight into the mode of action revealed that P13 (**38**) and C15 (**39**) were not inhibitors of virus attachment and that the inhibitory effect occurred early in the virus life cycle. The selection of virus resistant to P13 (**38**) and C15 (**39**) identified changes in the F protein with T400I and, in some clones, N197T emerging in response to selective pressure by P13 (**38**), while a D489G change conferred resistance to C15 (**39**).

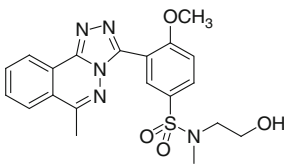

38 (P13)

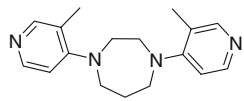

39 (C15)

5 Inhibitors of Respiratory Syncytial Virus Fusion: Interfering with an Intramolecular Protein-Protein Interaction

Evidence that fusion inhibition is the mode of action for the RSV inhibitors described above has been based on the generation of resistant virus with changes mapped to the F protein, time-of-addition experiments that indicate interference early in the virus life cycle and demonstration of activity in an assay that specifically differentiates inhibition of virus fusion from binding to host cell receptors [129–131]. Figure 4 provides a visual representation of the resistance mutations that have arisen in the RSV F protein in response to selective pressure from BABIM (**5**), VP-14637 (**10**), BMS-433771 (**13**), TMC-353121 (**33**), BTA-9881, P13 (**38**) and C15 (**39**), mapped onto the structure of the F protein. The levels of resistance to the individual molecules are summarized in Table 3. Most notably, there is

Table 3 Resistance mutations arising in response to selective pressure by RSV fusion inhibitors

Mutation	BMS-433771 (**13**)	BABIM (**5**)	CL-387626 (**8**)	VP-14637 (**10**)	JNJ-2408068 (**32**)	TMC-353121 (**33**)	BTA-9881	P13 (**38**)	C15 (**39**)
F140I	>1,250	>1,250							
V144A	150								
N197T								Resistant	
T335I							76		
D392G	35								
K394R	>1,250					30,000 w/S398L			
S398L						194			
T400A				>1,000					
T400I								Resistant	
D486N						2,474			
F488I			1,698	>10,000	>10,000				
F488L			610	>10,000	>10,000				
F488Y				Resistant					
D489Y	>1,250		261	>10,000	>10,000		Resistant		
D489G									Resistant

considerable cross-resistance between these compounds despite their significant structural differences, and the experimental data indicates commonality in their mode of fusion inhibition.

In an effort to more precisely map the binding sites of fusion inhibitors, radiolabeled affinity probes have been used to localize the binding site on the F protein. Binding of the tritiated azide **40**, EC_{50} = 200 nM, localized to the virus F protein and was competitively inhibited by analogues in this series [94]. Surface plasmon resonance experiments suggested that these molecules bound to HR-N and the HR-N/HR-C complex but not to HR-C, with binding to HR-N of lower affinity than for the whole F protein where affinity constants were in the 50–100 nM range [94]. These results were interpreted to suggest that RFI-641 (**9**) and related compounds associated with the loop or hinge region between the heptad repeats.

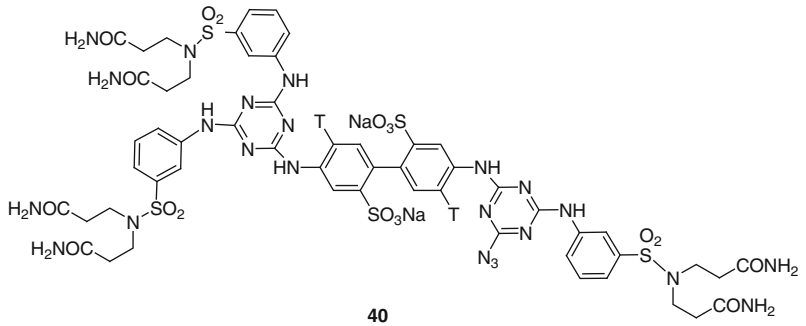

40

The iodinated diazirine BMS-356188 (**41**), EC_{50} = 38 nM, provided detailed information on the binding site of the Bristol-Myers Squibb series [132, 133]. Experiments with **41** revealed that the RSV F1 protein subunit was specifically labeled upon photo-activation of the diazirine to afford a highly reactive carbene species when incubated with virus. Labeling of the F1 protein was reduced in a concentration-dependent fashion when BMS-433771 (**13**) was included in the experiment, confirming that the two molecules share the same binding site. The labeled F1 subunit was digested with cyanogen bromide, which localized the binding site to an 11–13 kDa, 115 residue fragment comprising amino acids 137–251 [133]. Further degradation by exposure to the endoprotease Glu-C (*Staphylococcus aureus* V8 protease), which specifically cleaves at the amide bond of glutamate residues, isolated the label to residues 164–218 of the F1 protein, the N-terminal heptad repeat, HR-N. Subsequent experiments were conducted with the synthetic peptides that were used to determine the structure of the HR-N trimer and labeling of the assembled fusion core with **41** was examined [8, 133]. Affinity labeling was promoted optimally in the presence of RFI-641 (**9**) or, to a lesser extent, 20% trifluoroethanol, reagents considered to stabilize the helical trimeric form of HR-N. Sequencing of the labeled HR-N42 peptide in conjunction with mass spectrometric analysis identified Tyr198 as the amino acid that was predominantly labeled by the carbene derived from **39**, a process inhibited by BMS-433771 (**13**). Labeling of several adjacent amino acids

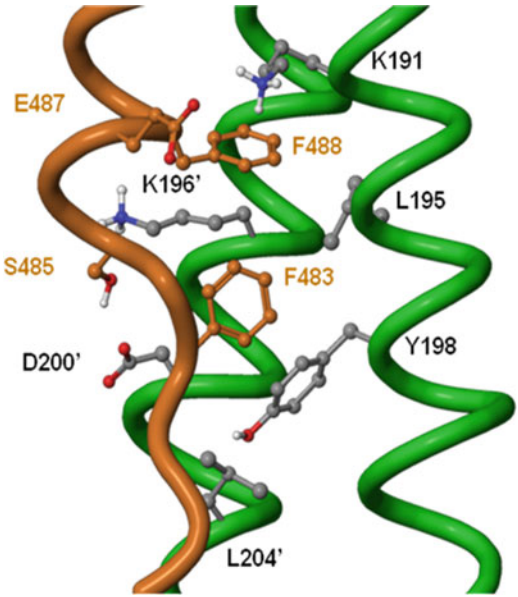

Fig. 5 Key interacting amino acid residues that are projected from HR-C to the hydrophobic pocket of the RSV HR-N trimer

was also observed that localized the binding site to the hydrophobic cavity in the HR-N trimer that accommodates Phe483, Phe488 and Ile492 from HR-C and which was identified by Kim as a potential site for drug action (Fig. 5) [8, 133]. Binding poses for **41** and **13** were assessed by computer-aided docking studies and molecular dynamics simulations, with the favored mode of interaction placing the diazirine moiety proximal to Tyr198. This binding pose placed the benzimidazol-2-one heterocycle in the pocket that accommodates Phe488 in the fusion-active six-helix bundle complex, while the benzimidazole moiety mimicked Phe483, projecting the diazirine-containing side chain towards Tyr198, the observed site of labeling. In this arrangement, the diiodophenol moiety of **41** occupies the pocket filled by Ile492 of HR-C with the cyclopropyl ring of BMS-433771 (**13**) acting as a smaller surrogate. Interestingly, the proposed binding interactions between these inhibitors and the trimeric HR-N bundle are hydrophobic in nature and do not rely upon any hydrogen-bonds.

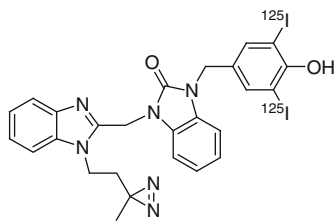

41 (BMS-356188)

Table 4 The evolution of structure-activity relationships for benzimidazole-based RSV fusion inhibitors that establish an interaction with Asp200

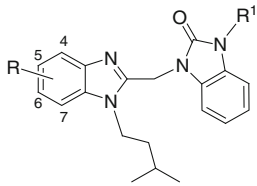

Compound	R	R^1	EC_{50} (μM)	CC_{50} (μM)
42	4-CH_2NH_2	*i*-Pr	0.715	7.0
43	4-CH_2OH	*i*-Pr	0.820	22.0
44	4-CO_2CH_3	*i*-Pr	230	49.2
45	5-CH_2NH_2	*i*-Pr	0.002	3.9
46	5-CH_2OH	*i*-Pr	0.050	31.6
47	5-CO_2NH_2	*i*-Pr	0.166	23.4
48	5-CO_2H	*i*-Pr	238	17.3
49	6-CH_2NH_2	*i*-Pr	0.095	28.1
50	6-$CH_2CH_2NH_2$	*i*-Pr	7.11	57.0
51	6-CH_2OH	*i*-Pr	0.134	81.6
52	6-CO_2NH_2	*i*-Pr	123	49.9
53	6-CO_2H	*i*-Pr	238	125
54	7-CH_2NH_2	*i*-Pr	192	11.0
55	7-CH_2OH	*i*-Pr	246	246
56	7-CO_2CH_3	*i*-Pr	230	25.3
57	5-NH_2	*i*-Pr	0.125	32.2
58	5-$CH_2CH_2NH_2$	*i*-Pr	0.002	3.92
59	5-CH_2NHCH_3	*i*-Pr	0.057	1.48
60	5-$CH_2N(CH_3)_2$	*i*-Pr	183	5.65
61	5-$CH_2NHCOCH_3$	*i*-Pr	0.631	178
62	5-$C(CH_3)_2NH_2$	*i*-Pr	0.694	3.27
63	5-$C(NH)NH_2$	2-Propenyl	0.004	10.8
64	5-$C(NOH)NH_2$	2-Propenyl	0.005	3.47

The hypothesized binding pose places the C-5 and C-6 atoms of the benzimidazole ring proximal to Asp200, precipitating the hypothesis that the introduction of basic or polar substituents at these sites of the heterocycle may establish additional productive interactions with the acid moiety. The model also predicts that substituents at C-7 of the benzimidazole ring would be poorly tolerated while C-4 would be more accommodating of substitution but, nevertheless, restricted in size since these sites are in close proximity with the protein. These hypotheses were explored experimentally with the synthesis and evaluation of the series of compounds compiled in Table 4, which systematically survey common substituents at the C-4, C-5, C-6 and C-7 sites of the benzimidazole heterocycle. It is clear from

the data that the structure-activity relationships are concordant with the proposed binding mode, with substituents at C-4 moderately tolerated while all C-7 substituted analogues are poorly active. An aminomethyl moiety at C-5 afforded **45**, a potent antiviral agent but the same substituent at C-6 confers an almost 50-fold reduction in potency (**49**), suggesting that interactions with Asp200 are more readily established from C-5 of the core heterocycle. With this information in hand, substituents at C-5 were explored in greater depth with the results furthering the hypothesis that this site of the heterocycle ring is close to Asp200. Most notably, the mono- and dimethyl-amine derivatives **59** and **60**, respectively, and the carboxylic acid **48** are weaker RSV inhibitors, whereas the amidine **63** is a potent antiviral, a result recapitulated by the nonbasic hydroxyamidine **64**. This result suggests that in addition to a salt bridge interaction, hydrogen-bonding is sufficient to establish a relationship with Asp200, a notion reinforced by the potent antiviral activity associated with the hydroxymethyl derivative **46**. Most interestingly, the RSV inhibition associated with amidine **63** is strongly suggestive of structural overlap with BABIM (**5**)**,** a molecule that projects a similar topological arrangement of heterocycles to that of the benzotriazole **15** that formed part of the original discovery of this chemotype [107].

The potency of benzylamine **45** towards wild-type virus is similar to that of BMS-433771 (**13**) and the unsubstituted analogue. However, the positive effect of a basic amine moiety at C-5 is most effectively demonstrated by the potency that the amine **45** expressed towards the K394R virus that confers resistance to this class of RSV fusion inhibitor. Amine **45** inhibits K394R virus with an EC_{50} of 20 nM, over 1,000-fold more potent than BMS-433771 (**13**), a result that supports the hypothesized binding mode [16, 111].

The most definitive data on the mode of binding of RSV fusion inhibitors to the HR-N trimer have been secured by solving an X-ray cocrystal structure of TMC-353121 (**33**) bound to the six-helix HR-N bundle, data that provide interesting insights into the mode of antiviral action [134]. Initial experiments focused on the binding of the diazirine **65**, which was labeled with ^{125}I and is a potent inhibitor of RSV, $pIC_{50} = 8.0$. Irradiation of **65** in the presence of the HR-N trimeric core IQN57 resulted in binding, providing that the HR-C element C39 was also included in solution. In the absence of C39, **65** failed to bind while the D489N mutant of C39 exhibited reduced binding, as did an IQN57 derivative in which Tyr198 was mutated to an alanine, data that suggest that this class of fusion inhibitor interacts with both HR-N and HR-C. This hypothesis was confirmed by cocrystallization of TMC-353121 (**33**) with N52, a 52-residue peptide derived from HR-N, and C39 which revealed that the inhibitor makes several hydrophobic and electrostatic contacts with both HR-N and HR-C. The hydroxyl substituent of the hydroxypyridine moiety of TMC-353121 (**33**) establishes a hydrogen-bond with Asp200 and the heterocycle ring engages in a π–π stacking interaction with Tyr198 and makes several hydrophobic contacts with the binding site. The NH attached to C-2 of the benzimidazole ring of TMC-353121 (**33**) interacts with D486 of HR-C via a hydrogen-bond donor interaction, and a water molecule mediates interactions between E487 of HR-C and the inhibitor. Both D486 and E487 adopt different rotameric states compared to the native structure

Table 5 Structure-activity relationships associated with TMC-353121 (**33**)

Compound	Structure	pEC_{50}
33 (TMC-35312, R═H) **66** (R═CH_3)	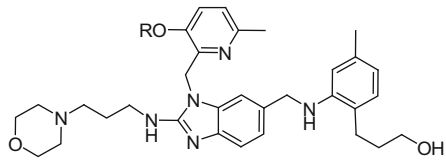	9.9 8.6
67	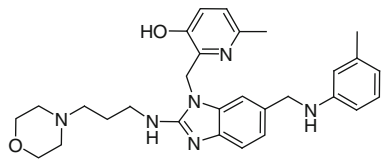	8.6
68	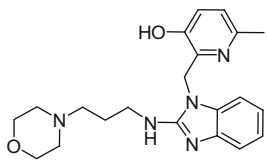	6.8
69 (R═NH_2) **70** (R═H)	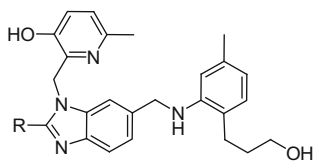	10.5 7.9

that allows interaction with TMC-353121 (**33**). The binding mode allows Phe488 to remain largely unperturbed in its binding pocket in HR-N, preserving the interactions observed in the absence of inhibitor but Phe483 is displaced by TMC-353121 (**33**). Thermal shift measurements indicate that TMC-353121 (**33**) stabilizes the six-helical bundle assembly, detected by the 7°C increase in the melting temperature (T_m). The binding mode in the X-ray structure exhibited good consistency with the structure-activity relationships developed for TMC-353121 (**33**), data summarized in Table 5. Methylation of the pyridine hydroxyl (**66**) reduced potency by 1.3 $\log_{10}$, reflecting the importance of this moiety in the array of hydrogen-bonding interactions. Deleting the hydoxypropyl (**67**) moiety also eroded activity by 1.3 $\log_{10}$ while further truncation to **68** resulted in almost an additional order of magnitude loss of antiviral activity. The morpholinoethyl side chain was not an important contributor to antiviral activity based on the potency of **69** but the 2-amino substituent was critical since omission afforded **70**, a compound 100-fold weaker than TMC-353121 (**33**) and 2.6 $\log_{10}$ less active than **69** [134].

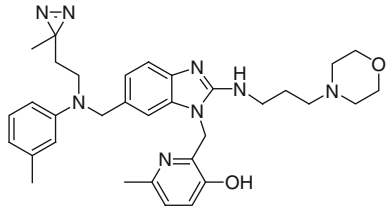

65 (TMC-429962)

The scenario that emerges from these data is one in which TMC-353121 (**33**) does not overtly prevent the formation of the critical six-helix bundle but rather is captured by the complex in a sandwich-like arrangement that leads to a distorted but stabilized structure in which four key residues of HR-C are unable to fully engage the core of the trimeric HR-N. The crystallographic structure also provides insight into the development of resistance with the D486N mutation interfering with the hydrogen-bond established between Asp486 and the benzimidazole 2-NH_2 substituent of TMC-353121 (**33**), further reinforcing the critical nature of this structural element.

The proposed binding mode of BMS-433771 (**13**) is quite different to that determined by the X-ray crystallographic analysis of TMC-353121 (**33**) bound to elements of the six-helix bundle. BMS-433771 (**13**) is thought to occupy the hydrophobic pockets filled by the HR-C residues Phe483, Phe488 and Ile492, binding along the groove between two of the helices with the axis of the molecule aligned with the HR-C backbone. In contrast, TMC-353121 (**33**) associates in a fashion that is essentially orthogonal, binding across two of the helices of the HR-N trimeric core, a binding mode that fully preserves the interaction between Phe488 of HR-C and the HR-N core (Figs. 5 and 6). The mode of interaction of BMS-433771 (**13**) with HR-C residues is unknown and it is likely that these will fold quite differently around the inhibitor than that observed with TMC-353121 (**33**), providing additional productive interactions [134].

The X-ray crystallographic structure of TMC-353121 (**33**) bound to elements of the RSV six-helix bundle provides key insights into the mode of action of this compound that may be extrapolated to other fusion inhibitors. Whereas the precise mode of action of TMC-353121 (**33**) remains somewhat enigmatic, it is clear that the compound does not act by simply preventing the formation of the fusion core but rather leads to a distorted structure that presumably affects subsequent events in the fusion process that are unresolved. The formation of a fusion pore between the host and virus membranes is a key step following F protein rearrangement and the first stages of self-association between HR-N and HR-C, a process that has proven difficult to study [135–139]. Both the number of fusion trimers required to promote fusion pore generation and the precise temporal occurrence of events in the process are controversial and may differ between viruses in a subtle fashion. The simple act of drawing the two membranes into close proximity has been shown to be

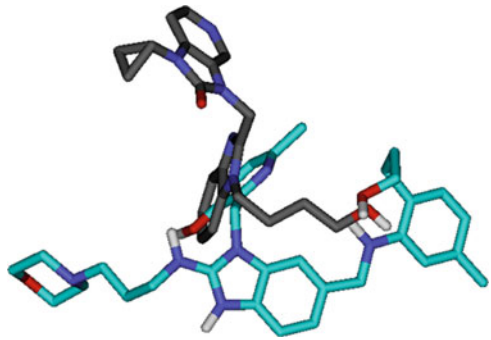

Fig. 6 Overlay of the proposed binding mode of BMS-433771 (**12**) (*gray*) with the X-ray crystallographic structure of TMC-353121 (**33**) (*blue*) bound to the RSV six-helix bundle

insufficient to promote full fusion and elements of the fusion peptide play an important role in this stage of the process [140–142]. Interactions between the fusion peptide and C-terminus transmembrane domain during the later stages of fusion are a feature of both the lipid-centric and the pinprick models of viral fusion and are of greater importance in the latter model [135]. The distortion in the six-helix bundle induced by RSV fusion inhibitors may compromise interactions between fusion protein trimers that are cooperative in nature and facilitate the process of membrane apposition [143]. Alternatively, a complex between an RSV fusion inhibitor and the six-helix bundle has the potential to interfere with the association of the C-terminus transmembrane segment and the fusion peptide that may be of importance during the final stages of membrane fusion.

6 Conclusion

Broad screening campaigns have proven to be a very effective approach to the identification of RSV fusion inhibitors and several structurally diverse chemotypes that appear to function by common underlying mechanistic themes have been profiled in some detail. The six-helix bundle core adopted by the RSV F protein in its fusion-competent state is a structural motif common to several viruses, including the retroviruses HIV-1, simian immunodeficiency virus, Moloney murine leukemia virus and human T-cell leukemia virus type-1, and influenza, ebola and simian parainfluenza virus 5 [1]. Interfering with six-helix bundle formation is the mode of action of enfuvirtide, a 36-residue peptide derived from HR-C that was granted accelerated approval on March 13, 2003 by the FDA as a treatment for HIV-1 infection with traditional approval occurring on October 15, 2004. The synthesis of peptides derived from the HR-C elements of type 1 virus fusion proteins has proven to be a useful and general strategy for identifying inhibitors of six-helix bundle formation and virus entry in vitro. However, to date, RSV is unique in that this process is susceptible to interference by small-molecule

inhibitors. Moreover, the inhibitors that have been described represent a broad range of structural diversity but appear to share remarkable similarities in their underlying mode of action. Although the characterization of RSV fusion inhibitors has illuminated fundamental aspects of the virus fusion process, the precise mechanism by which this intramolecular protein-protein interaction is ultimately compromised is enigmatic and remains as a subject of considerable interest to the virology scientific community.

References

1. Eckert DM, Kim PS (2001) Mechanisms of viral membrane fusion and its inhibition. Annu Rev Biochem 70:777–810
2. Peisajovich SG, Shai Y (2002) New insights into the mechanism of virus-induced membrane fusion. Trends Biochem Sci 27:183–190
3. Colman PM, Lawrence MC (2003) The structural biology of type I viral membrane fusion. Nat Rev Mol Cell Biol 4:309–319
4. Smith AE, Helenius A (2004) How viruses enter animal cells. Science 304:237–242
5. Earp LJ, Delos SE, Park HE, White JM (2005) The many mechanisms of viral membrane fusion proteins. Curr Top Microbiol Immunol 285:25–66
6. Lamb RA, Jardetzky TS (2007) Structural basis of viral invasion: lessons from paramyxovirus F. Curr Opin Struct Biol 17:427–436
7. Harrison SC (2008) Viral membrane fusion. Nat Struct Mol Biol 15:690–698
8. Zhao X, Singh M, Malashkevich VN, Kim PS (2000) Structural characterization of the human respiratory syncytial virus fusion protein core. Proc Natl Acad Sci USA 97:14172–14177
9. Chan DC, Chutkowski CT, Kim PS (1998) Evidence that a prominent cavity in the coiled coil of HIV type 1 gp41 is an attractive drug target. Proc Natl Acad Sci USA 95:15613–15617
10. Debnath AK (2006) Prospects and strategies for the discovery and development of small-molecule inhibitors of six-helix bundle formation in class 1 viral fusion proteins. Curr Opin Investig Drugs 7:118–127
11. Wild C, Oas T, McDanal C et al (1992) A synthetic peptide inhibitor of human immunodeficiency virus replication: correlation between solution structure and viral inhibition. Proc Natl Acad Sci USA 89:10537–10541
12. Wild C, Greenwell T, Shugars D et al (1995) The inhibitory activity of an HIV type 1 peptide correlates with its ability to interact with a leucine zipper structure. AIDS Res Hum Retrovir 11:323–325
13. Lu M, Blacklow SC, Kim PS (1995) A trimeric structural domain of the HIV-1 transmembrane glycoprotein. Nat Struct Biol 2:1075–1082
14. Chan DC, Fass D, Berger JM, Kim PS (1997) Core structure of gp41 from the HIV envelope glycoprotein. Cell 89:263–273
15. Del Vecchio AM, Sarisky RT (2006) Cold virus fusion or stopping fusion cold – inhibitors of the human respiratory syncytial virus F protein. Recent Pat AntiInfect Drug Discov 1:247–254
16. Meanwell NA, Krystal M (2007) Respiratory syncytial virus – the discovery and optimization of orally bioavailable fusion inhibitors. Drugs Future 32:441–455
17. Carter M, Cockerill GS (2008) Inhibitors of respiratory syncytial virus. Annu Rep Med Chem 43:229–245
18. Bonfanti J-F, Roymans D (2009) Prospects for the development of fusion inhibitors to treat human respiratory syncytial virus infection. Curr Opin Drug Discov Dev 12:479–487

19. Olszewska W, Openshaw P (2009) Emerging drugs for respiratory syncytial virus infection. Exp Opin Emerg Drugs 14:207–217
20. Murineddu G, Murruzzu C, Pinna GA (2010) An overview on different classes of viral entry and respiratory syncytial virus (RSV) fusion inhibitors. Curr Med Chem 17:1067–1091
21. Collins PL, McIntosh K, Chanock RM (2002) Respiratory syncytial virus. In: Knipe DM, Howley PM (eds) Fields virology. Raven, New York
22. Blount RE Jr, Morris JA, Savage RE (1956) Recovery of cytopathogenic agent from chimpanzees with coryza. Proc Soc Exp Biol Med 92:544–549
23. Chanock R, Roizman B, Myers R (1957) Recovery from infants with respiratory illness of a virus related to chimpanzee coryza agent (CCA). I. Isolation, properties and characterization. Am J Hyg 66:281–290
24. Chanock R, Finberg L (1957) Recovery from infants with respiratory illness of a virus related to chimpanzee coryza agent (CCA). II. Epidemiologic aspects of infection in infants and young children. Am J Hyg 66:291–300
25. Rowe DS, Michaels RH (1960) Isolation of the respiratory syncytial virus from a patient with pneumonia. Pediatrics 6:623–629
26. Tang Y-W, Crowe JE Jr (2007) Respiratory syncytial virus and human metapneumovirus. In: Murray PR (ed) Manual of clinical microbiology, 9th edn. ASM Press, New York
27. Griffin MR, Walker FJ, Iwane MK et al (2004) Epidemiology of respiratory infections in young children insights from the new vaccine surveillance network. Pediatr Infect Dis J 23: S188–S192
28. Glezen WP (2004) The changing epidemiology of respiratory syncytial virus and influenza impetus for new control measures. Pediatr Infect Dis J 23:S202–S206
29. Washburne JF, Bocchini JA Jr, Jamison RM (1992) Summertime respiratory syncytial virus infection: epidemiology and clinical manifestations. South Med J 85:579–583
30. Halstead DC, Jenkins SG (1998) Continuous non-seasonal epidemic of respiratory syncytial virus infection in the southeast United States. South Med J 91:433–436
31. Ottolini MG, Hemming VG (1997) Prevention and treatment recommendations for respiratory syncytial virus infection. Background and clinical experience 40 years after discovery. Drugs 54:867–884
32. Simoes EAF (1997) Respiratory syncytial virus infection: pathogenesis, treatment and prevention. Curr Opin Infect Dis 10:213–220
33. Holberg CJ, Wright AL, Martinez FD et al (1991) Risk factors for respiratory syncytial virus-associated lower respiratory illnesses in the first year of life. Am J Epidemiol 133:1135–1151
34. Glezen WP, Taber LH, Frank AL, Kasel JA (1986) Risk of primary infection and reinfection with respiratory syncytial virus. Am J Dis Child 140:543–546
35. Anderson LJ, Parker RA, Strikas RL (1990) Association between respiratory syncytial virus outbreaks and lower respiratory tract deaths of infants and young children. J Infect Dis 161:640–646
36. Nicholson KG (1996) Impact of influenza and respiratory syncytial virus on mortality in England and Wales form January 1975 to December 1990. Epidemiol Infect 116:51–63
37. Shay DK, Holman RC, Newman RD et al (1999) Bronchiolitis-associated hospitalizations among US children, 1980–1996. JAMA 282:1440–1446
38. Thompson WW, Shay DK, Weintraub E et al (2003) Mortality associated with influenza and respiratory syncytial virus in the United States. JAMA 289:179–186
39. Breese Hall C, Powell KR, MacDonald NE et al (1986) Respiratory syncytial viral infection in children with compromised immune function. New Engl J Med 315:77–81
40. Englund JA, Sullivan CJ, Jordan MC et al (1988) Respiratory syncytial virus infection in immunocompromised adults. Ann Intern Med 109:203–208
41. Hertz MI, Englund JA, Snover D et al (1989) Respiratory syncytial virus-induced acute lung injury in adult patients with bone marrow transplants: a clinical approach and review of the literature. Medicine 68:269–281

42. Ebbert JO, Limper AH (2005) Respiratory syncytial virus pneomonitis in immunocompromised adults: clinical features and outcome. Respiration 72:263–269
43. Ljungman P (1997) Respiratory virus infections in bone marrow transplant recipients, the European perspective. Am J Med 102:44–47
44. Flamant C, Hallelel F, Nolent P et al (2005) Severe respiratory syncytial virus bronchiolitis in children: from short mechanical ventilation to extracorporeal membrane oxygenation. Eur J Pediatr 164:93–98
45. Hashem M, Hall CB (2003) Respiratory syncytial virus in healthy adults: the cost of a cold. J Clin Virol 27:14–21
46. Dowell SF, Anderson LJ, Gary HE Jr et al (1996) Respiratory syncytial virus is an important cause of community-acquired lower respiratory infection among hospitalized adults. J Infect Dis 174:456–462
47. Mlinaric-Galinovic G, Falsey AR, Walsh EE (1996) Respiratory syncytial virus infection in the elderly. Eur J Clin Dis 15:777–781
48. Han LL, Alexander JP, Anderson LJ (1999) Respiratory syncytial virus pneumonia among the elderly: an assessment of the disease burden. J Infect Dis 179:25–30
49. Walsh EE, Peterson DR, Falsey AR (2004) Risk factors for severe respiratory syncytial virus infection in elderly persons. J Infect Dis 189:233–238
50. Falsey AR, Hennessey PA, Formica MA et al (2005) Respiratory syncytial virus infection in elderly and high-risk adults. New Engl J Med 352:1749–1759
51. Falsey AR, Walsh EE (2005) Respiratory syncytial virus infection in elderly adults. Drugs Aging 22:577–587
52. Zambon MC, Stockton JD, Clewley JP, Fleming DM (2001) Contribution of influenza and respiratory syncytial virus to community cases of influenza-like illness: an observational study. Lancet 358:1410–1416
53. Crowcroft NS, Cutts F, Zambon MC (1999) Respiratory syncytial virus: an underestimated cause of respiratory infection, with prospects for a vaccine. Commun Dis Public Health 2:234–241
54. Cane PA (2001) Molecular epidemiology of respiratory syncytial virus. Rev Med Virol 11:103–116
55. Melero JA (2007) Molecular biology of human respiratory syncytial virus. Perspect Med Virol 14:1–42
56. Ahmadian G, Chambers P, Easton AJ (1999) Detection and characterization of proteins encoded by the second ORF of the M2 gene of pneumoviruses. J Gen Virol 80:2011–2016
57. Melero JA, Garcia-Barreno B, Martinez I et al (1997) Antigenic structure, evolution and immunobiology of human respiratory syncytial virus attachment (G) protein. J Gen Virol 78:2411–2418
58. Krusat T, Streckert HJ (1997) Heparin-dependent attachment of respiratory syncytial virus (RSV) to host cells. Arch Virol 142:1247–1254
59. Harris J, Werling D (2003) Binding and entry of respiratory syncytial virus into host cells and initiation of the innate immune response. Cell Microbiol 5:671–680
60. Malhotra R, Ward M, Bright H et al (2003) Isolation and characterisation of potential respiratory syncytial virus receptor(s) on epithelial cells. Microbes Infect 5:123–133
61. Karron RA, Buonagurio DA, Georgiu AF et al (1997) Respiratory syncytial virus (RSV) SH and G proteins are not essential for viral replication in vitro: clinical evaluation and molecular characterization of a cold-passaged, attenuated RSV subgroup B mutant. Proc Natl Acad Sci USA 94:13961–13966
62. Kahn J, Schnell MJ, Buonocore L et al (1999) Recombinant vesicular stomatitis virus expressing respiratory syncytial virus (RSV) glycoproteins: RSV fusion protein can mediate infection and cell fusion. Virology 254:81–91
63. Feldman SA, Audet S, Beeler JA (2000) The fusion glycoprotein of human respiratory syncytial virus facilitates virus attachment and infectivity *via* an interaction with cellular heparan sulfate. J Virol 74:6442–6447

64. Techaarpornkul S, Barretto N, Peeples ME (2001) Functional analysis of recombinant respiratory syncytial virus deletion mutants lacking the small hydrophobic and/or attachment glycoprotein gene. J Virol 75:6825–6834
65. González-Reyes L, Ruiz-Argüello MB, García-Barreno B et al (2001) Cleavage of the human respiratory syncytial virus fusion protein at two distinct sites is required for activation of membrane fusion. Proc Natl Acad Sci USA 98:9859–9864
66. Zimmer G, Budz L, Herrler G (2001) Proteolytic activation of respiratory syncytial virus fusion protein. Cleavage at two furin consensus sequences. J Biol Chem 276:31642–31650
67. Behera AK, Matsuse H, Kumar M et al (2001) Blocking intercellular adhesion molecule-1 on human epithelial cells decreases respiratory syncytial virus infection. Biochem Biophys Res Commun 280:188–195
68. Tayyari F, Marchant D, Moraes TJ et al (2011) Identification of nucleolin as a cellular receptor for human respiratory syncytial virus. Nat Med 17:1132–1135
69. Fuentes S, Tran KC, Luthra P et al (2007) Function of the respiratory syncytial virus small hydrophobic protein. J Virol 81:8361–8366
70. Cowton VM, McGivern DR, Fearns R (2006) Unravelling the complexities of respiratory syncytial virus RNA synthesis. J Gen Virol 87:1805–1821
71. Noton SL, Cowton VM, Zack CR et al (2010) Evidence that the polymerase of respiratory syncytial virus initiates RNA replication in a nontemplated fashion. Proc Natl Acad Sci USA 107:10226–10231
72. Green N, Ott RD, Isaacs RJ, Fang H (2008) Cell-based assays to identify inhibitors of viral disease. Exp Opin Drug Discov 3:671–676
73. Stockwell BR (2004) Exploring biology with small organic molecules. Nature 432:846–854
74. Daelemans D, Pauwels R, De Clercq E, Pannecouque C (2011) A time-of-addition approach to target identification of antiviral compounds. Nat Protoc 6:925–933
75. Mason SW, Lawetz C, Gaudette Y et al (2004) Polyadenylation-dependent screening assay for respiratory syncytial virus RNA transcriptase activity and identification of an inhibitor. Nucleic Acids Res 32:4758–4767
76. Liuzzi M, Mason SW, Cartier M et al (2005) Inhibitors of respiratory syncytial virus replication target cotranscriptional mRNA guanylylation by viral RNA-dependent RNA polymerase. J Virol 79:13105–13115
77. Sudo K, Miyazaki Y, Kojima N et al (2005) YM-53403, a unique anti-respiratory syncytial virus agent with a novel mechanism of action. Antiviral Res 65:125–131
78. Carter MC, Alber DG, Baxter RC et al (2006) 1,4-Benzodiazepines as inhibitors of respiratory syncytial virus. J Med Chem 49:2311–2319
79. Henderson EA, Alber DG, Baxter RC et al (2007) 1,4-Benzodiazepines as inhibitors of respiratory syncytial virus. The identification of a clinical candidate. J Med Chem 50:1685–1692
80. Chapman J, Abbott E, Alber DG et al (2007) RSV604, a novel inhibitor of respiratory syncytial virus replication. Antimicrob Agents Chemother 51:3346–3353
81. Dent J, Grieve S, Harland R et al (2005) Multiple-dose safety and pharmacokinetics of A-60444, a novel compound active against respiratory syncytial virus (RSV). In: 45th interscience conference on antimicrobial agents chemotherapy, Washington, DC, Dec 16–19, Abstract F-483
82. Kimura K, Mori S, Tomita K et al (2000) Antiviral activity of NMSO3 against respiratory syncytial virus infection in vitro and in vivo. Antiviral Res 47:41–51
83. Wyde PR, Moylett EH, Chetty SN et al (2004) Comparison of the inhibition of human metapneumovirus and respiratory syncytial virus by NMSO3 in tissue culture assays. Antiviral Res 63:51–59
84. Kimura K, Ishioka K, Hashimoto K et al (2004) Isolation and characterization of NMSO3-resistant mutants of respiratory syncytial virus. Antiviral Res 61:165–171
85. Nakamura M, Terada M, Kamada M et al (2003) Mechanistic effect of NMSO3 on replication of human immunodeficiency virus. Antivir Chem Chemother 14:171–176

86. Dubovi EJ, Geratz JD, Tidwell RR (1980) Inhibition of respiratory syncytial virus by bis(5-amidino-2-benzimidazolyl)methane. Virology 103:502–504
87. Dubovi EJ, Geratz JD, Shaver SR, Tidwell RR (1981) Inhibition of respiratory syncytial virus-host cell interactions by mono- and diamidines. Antimicrob Agents Chemother 19:649–656
88. Tidwell RR, Geratz JD, Dubovi EJ (1983) Aromatic amidines. Comparison of their ability to block respiratory syncytial virus induced cell fusion and to inhibit plasmin, urokinase, thrombin, and trypsin. J Med Chem 26:294–298
89. Dubovi EJ, Geratz JD, Tidwell RR (1983) Enhancement of respiratory syncytial virus-induced cytopathology by trypsin, thrombin, and plasmin. Infect Immun 40:351–358
90. Cianci C, Yu K-L, Combrink K et al (2004) Orally active fusion inhibitor of respiratory syncytial virus. Antimicrob Agents Chemother 48:413–422
91. Tidwell RR, Geratz J, Dieter C et al (1984) Suppression of respiratory syncytial virus infection in cotton rats by bis(5-amidino-2-benzimidazolyl)methane. Antimicrob Agents Chemother 26:591–593
92. Ding W, Mitsner B, Krishnamurthy G et al (1998) Novel and specific respiratory syncytial virus inhibitors that target virus fusion. J Med Chem 41:2671–2675
93. Wyde PR, Moore-Poveda DK, O'Hara B et al (1998) CL387626 exhibits marked and unusual antiviral activity against respiratory syncytial virus in tissue culture and in cotton rats. Antiviral Res 38:31–42
94. Aulabaugh A, Ding W, Ellestad GA et al (2000) Inhibition of respiratory syncytial virus by a new class of chemotherapeutic agents. Drugs Future 25:287–294
95. Gazumyan A, Mitsner B, Ellestad GA (2000) Novel anti-RSV dianionic dendrimer-like compounds: design, synthesis and biological evaluation. Curr Pharm Des 6:525–546
96. Nikitenko A, Raifeld Y, Mitsner B, Newman H (2005) Pyrimidine containing RSV fusion inhibitors. Bioorg Med Chem Lett 15:427–430
97. Nikitenko A, Raifeld YE, Wang TZ (2001) The discovery of RFI-641 as a potent and selective inhibitor of the respiratory syncytial virus. Bioorg Med Chem Lett 11:1041–1044
98. Razinkov V, Gazumyan A, Nikitenko A et al (2001) RFI-641 inhibits entry of respiratory syncytial virus via interactions with fusion protein. Chem Biol 8:645–659
99. Razinkov V, Huntley C, Ellestad G et al (2002) RSV entry inhibitors block F-protein mediated fusion with model membranes. Antiviral Res 55:189–200
100. Huntley CC, Weiss WJ, Gazumyan A et al (2002) RFI-641, a potent respiratory syncytial virus inhibitor. Antimicrob Agents Chemother 46:841–847
101. Weiss WJ, Wyde P, Prince G et al (2000) Efficacy of RFI-641, a novel fusion inhibitor, in animal models of RSV infection. In: 40th interscience conference on antimicrobial agents and chemotherapy, Abstract H-186
102. Weiss WJ, Murphy T, Lynch ME et al (2003) Inhalation efficacy of RFI-641 in an African green monkey model of RSV infection. J Med Primatol 32:82–88
103. McKimm-Breschkin J (2000) VP-14637 ViroPharma. Curr Opin Investig Drugs 1:425–427
104. Nitz TJ, Pevear DC (1999) Preparation of heterocyclyl-substituted methylidynetrisphenol derivatives and related compounds for treating or preventing pneumovirus infection and associated diseases. World Patent Application WO1999/38508 A1
105. Wyde PR, Laquerre S, Chetty SN et al (2005) Antiviral efficacy of VP14637 against respiratory syncytial virus in vitro and in cotton rats following delivery by small droplet aerosol. Antiviral Res 68:18–26
106. Cianci C, Meanwell N, Krystal M (2005) Antiviral activity and molecular mechanism of an orally active respiratory syncytial virus fusion inhibitor. J Antimicrob Chemother 55:289–292
107. Yu K-L, Zhang Y, Civiello RL et al (2003) Fundamental structure-activity relationships associated with a new structural class of respiratory syncytial virus inhibitor. Bioorg Med Chem Lett 13:2141–2144

108. Yu K-L, Zhang Y, Civiello RL et al (2004) Respiratory syncytial virus inhibitors. Part 2: benzimidazol-2-one derivatives. Bioorg Med Chem Lett 14:1133–1137
109. Yu K-L, Wang XA, Civiello RL et al (2006) Respiratory syncytial virus fusion inhibitors. Part 3: water-soluble benzimidazol-2-one derivatives with antiviral activity in vivo. Bioorg Med Chem Lett 16:1115–1122
110. Yu K-L, Sin N, Civiello RL et al (2007) Respiratory syncytial virus fusion inhibitors. Part 4: optimization for oral bioavailability. Bioorg Med Chem Lett 17:895–901
111. Wang XA, Cianci CW, Yu K-L et al (2007) Respiratory syncytial virus fusion inhibitors. Part 5: optimization of benzimidazole substitution patterns towards derivatives with improved activity. Bioorg Med Chem Lett 17:4592–4598
112. Combrink KD, Gulgeze HB, Thuring JW et al (2007) Respiratory syncytial virus fusion inhibitors. Part 6: an examination of the effect of structural variation of the benzimidazol-2-one heterocycle moiety. Bioorg Med Chem Lett 17:4784–4790
113. Sin N, Venables BL, Combrink KD et al (2009) Respiratory syncytial virus fusion inhibitors. Part 7: structure-activity relationships associated with a series of isatin oximes that demonstrate antiviral activity in vivo. Bioorg Med Chem Lett 19:4857–4862
114. Cianci C, Genovesi EV, Lamb L et al (2004) Oral efficacy of a respiratory syncytial virus inhibitor in rodent models of infection. Antimicrob Agents Chemother 48:2448–2454
115. Pagani F, Sparatore F (1965) Benzotriazolylalkyl benzimidazoles and their dialkylaminoalkyl derivatives. Boll Chim Farm 104:427–431
116. Paglietti G, Boido V, Sparatore F (1975) Dialkylaminoalkylbenzimidazoles of pharmacological interest IV. Il Farmaco Ed Sci 30:505–511
117. Tonelli M, Paglietti G, Boido V et al (2008) Antiviral activity of benzimidazole derivatives. I. Antiviral activity of 1-substituted-2-[(benzotriazol-1/2-yl)methyl]benzimidazoles. Chem Biodivers 5:2386–2401
118. Andries K, Moeremans M, Gevers T et al (2003) Substituted benzimidazoles with nanomolar activity against respiratory syncytial virus. Antiviral Res 60:209–219
119. Wyde PR, Chetty SN, Timmerman P et al (2003) Short duration aerosols of JNJ 2408068 (R170591) administered prophylactically or therapeutically protect cotton rats from experimental respiratory syncytial virus infection. Antiviral Res 60:221–231
120. Bonfanti J-F, Doublet F, Fortin J et al (2007) Selection of a respiratory syncytial virus fusion inhibitor clinical candidate. Improving the pharmacokinetic profile using the structure-property relationship. J Med Chem 50:4572–4584
121. Bonfanti JF, Meyer C, Doublet F et al (2008) Selection of a respiratory syncytial virus fusion inhibitor clinical candidate. 2. Discovery of a morpholinopropylaminobenzimidazole derivative (TMC353121). J Med Chem 51:875–896
122. Rouan M-C, Gevers T, Roymans D et al (2010) Pharmacokinetics-pharmacodynamics of a respiratory syncytial virus fusion inhibitor in the cotton rat model. Antimicrob Agents Chemother 54:4534–4539
123. Olszewska W, Ispas G, Schnoeller C et al (2011) Antiviral and lung protective activity of a novel RSV fusion inhibitor in a mouse model. Eur Respir J 38:401–408
124. Bond S, Sanford VA, Lambert JN et al (2005) Preparation of polycyclic agents for the treatment of respiratory syncytial virus infections. World Patent Application WO2005/061513 A1
125. Mitchell JP, Draffan AG, Sanford VA et al (2008) Polycyclic imidazole derivatives as antiviral agents and their preparation, pharmaceutical compositions and use in the treatment of RSV infections. World Patent Application WO2008/037011 A1
126. Mitchell JP, Pitt G, Draffan AG, Mayes PA, Andrau L, Anderson K (2011) Compounds for treating respiratory syncytial virus infections. World Patent Application WO2011/094823 A1
127. Information available at Biota's website http://www.biota.com.au/uploaded/154/1021724_171101uscorporatepresenta.pdf
128. Lundin A, Bergstroem T, Bendrioua L et al (2010) Two novel fusion inhibitors of human respiratory syncytial virus. Antiviral Res 88:317–332

129. Morton CJ, Cameron R, Lawrence LJ et al (2003) Structural characterization of respiratory syncytial virus fusion inhibitor escape mutants: homology model of the F protein and a syncytium formation assay. Virology 311:275–288
130. Douglas JL, Panis ML, Ho E et al (2003) Inhibition of respiratory syncytial virus fusion by the small molecule VP-14637 via specific interactions with F protein. J Virol 77:5054–5064
131. Douglas JL, Panis ML, Ho E et al (2005) Small molecules VP-14637 and JNJ-2408068 inhibit respiratory syncytial virus fusion by similar mechanisms. Antimicrob Agents Chemother 49:2460–2466
132. Dischino DD, Cianci CW, Civiello R et al (2003) Development of a photoaffinity label for respiratory syncytial virus inhibitors. J Label Compd Radiopharm 46:1105–1116
133. Cianci C, Langley DR, Dischino DD et al (2004) Targeting a binding pocket within the trimer-of-hairpins: small-molecule inhibition of viral fusion. Proc Natl Acad Sci USA 101:15046–15051
134. Roymans D, De Bondt HL, Arnoult E et al (2010) Binding of a potent small-molecule inhibitor of six-helix bundle formation requires interactions with both heptad-repeats of the RSV fusion protein. Proc Natl Acad Sci USA 107:308–313
135. Donald JE, Zhang Y, Fiorin G et al (2011) Transmembrane orientation and possible role of the fusogenic peptide from parainfluenza virus 5 (PIV5) in promoting fusion. Proc Natl Acad Sci USA 108:3958–3963
136. Markosyan RM, Cohen FS, Melikyan GB (2003) HIV-1 envelope proteins complete their folding into six-helix bundles immediately after fusion pore formation. Mol Biol Cell 14:926–938
137. Markosyan RM, Leung MY, Cohen FS (2009) The six-helix bundle of human immunodeficiency virus env controls pore formation and enlargement and is initiated at residues proximal to the hairpin turn. J Virol 83:10048–10057
138. Lee KK (2010) Architecture of a nascent viral fusion pore. EMBO J 29:1299–1311
139. Imai M, Mizuno T, Kawasaki K (2006) Membrane fusion by single influenza hemagglutinin trimers. Kinetic evidence from image analysis of hemagglutinin-reconstituted vesicles. J Biol Chem 281:12729–12735
140. Kemble GW, Danieli T, White JM (1994) Lipid-anchored influenza hemagglutinin promotes hemifusion, not complete fusion. Cell 76:383–391
141. Steinhauer DA, Wharton SA, Skehel JJ, Wiley DC (1995) Studies of the membrane fusion activities of fusion peptide mutants of influenza virus hemagglutinin. J Virol 69:6643–6651
142. Qiao H, Armstrong RT, Melikyan GB et al (1999) A specific point mutant at position 1 of the influenza hemagglutinin fusion peptide displays a hemifusion phenotype. Mol Biol Cell 10:2759–2769
143. Dobay MP, Dobay A, Bantang J, Mendoza E (2011) How many trimers? Modeling influenza virus fusion yields a minimum aggregate size of six trimers, there of which are fusogenic. Mol Biosyst 7:2741–2749

Top Med Chem 8: 197–230
DOI: 10.1007/978-3-642-28965-1_6

Rational Design Strategies for Developing Synthetic Inhibitors of Helical Protein Interfaces

Andrew B. Mahon, Stephen E. Miller, Stephen T. Joy, and Paramjit S. Arora

Contents

Abstract Cellular function depends on highly specific interactions between biomolecules (proteins, RNA, DNA, and carbohydrates). A basic limitation of drug development is the inability of traditional "small-molecule" pharmaceuticals to specifically target large protein interfaces, many of which are desirable drug targets. α-Helices, ubiquitous elements of protein structures, play fundamental roles in many protein-protein interactions. Stable mimics of α-helices that can predictably disrupt these interactions would be invaluable as tools in molecular biology, and as leads in drug discovery. The past decade has seen exciting progress in the molecular design of these protein domain mimetics and their remarkable potential to inhibit challenging interactions. Key challenges in the field include identification of suitable targets and bioavailability of medium-sized molecules, which do not conform to empirical rules followed in traditional drug design. Stabilized α-helices bypass some of the strict limitations that have been

A.B. Mahon • S.E. Miller • S.T. Joy • P.S. Arora (✉)
Department of Chemistry, New York University, New York, NY 10003, USA
e-mail: arora@nyu.edu

placed on drug discovery. When designing potential drug candidates, medicinal chemists often adhere to the Lipinski rules, which stipulate that the molecular mass of a drug should not exceed 500 Da. Recent findings suggest that large synthetic α-helices can traffic into the cell and efficiently compete with cellular protein-protein interactions, contrary to predictions based on the Lipinski rules. Although these molecules have undoubtedly proven their value as probes for decoding biological complexity, the next big question is whether these molecules can become therapeutics. This chapter discusses the properties of protein-protein interactions, emerging rules for identifying protein targets and design criteria guiding construction of helix mimetics.

Keywords Helix mimetics • Inhibitors • Protein-protein interactions

1 Introduction

Protein-protein interactions (PPIs) are essential for the control of cellular processes, and the misregulation of these interactions is often implicated in disease states [1]. Despite their fundamental role in cellular function, PPIs are not generally considered attractive targets for drug design because of their large, and often flat, contact surfaces [2–4]. This is well illustrated by comparing the small number (324 in 2006) of proteins targeted by FDA approved drugs relative to the large number of potential disease-related targets in the human genome [5, 6].

In recent years, however, a number of groups have reported the successful inhibition of PPIs, once considered "undruggable," using low molecular weight synthetic molecules [2, 7, 8]. For example, numerous inhibitors of the p53/HDM2 interaction have been developed, of which MI-219 and nutlin-3 are the most well known [9–12]. BH3/Bcl-2 interactions have also been targeted using small molecule ligands, e.g., A-385358 and ABT-737 [13–16]. Other well-known small-molecule PPI targets include the human papillomavirus E1-E2 interaction [17], Smac/IAP interaction [18–21], gp41 assembly and reorganization [22], and Myc/Max dimerization inhibitors (Fig. 1) [23, 24].

A promising rational design approach for the discovery of PPI inhibitors is centered on the role of protein secondary structures at protein interfaces. Analysis suggests that although protein interfaces are large, often a small subset of the residues contributes significantly to the free energy of binding [25–28]. These "hot spot" residues are commonly located on secondary structures in proteins [4, 29, 30]. It has been demonstrated that synthetic molecules that reproduce key elements of energetically significant protein secondary structures can inhibit chosen interfaces with high affinity and specificity [31–42].

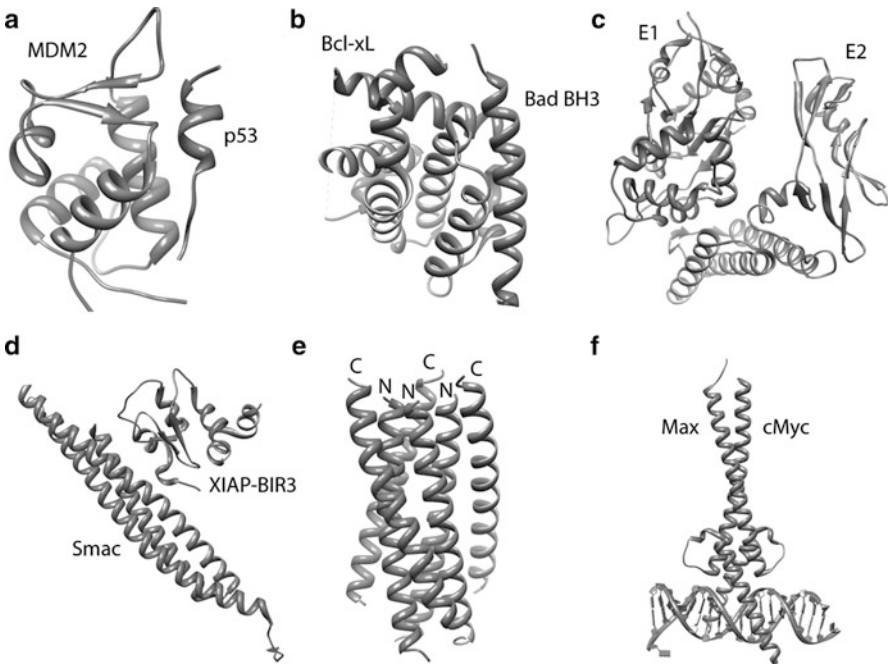

Fig. 1 X-ray crystal structure representations of well-known small molecule PPI targets. (**a**) p53 activation domain bound to MDM2 (PDB code: 1ycr); (**b**) Bad BH3 domain bound to Bcl-xL (PDB code: 2bzw); (**c**) HPV18 E2 activation domain bound to the helicase domain of E1 (PDB code: 1tue); (**d**) Smac bound to the XIAP-BIR3 domain (PDB code: 1g73); (**e**) HIV-1 gp41 core six-helix bundle with N and C regions labelled (PDB code: 1i5x); (**f**) The c-Myc-Max DNA recognition complex (PDB code: 1nkp)

2 Identification of Inhibitable Protein Complexes

The preliminary successes in targeting protein-protein interactions have given rise to an important question: *What types of PPIs are "inhibitable?"* A number of studies have focused on predicting the physicochemical properties of small-molecule protein-protein interaction inhibitors, [43–49] and methods for gauging the "inhibitability" of protein complexes have been proposed [46]. Jochim and Arora described a computational alanine scanning method to identify helical interfaces in the Protein Data Bank (PDB) [50].

Complexes that feature α-helices at interfaces were studied because α-helices constitute the largest class of protein secondary structure and mediate many protein interactions [30, 51]. Helices located within the protein core are vital for the overall stability of protein tertiary structure, whereas exposed α-helices on protein surfaces constitute central bioactive regions for the recognition of numerous proteins, DNAs, and RNAs. Importantly, helix mimetics have emerged as a highly effective class of PPI inhibitors [32, 36, 44, 52–55].

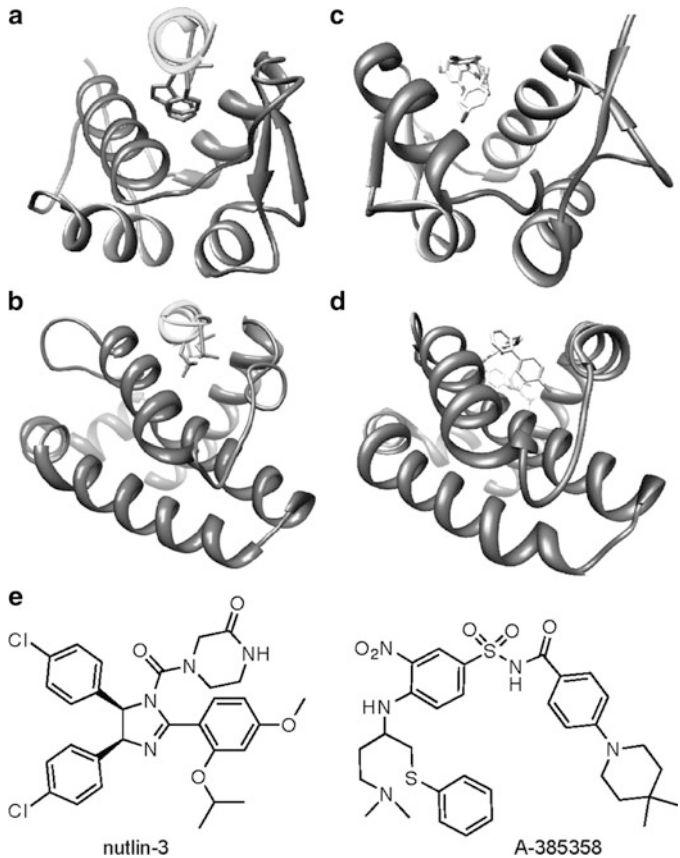

Fig. 2 (**a**) The p53/MDM2 interaction (PDB code: 1ycr). A helix in the p53 activation domain resides in a deep hydrophobic groove. (**b**) The proapoptotic protein partner Bak bound to the antiapoptotic protein Bcl-xL (PDB code: 1BXL). (**c**) Nutlin-3 binds to MDM2 in the same hydrophobic groove occupied by the p53 helix (PDB code: 1rv1). (**d**) ABT-385358 targets Bcl-xL at the site of its proapoptotic binding partners (PDB code: 2o22). (**e**) The structures of nutlin-3 and A-385358 (Reprinted with permission from Jochim and Arora [50], Copyright (2010) American Chemical Society)

Alanine scanning mutagenesis offers a powerful approach for identifying hot spot residues [56]. For example, in the well-studied p53/HDM2 interaction, three residues (F19, W23, and L26) from a helix in the p53 activation domain reside in a deep hydrophobic groove (Fig. 2a) [12]. Mutation of any of these residues to alanine leads to a significant (>2 kcal/mol) decrease in the stability of the resulting complex [57]. Similar alanine scanning results are obtained with proapoptotic partners of the antiapoptotic protein Bcl-xL (Fig. 2b) [14]. The complex between transcription factor p53 and its regulator HDM2 is inhibited by nutlins (Fig. 2c), [10, 58] and there are highly potent small-molecule antagonists, including ABT-737 and A-385358, of the interactions between Bcl-xL and BH3 domains (Fig. 2d) [15, 59].

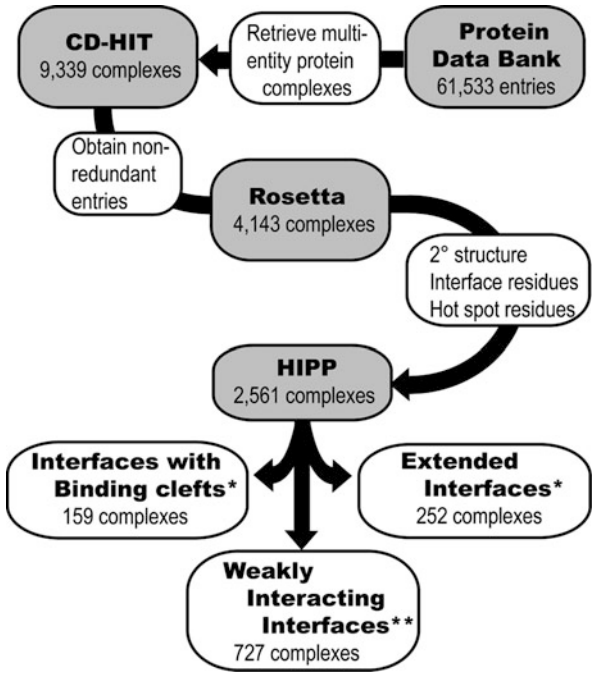

Fig. 3 Evaluation of structures from the Protein Data Bank to identify and assess helical interfaces in protein–protein (HIPP) interactions. The helical interfaces were segregated based on binding interfaces and computational alanine scanning mutagenesis analysis. *$\Delta\Delta G_{avg} \geq 2$ kcal/mol; **$\Delta\Delta G_{avg} = 1$–2 kcal/mol (Reprinted with permission from Jochim and Arora [50], Copyright (2010) American Chemical Society)

The characteristics of these interactions indicate that they can be inhibited with nanomolar affinity by small molecules because the critical residues lie within a small radius of each other on one of the partner proteins, allowing their arrangement on a low molecular weight scaffold. For instance, the two chlorobenzene groups in nutlin-3 span 6 Å (Fig. 2e), and occupy the binding pockets of the key tryptophan and leucine residues from the p53 helix [10]. Similarly, A-385358 targets the same key pockets on Bcl-xL as the helical BH3 domains [60]. Jochim and Arora used these examples of successfully inhibited PPIs as a guide to identify PPIs as likely targets for small molecule inhibitors from the PDB [61].

Initially, a full set of α-helical interfaces in the PDB was identified (Fig. 3). The PDB (version 08/04/2009) was queried for structures containing more than one protein entity [51]. This query extracted 9,339 complexes. Complexes were clustered according to sequence similarity of all protein chains in each complex using the CD-HIT [62] sequence alignment program at a 95% similarity threshold. This yielded a dataset of 4,143 unique protein complexes. For each <4 Å resolution structure, potential chain partners belonging to separate molecules as specified in the PDB file were extracted. Identification of secondary structure, interfacial

residues, and hot spot residues was accomplished using the Rosetta suite of programs [63–65]. Rosetta determines secondary structure by calculating the ϕ and φ angles of the protein backbone. Helical segments were defined as those that contain at least four contiguous residues with ϕ and φ angles characteristic of an α-helix, or the closely related 3_{10}-helix [51]. An interfacial residue was defined as a residue that has at least one atom within a 5 Å radius of an atom belonging to a binding partner in the protein complex. Hot spot residues were predicted using a computational alanine scan [64, 65]. Hot spot residues were defined as residues that upon mutation to alanine are predicted to decrease the binding energy by a threshold value $\Delta\Delta G_{bind} \geq 1.0$ kcal/mol, as measured in Rosetta energy units. This method identified 2,561 PDB entries possessing helix interfaces in protein-protein (HIPP) interactions and suggests that roughly 62% of the protein complexes in the PDB feature helical interfaces.

Analysis of the energetic contributions and spatial arrangement of the hot spot residues in the helix of p53 in the p53/HDM2 interaction and the BH3 helix of Bak in the Bcl-xL/Bak interaction gave insight into the reason that HDM2 and Bcl-xL are tractable targets for inhibition by small molecules. For both complexes, the calculated average $\Delta\Delta G_{bind}$ of the hot spot residues in the helix of the protein partner (p53 in the p53/HDM2 complex and Bak in the Bcl-xL/Bak complex) is >2 kcal/mol and the radius between the hot spot residues in the helix of the protein partners was on the order of 7 Å. Using these characteristics as a guide, HIPP interactions were screened for interactions that possess the same features. These interactions partition into three broad categories: (1) receptors that contain a *cleft* for helix binding (Fig. 4a), as in the p53/HDM2 complex, where at least two nearby residues contribute strongly to binding; (2) *extended* interfaces that require multiple contacts from two to five turn helices featuring two or more residues that contribute strongly to binding (Fig. 4b); and (3) receptors with clefts and extended interfaces characterized by weaker interactions [66]. For the purposes of the study, hot spot residues were defined as strong or weak contributors based on the change in free energy ($\Delta\Delta G_{avg}$) when these residues on a given helix are mutated to alanine, with a $\Delta\Delta G_{avg}$ cutoff of 2 kcal/mol. Receptors with clefts are targeted by helices with two or more hot spot residues within a 7 Å radius, while the extended interfaces category features a distribution of hot spot residues over a larger distance of 7–30 Å (Fig. 3). Category 2 consists of interfaces where the helical segment spans 20 residues or roughly five helical turns; longer sequences were placed in category 3. Calculations that determined the proportion of hot spots residing on the helix versus the rest of the chain were used to determine if a simple mimic of an interfacial helix could inhibit a large interface. It should be noted that analysis of PDB structures is complicated by the fact that a number of the complexes in the PDB do not have full-length proteins, and in fact a number of the relevant complexes only consist of a truncated helical domain.

From the above described analysis, there were 159 complexes predicted to be targets for small molecules and another 252 interfaces that could potentially be inhibited by helix mimetics. The remaining complexes that did not meet the criteria

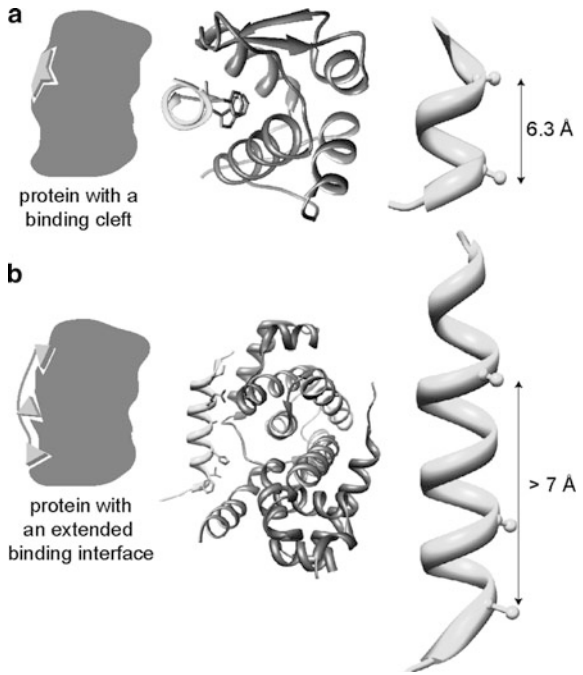

Fig. 4 Helical interfaces may be divided between those that feature clefts for binding (**a**) and those with extended interfaces (**b**). The p53/MDM2 (PDB code: 1ycr) (**a**) and cyclin-dependent kinase6/D-type viral cyclin (PDB code: 1g3n) (**b**) complexes are representative examples of binding cleft and extended interfaces, respectively. The distance between flanking hot spot residues in the helix of the protein partner of a binding cleft target spans a radius of 7 Å or less (**a**) and greater than 7 Å but less than 30 Å (**b**) for an extended interface target (Reprinted with permission from Jochim and Arora [50], Copyright (2010) American Chemical Society)

of the first two categories featured weaker interactions between the candidate helix and the protein receptor. Full lists of complexes that fall into each of the three aforementioned categories, along with the sequence information for each PDB entry have been reported [50]. This analysis suggests that the current PDB has roughly 400 targets for helix mimetics or small molecules that reproduce the organization of the key functionality at the interfaces. These predictions could substantially enhance current numbers of druggable targets.

Helical interfaces are involved in a broad range of functions from enzymatic activity to gene regulation (Fig. 5) [50, 51, 67]. Interfaces with binding clefts are involved in a comparable range of functions as extended interfaces. The utility of classifying PPIs according to the inhibitability criteria outlined above is demonstrated by the identification of hypoxia-inducible genes and Ras signaling as tractable targets for synthetic α-helices. Subsequently, both pathways were successfully inhibited with cell permeable α-helix mimetics [54, 68].

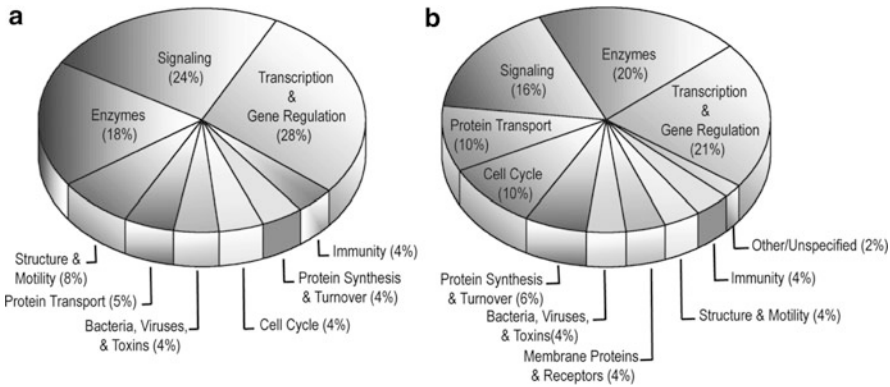

Fig. 5 Classification of (**a**) helical interfaces with binding clefts and (**b**) extended helical interfaces by function (Reprinted with permission from Jochim and Arora [50], Copyright (2010) American Chemical Society)

3 Composition and Topologies of Helical Protein Interfaces

In this section, the composition and characteristics of helical domains identified to be critical for protein complex formation is discussed. This analysis allows prediction of the type of helix mimetic that is best suited for the type of helical interface.

Three general strategies have been used to develop helix mimetics: helix stabilization, helical foldamers, and helical surface mimetics (Fig. 13) [52, 69]. Helix stabilizing methods based on side-chain crosslinks [38, 70] and hydrogen-bond surrogates [71] preorganize amino acid residues and initiate helix formation. Helical foldamers, [31, 72] such as β-peptides [73–75] and peptoids, [76] are composed of amino acid analogs and are capable of adopting conformations similar to those found in natural proteins. Helical surface mimetics utilize conformationally restricted scaffolds with attached functional groups that resemble the i, $i + 3$, $i + 4$, and $i + 7$ pattern of side-chain positioning on an α-helix (Fig. 6a). Surface mimetics typically impart functionality from one face of the helix, [77] while stabilized peptide helices and foldamers are able to reproduce functionality present on multiple faces of the target helix. A key advantage of helix surface mimicry is that it affords low molecular weight compounds as modulators of protein interactions [78–83].

A study by Bullock et al. revealed that roughly 60% of helical interfaces in the HIPP dataset feature helices with hot spot residues on one face of the helix (Fig. 6b, d), a third of the complexes utilize helices with hot spots on two faces (Fig. 6b, e), and roughly 10% require all three faces for interaction with the target protein partner (Fig. 6b, f). The full list of PPIs that correspond to each category is published elsewhere [67]. Overall percent occurrences of hot spot residues at the first 12 positions in interfacial helices are depicted in Fig. 6c. The results of the study indicate that helix surface mimetics may prove to be a highly effective class of synthetic

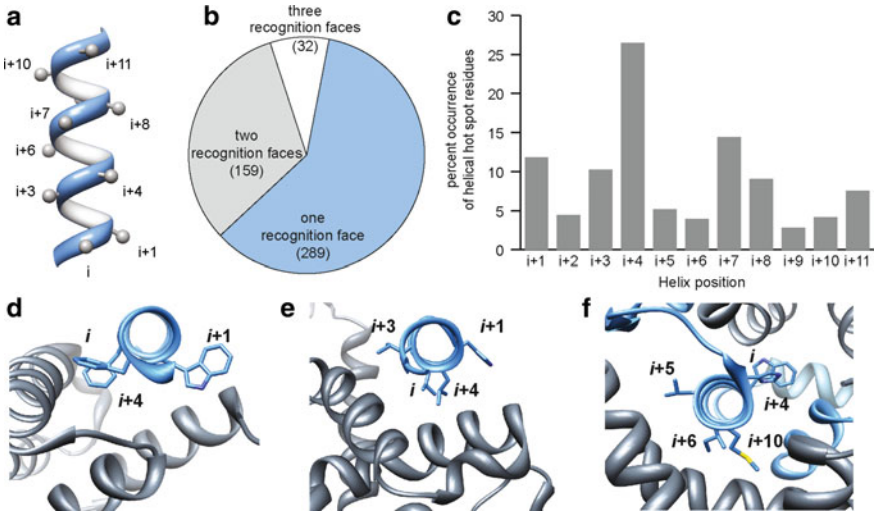

Fig. 6 Energetic contributions of residues on different faces of interfacial helices. (**a**) Positioning of side-chain residues on a canonical α-helix, (**b**) percent occurrence of hot spot residues on one, two, or three helical faces (total number helices in each category shown in parentheses), (**c**) percent occurrence of hot spot residues as a function of helix position, (**d–f**) examples of protein complexes with hot spot residues on one face, two faces, and three faces (PDB codes: 1xl3, 1xiu, and 1or7) (Adapted with permission from Bullock et al. [67], Copyright (2011) American Chemical Society)

inhibitors; however, a significant fraction of PPIs will require mimetics that array protein-like functionality on multiple faces. Figure 7 shows the targeting potential of various helix mimetics. Terphenyls, the prototypical helix surface mimetics, imitate one helical face, side-chain crosslinked helices can reproduce functionality of up to two faces; although the linker itself may interact with the protein pocket. Hydrogen bond surrogate (HBS) helices and β-peptide foldamers potentially afford complete replicas of functionality present on protein α-helices. The functions of protein complexes featuring PPIs with hot spots on different numbers of helical faces as defined in the PDB is shown in Fig. 8. Some interactions could fall into more than one functional category. The four largest categories for each type are gene regulation, enzymatic function, cell cycle, and signaling.

The percentage of each helical residue that contributes strongly to binding is represented in Fig. 9. Glycine and proline residues were exempted from alanine scanning since substitutions at these positions may cause a conformational change in the protein backbone. Leucine dominates the interface region (Fig. 9a), which is not surprising as leucine is also the most prevalent residue in proteins in general. When normalized for natural abundance, [84] aromatic residues and arginine, along with leucine, are overrepresented as hot spots at helical interfaces in comparison to polar residues (Fig. 9c). These results correspond with previous studies of the types

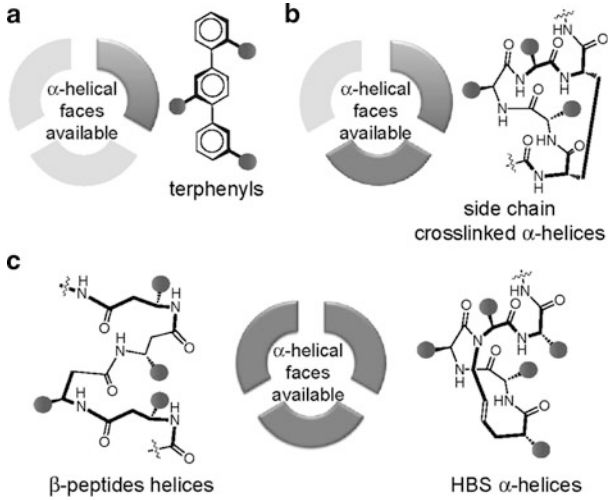

Fig. 7 Potential of various helix mimetics to reproduce functionality of one, two, or all three faces of protein α-helices (Reprinted with permission from Bullock et al. [67], Copyright (2011) American Chemical Society)

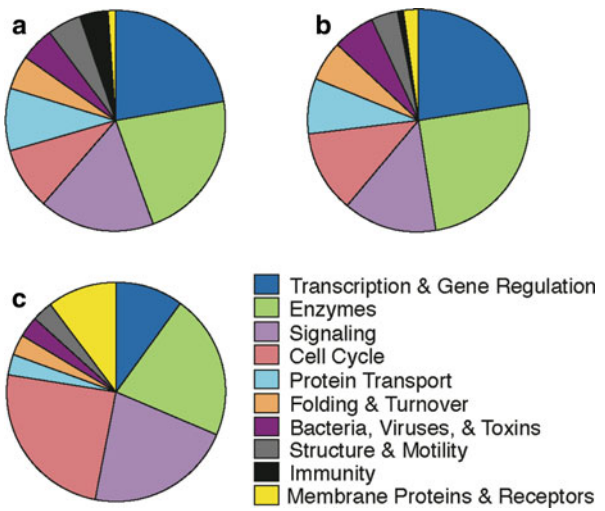

Fig. 8 Functions associated with protein-protein interactions featuring hot spots on (**a**) one helical face, (**b**) two helical faces, and (**c**) three helical faces (Reprinted with permission from Bullock et al. [67], Copyright (2011) American Chemical Society)

of amino acids appearing as hot spot residues in protein interfaces (Fig. 10); [25, 29, 30, 85, 86] although the dataset studied by Bullock et al. is considerably larger than those previously examined. It is expected that the data represented in Fig. 9 will help in guiding the design of helix mimetic libraries [79, 82, 83, 87–89].

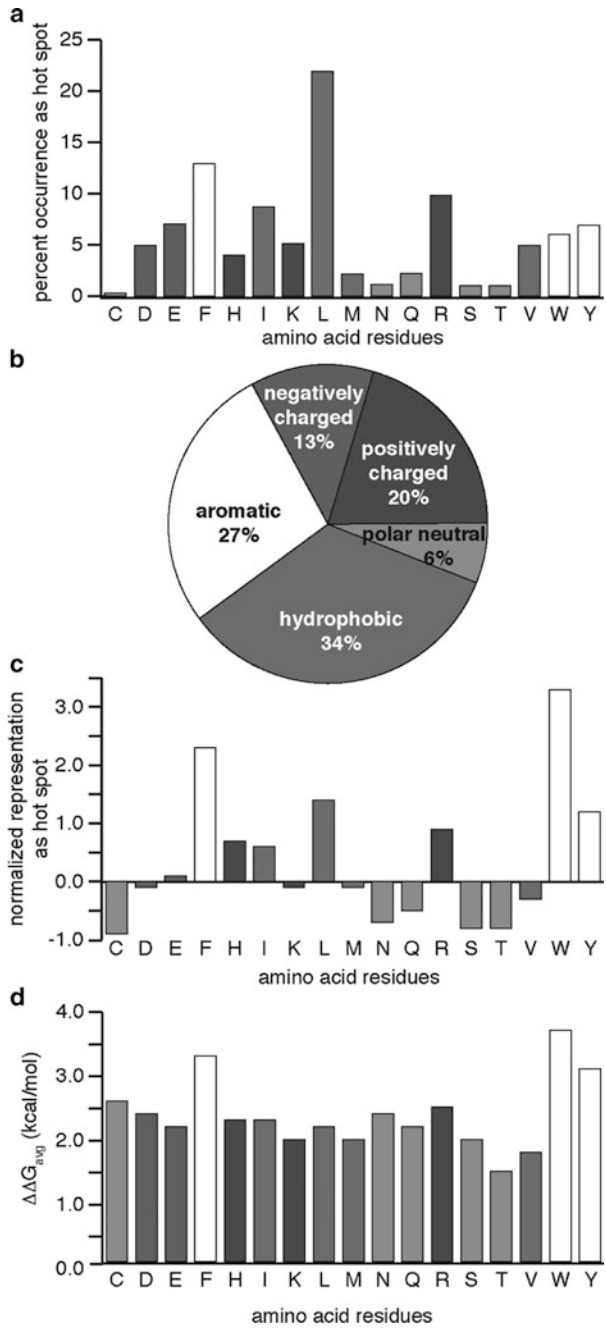

Fig. 9 (**a**) Percent occurrence of hot spot amino acids in helix-mediated protein interfaces, (**b**) percent occurrence of hot spot residues classified into similar groups, (**c**) representation of hot spot amino acids normalized to natural abundance of amino acids in proteins, and (**d**) average predicted decrease in binding energy of helical interfaces upon mutation of hot spot residues to alanine (Reprinted with permission from Bullock et al. [67], Copyright (2011) American Chemical Society)

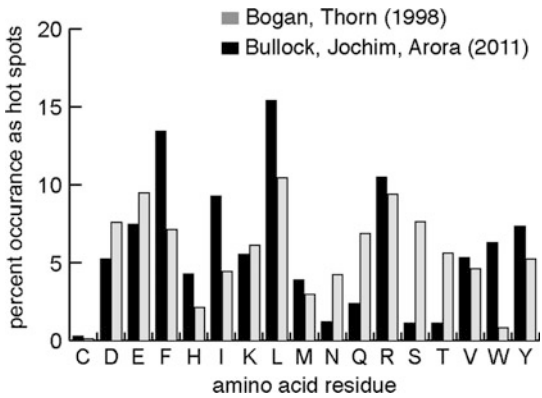

Fig. 10 Comparison of amino acid preferences in hot spots from Bullock et al. [67] and Bogan and Thorn [25] (Reprinted with permission from Bullock et al. [67], Copyright (2011) American Chemical Society)

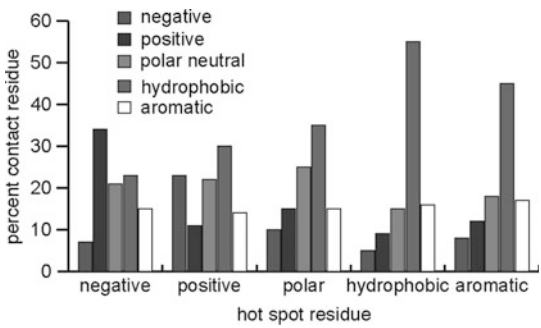

Fig. 11 Classification of contact residues on partner proteins. Residues on the partner protein that are within 5 Å of the helical hot spot residue were analyzed within Rosetta (Reprinted with permission from Bullock et al. [67], Copyright (2011) American Chemical Society)

Hydrophobic and aromatic residues constitute a majority of hot spot residues; however, polar and charged residues are also significant contributors at interfaces (Fig. 9b) [90]. This analysis supports the common perception that PPIs are generally hydrophobic but also feature key polar interactions that appreciably influence the binding energy landscape [28]. This view is further supported by the evaluation of residues on the partner protein that are within 5 Å of the helical hot spot residue (Fig. 11). Not surprisingly a majority of residues that are within the specified radius of a hydrophobic residue are themselves hydrophobic, which is consistent with the

hypothesis that the burial of a hot spot in a hydrophobic environment is a major stabilizing influence [25]. In this respect, it is interesting to note that, on average, mutations of aromatic residues to alanine are more destabilizing than substitution of other interfacial residues, with the effect being dependent on the size of the aromatic ring (Fig. 9d).

Helical PPIs have so far been successfully targeted by a diverse array of mimetics [32, 34, 36, 38, 41, 68]. Preliminary success in this field validates helix design concepts from multiple research groups and provides an impetus for designing inhibitors of interactions previously considered to be intractable to inhibition by synthetic ligands. A key motivation for research in our laboratory is to bridge the significant chasm between the elegant design of helix mimetics and their sporadic use in biology. Analysis of the HIPP dataset discussed above provides a list of targets to be considered for different classes of helix mimetics based on the number of contact surfaces the target helix utilizes for interactions with partner proteins.

4 Strategies for Mimicking the α-Helical Conformation

α-Helices constitute the largest class of protein secondary structures, and play a major role in mediating PPIs [29, 91]. Significantly, the average length of helical domains in proteins is rather small, spanning two to three helical turns (or 8–12 residues) [51, 92]. Figure 12 shows a selection of complexes in which a short α-helical domain targets a biomolecule. These complexes and the hot spot analyses discussed above suggest that it may be possible to develop short helices that participate in selective interactions with biomolecules. However, peptides rarely retain their conformation once excised from the parent protein; much of their ability to specifically bind their intended targets is lost because they adopt an ensemble of shapes rather than the biologically relevant one. The proteolytic instability of peptides is an additional factor that limits their utility as reagents in molecular biology and drug discovery. In principle, stabilization of peptides in helical structures should not only reduce their conformational heterogeneity, but also substantially increase their resistance to proteases as these enzymes typically bind their substrates in an extended conformation [93]. The proteolytic stability of a helix should thus be directly proportional to its conformational stability. The chemical biology community has focused much of its attention on studying different approaches to either stabilize the α-helical conformation in peptides or mimic this domain with nonnatural scaffolds [94].

Figure 13 illustrates the different approaches that have been adopted either to stabilize or mimic an α-helix, with the overall aim of endowing peptidic and nonpeptidic oligomers with conformational rigidity, proteolytic stability, and the desired array of protein-like functionality. As stated in Sect. 3, these approaches can be divided into three general categories: helix stabilization, helical foldamers, and helical surface mimetics. Below, each helix mimetic strategy is described with specific examples illustrating the potential of these methods to target PPIs.

Fig. 12 The α-helix is a ubiquitous element in biomolecular recognition. (**a**) MATa1/MATα2-3A heterodimer bound to DNA (PDB code:1LE8), (**b**) complex of the WH2 domain of WAVE with Actin-DNAse I (PDB code: 2A40), (**c**) endothelial nitric oxide synthase peptide bound to calmodulin (PDB code: 1NIW)

4.1 Side-Chain Crosslinked α-Helices

The classical strategy to stabilize the α-helical conformation in peptides employs covalent bonds between the i and $i + 4$ or i and $i + 7$ side-chain groups (Fig. 14). Earliest side-chain crosslinks utilized lactam, disulfide, and metal-mediated bridges [95–104]. Helices containing lactam-bridges and disulfide links have been shown to successfully target their intended receptors [100, 105–109]. While lactam crosslinks can improve the proteolytic stability of peptide mimetics, disulfide bonds are less desirable because they are chemically labile.

Side-chain crosslinked helices obtained from an olefin metathesis reaction were first described by Blackwell and Grubbs [110], and more recently by Schafmeister and Verdine [70]. These researchers carefully examined linker length and stereochemistry to arrive at the optimal design. The hydrocarbon-stapled helices were subsequently shown to target antiapoptotic proteins HDM2 and Bcl-2 BH3 domain proteins in cell culture and animal models [37, 111]. The hydrocarbon linker was employed because it was expected to be chemically more stable than linkers built from amide or disulfide bonds; but, significantly, these hydrocarbon-stapled helices have also shown an increased tendency to penetrate cell membranes, possibly due to the lipophilic nature of the linker. Debnath and

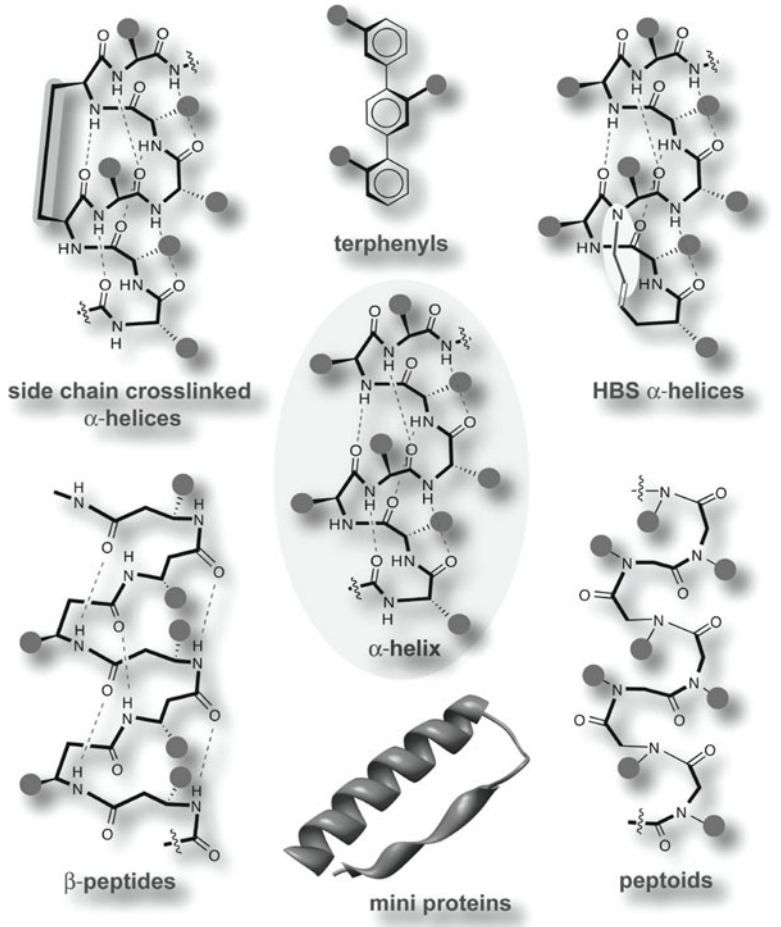

Fig. 13 Stabilized helices and nonnatural helix mimetics: several strategies that stabilize the α-helical conformation in peptides or mimic this domain with nonnatural scaffolds have been described. Recent advances include β-peptide helices, terphenyl helix-mimetics, mini-proteins, peptoid helices, side-chain crosslinked α-helices, and the hydrogen bond surrogate (HBS) derived α-helices. *Circles* represent amino acid side-chain functionality (Reprinted from Henchey et al. [52], Copyright (2008) with permission from Elsevier)

coworkers also discovered that the hydrocarbon-stapled helices can penetrate cells and target HIV-1 capsid assembly [112].

The lactam-bridged and hydrocarbon-stapled helices feature flexible crosslinks. Entropic considerations would suggest that rigid linkers might afford more stable helices. Two groups have recently studied the effect of linker flexibility on helix stability. Woolley and coworkers found that a rigid aromatic linker that matches the distance between the i and $i + 11$ side-chains provides much greater stability

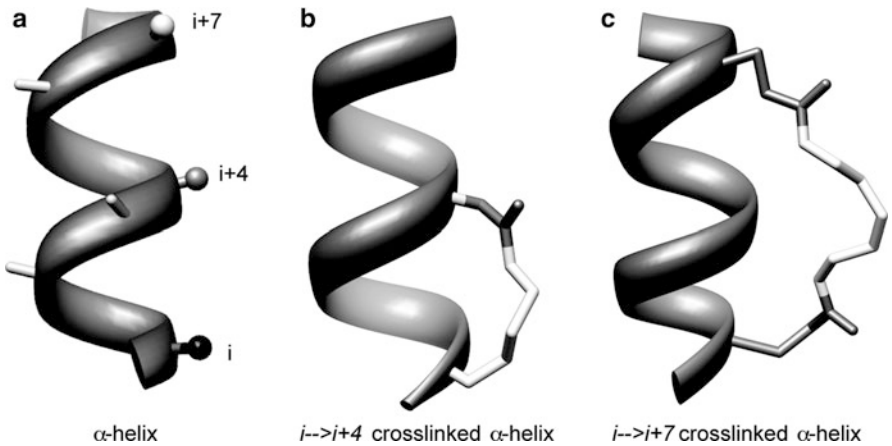

Fig. 14 Side-chain crosslinked α-helical peptides with lactam bridges. (**a**) Depicts the i, $i + 4$, and $i + 7$ residues with side-chains all on the same face of the helix; (**b**) and (**c**) are solution structures $i \rightarrow i + 4$ (BMRB accession number: 3z0q0z3) and $i \rightarrow i + 7$ (PDB code: 1gzl) side-chain cross-links respectively

than a flexible linker [113]. Fujimoto et al. performed a detailed examination of various flexible and rigid linkers, and crosslinking positions on the helix [114]. They hypothesized and demonstrated that rigid linkers that are shorter than the target helix pitch lead to more stable helices. These interesting findings may lead to reevaluation of linker lengths in side-chain crosslinked helices.

Of the many side-chain crosslinking strategies developed for producing α-helical PPI inhibitors, hydrocarbon stapling and lactam bridges have proven to be the most promising. Examples below illustrate the PPI-targeting potential of these bridged peptides.

4.1.1 Inhibition of Respiratory Syncytial Virus (RSV) Cell Fusion

The trimeric RSV F glycoprotein is found on the virion surface, with a prefusion configuration [115]. Upon host cell receptor engagement, conformational reorganization results in a postfusion six α-helix bundle that consists of three heptad repeat N-terminal and three heptad repeat C-terminal domains. Formation of the six α-helix bundle enables virus-cell membrane fusion (Fig. 15). Shepherd et al. designed a doubly stitched lactam-bridged peptide based on a region of the C-terminal heptad repeat domain. This constrained α-helical peptide is a potent inhibitor of RSV fusion, with an IC_{50} of 190 pM [38, 109].

4.1.2 Inhibition of Bcl-2 Family Proteins

Bcl-2 is a member of a family of proteins essential for the control of apoptosis. Overexpression of Bcl-2 prosurvival proteins is consistently associated with

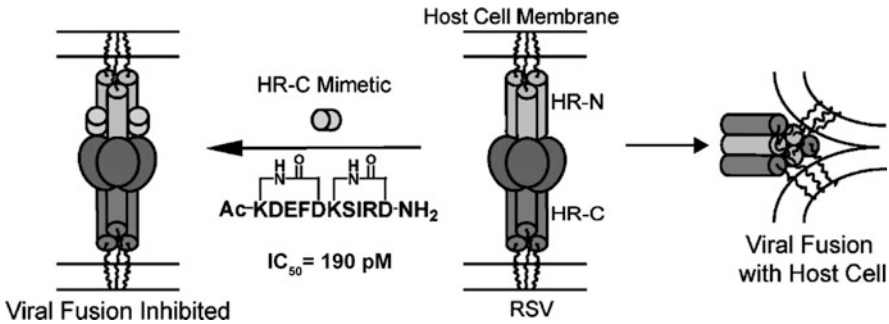

Fig. 15 Inhibition of RSV F glycoprotein six-helix bundle formation to prevent virus-cell fusion. A heptad repeat (HR) C terminal domain lactam-bridged α-helix mimetic binds to the HR N terminal domain, preventing conformation change (Reprinted with permission from Shepherd et al. [109], Copyright (2006) American Chemical Society)

malignant disease [116]. Bcl-2 family proteins are characterized by the presence of up to four Bcl homology (BH) domains—all of which include α-helical segments. Antiapoptotic proteins (e.g. Bcl-2 and Bcl-xL) display sequence conservation in all BH domains. Proapoptotic proteins are divided into multidomain members (e.g., Bax and Bak) and BH3 only members (e.g., Bid and Bad) that only display sequence similarity in the BH3 α-helical domain. The amphipathic BH3 α-helical domain of proapoptotic family members is a required death domain that binds the hydrophobic groove formed by the juxtaposition of BH1, BH2, and BH3 domains of antiapoptotic multidomain members. Due to their role in triggering mitochondrial apoptosis, a number of stapled peptide α-helix mimetics based on BH3 domains have been developed [117–120]. The crystal structure of an Mcl-1 BH3 domain stapled peptide in complex with Mcl-1 was recently reported [121].

Verdine and coworkers reported their first success with Bcl-2 family proteins using a stapled peptide analog of the proapoptotic Bid BH3 domain [37]. The hydrocarbon-crosslinked peptide was shown to bind Bcl-xL at the same binding site as wild-type Bid BH3 and with increased affinity. Importantly, the hydrocarbon crosslink rendered the stapled peptide cell permeable, where the wild-type peptide was not. In cell-based assays, stapled Bid BH3 was shown to sensitize cancer cells to Bax mediated apoptosis. In mice with leukemia xenografts, stapled Bid BH3 treatment consistently suppressed tumor growth.

4.1.3 Inhibition of the NOTCH Transactivation Complex

NOTCH proteins participate in conserved pathways that regulate cellular differentiation, proliferation, and cell death. Mammalian NOTCH receptors are single-pass transmembrane proteins that transmit juxtacrine signals initiated by ligands of the Delta, Serrate, or Lag-2 family [122, 123]. When ligands bind to the extracellular domain of NOTCH1, sequential proteolytic processing events lead to the

intracellular domain of NOTCH (ICN1) being released and translocating to the nucleus, where it loads onto the DNA bound transcription factor CSL. Engagement of CSL with ICN1 creates a long shallow groove along the PPI. The shallow groove serves as a binding site for coactivator proteins, e.g., MAML proteins. The ICN-CSL-MAML complex recruits core transcription machinery effecting activation of NOTCH-dependent target genes (Fig. 16a, b). Loss-of-function mutations have been observed for a number of diseases, and gain-of-function mutations in the NOTCH pathway are causally linked to cancer. Most efforts aimed at antagonizing the NOTCH pathway have focused on blocking ICN1 release using small-molecule inhibitors of the γ-secretase complex [124]. Small molecules, however, have toxicity issues and some cell lines are resistant to GSI inhibitors.

A stapled peptide inhibitor of the NOTCH transactivation complex, based on dnMAML-1, a continuous α-helix at the ICN1–CSL groove, was found to have sub-micromolar binding to the CSL complex in vitro [36, 55]. RT-PCR experiments revealed that treatment of T-ALL cells with stapled dnMAML-1 peptide resulted in downregulation of canonical NOTCH1 targets (Fig. 16c). The stapled peptide was found to be a specific inhibitor of T-cell leukemia in mouse models.

4.2 Hydrogen Bond Surrogate α-Helices

In a classical α-helix, a hydrogen bond between the C═O of the *i* amino acid residue and the NH of the $i + 4$ amino acid residue stabilizes the structure (Fig. 17). Arora and colleagues have reported a strategy for α-helix stabilization that involves replacement of one of the main chain hydrogen bonds with a covalent linkage [71]. To mimic the C═O—H–N hydrogen bond as closely as possible, the investigators envisioned a covalent bond of the type C═X–Y–N, where X and Y would be part of the *i* and the $i + 4$ residues. The exceptional functional group tolerance displayed by olefin metathesis catalysts (of general formula: $L_2X_2Ru{=}CHPh$) for the facile introduction of nonnative carbon–carbon constraints in the preparation of peptidomimetics suggested that X and Y could be pictured as two carbon atoms connected through an olefin metathesis reaction (Fig. 17) [125, 126]. The main chain hydrogen bond surrogate strategy is attractive because the placement of the crosslink within a helix is not expected to block solvent-exposed molecular recognition surfaces of the molecule. Implementation of this strategy results in a highly stabilized, internally crosslinked α-helix. HBS peptides have been shown to successfully modulate protein-biomolecule interactions in cell-free and cell culture assays.

This strategy is expected to yield highly stable short helices based on the hypothesis that helix nucleation is an entropically and enthalpically disfavored process; therefore, factors that stabilize the first turn of the helix should promote helix formation (Fig. 18). The Zimm-Bragg [127] and Lifson-Roig [128] models for helix-coil transition predict that nucleation of the helix in a random coil is the slowest step, and subsequent growth of the helix is rapid. The peptide is considered

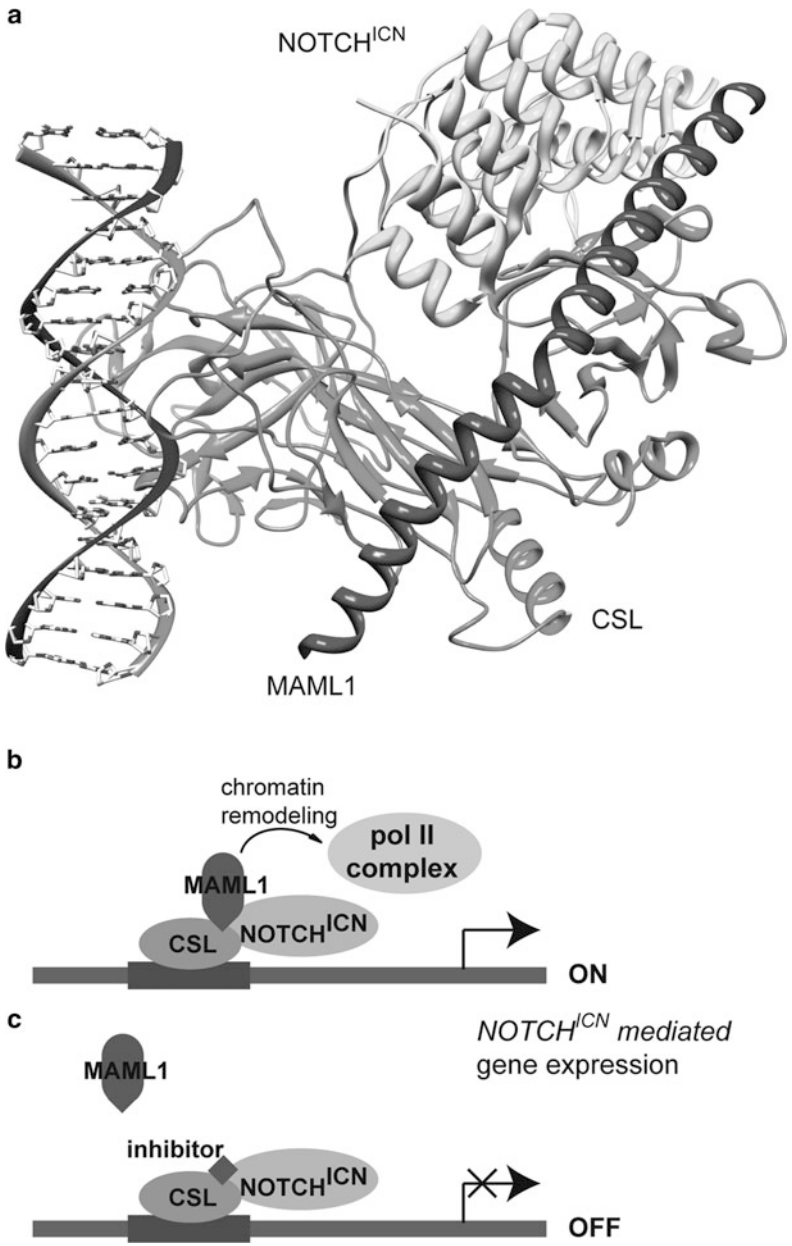

Fig. 16 (**a, b**) Transcription of Notch genes is controlled by the interaction of DNA-bound transcription factor CSL and Notch^{ICN} heterodimer with transcription coactivator MAML1. (PDB code: 2f8x) (**c**) Competitive inhibition of the CSL/Notch^{ICN} complex with MAML1 leads to downregulation of target genes

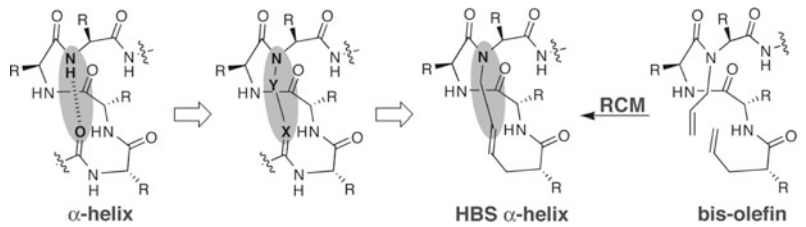

Fig. 17 Nucleation of short α-helices by replacement of an N-terminal *i* and $i + 4$ hydrogen bond (C═O—H–N) with a covalent link (C═X–Y–N). The hydrogen bond surrogate-based (HBS) α-helices contain a carbon–carbon bond derived from a ring-closing metathesis reaction (Reprinted with permission from Patgiri et al. [71], Copyright (2008) American Chemical Society)

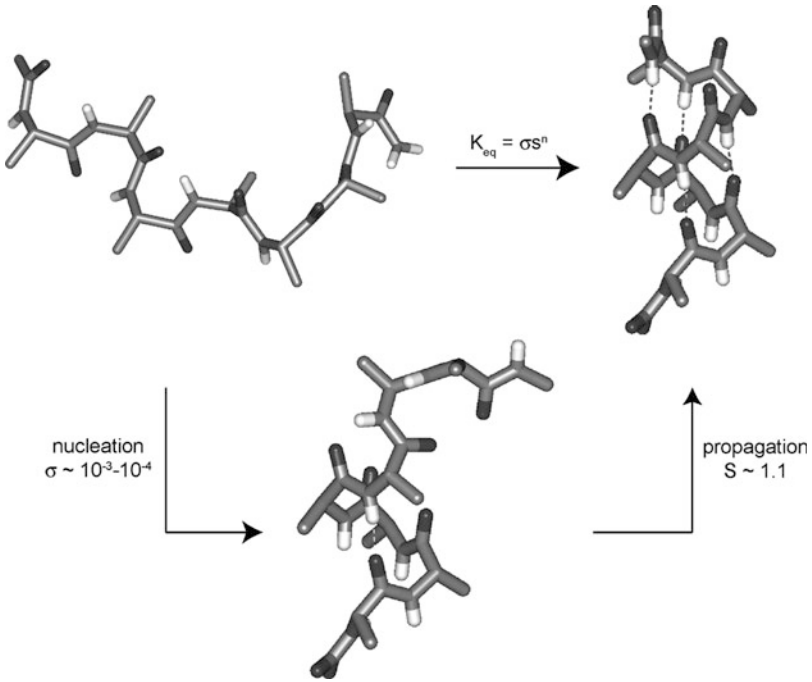

Fig. 18 Models for helix-coil transition predict that the nucleation of the helix in a random coil is the rate-determining step, and subsequent growth of the helix is rapid

to fold via two processes governed by a nucleation parameter (σ in Zimm-Bragg notation) and a propagation parameter, *s*. The propagation parameter is related to the helix propensity of individual amino acids. For a peptide with *n* residues, the equilibrium constant for the helix-coil transition, K_{eq} is described as: $K_{eq} = \sigma s^n$.

The value of the nucleation constant σ is typically very low, about 10^{-3} to 10^{-4} and the propagation parameter *s* is typically around unity [129]. By constraining the

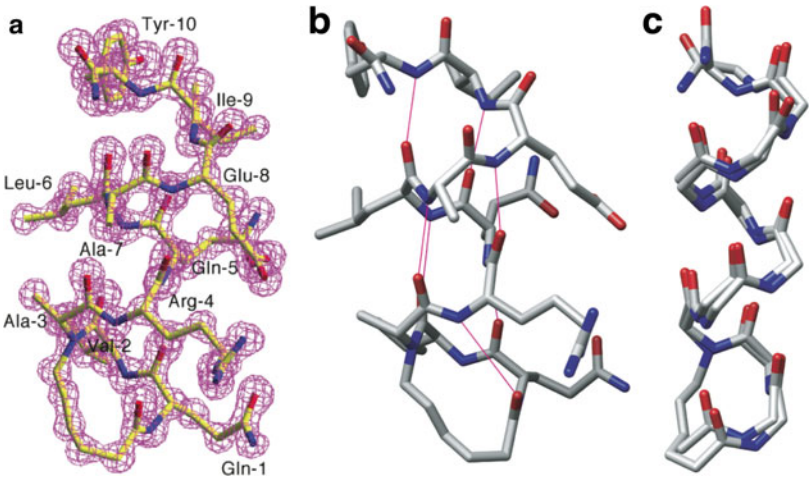

Fig. 19 (**a**) Crystal structure of the HBS α-helix with electron density map superimposed onto the refined molecular model. (**b**) Putative i and $i + 4$ hydrogen bonds (*magenta lines*) in crystal structure–derived molecular model of HBS helix. (**c**) Overlay of crystal structure and a model of an idealized α-helix (Reprinted with permission from Patgiri et al. [71], Copyright (2008) American Chemical Society)

first four residues of the helix the intrinsic nucleation propensities should be overwhelmed and set $\sigma \approx 1$. Thus, if done properly, forming the first α-turn through covalent stitching should favor the helix formation by ~4 kcal/mol.

The hydrogen bond surrogate approach offers two attractive features. (1) As discussed above, this approach provides peptide stabilization with strict preservation of the helix surfaces. (2) The inherent generality of this approach potentially allows access to several protein secondary structures from a single short peptide. A peptide strand can adopt a variety of secondary structures (α-helices, 3_{10}-helices, π-helices, and β-sheets) within the context of proteins. The HBS approach has been shown to stabilize the difficult π-helix conformation in a short peptide, highlighting the versatility of this approach [130].

Extensive NMR and circular dichroism [131, 132] spectroscopy was used to examine the structure and stability of HBS α-helices; the conformation of these compounds is also supported by an X-ray crystal structure that is presented in Fig. 19 [133]. These studies demonstrate that the HBS approach affords stable, short α-helices from biologically relevant sequences.

HBS helices have proven to be remarkably effective tools for the regulation of protein interactions. Significantly, HBS helices outperform their unconstrained counterparts in cell culture studies reflecting their enhanced metabolic stability and cellular uptake properties. The potential of HBS helices has been demonstrated with inhibitors designed to modulate HIV fusion [35], transcription of hypoxia inducible genes [54], p53/HDM2 [33], and Ras/Sos interactions [134]. The selected examples below highlight the potential of HBS helices as inhibitors of PPIs.

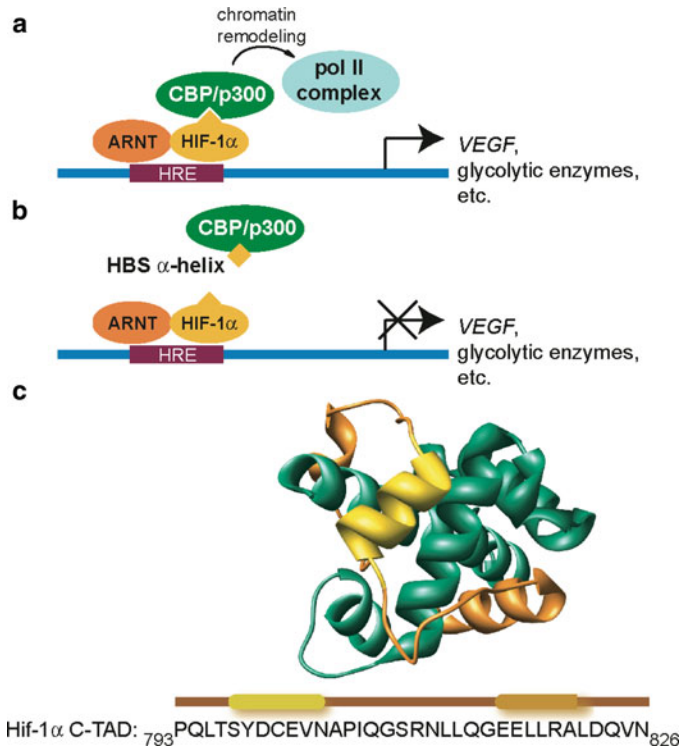

Fig. 20 (**a**) Transcription of hypoxia inducible genes is controlled by the interaction of DNA-bound HIF-1α/ARNT heterodimer with transcription coactivator CBP/p300. (**b**) Competitive inhibition of the HIF-1R C-TAD complex with CBP/p300 CH1 domain leads to downregulation of *VEGF* transcription. (**c**) α-Helices from the C-TAD$_{793–826}$ domain of HIF-1α bind to the cysteine-histidine rich 1 (CH1) region of CBP/p300. HIF-1α is shown in *orange* and *yellow* colors, and CBP/p300 in *green* (PDB code 1L8C) (Reprinted with permission from Henchey et al. [54], Copyright (2010) American Chemical Society)

4.2.1 Modulation of HIF-1α p300/CBP Interaction

Transcription of hypoxia-inducible genes is important for cancer growth and metastasis. Regulation of the transcription process is mediated by binding of the CH1 region of coactivator p300 (or CREB binding protein) and the C-terminal transactivation domain (C-TAD$_{786–826}$) of hypoxia inducible factor 1α (HIF-1α). Structural analysis shows that two helical domains of HIF-1α C-TAD are important for recognition of p300/CBP and are, therefore, potential structures on which to base synthetic mimics to inhibit the interaction (Fig. 20). Interference with this interaction is intended to downregulate expression of vascular endothelial growth factor (VEGF) and its receptor VEGFR2, which are involved in angiogenesis. HBS helix mimics of the CH1 domain of HIF-1α have been shown to downregulate transcription of the VEGF gene in HeLa cells under hypoxic conditions [54]. Cell

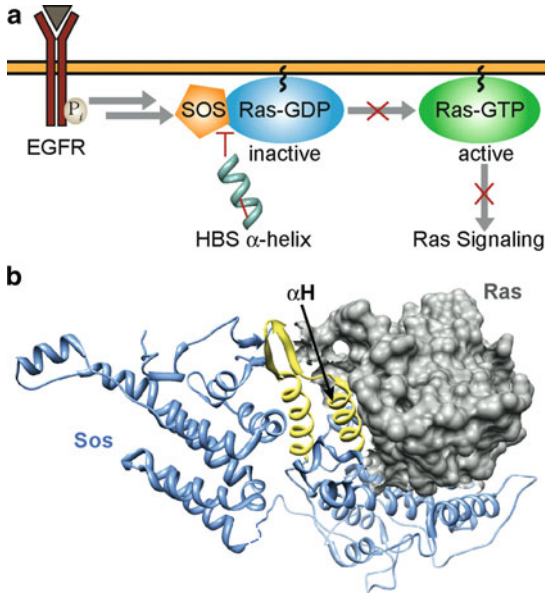

Fig. 21 The Ras-Sos interface and rational design of synthetic inhibitors. (**a**) Schematic depiction of the major transduction steps in the RTK-Sos-Ras-ERK pathway. Binding of growth factor to RTK leads to its phosphorylation triggering recruitment of Sos to the plasma membrane. Membrane-localized Sos activates Ras by facilitating exchange of GDP for GTP. Activated Ras stimulates the ERK-MAP kinase cascade through the sequential phosphorylation of Raf, MEK and ERK. (**b**) *Ribbon* diagram showing the region within the Ras-Sos interface containing the Sos helical hairpin (*yellow*) (PDB code 1NVW). The hairpin inserts into the flexible switch regions of Ras (*grey surface*). The αH motif makes direct contacts with the switch regions of Ras. Mimics of this helix have been shown to modulate Ras signaling (Reprinted with permission from Patgiri et al. [135], Copyright (2011) Nature Publishing Group)

viability assays revealed HBS helices to be less cytotoxic than chetomin, a known inhibitor of the interactions between HIF-1α and p300/CBP.

4.2.2 Regulation of Ras Signaling

Aberrant receptor tyrosine kinase (RTK) signaling is a major underlying cause of various developmental disorders and hyperproliferative diseases [134]. A primary transduction mechanism by which RTK signals are propagated to intracellular pathways involves the ligand-dependent activation of the small guanine nucleotide binding protein Ras (Fig. 21) [136]. Accordingly, design of Ras inhibitors has been an active area of research for anticancer therapy [137, 138]. The rate-limiting step in Ras activation process is the conversion of Ras-GDP to Ras-GTP through an exchange reaction that is catalyzed by the Ras specific guanine nucleotide exchange factor Sos (Fig. 21). Inhibitors of the Ras-Sos interactions would be valuable as

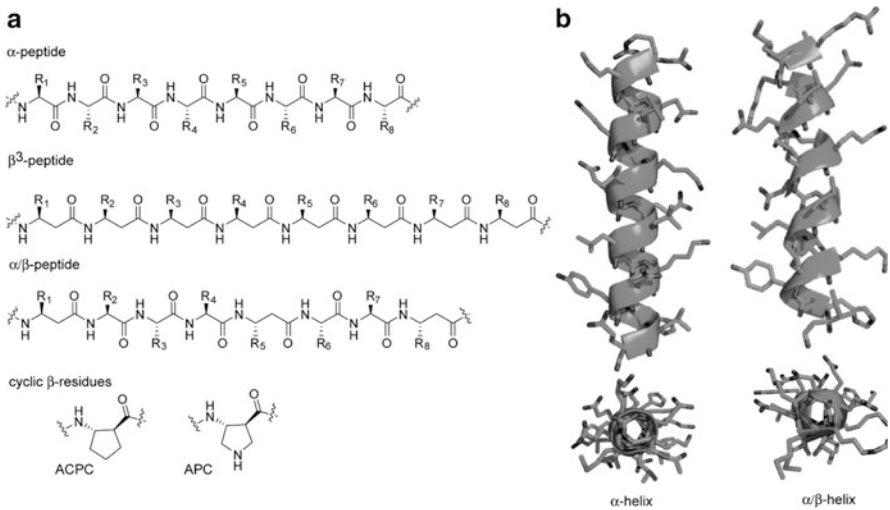

Fig. 22 α-Helix and α/β-peptide foldamers array side-chain functionality in similar fashion: (**a**) backbone sequences of α-, β-, and α/β-helices, and structures of cyclic β-residues. (**b**) Comparison of the α- and α/β-helices (PDB codes 2ZTA and 3C3F) (Reprinted from Guarracino and Arora [139], Copyright (2009) with permission from Elsevier)

tools to dissect this complex signaling pathway and as leads for anticancer drug design. Patgiri et al. recently described the design of a cell-permeable HBS α-helix based on the guanine nucleotide exchange factor Sos that interferes with Ras-Sos interaction and downregulates Ras signaling in response to receptor tyrosine kinase activation [135]. Significantly, the unconstrained peptide derivative remains inactive, highlighting the remarkable potential of stabilized helices and helix mimetics in inhibiting previously untargeted PPIs.

4.3 β-Peptide Foldamers

Helical foldamers, [31, 72] such as β-peptides [73–75] and peptoids, [76] are composed of amino acid analogs and are capable of adopting conformations similar to those found in natural proteins. β-Peptide foldamers are built from β-amino acid residues and have been shown to inhibit various protein-protein complexes (Fig. 22) [31, 72, 73, 140, 141]. The salient feature of these nonpeptidic oligomers is that they display protein-like functionality to target biomolecular receptors while resisting proteolytic degradation [74]. Recent studies have shown that foldamers composed of heterogeneous backbones consisting of α- and β-amino acid residues are also capable of adopting diverse sets of stable conformations [142]. Pioneering studies from the Gellman, Schepartz and Seebach groups have demonstrated the vast potential of these nonnatural oligomers to modulate a variety of protein targets

including those involved in transcription [32, 75, 143]. Cell-penetrating β-peptides that mimic the p53 activation domain were shown to upregulate cellular levels of p53, p21 and HDM2 [40]. The Gellman and Schepartz groups have utilized combinatorial chemistry strategies to generate diverse sets of β-peptide ligands for protein targets [89, 144].

Multiple methods for controlling the helical structure of β-peptides have been described. The Gellman group has pioneered the use of cyclic β-amino acid residues to lock the oligomer backbone into favorable positions. Constraining the desired Cα–Cβ torsional angles in cyclic compounds (e.g., ACPC and APC, Fig. 22a) improves helicity by reducing flexibility [72]. Other approaches for stabilizing the β-peptide conformation include insertion of favorable salt-bridging interactions along one face of the helix and control of the helical macrodipole [145]. More recently, α-, β-, and cyclic β-amino acid residues were combined to create heterogeneous backbones with diverse projection of side-chain functionality [74]. The ability of foldamers to take on a variety of helical shapes is advantageous in the design of therapeutics that better imitate protein secondary structures [31].

4.3.1 HIV Entry Inhibitors

In a recent manuscript, Gellman and coworkers described the design, characterization, and potent activity of α/β-peptides that mimic a long α-helix involved in HIV viral entry [32]. Viral entry is facilitated by conformational changes that the HIV membrane protein gp41 undergoes to form a six-helix bundle during the fusion of the host and viral membranes. The six-helix bundle consists of three helices from the C-terminal heptad repeat domain and three helices from the N-terminal heptad repeat domain [146]. Prevention of bundle formation using α-peptides (or mimics thereof) derived from the C-terminal region is central to anti-HIV entry drug design efforts. One drug in current use, enfuvirtide (Fuzeon), is a 36-amino acid α-peptide comprising residues from the C-terminal region of gp41. As enfuvirtide is composed solely of α-amino acids, it is susceptible to protease degradation and, therefore, can be highly unstable as a therapeutic agent.

Discovery of potent nonnatural, peptide-based gp41 mimics or small molecules capable of disrupting six-helix bundle formation has been a difficult challenge. Gellman and coworkers began their α/β-peptide designs by mimicking a previously described α-peptide helix [32]. Acyclic β^3-amino acid substitution into the α-peptide sequence provided modest inhibitors with in vitro activity in the micromolar range. Replacement of key acyclic β-residues with ACPC and APC resulted in rigidified chimeric α/β-peptides with a remarkable 380-fold binding enhancement. The optimization studies provided highly effective constructs with low nanomolar activities in cell-cell fusion and HIV antiinfectivity assays. Importantly, helical propensity in α/β-peptides correlated well with inhibitory potency and resistance against proteolytic degradation.

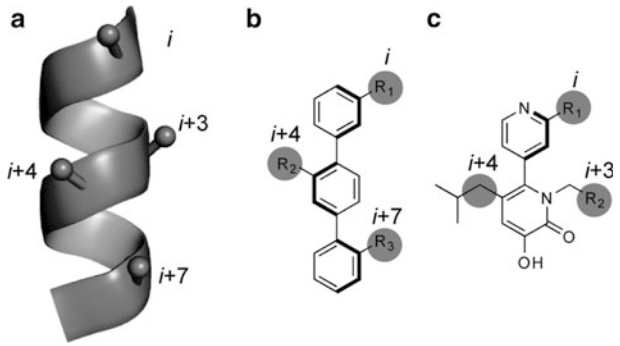

Fig. 23 Nonpeptidic helix mimetics such as (**b**) terphenyls and (**c**) pyridylpyridone derivatives array protein like functionality to mimic their arrangement on an α-helix (**a**) (Reprinted from Guarracino et al. [148], Copyright (2011) with permission from Wiley)

This work highlights the potential of the foldamer strategy to create faithful mimics of the α-helix that are endowed with conformational and proteolytic stability. The mechanism used by the HIV virus to enter cells is also employed by other Class I viruses to target host cells [147]. Success of the outlined strategy suggests that α/β-helices may be effective scaffolds for the generation of potent inhibitors or antigens against these viruses.

4.4 Helix Surface Mimetics

In many protein complexes, one face of the α-helix featuring the i, $i + 4$, and $i + 7$ residues participates in PPIs. Helical surface mimetics take advantage of this feature by capturing the functionality of the primary face of the helix on a nonpeptidic scaffold. Hamilton and coworkers pioneered the development of helical surface mimetics with terphenyl and related scaffolds (Fig. 23); [41, 149] however, since this earlier work, a number of new scaffold designs have been described [78–83]. Molecular modeling and crystal structures suggest that these scaffolds project protein-like functionality in a manner reminiscent of the i, $i + 4$ (or $i + 3$), and $i + 7$ positions of a canonical α-helix. Terphenyl derivatives displaying key p53 binding residues were able to selectively inhibit the p53/HDM2 interaction in vitro with high affinity [149]. The same group also demonstrated that pyridylpyridone derivatives can effectively mimic the conserved nuclear receptor box motif, LXXLL, and target the interaction of estrogen receptor and its coactivator responsible for the expression of estrogen-activated genes [150, 151].

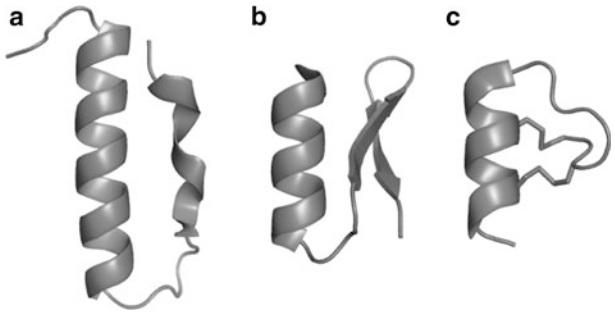

Fig. 24 Miniature proteins that display stable helical folds and regulate transcription: (**a**) avian pancreatic protein (PDB code: 1 ppt), (**b**) scorpion toxin miniprotein (PDB code: 1r1g), and (**c**) apamin (PDB code: 3iux) (Reprinted from Guarracino et al. [148], Copyright (2011) with permission from Wiley)

4.5 Miniproteins

Well-folded miniature proteins that present solvent-exposed helices can serve as templates for the development of novel ligands for transcription factors and cofactor protein interactions [52]. Schepartz and coworkers have engineered avian pancreatic polypeptide (aPP, Fig. 24) scaffolds with the recognition epitope from the CREB KID transcription activation domain to target the KIX domain of coactivator CBP with high affinity [152, 153]. Fusion of the CREB miniature protein with a heterologous DNA-binding domain provided artificial ligands that activated the transcription through the CBP/p300 pathway [153]. An attractive feature of miniprotein scaffolds is that they may be diversified using common protein evolution strategies, such as phage display. Several miniproteins including aPP, and α-helical scaffolds derived from scorpion toxin and apamin, have been designed to target the interaction between the activation domain of p53 and HDM2.

5 Future Outlook and Challenges

Development of specific ligands for protein targets that help decode the complexities of PPI networks is a key goal for the field of chemical biology. Despite the emergence of powerful *in silico* and experimental high-throughput screening strategies, the discovery of synthetic ligands that selectively modulate PPIs remains a challenge for organic and medicinal chemists. This chapter discussed rational-design approaches for the discovery of PPI inhibitors. Fundamentally, these synthetic methods seek to adapt nature's protein recognition principles. The distinguishing element of these approaches is that they offer medium-sized molecules that potentially target protein surfaces with a larger number of contacts, and higher specificity, than traditional small molecules. The past decade has seen significant progress in the design of protein domain mimetics and their potential to bind their cognate receptors.

Significantly, the preliminary success in the field has brought into question a basic tenet of drug discovery that only molecules of a certain size may enter cells.

Associated with this enormous preliminary promise are several hurdles that need to be overcome for the outlined strategies to result in human therapeutics. These include cellular uptake, synthesis scale-up, evaluation of specificity for the chosen interaction, oral availability and metabolic stability, and immunogenicity. Several constrained peptide sequences have been shown to be cell permeable but the exact mechanisms controlling uptake are not clear; e.g., the effect of sequence on permeability remains to be determined. Several of the synthetic approaches require transition metal catalysis, which may become a significant obstacle in terms of cost and synthetic efficiency, especially for difficult sequences. The medium-sized molecules discussed in this chapter are inherently more specific for target proteins than typical small-molecule inhibitors because they use multiple contact points. However, proteins have not only evolved to bind larger molecules, they often interact with several natural partners at the same interface, making it a challenging proposition to achieve specific regulation of a single pathway. Additionally, the dynamic nature of protein surfaces may complicate specific targeting of chosen receptors.

Despite the various obstacles that need to be overcome, the examples outlined herein suggest that these medium-sized molecules will play important roles as tools for decoding biological complexity and, potentially, as leads for drug discovery.

Acknowledgments We thank the National Institutes of Health (GM073943) and National Science Foundation (CHE 0848410) for financial support.

References

1. Ryan DP, Matthews JM (2005) Protein-protein interactions in human disease. Curr Opin Struct Biol 15:441–446
2. Arkin MR, Wells JA (2004) Small-molecule inhibitors of protein-protein interactions: progressing towards the dream. Nat Rev Drug Discov 3:301–317
3. Hajduk PJ, Greer J (2007) A decade of fragment-based drug design: strategic advances and lessons learned. Nat Rev Drug Discov 6:211–219
4. Lo Conte L, Chothia C, Janin J (1999) The atomic structure of protein-protein recognition sites. J Mol Biol 285:2177–2198
5. Overington JP, Al-Lazikani B, Hopkins AL (2006) How many drug targets are there? Nat Rev Drug Discov 5:993–996
6. Vitkup D, Melamud E, Moult J, Sander C (2001) Completeness in structural genomics. Nat Struct Biol 8:559–566
7. Vassilev L, Fry D (eds) (2011) Small molecule inhibitors of protein-protein interactions, vol 348, Current topics in microbiology and immunology. Springer, Heidelberg/Dordecht/London/New York
8. Berg T (2008) Inhibition of transcription factors with small organic molecules. Curr Opin Chem Biol 12:464–471
9. Shangary S, Wang S (2008) Targeting the MDM2-p53 interaction for cancer therapy. Clin Cancer Res 14:5318–5324

10. Vassilev LT, Vu BT, Graves B et al (2004) In vivo activation of the p53 pathway by small-molecule antagonists of MDM2. Science 303:844–848
11. Chene P (2003) Inhibiting the p53-MDM2 interaction: an important target for cancer therapy. Nat Rev Cancer 3:102–109
12. Kussie PH, Gorina S, Marechal V et al (1996) Structure of the MDM2 oncoprotein bound to the p53 tumor suppressor transactivation domain. Science 274:948–953
13. Oltersdorf T, Elmore SW, Shoemaker AR et al (2005) An inhibitor of Bcl-2 family proteins induces regression of solid tumours. Nature 435:677–681
14. Sattler M, Liang H, Nettesheim D et al (1997) Structure of Bcl-x(L)-Bak peptide complex: recognition between regulators of apoptosis. Science 275:983–986
15. Shoemaker AR, Oleksijew A, Bauch J et al (2006) A small-molecule inhibitor of Bcl-XL potentiates the activity of cytotoxic drugs in vitro and in vivo. Cancer Res 66:8731–8739
16. Wendt MD, Shen W, Kunzer A et al (2006) Discovery and structure-activity relationship of antagonists of B-cell lymphoma 2 family proteins with chemopotentiation activity in vitro and in vivo. J Med Chem 49:1165–1181
17. Wang Y, Coulombe R, Cameron DR et al (2004) Crystal structure of the E2 transactivation domain of human papillomavirus type 11 bound to a protein interaction inhibitor. J Biol Chem 279:6976–6985
18. Cheng RP, DeGrado WF (2001) De novo design of a monomeric helical beta-peptide stabilized by electrostatic interactions. J Am Chem Soc 123:5162–5163
19. Liu Z, Sun C, Olejniczak ET et al (2000) Structural basis for binding of Smac/DIABLO to the XIAP BIR3 domain. Nature 408:1004–1008
20. Oost TK, Sun C, Armstrong RC et al (2004) Discovery of potent antagonists of the antiapoptotic protein XIAP for the treatment of cancer. J Med Chem 47:4417–4426
21. Sun H, Nikolovska-Coleska Z, Yang C-Y et al (2004) Structure-based design of potent, conformationally constrained Smac mimetics. J Am Chem Soc 126:16686–16687
22. Glattli A, Daura X, Bindschadler P et al (2005) On the influence of charged side chains on the folding-unfolding equilibrium of beta-peptides: a molecular dynamics simulation study. Chemistry 11:7276–7293
23. Berg T, Cohen SB, Desharnais J et al (2002) Small-molecule antagonists of Myc/Max dimerization inhibit Myc-induced transformation of chicken embryo fibroblasts. Proc Natl Acad Sci USA 99:3830–3835
24. Kiessling A, Sperl B, Hollis A et al (2006) Selective inhibition of c-Myc/Max dimerization and DNA binding by small molecules. Chem Biol 13:745–751
25. Bogan AA, Thorn KS (1998) Anatomy of hot spots in protein interfaces. J Mol Biol 280:1–9
26. Moreira IS, Fernandes PA, Ramos MJ (2007) Hot spots–a review of the protein-protein interface determinant amino-acid residues. Proteins 68:803–812
27. Clackson T, Wells JA (1995) A hot-spot of binding-energy in a hormone-receptor interface. Science 267:383–386
28. Keskin Z, Gursoy A, Ma B, Nussinov R (2008) Principles of protein-protein interactions: what are the preferred ways for proteins to interact? Chem Rev 108:1225–1244
29. Guharoy M, Chakrabarti P (2007) Secondary structure based analysis and classification of biological interfaces: identification of binding motifs in protein-protein interactions. Bioinformatics 23:1909–1918
30. Jones S, Thornton JM (1995) Protein-protein interactions – a review of protein dimer structures. Prog Biophys Mol Biol 63:31–65
31. Goodman CM, Choi S, Shandler S, DeGrado WF (2007) Foldamers as versatile frameworks for the design and evolution of function. Nat Chem Biol 3:252–262
32. Horne WS, Johnson LM, Ketas TJ et al (2009) Structural and biological mimicry of protein surface recognition by α/β-peptide foldamers. Proc Natl Acad Sci USA 106:14751–14756
33. Henchey LK, Porter JR, Ghosh I, Arora PS (2010) High specificity in protein recognition by hydrogen-bond-surrogate α-helices: selective inhibition of the p53/MDM2 complex. Chembiochem 11:2104–2107

34. Ko E, Liu J, Burgess K (2011) Minimalist and universal peptidomimetics. Chem Soc Rev 40:4411–4421
35. Wang D, Lu M, Arora PS (2008) Inhibition of HIV-1 fusion by hydrogen-bond-surrogate-based α helices. Angew Chem Int Ed 47:1879–1882
36. Moellering RE, Cornejo M, Davis TN et al (2009) Direct inhibition of NOTCH transcription factor complex. Nature 462:182–190
37. Walensky LD, Kung AL, Escher I et al (2004) Activation of apoptosis in vivo by a hydrocarbon-stabled BH3 helix. Science 305:1466–1470
38. Harrison RS, Shepherd NE, Hoang HN et al (2010) Downsizing human, bacterial, and viral proteins to short water-stable α helices that maintain biological potency. Proc Natl Acad Sci USA 107:11686–11691
39. Smith BA, Daniels DS, Coplin AE et al (2008) Minimally cationic cell-permeable miniature proteins via α-helical arginine display. J Am Chem Soc 130:2948–2949
40. Harker EA, Schepartz A (2009) Cell-permeable β-peptide inhibitors of p53/hDM2 complexation. Chembiochem 10:990–993
41. Cummings CG, Hamilton AD (2010) Disrupting protein-protein interactions with non-peptidic, small molecule α-helix mimetics. Curr Opin Chem Biol 14:341–346
42. Hammond MC, Harris BZ, Lim WA, Bartlett PA (2006) β strand peptidomimetics as potent PDZ domain ligands. Chem Biol 13:1247–1251
43. Bourgeas R, Basse MJ, Morelli X, Roche P (2010) Atomic analysis of protein-protein interfaces with known inhibitors: the 2P2I database. PLoS One 5:e9598
44. Davis JM, Tsou LK, Hamilton AD (2007) Synthetic non-peptide mimetics of α-helices. Chem Soc Rev 36:326–334
45. Duca M, Vekhoff P, Oussedik K et al (2008) The triple helix: 50 years later, the outcome. Nucleic Acids Res 36:5123–5138
46. Higueruelo AP, Schreyer A, Bickerton GR et al (2009) Atomic interactions and profile of small molecules disrupting protein-protein interfaces: the TIMBAL database. Chem Biol Drug Des 74:457–467
47. Jamieson AC, Miller JC, Pabo CO (2003) Drug discovery with engineered zinc-finger proteins. Nat Rev Drug Discov 2:361–368
48. Ray A, Norden B (2000) Peptide nucleic acid (PNA): its medical and biotechnical applications and promise for the future. FASEB J 14:1041–1060
49. Reynes C, Host H, Camproux AC et al (2010) Designing focused chemical libraries enriched in protein-protein interaction inhibitors using machine-learning methods. PLoS Comput Biol 6:e1000695
50. Jochim AL, Arora PS (2010) Systematic analysis of helical protein interfaces reveals targets for synthetic inhibitors. ACS Chem Biol 5:919–923
51. Jochim AL, Arora PS (2009) Assessment of helical interfaces in protein-protein interactions. Mol Biosyst 5:924–926
52. Henchey LK, Jochim AL, Arora PS (2008) Contemporary strategies for the stabilization of peptides in the α-helical conformation. Curr Opin Chem Biol 12:692–697
53. Kritzer JA, Lear JD, Hodsdon ME, Schepartz A (2004) Helical β-peptide inhibitors of the p53-hDM2 interaction. J Am Chem Soc 126:9468–9469
54. Henchey LK, Kushal S, Dubey R et al (2010) Inhibition of hypoxia inducible factor 1–transcription coactivator interaction by a hydrogen bond surrogate α-helix. J Am Chem Soc 132:941–943
55. Nam Y, Sliz P, Song L et al (2006) Structural basis for cooperativity in recruitment of MAML coactivators to Notch transcription complexes. Cell 124:973–983
56. Cunningham BC, Wells JA (1989) High-resolution epitope mapping of hGH-receptor interactions by alanine-scanning mutagenesis. Science 244:1081–1085
57. Tovar C, Rosinski J, Filipovic Z et al (2006) Small-molecule MDM2 antagonists reveal aberrant p53 signaling in cancer: implications for therapy. Proc Natl Acad Sci USA 103:1888–1893

58. Fechter EJ, Olenyuk B, Dervan PB (2004) Design of a sequence-specific DNA bisintercalator. Angew Chem Int Ed Engl 43:3591–3594
59. Vassilev LT (2007) MDM2 inhibitors for cancer therapy. Trends Mol Med 13:23–31
60. White RJ, Sharrocks AD (2010) Coordinated control of the gene expression machinery. Trends Genet 26:214–220
61. Berman HM, Westbrook J, Feng Z et al (2000) The protein data bank. Nucleic Acids Res 28:235–242
62. Li W, Jaroszewski L, Godzik A (2001) Clustering of highly homologous sequences to reduce the size of large protein databases. Bioinformatics 17:282–283
63. Kuhlman B, Baker D (2000) Native protein sequences are close to optimal for their structures. Proc Natl Acad Sci USA 97:10383–10388
64. Kortemme T, Baker D (2002) A simple physical model for binding energy hot spots in protein-protein complexes. Proc Natl Acad Sci USA 99:14116–14121
65. Kortemme T, Kim DE, Baker D (2004) Computational alanine scanning of protein-protein interfaces. Sci STKE 2004:pl2
66. Murray JK, Gellman SH (2007) Targeting protein-protein interactions: lessons from p53/MDM2. Biopolymers 88:657–686
67. Bullock BN, Jochim AL, Arora PS (2011) Assessing helical protein interfaces for inhibitor design. J Am Chem Soc 133:14220–14223
68. Arora PS, Ansari AZ, Best TP et al (2002) Design of artificial transcriptional activators with rigid poly-L-proline linkers. J Am Chem Soc 124:13067–13071
69. Edwards TA, Wilson AJ (2011) Helix-mediated protein-protein interactions as targets for intervention using foldamers. Amino Acids 41:743–754
70. Schafmeister CE, Po J, Verdine GL (2000) An all-hydrocarbon cross-linking system for enhancing the helicity and metabolic stability of peptides. J Am Chem Soc 122:5891–5892
71. Patgiri A, Jochim AL, Arora PS (2008) A hydrogen bond surrogate approach for stabilization of short peptide sequences in alpha-helical conformation. Acc Chem Res 41:1289–1300
72. Gellman SH (1998) Foldamers: a manifesto. Acc Chem Res 31:173–180
73. Cheng RP, Gellman SH, DeGrado WF (2001) β-peptides: from structure to function. Chem Rev 101:3219–3232
74. Horne WS, Gellman SH (2008) Foldamers with heterogeneous backbones. Acc Chem Res 41:1399–1408
75. Seebach D, Gardiner J (2008) β-peptidic peptidomimetics. Acc Chem Res 41:1366–1375
76. Yoo B, Kirshenbaum K (2008) Peptoid architectures: elaboration, actuation, and application. Curr Opin Chem Biol 12:714–721
77. Marimganti S, Cheemala MN, Ahn JM (2009) Novel amphiphilic α-helix mimetics based on a bis-benzamide scaffold. Org Lett 11:4418–4421
78. Plante JP, Burnley T, Malkova B et al (2009) Oligobenzamide proteomimetic inhibitors of the p53-hDM2 protein-protein interaction. Chem Commun 34:5091–5093
79. Shaginian A, Whitby LR, Hong S et al (2009) Design, synthesis, and evaluation of an α-helix mimetic library targeting protein-protein interactions. J Am Chem Soc 131:5564–5572
80. Restorp P, Rebek J Jr (2008) Synthesis of α-helix mimetics with four side-chains. Bioorg Med Chem Lett 18:5909–5911
81. Tosovska P, Arora PS (2010) Oligooxopiperazines as nonpeptidic α-helix mimetics. Org Lett 12:1588–1591
82. Lee JH, Zhang Q, Jo S et al (2011) Novel pyrrolopyrimidine-based α-helix mimetics: cell-permeable inhibitors of protein-protein interactions. J Am Chem Soc 133:676–679
83. Buhrlage SJ, Bates CA, Rowe SP et al (2009) Amphipathic small molecules mimic the binding mode and function of endogenous transcription factors. ACS Chem Biol 4:335–344
84. Nelson DL, Lehninger AL, Cox MM (2008) Principles of biochemistry, 5th edn. W.H Freeman, New York
85. Kossiakoff AA, Koide S (2008) Understanding mechanisms governing protein-protein interactions from synthetic binding interfaces. Curr Opin Struct Biol 18:499–506

86. Argos P (1988) An investigation of protein subunit and domain interfaces. Protein Eng 2:101–113
87. Ko E, Liu J, Perez LM et al (2010) Universal peptidomimetics. J Am Chem Soc 133:462–477
88. Campbell F, Plante JP, Edwards TA et al (2010) N-alkylated oligoamide α-helical proteomimetics. Org Biomol Chem 8:2344–2351
89. Murray JK, Farooqi B, Sadowsky JD et al (2005) Efficient synthesis of a β-peptide combinatorial library with microwave irradiation. J Am Chem Soc 127:13271–13280
90. Sheinerman FB, Norel R, Honig B (2000) Electrostatic aspects of protein-protein interactions. Curr Opin Struct Biol 10:153–159
91. Jones S, Thornton JM (1996) Principles of protein-protein interactions. Proc Natl Acad Sci USA 93:13–20
92. Barlow DJ, Thornton JM (1988) Helix geometry in proteins. J Mol Biol 201:601–619
93. Tyndall JD, Nall T, Fairlie DP (2005) Proteases universally recognize β strands in their active sites. Chem Rev 105:973–999
94. Garner J, Harding MM (2007) Design and synthesis of α-helical peptides and mimetics. Org Biomol Chem 5:3577–3585
95. Felix AM, Heimer EP, Wang CT et al (1988) Synthesis, biological activity and conformational analysis of cyclic GRF analogs. Int J Pept Protien Res 32:441–454
96. Osapay G, Taylor JW (1992) Multicyclic polypeptide model compounds.2. Synthesis and conformational properties of a highly α-helical uncosapeptide constrained by 3 side-chain to side-chain lactam bridges. J Am Chem Soc 114:6966–6973
97. Phelan JC, Skelton NJ, Braisted AC, McDowell RS (1997) A general method for constraining short peptides to an α-helical conformation. J Am Chem Soc 119:455–460
98. Taylor JW (2002) The synthesis and study of side-chain lactam-bridged peptides. Biopolymers 66:49–75
99. Jackson DY, King DS, Chmielewski J et al (1991) General-approach to the synthesis of short α-helical peptides. J Am Chem Soc 113:9391–9392
100. Leduc AM, Trent JO, Wittliff JL et al (2003) Helix-stabilized cyclic peptides as selective inhibitors of steroid receptor-coactivator interactions. Proc Natl Acad Sci USA 100:11273–11278
101. Ghadiri MR, Choi C (1990) Secondary structure nucleation in peptides – transition-metal ion stabilized α-helices. J Am Chem Soc 112:1630–1632
102. Kelso MJ, Beyer RL, Hoangt HN et al (2004) α-turn mimetics: short peptide α-helices composed of cyclic metallopentapeptide modules. J Am Chem Soc 126:4828–4842
103. Ruan FQ, Chen YQ, Hopkins PB (1990) Metal-ion enhanced helicity in synthetic peptides containing unnatural, metal-ligating residues. J Am Chem Soc 112:9403–9404
104. Brunel FM, Dawson PE (2005) Synthesis of constrained helical peptides by thioether ligation: application to analogs of gp41. Chem Commun 20:2552–2554
105. Judice JK, Tom JY, Huang W et al (1997) Inhibition of HIV type 1 infectivity by constrained α-helical peptides: implications for the viral fusion mechanism. Proc Natl Acad Sci USA 94:13426–13430
106. Sia SK, Carr PA, Cochran AG et al (2002) Short constrained peptides that inhibit HIV-1 entry. Proc Natl Acad Sci USA 99:14664–14669
107. Geistlinger TR, Guy RK (2003) Novel selective inhibitors of the interaction of individual nuclear hormone receptors with a mutually shared steroid receptor coactivator 2. J Am Chem Soc 125:6852–6853
108. Mills NL, Daugherty MD, Frankel AD, Guy RK (2006) An α-helical peptidomimetic inhibitor of the HIV-1 Rev-RRE interaction. J Am Chem Soc 128:3496–3497
109. Shepherd NE, Hoang HN, Desai VS et al (2006) Modular α-helical mimetics with antiviral activity against respiratory syncitial virus. J Am Chem Soc 128:13284–13289
110. Blackwell HE, Grubbs RH (1998) Highly efficient synthesis of covalently cross-linked peptide helices by ring-closing metathesis. Angew Chem Int Ed Engl 37:3281–3284

111. Bernal F, Tyler AF, Korsmeyer SJ et al (2007) Reactivation of the p53 tumor suppressor pathway by a stapled p53 peptide. J Am Chem Soc 129:2456–2457
112. Zhang H, Zhao Q, Bhattacharya S et al (2008) A cell-penetrating helical peptide as a potential HIV-1 inhibitor. J Mol Biol 378:565–580
113. Zhang FZ, Sadovski O, Xin SJ, Woolley GA (2007) Stabilization of folded peptide and protein structures via distance matching with a long, rigid cross-linker. J Am Chem Soc 129:14154–14155
114. Fujimoto K, Kajino M, Inouye M (2008) Development of a series of cross-linking agents that effectively stabilize α-helical structures in various short peptides. Chem Eur J 14:857–863
115. Debnath AK (2006) Prospects and strategies for the discovery and development of small-molecule inhibitors of six-helix bundle formation in class 1 viral fusion proteins. Curr Opin Investig Drugs 7:118–127
116. Labi V, Grespi F, Baumgartner F, Villunger A (2008) Targeting the Bcl-2-regulated apoptosis pathway by BH3 mimetics: a breakthrough in anticancer therapy? Cell Death Differ 15:977–987
117. Walensky LD, Pitter K, Morash J et al (2006) A stapled BID BH3 directly binds and activates BAX. Mol Cell 24:199–210
118. Gavathiotis E, Reyna DE, Davis ML et al (2010) BH3-triggered structural reorganization drives the activation of proapoptotic BAX. Mol Cell 40:481–492
119. Gavathiotis E, Suzuki M, Davis ML et al (2008) BAX activation is initiated at a novel interaction site. Nature 455:1076–1081
120. Danial NN, Walensky LD, Zhang CY et al (2008) Dual role of proapoptotic BAD in insulin secretion and beta cell survival. Nat Med 14:144–153
121. Stewart ML, Fire E, Keating AE, Walensky LD (2010) The MCL-1 BH3 helix is an exclusive MCL-1 inhibitor and apoptosis sensitizer. Nat Chem Biol 6:595–601
122. Lai EC (2004) Notch signaling: control of cell communication and cell fate. Development 131:965–973
123. Nam Y, Aster JC, Blacklow SC (2002) Notch signaling as a therapeutic target. Curr Opin Chem Biol 6:501–509
124. Real PJ, Tosello V, Palomero T et al (2009) γ-Secretase inhibitors reverse glucocorticoid resistance in T cell acute lymphoblastic leukemia. Nat Med 15:50–58
125. Trnka TM, Grubbs RH (2001) The development of $L_2X_2Ru{=}CHR$ olefin metathesis catalysts: an organometallic success story. Acc Chem Res 34:18–29
126. Hoveyda AH, Gillingham DG, Van Veldhuizen JJ et al (2004) Ru complexes bearing bidentate carbenes: from innocent curiosity to uniquely effective catalysts for olefin metathesis. Org Biomol Chem 2:8–23
127. Zimm BH, Bragg JK (1959) Theory of the phase transition between helix and random coil in polypeptide chains. J Chem Phys 31:526–535
128. Lifson S, Roig A (1961) On the theory of helix-coil transitions in polypeptides. J Chem Phys 34:1963–1974
129. Scholtz JM, Baldwin RL (1992) The mechanism of alpha-helix formation by peptides. Annu Rev Biophys Biomol Struct 21:95–118
130. Chapman R, Kulp JL III, Patgiri A et al (2008) Trapping a folding intermediate of the alpha-helix: stabilization of the pi-helix. Biochemistry 47:4189–4195
131. Wang D, Chen K, Kulp JL III, Arora PS (2006) Evaluation of biologically relevant short α-helices stabilized by a main-chain hydrogen-bond surrogate. J Am Chem Soc 128:9248–9256
132. Wang D, Chen K, Dimartino G, Arora PS (2006) Nucleation and stability of hydrogen-bond surrogate-based α-helices. Org Biomol Chem 4:4074–4081
133. Liu J, Wang D, Zheng Q et al (2008) Atomic structure of a short α-helix stabilized by a main chain hdrogen surrogate. J Am Chem Soc 130:4334–4337
134. Blume-Jensen P, Hunter T (2001) Oncogenic kinase signalling. Nature 411:355–365

135. Patgiri A, Yadav KK, Arora PS, Bar-Sagi D (2011) An orthosteric inhibitor of the Ras-Sos interaction. Nat Chem Biol 7:585–587
136. Buday L, Downward J (2008) Many faces of Ras activation. Biochim Biophys Acta 1786:178–187
137. Downward J (2003) Targeting RAS signalling pathways in cancer therapy. Nat Rev Cancer 3:11–22
138. Joerger AC, Fersht AR (2008) Structural biology of the tumor suppressor p53. Annu Rev Biochem 77:557–582
139. Guarracino DA, Arora PS (2009) Making strides in peptide-based therapeutics. Chem Biol 16:919–920
140. Seebach D, Hook DF, Glattli A (2006) Helices and other secondary structures of β- and γ-peptides. Biopolymers 84:23–37
141. Choi SH, Guzei IA, Spencer LC, Gellman SH (2010) Crystallographic characterization of 12-helical secondary structure in β-peptides containing side chain groups. J Am Chem Soc 132:13879–13885
142. Hook DF, Bindschadler P, Mahajan YR et al (2005) The proteolytic stability of 'designed' β-peptides containing α-peptide-bond mimics and of mixed α, β-peptides: application to the construction of MHC-binding peptides. Chem Biodivers 2(5):591–632
143. Kritzer JA, Stephens OM, Guarracino DA et al (2005) β-Peptides as inhibitors of protein-protein interactions. Bioorg Med Chem 13:11–16
144. Kritzer JA, Luedtke NW, Harker EA, Schepartz A (2005) A rapid library screen for tailoring β-peptide structure and function. J Am Chem Soc 127:14584–14585
145. Kritzer JA, Tirado-Rives J, Hart SA et al (2005) Relationship between side chain structure and 14-helix stability of β3-peptides in water. J Am Chem Soc 127:167–178
146. Chan DC, Fass D, Berger JM, Kim PS (1997) Core structure of gp41 from the HIV envelope glycoprotein. Cell 89:263–273
147. Dimitrov DS (2004) Virus entry: molecular mechanisms and biomedical applications. Nat Rev Microbiol 2:109–122
148. Guarracino DA, Bullock BN, Arora PS (2011) Protein-protein interactions in transcription: a fertile ground for helix mimetics. Biopolymers 95:1–7
149. Yin H, Lee GI, Park HS et al (2005) Terphenyl-based helical mimetics that disrupt the p53/HDM2 interaction. Angew Chem Int Ed Engl 44:2704–2707
150. Shiau AK, Barstad D, Loria PM et al (1998) The structural basis of estrogen receptor/coactivator recognition and the antagonism of this interaction by tamoxifen. Cell 95:927–937
151. Becerril J, Hamilton AD (2007) Helix mimetics as inhibitors of the interaction of the estrogen receptor with coactivator peptides. Angew Chem Int Ed Engl 46:4471–4473
152. Rutledge SE, Volkman HM, Schepartz A (2003) Molecular recognition of protein surfaces: high affinity ligands for the CBPKIX domain. J Am Chem Soc 125:14336–14347
153. Volkman HM, Rutledge SE, Schepartz A (2005) Binding mode and transcriptional activation potential of high affinity ligands for the CBPKIX domain. J Am Chem Soc 127:4649–4658
154. Li C, Pazgier M, Li J et al (2010) Limitations of peptide retro-inverso isomerization in molecular mimicry. J Biol Chem 285:19572–19581
155. Kritzer JA, Zutshi R, Cheah M et al (2006) Miniature protein inhibitors of the p53-hDM2 interaction. Chembiochem 7:29–31
156. Li C, Liu M, Monbo J et al (2008) Turning a scorpion toxin into an antitumor miniprotein. J Am Chem Soc 130:13546–13548
157. Li C, Pazgier M, Liu M, Lu WY (2009) Apamin as a template for structure-based rational design of potent peptide activators of p53. Angew Chem Int Ed Engl 48:8712–8715

Top Med Chem 8: 231–258
DOI: 10.1007/978-3-642-28965-1_7

The Discovery of Navitoclax, a Bcl-2 Family Inhibitor

Michael D. Wendt

Contents

Abstract A case history of the Abbott Oncology Bcl-2/Bcl-xL inhibitors program is presented. The target proteins interact with other members of the Bcl family through surfaces that are very large and hydrophobic even compared to other PPIs that have been targeted by pharma. Resulting inhibitors are correspondingly large and hydrophobic and thus tend to be highly protein bound and possess low oral bioavailability. The Abbott drug discovery effort began with the creation of a soluble, stable version of Bcl-xL, and a solution structure of Bcl-xL bound to a native ligand. Structural support facilitated efforts to find chemical matter, which was accomplished through fragment screening. Structure-based drug design was also employed throughout the project, with the discovery process characterized by separate optimization of two widely separated hydrophobic hot spots. ABT-737, an IV-only compound, was initially selected as a development candidate. Later, efforts

M.D. Wendt (✉)
Department of R4N6 Bldg AP10, Cancer Research, Abbott Laboratories, 100 Abbott Park Road, Abbott Park, IL 60064, USA
e-mail: mike.d.wendt@abbott.com

to derive an orally bioavailable compound from the same chemical series produced navitoclax (ABT-263), an extremely potent Bcl-2/Bcl-xL inhibitor, currently in Phase II clinical trials for cancer.

Keywords Apoptosis • Bcl-2 family • Bcl-2 • Bcl-xL • Cancer • Oral bioavailability • Structure-based drug design

1 Introduction

Apoptosis, or programmed cell death, is a highly regulated process used to eliminate defective and unnecessary cells, and is important in normal development, tissue remodeling and immune response [1–3]. Disruption of this process is a prominent characteristic of several disease states, and is a hallmark of cancer. Defects in the apoptotic pathway confer a survival advantage to cancer cells that are subjected to normally apoptosis-inducing stresses such as hypoxia, inappropriate substratum attachment, genetic damage and abnormal cell cycle progression [4]. Most importantly, an aberrant apoptotic pathway also affects the susceptibility of cancer cells to chemotherapeutics and radiation. Agents capable of specifically restoring natural pathways for apoptosis should not only directly block progression of the tumorigenic phenotype, but should also potentiate existing therapies by overcoming resistance [5, 6].

The Bcl-2 family of proteins is composed of both proapoptotic (pro-death) and antiapoptotic (pro-survival) members acting through a complex series of protein-protein interactions to mediate the intrinsic apoptotic pathway [7–9]. The antiapoptotic family members (Bcl-xL, Bcl-2, Bcl-w, A1, Mcl-1) are characterized by four α-helical Bcl-2 homology (BH) domains, designated BH1–4. The pro-death proteins comprise two groups, those containing domains BH1–3, (Bax, Bak) and those with a single BH3 domain (Bad, Bik, Bid, Bim, Hrk, Bmf, Noxa and Puma). Interactions between these three subsets dictate the apoptotic fate of the cell. The BH3-only proteins are activated to initiate apoptosis in response to cellular stresses [10, 11]. Bax and Bak subsequently trigger apoptosis by oligomerizing and forming pores on the mitochondrial outer membrane, resulting in release of apoptotic factors and caspase-dependent cell death [12, 13]. Antiapoptotic Bcl-2 proteins (Bcl-2, Bcl-xL, Mcl-1, Bcl-2, A-1) block the apoptotic signal by directly binding to and sequestering their proapoptotic counterparts.

Cancer cells that are particularly reliant on antiapoptotic Bcl-2 proteins holding in check proapoptotic BH3-only proteins can be thought of as being “primed for death,” with the degree of priming dependent on the relative amounts of pro- and antiapoptotic proteins present at the mitochondria [14]. This suggests that a small molecule mimetic of BH3-only proteins might be active as a single agent. Alternately, such a compound could be used as an addition to cytotoxics or other chemotherapy, in cases where cancer cells require additional stresses in order to become sufficiently reliant for survival on blockade of the apoptotic program. Also,

a significant therapeutic window should exist for a BH3 mimetic between "primed for death" tumor cells and normal cells in an "unprimed" state.

Bcl-2 and Bcl-xL have been far more strongly associated with tumor progression, poor prognosis and drug resistance in cancer than other antiapoptotic family members. Prior to the outset of this work, Bcl-xL overexpression had in particular shown a more consistent correlation with intractability of cancer cell lines than had Bcl-2. As an illustration, an informatics study on the NCI 60 tumor cell line panel showed that Bcl-xL expression had a strong negative correlation with sensitivity to both 122 standard chemotherapeutic agents and a larger set of 1,200 cytotoxic agents [15]. This correlation was not observed for either Bcl-2 or Bax, and was more significant than that between cytotoxicity and p53 status.

2 Discovery of ABT-737

2.1 Structural Aspects of Bcl-xL

The Abbott NMR group spurred internal interest in Bcl-xL by generating an NMR structure of a Bcl-xL/Bak peptide complex. The NMR group used a biologically active version of Bcl-xL with deletions of both the COOH-terminal transmembrane helix and the majority of an unstructured loop [16]. An analogous structure of Bcl-xL complexed to a Bad-derived BH3 peptide followed (Fig. 1) [17], and a fluorescent polarization binding assay (FPA) using labeled Bax peptide as a ligand was developed not long after [18]. The initial drug discovery plan was to target Bcl-xL activity as a strategy for developing a small molecule that would act primarily as a potentiator in conjunction with standard cancer chemotherapies, while at the same time trying to develop structural and biological support for Bcl-2 parallel to that already present for Bcl-xL. It was known that structural homology between the two proteins is very high, particularly with regard to the binding site. Only four active site amino acid pairs vary between the two proteins [19]. Bcl-w also has a high degree of homology to both Bcl-xL and Bcl-2, whereas Mcl-1 and A1 possess much lower homology to Bcl-2/xL. Phylogenetic analysis has shown that those latter two members of the multidomain family are more distantly related to Bcl-2, Bcl-xL and Bcl-w [20]. Additionally, a recent paper reports major structural differentiation of Mcl-1 [21]. Throughout the course of this work, compounds consistently had Bcl-w affinity that closely tracked Bcl-2, while having essentially no affinity to Mcl-1 or A1.

Antiapoptotic Bcl-2 family proteins have conserved structures consisting of two hydrophobic α-helices surrounded by six or seven amphipathic α-helices [19, 21–23]. A large (620 $Å^2$) hydrophobic groove approximately 20 Å in length serves as the binding site for BH3 domains of their proapoptotic partners. As is common to many protein-protein interaction targets, the nature of these binding surfaces greatly impacted a number of issues throughout the project [24].

Fig. 1 Cartoon-and-stick representation of NMR-derived structure of Bad BH3 peptide bound to Bcl-xL

First and foremost, it was expected that any resulting clinical candidate would quite probably be very undruglike, with greater size and lower water solubility than is desirable. However, there were other aspects of the target family that made it very appealing, beyond the relatively well-understood biology. At the inception of lead optimization, patentable chemical matter was in hand (see below). Also, there was a high degree of confidence in the ability to generate structures of inhibitors bound to target proteins, which proved to be a highly valuable asset. Thus, investigators were motivated to target antiapoptotic Bcl-2 family proteins in spite of the anticipated low probability of working in conventionally druglike chemical space.

2.2 Compound Screening and Hit-to-Lead

The effort to find lead compounds for Bcl-xL was profoundly affected by the physical nature of the target. High throughput screening (HTS) of the Abbott compound repository against Bcl-xL was performed with the FPA noted above [18]. From a collection of $>$100,000 compounds, screening produced six compounds with IC_{50}

values below 10 μM, and several other hits with double-digit micromolar affinities. Unfortunately, all of the hits were extremely large and lipophilic, although many contained carboxylic acid groups somewhere within their structures. As a corollary to this, compounds had very low binding efficiencies, as their otherwise reasonable affinity levels appeared to be driven by the sheer quantity of hydrophobic interactions, rather than good fits with the Bcl-xL surface. Failed efforts to obtain NMR structures gave evidence for, at best, a lack of distinct binding modes, while some compounds appeared to not bind at all. This latter result indicated that many compounds were probably aggregators or denaturants; these large hydrophobic compounds in a more normal setting might be immediately thrown out by inspection, but with Bcl-xL being the target, these large, hydrophobic structures were not so obviously unlikely to be true binders. Qualitatively, this result was later duplicated in subsequent top-off screens of both Bcl-xL and Bcl-2.

With more experience in dealing with such a target, this result might have been expected. Many reviews of PPIs touch on the frequent failure of HTS toward PPI targets [25, 26]; and several authors have made note of the fact that industrial compound repositories do not specialize in compounds tailored to bind to this sort of target. Typically, HTS preferentially identifies molecules with moieties that interact with a highly polar active site or recognition element – such as a "hinge" region of a tyrosine kinase – which constitutes the primary source of affinity. Moreover, compounds identified by assays as actives, but which do not possess an identifiable interacting group, are more easily recognized as being spurious hits. Bcl-xL, lacking such a strongly interacting group, recognizes widely separated hydrophobic amino acid side chains, so virtually all of the binding energy available must come from burying hydrophobic surfaces. With no high-efficiency, specificity-defining interactions, the only possibility of identifying a legitimate hit compound would be if the compound repository happened to contain a particularly good-fitting molecule that also lacked any polar groups that would fail to find complementary moieties on the protein surface. Thus, the likelihood of finding such a compound – when targeting such a large surface – was very low.

Parallel to the HTS effort, fragment screening was also employed [27, 28]. This approach, in its infancy at the time, has often proved to be well-equipped to identify "hot spots," subregions of a protein-protein interface that, through their more concave surfaces, can generate a disproportionate amount of affinity relative to the rest of the protein surface when binding an appropriate ligand [29–31]. For Bcl-xL, hot spots were identified through alanine scanning of a Bak peptide bound to Bcl-xL [16]. Alanine scanning involves systematic mutation of residues of protein surfaces in an effort to locate key binding contacts [29]. Here, versions of the Bak peptide with single alanine substitutions had their affinities to Bcl-xL measured (Fig. 2a). The largest changes in affinity came from substitution of Leu78, which resulted in a 900-fold drop in affinity to Bcl-xL, and Ile85, which produced a 310-fold reduction. These are two of the residues that, on the α-helical Bak peptide, point straight down into the hydrophobic groove of Bcl-xL, which forms more locally concave surfaces in response to the two residues (Fig. 2b). Other residues with this orientation, Val74 and Ile81, showed less of a drop in affinity

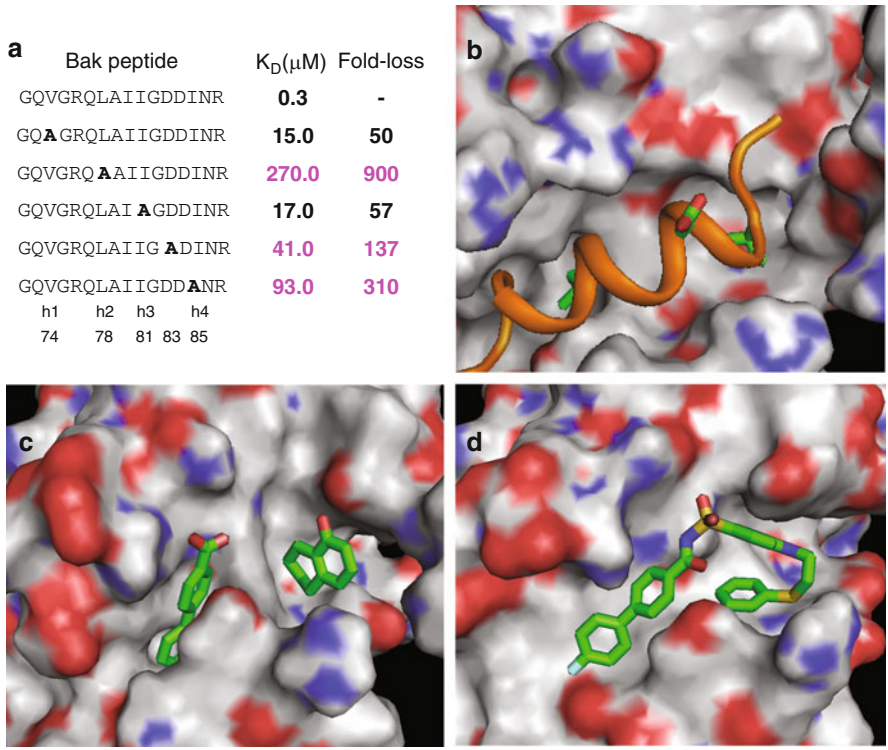

Fig. 2 (**a**) Alanine scan of Bak peptide bound to Bcl-xL. (**b–d**) Aligned views of NMR structures. (**b**) Bcl-xL/Bak peptide complex with key residues *highlighted*. (**c**) Bcl-xL complexed with fragment screening ligands **1** and **2**. The Phe97 side chain is situated between the two ligands. (**d**) Bcl-xL/**3** complex. The Phe97 side chain has rotated below the –SPh group of **3**, expanding the P4 pocket (Adapted from Ref. [34])

upon alanine replacement; therefore, of these four hydrophobic residues (h1–h4) and their corresponding interaction pockets (P1–P4), the h2–P2 and h4–P4 pairs appeared to be of particular importance. One other residue was identified by the alanine scan, Asp83, which is solvent-exposed and forms a salt bridge with Arg139 of Bcl-xL. Replacement of Asp83 with alanine resulted in a 137-fold loss of affinity.

An advantage of fragment screening is that screening libraries comprises smaller compounds which can bind deeply to hydrophobic hot spots, whereas larger compounds will often only be able to fit a part of their surfaces into them, and will bind less efficiently. The small fragments, which because of their size will individually bind with lower affinity than HTS hits, can then in theory be linked together to form a more tightly bound lead compound. For Bcl-xL, NMR screening [32] of a 10,000 compound library with an average molecular weight of 210 produced a small cluster of compounds, including the fluorobiphenyl acid **1** (Fig. 3) [33, 34]. A second round of screening in the presence of **1** produced another group

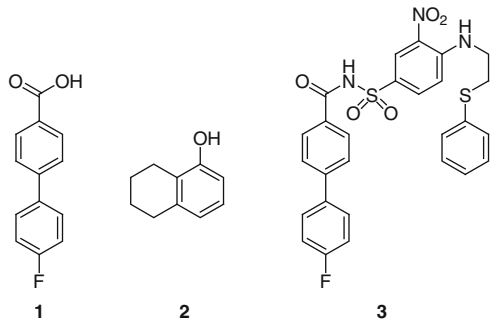

Fig. 3 Fragment screening hits **1** and **2**, and lead compound **3**

of hydrophobic compounds of similar size, such as the tetrahydronaphthol **2** (Fig. 3). Gratifyingly, the binding sites for these two compounds coincided with P2 and P4, the two major hydrophobic hot spots identified through alanine scanning [16]. In Fig. 2c, **1** and **2** are shown in the P2 and P4 pockets, and **1** is also interacting with Arg139 through its carboxylate. This provided encouragement that although the ligands **1** and **2** bound with only 300 and 4,300 μM affinities, respectively, a meaningful starting point had been identified from which to generate lead compounds.

In order to maximize the value of the two fragments, it was necessary to link them into one lead compound. However, all efforts to join the fragments, using a variety of linkers via the *ortho*-position of the benzoic acid, failed to produce a significantly more potent compound. It was eventually determined that the side chain of Phe97 was forcing the linking groups to take a more circuitous and disfavored path to the second site (Fig. 2c). Fortunately, an acylsulfonamide isostere was found to be equal in binding affinity to the acid. The acylsulfonamide pK_a was very close to that of the carboxylic acid **1**, and also provided a vector toward the second site that would not be blocked by the Phe97 side chain. This constituted a key breakthrough, as two rounds of directed parallel synthesis very quickly resulted in compound **3** (Bcl-xL IC_{50} = 93 nM, Table 1 and Fig. 3) [33, 34]. The first library synthesis, using **1** and a number of sulfonamides, produced compound **4** (Table 1), which was as potent as anything previously made in the effort to link **1** and **2**. Nevertheless, it did not appear from either modeling or NMR structural analysis that the unattractive bicyclic hydrazone was interacting with Bcl-xL. The nitroaryl group did occupy part of the P4 pocket, so a second library was made by reacting the nitroaryl **5** with ~100 amines, producing a sizable group of sub-μM compounds with hydrophobic amine tails, such as **6**. One of these compounds, the thiophenyl **3**, had noticeably better affinity than the others. Compounds with similar linking groups, such as **7** and **8**, were less potent, indicating that the dimethylene linker of **3** was near-optimal; this was verified through subsequent, more throrough medicinal chemistry work.

An NMR structure of **3** bound to Bcl-xL shows that **3** spans most of the length of the BH3-binding groove of Bcl-xL (Fig. 2d). Comparison with the tertiary complex

Table 1 Discovery of lead compound **3** by library syntheses

	Compound	R	Bcl-xL FPA IC_{50} (μM)
	4	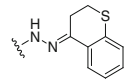	3.5
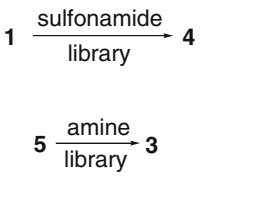	**5**	Cl	>10
	6	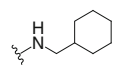	0.33
	7	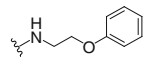	1.20
	3	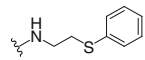	0.093
	8	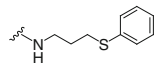	0.70

Adapted from Ref. [24]

indicates that the acylsulfonamide pulls the biphenyl group upward within the groove, and changes its angle relative to the Bcl-xL surface. This also places the acylsulfonamide group farther from Arg139 than the carboxylate of **1**, which eliminates the salt bridge. The precise nature of the interaction of Arg139 with **3** and later acylsulfonamides is not entirely clear; nevertheless, eliminating the negative charge consistently abrogated both affinity and cellular activity. Most importantly, the amine tail of **3** assumes a surprising "bent-back" π-stacked conformation within the groove, with its phenylthio group tucked under the nitrophenyl ring. In order to accommodate this hydrophobic collapse, movement of the Phe97 side chain expands the P4 hot spot, allowing the formation of an extended π-network with the Tyr194 side chain (Fig. 2d). The phenylthio group occupies the canonical h4 position, with the nitroaryl group also present in the hydrophobic pocket, as are the h4 + 4 residues of Bak and Bad. Finally, the bent-back conformation appears to be the dominant conformation in solution; thus, the molecule is largely in a preorganized conformational state, reducing the entropic barrier to target binding, and also reducing the effective surface area of **3**.

The serendipitous discovery of a ligand with the bent-back feature was important for several reasons. In addition to the large affinity gain, the conformation of **3** allowed for further growth into the region the other amine tails were occupying.

While **3** had less than an order of magnitude more affinity than some other compounds in the second library, all of this affinity came from filling the P4 pocket, so it remained to grow into the "tail" region and pick up still more affinity. Most importantly, the nitrophenyl sulfonamide **5** alone demonstrates that a single aromatic ring within P4 improves affinity by only a small amount. The bent-back conformation satisfied the P4 binding pocket in a way that might have been very difficult to access in a slower, more piecemeal fashion, as half-completed π-stacks are not particularly compelling as leads, and the expanded P4 pocket had not yet manifested as a target. Even had it done so, it would have constituted an impressive bit of design work to first target a π-stack within the pocket, and then to achieve it via such a structure.

The stacked phenyl arrangement of **3** bears little resemblance to fragment **2** in the original tertiary structure; yet, finding a second-site ligand helped validate the results of the alanine scan, and thereby set a strategy for the elaboration of **1**, which ultimately led to a ligand for the P4 pocket, which improved the binding by approximately three orders of magnitude compared to **1** and presented a clear path forward to make additional improvements.

2.3 Bcl-xL Inhibitors

Although **3** bound to Bcl-xL with a K_i of 36 nM in the FPA assay, the same assay run with 1% serum resulted in a 69-fold lower affinity. As lead compounds were very likely to continue becoming more hydrophobic during subsequent optimization, it seemed prudent to begin trying to address the serum deactivation issue immediately [35]. Most of the serum binding was traced to domain III of human serum albumin (HSA-III), as Bcl-xL/**3** affinity in the presence of the 1% serum equivalent of HSA-III alone showed a 68-fold drop. HSA-III is known to bind medium- and long-chain fatty acids and aromatic anions, which are similar in character to **3** [36, 37]. The group planned to append substituents to **3** that would be accommodated by Bcl-xL but not HSA-III, a task for which NMR-derived structures were again helpful. A comparison of two complexed structures, one of **3** bound to Bcl-xL, and the other a close analog of **3** bound to HSA-III, suggested two appropriate modification sites, where added polar groups might be expected to decrease HSA-III affinity while maintaining or improving Bcl-xL affinity [38]. The first site was that which was occupied by a majority of amine tails created in the second library synthesis. The amines used in that library were of various sizes, but almost all were nonpolar except for the amino groups themselves, and the binding data amply demonstrated that this area tolerates hydrophobic groups, in spite of its being more solvent-exposed than the binding groove proper. Polar moieties in that region, if tolerated, would also be expected to inhabit a tight hydrophobic pocket of albumin, and thus reduce the serum deactivation. Likewise, the second site identified for modifications was at the opposite, biphenyl end of **3**. Bound to Bcl-xL, **3** extends down only to the lip of the P2 region, allowing for a great deal

Table 2 SAR of changes addressed toward protein binding

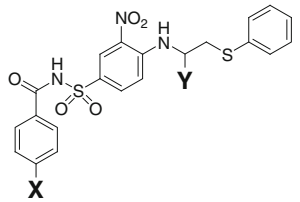

Compound	X	Y	Bcl-xL FPA K_i (μM)		FL5.12 Bcl-xL EC_{50} (μM)	
			0% HS	10% HS	Gelatin	3% FBS
3	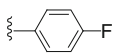	H	0.036	≫10	1.4	25
9	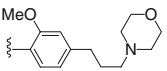	H	0.010	4.3	–	–
10	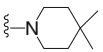	H	0.019	>10	1.2	18
11	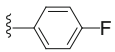		0.0035	0.35	0.72	7.8
12	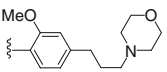		<0.0005	0.15	0.40	2.1
13	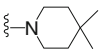		0.0008	0.50	0.47	5.1

of growth. Expectations were that affinity could be gained by adding hydrophobic groups further down the groove, but it also seemed possible that a polar group might be accommodated beyond P2 without much loss in potency. The binding groove of Bcl-xL is not as solvent-exposed as the amine tail region except at its very bottom; however, by comparison, the fluorophenyl group of the analog of **3** in HSA-III is surrounded by nonpolar residues [35]. Additionally, HSA-III is known to have low affinity to compounds containing groups such as amines, amides and carbamates; therefore, the majority of work focused on adding those groups [38].

Because the binding pockets of both HSA and Bcl-xL are able to undergo conformational changes, it was not clear if this structure-based approach would succeed. At the site near P2, appending amines or amides to the lower portion of the

groove was largely unsuccessful (Table 2). Below P2, some polar groups appeared to lessen serum deactivation, and did not reduce affinity, such as with **9**, but the overall effect was smaller than hoped for. Although amides and basic amines seemed to have a small serum effect, even at the bottom of the groove there was a sensitivity to charge state, as the less basic morpholine of **9** produced the highest affinity. Also, polar groups needed to be situated very far down toward the P1 end of the binding groove in order to be tolerated at all. The end result of this was less atom-efficient compounds, and a synthetic dead end. However, by substituting various rings for the fluorophenyl group of **3**, the piperidine of **10** was found to provide similar affinity and reduced serum deactivation in a much more atom-efficient manner, and this compound also provided a hope of further elaboration in the future.

In short, it proved impossible to situate a polar group inside of the binding groove without sacrificing a great deal of affinity. This proved true on a number of other occasions during lead optimization, where in the course of SAR work on each substructure of lead compounds, appending or substituting polar groups invariably caused a meaningful loss of affinity or potency. The only exception to this lay in changes made outside of the binding groove. With regard to the second modification site, amines (**11**) built off of the CCSPh tail provided not only a small affinity boost in the binding assay – commensurate with what was achieved in this area with nonpolar groups – but greatly improved affinity in the presence of serum, and activity in the cell assay. A two-atom linker with R-stereochemistry was found to be optimal for cellular potency. Amides and less basic amines had more moderate effects [35]. Combining the best modifications at both sites gave compounds **12** and **13**, which had much better affinity in the presence of serum, and showed submicromolar activity in cells.

Several compounds in addition to **12** and **13** began to show mechanism-based levels of cellular activity, with EC_{50} values distinct from those of enantiomers or other compounds with weaker affinity. Cellular data were obtained using Bcl-xL-transfected FL5.12 cells in both the absence and presence of 3% fetal bovine serum (FBS). FL5.12 is an IL-3 dependent murine pro-B lymphoid cell line characterized by low to moderate Bcl-xL and Bcl-2 expression levels. Transfection with human Bcl-xL produced cells expressing roughly tenfold higher protein levels, allowing them to survive in the absence of IL-3. **13** was effective in negating the survival advantage toward cytokine withdrawal provided by Bcl-xL expression. Additionally, **13** was found to enhance the cytotoxic activity of UV radiation and multiple cytotoxic agents against human tumor cell lines. However, **13** had little or no single agent efficacy against a broad panel of tumor cell lines [39].

While **13** had good affinity toward Bcl-xL ($K_i = 0.8$ nM), it bound much less tightly to Bcl-2 ($K_i = 67$ nM). A wealth of literature existed on the importance of Bcl-2 in cancer, particularly the identification of the t(14;18) chromosomal translocation involving Bcl-2 overexpression in non-Hodgkin's lymphoma [40]. At roughly this stage of the discovery effort, a stable, soluble Bcl-2 mutant also became available. One mutant had the same COOH-terminal deletion as the Bcl-xL construct, along with the deletion of most of the unstructured loop. However, the remaining 15 residues of the unstructured loop are much more hydrophobic in Bcl-2 than in Bcl-xL, and it proved beneficial to use the corresponding residues of Bcl-xL

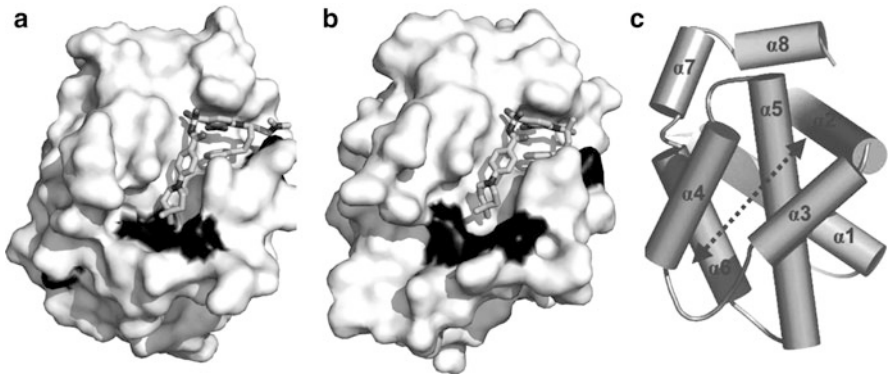

Fig. 4 (**a**, **b**) X-ray structures of **13**/Bcl-xL and analog/Bcl-2 complexes. Connolly surfaces deriving from amino acid changes are in *black* and are at P2, Ala104Asp and Leu108Met (α3), and Ser122Arg (α4), and outside P4, Glu96Asp. (**c**) Schematic of 3D structure of Bcl-xL and Bcl-2 with labeled helices. The *dotted line* is the axis of the binding groove (Reproduced by permission of The Royal Society of Chemistry, Wendt [42])

for the truncated loop of the Bcl-2 construct [19]. With this new version of Bcl-2, analogous FPA and FL5.12 assays were introduced for Bcl-2, and structure-based design of compounds via NMR- and X-ray-derived complexed structures of Bcl-2 began to contribute to the design process, just as with Bcl-xL. Focus turned to broadening the effect of project compounds by improving their potency against Bcl-2.

2.4 Dual Bcl-xL/Bcl-2 Inhibitors

Assaying previously synthesized compounds against Bcl-2 showed that most of the more elaborated compounds were, like **13**, roughly 100-fold selective for Bcl-xL. In other words, this was not unexpected, as compounds had up to this point been optimized solely against Bcl-xL. Yet, the exact source of this selectivity was somewhat mysterious, as the tertiary structures of the proteins are very similar [19, 41]. Figure 4 compares X-ray structures of a **13**/Bcl-xL complex and a Bcl-2-complex of a close analog of **13** without the amine tail, with the black surfaces deriving from residues that differ between the two proteins. The surfaces involved in binding to project compounds up to this point were essentially identical, particularly in the P4 area. It was later determined that the Glu96Asp change from Bcl-xL to Bcl-2 was responsible for some of the Bcl-xL selectivity of compounds with an amine tail, such as **13**. The longer glutamic acid side chain of Bcl-xL makes a closer interaction with amines than the corresponding Asp of Bcl-2. The presence of an amino group was in any case required, and was maintained going forward.

Most of the structural differences between the two proteins appeared to be in portions of the binding groove that had yet to be accessed. The Bcl-2 groove is very slightly wider than the Bcl-xL groove throughout, and appears to extend a bit farther down beyond P1, due to slightly different folds of the α3 helices forming

the right-hand sides of the grooves; these differences could not have been predicted from the secondary structures of the two proteins. It is clear from Fig. 4, however, that the major structural differences lay in or near the P2 hot spot. Three amino acid changes, two at the end of the α3 helix, and one at the beginning of α4, account for the structural changes. The most important of these is the substitution of Met108 in Bcl-2 for Leu108 in Bcl-xL. The more flexible side chain of the methionine allows for more distortion of the Bcl-2 structure around P2. Accessing this pocket more effectively, and growing compounds in that direction was expected to increase affinity to both proteins, and to preferentially increase Bcl-2 affinity.

Accordingly, the medicinal chemistry group began to probe this area with increasingly large hydrophobic groups [43]. Chemists built off of the vectors provided by the 4,4-disubstituted piperidine of **13**, in anticipation that one vector could be used to interact with the protein surface while the other, projecting toward solvent, could be used to attach a polar group that might both improve solubility and decrease protein binding. A 4-piperidone building block allowed for easy access to a series of methoxy-containing compounds such as **14–16** (Table 3). This series, as hoped for, registered improved Bcl-2 affinity with increasing bulk, with the benzyl group essentially achieving parity between Bcl-2 and Bcl-xL. Within this series, *ortho*-substitution was preferred, and eventually led to the *ortho*-phenyl **16**. The methoxy group was replaced with more polar moieties, again with particular concentration on amides and amines. These compounds were equipotent to their corresponding methoxy compounds in binding assays, but were more than tenfold less potent in cellular assays, again demonstrating the hazards of adding polar surface area to these large molecules.

Also from the 4-piperidone intermediate, a series of 4-benzylidene piperidines was accessed, which provided a different vector for the hydrophobic group and eliminated the ineffective polar group pointing into solvent. Simple benzylidenes such as **17** were effective in both improving the affinity against Bcl-2 and in improving the potency in the FL5.12 cell assay, but although the hydrophobic groups in the ortho-position were again the preferred mode of substitution, these substituents did not improve compound performance to the same degree as in the disubstituted piperidine series. Instead, larger substituents (**18**) seemed to occupy a plateau of potency defined by the trifluoromethyl group of **17**. It became apparent that the benzylidene geometry, much different from that of the benzylpiperidine, prevented optimal interaction with the P2 regions of the Bcl-2 and Bcl-xL surfaces [43].

Replacing the piperidine ring with a piperazine created a different synthetically tractable isostere that also eschewed the polar substituent, and supplied a vector for a hydrophobic group that differed only slightly from that of the disubstituted piperidine. Based on the experiences with situating amino groups near and below P2, as with **9** or **12**, a small potency drop was expected due to the basicity of the piperazine. There did prove to be a small cost associated with the piperazine, as for example, the benzyl **19** was somewhat less potent than the corresponding piperidine **15**. However, with further elaboration this series became equipotent with piperidines, and the ortho-phenyl **20** proved equal to or better than the corresponding piperidine **16**.

As a result, neither the FPA nor the serum-free FL5.12 assay was able to distinguish between the best compounds, and the FL5.12 assays with 3% serum

Table 3 SAR of P2-targeted groups

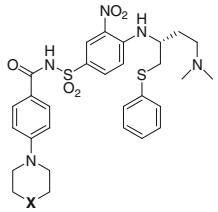

		FPA (nM)			FL5.12 cells (μM)	
		K_i		10% HS	EC_{50}	
	X	Bcl-2	Bcl-xL	Bcl-xL	Bcl-2	Bcl-xL
13		67	0.8	360	2.2	0.47
14	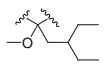	2.2	<0.5	140	0.40	0.33
15	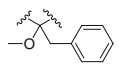	8.1	1.8	150	0.93	0.68
16	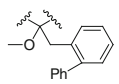	<1.0	<0.5	35	0.020	0.035
17		2.0	<0.5	300	0.21	0.15
18		<1	<0.5	83	0.18	0.16
19	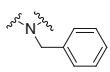	40	2.6	300	1.7	1.1
20	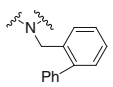	<1.0	<0.5	37	0.016	0.018
21	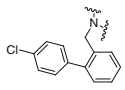	<1.0	<0.5	<60	0.008	0.030

Adapted from Ref. [24]

(FBS) drove further work. EC_{50} values for **20** in that assay were 1.3 and 1.2 μM for Bcl-2 and Bcl-xL, respectively. Further, SAR work on the terminal phenyl ring showed that nonpolar para groups promoted superior efficacy in the presence of serum [43]. Although **20** and the chloro-substituted **21** appear similar based on the data in Table 3, in the 3% serum FL5.12 assay **21** improved to 0.050 and 0.22 μM

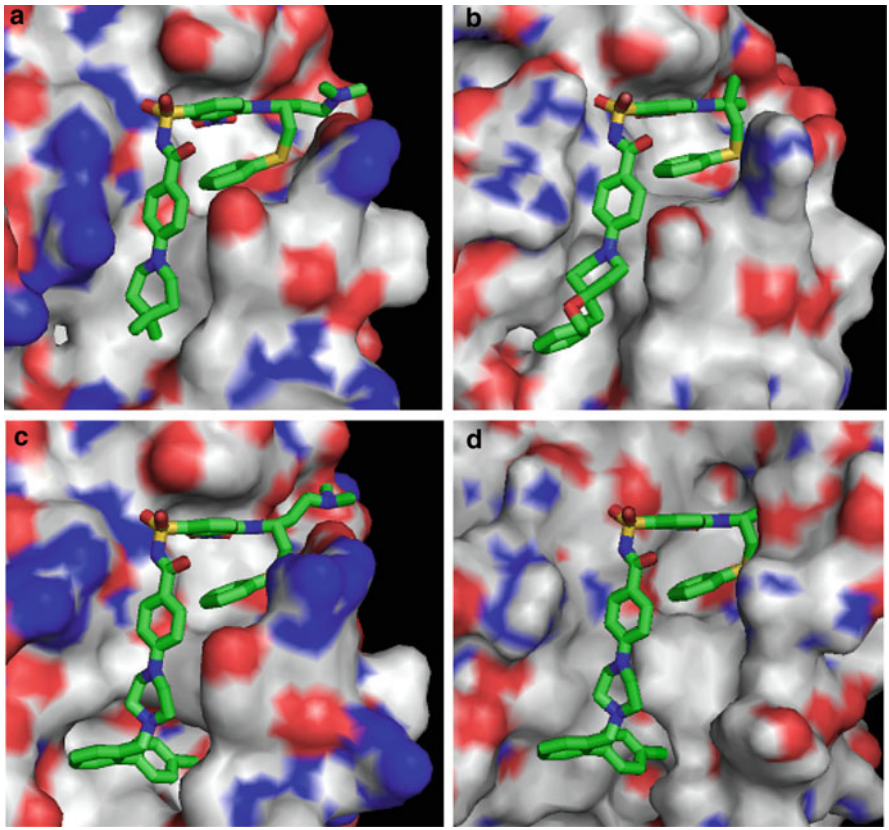

Fig. 5 Aligned Connolly surfaces of inhibitors bound to Bcl-xL. (**a**) X-ray structure of **13**. (**b**) NMR structure of derivative of **15**. (**c**) X-ray crystal structure of ABT-737 (**21**). (**d**) Structure of **21** overlaid onto Bcl-xL surface derived from NMR structure of Bcl-xL/Bad peptide complex (Reprinted with permission from Informa Healthcare, Wendt [24])

for Bcl-2 and Bcl-xL, respectively. Interestingly, as the corresponding methoxypiperidine compound did not show the same late improvement with para-additions, it appears that it was not able to situate the terminal phenyl group within P2 in quite the same way. Compound **21** thus achieved >250-fold (Bcl-2) and >20-fold (Bcl-xL) better potency than the piperidine **13**, further illustrating the success of the strategy for introducing more Bcl-2 affinity, and **21** was identified as the first development candidate, ABT-737.

It was particularly helpful during this part of the project, centering on the development of a ligand for the P2 pocket, to obtain a number of NMR and X-ray crystal structures of bound compounds. These structures indicated a profound capacity of both Bcl-2 and Bcl-xL to alter their structure in the vicinity of P2, an effect that is now understood to be very common among protein-protein hot spots [44]. Figure 5 shows four structures of compounds bound to Bcl-xL, illustrating a

great deal of conformational flexibility in this part of the protein surface. Compared to **13**, a version of the 4-methoxy-4-benzylpiperidine, **15**, with a different h4 tail only causes a slight change in the protein surface. However, **21** achieves a much greater degree of penetration into an expanded P2 hot spot induced by the ligand [45]. Many other compounds produced varying degrees of induced changes in the P2 protein surfaces of both Bcl-xL and Bcl-2. Figure 5c, d show that the deep P2 and P4 pockets induced by **21** are similar to those induced by the Bad peptide, although the hot spots are better defined in the Bcl-xL/**21** structure [17], as the much larger peptide ligand creates a wider binding groove and the presence of the N-terminal tail induces additional changes to the loop between helices 3 and 4. It is not clear from the above compound development if efficient P2 occupancy bears some intrinsic Bcl-2-selectivity; however, Bcl-2-selective compounds have been reported that bind only to P2 and the lower part of the groove [46–48].

2.5 ABT-737 as a Tool Compound

ABT-737 (**21**) has excellent activity against primary patient-derived samples of follicular lymphoma [34], and the primary chronic lymphocytic leukemia (CLL) cells are extremely sensitive, undergoing rapid apoptosis upon ABT-737 treatment ($EC_{50} = 4.5$, 7.0 nM) [49, 50]. This activity appears to be independent of prior treatment history and prognostic factors associated with CLL progression.

ABT-737 has been supplied to, and is still being used by a large number of outside research groups. Many of these laboratories have shown ABT-737 to be very effective ($EC_{50} < 100$ nM) in primary patient samples of multiple types of blood-borne cancers [51–57]. Also, ABT-737 has been shown to have single-agent activity against small-cell lung cancer (SCLC) cell lines [34, 58]. Overexpression of Bcl-2 occurs in 55–90% of SCLC cases, and may be important in the initiation, growth and apoptotic resistance of SCLC [59–63]. Efficacy in combination chemotherapy has been shown with etoposide in SCLC xenograft models [64], and in several other settings [65–67]. Additionally, the selectivity of ABT-737 within the Bcl-2 protein family has rendered it invaluable as a tool compound for biological studies. Several laboratories have used ABT-737 to further the understanding of mechanisms of action of Bcl-2 family proteins [49, 50, 68–70]. In particular, confirmation of Mcl-1 as a resistance factor and identification of settings in which Mcl-1-derived resistance may be circumvented, have been the subject of a number of reports [51, 55, 71, 72].

3 Discovery of Navitoclax (ABT-263)

3.1 Orally Bioavailable Derivatives of ABT-737

The extremely low water solubility (<1 μg/mL) and high lipophilicity of ABT-737 made IV formulation particularly challenging. Additionally, preclinical animal models had demonstrated that ABT-737 was maximally efficacious when dosed on a continuous, daily basis. While ABT-737 was in preclinical development, then, discovery work continued with the goal of discovering an orally bioavailable compound with similar potency within the acylsulfonamide series [73]. Given the high molecular weight (813), high lipophilicity and poor oral pharmacokinetics (~5% F) of ABT-737, the chance of success in this endeavor may have been considered too unlikely to invest resources in. However, the group already had in hand examples of small modifications to ABT-737 that imparted greatly improved oral plasma levels. In Table 4, data for two close analogs of ABT-737 from a pharmacokinetic (PK) screen using Sprague-Dawley rats are shown. In the first, substitution of a morpholine for the dimethylamino group (**22**) produced a fourfold improvement in plasma levels, which later proved to be a typical shift for dimethylamine-morpholine compound pairs. However, the morpholine substitution also reliably produced a roughly commensurate decrease in potency both in vitro and in vivo. Similar, though more profound, changes resulted from replacement of the nitro group with a trifluoromethyl to give **23**. This compound had vastly improved oral PK, with both much higher plasma levels and a long half-life, but again, this was accompanied by an equally large drop in cellular potency, The functional outcome of these often competing effects was measured with the ratio AUC/EC_{50}, which used data from the rat PK model and a cellular assay using H146 cells, a SCLC line expressing high levels of Bcl-xL and some Bcl-2, in 10% serum, thus taking into account both plasma exposure and cellular potency. This PK/PD ratio showed that neither **22** nor **23** constituted an overall improvement, but the compounds did demonstrate that ABT-737 could be modified to make derivatives that had acceptable PK parameters. It was then a matter of finding modifications to ABT-737 that had similar effects on pharmacokinetics but maintained potency.

Much of the post-ABT-737 medicinal chemistry concentrated on modifications to these two areas. This had the added benefits of addressing two other issues. First, dimethylamino group demethylation constituted a small metabolic liability, and any new amino functionality would probably result in an improvement in that area. Second, although the nitro group had never shown more than trace metabolism in various assays, it remained a potential toxicology concern. To these two areas of focus was added a third, consisting of further work on the h2 fragment. This was undertaken not because of any expectation of PK effects similar to the other two areas of concern, but because as the chlorobiphenyl group of ABT-737 was installed near the end of that phase of the project, SAR of that part of the molecule had not yet been fully explored. The three areas were investigated simultaneously at first, under the assumption that effects of modifications in each area would be independent of one another.

Table 4 Rat pharmacokinetic parameters of ABT-737 (**21**) and derivatives after 5 mpk oral dose

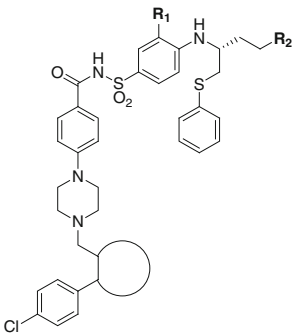

	Ring	R_1	R_2	AUC[a]	F%	EC_{50}[b]	AUC/EC_{50}
21		NO_2		0.23	5.9	87	2.6
22		NO_2		0.99	16	570	1.7
23		CF_3		3.7	24	2,200	1.7
24		SO_2CF_3		0.87	8.7	39	19
25		SO_2CF_3		0.91	13	21	43
26		SO_2CF_3		2.9	14	28	104

Adapted by permission of The Royal Society of Chemistry, Wendt [42]
[a]0–8 h, μg/mL
[b]nM, H146 SCLC cells, 10% serum

3.2 Compound Optimization

Immediately after the discovery of **3**, extensive substitution of the nitro group had been performed, and this was periodically revisited throughout the project. While initially, groups such as chloro and trifluoromethyl were close to the nitro in affinity, none of the substitutions or modifications synthesized produced compounds that were adequate in terms of cellular potency. In fact, at this point in the project, the 30-fold less potent trifluoromethyl substitution noted above was the next-best option at that position. However, as oral pharmacokinetics now became a priority, many substitutions in addition to the trifluoromethyl group outperformed the nitro group, although to a lesser extent, in the rat PK model. It soon became clear that the nitro group was in fact a particularly poor substituent as regards oral bioavailability. Ultimately over two dozen compounds with different aryl substitutions were examined. Most of these were solely replacements for the nitro group, while some others explored additional fluoro substitutions on the aromatic ring, as that seemed a way to modify the acidity of the acylsulfomamide without greatly altering hydrophobicity.

The result of this was that a very strong correlation between lower acylsulfonamide acidity and higher oral exposure was found. This indicated that a reduction in charged species was a strong determinant of absorption. However, an equally strong correlation was found between lower acidity and a reduction in cellular potency. Additionally, the binding pocket seemed to require a relatively lipophilic group for good affinity, so most electron-withdrawing groups were complete failures, as they had been in past SAR studies.

The mostly contradictory requirements of small size, high lipophilicity and strong electron-withdrawing capability resulted in a near-monotonic tradeoff between potency and oral exposure. It was surprising, then, that a substituent was found that did not adhere to this tradeoff. One nitro replacement that had been looked at during a very early stage of the project was a methylsulfonyl group, which, seemingly too polar and perhaps too large, fared poorly. At this time, the same substitution again resulted in a much less potent compound, and also did not perform well enough in the rat PK assay to warrant further consideration. However, when further modification produced compound **24**, with a trifluomethylsulfonyl, or trifloyl group, small improvements over the nitro group in both potency and oral exposure were achieved. Table 4 shows an eightfold improvement in the AUC/EC_{50} ratio for **24** compared to ABT-737 (**21**). The trifloyl group has similar electron withdrawing capacity to a nitro group, producing a similar acylsulfonamide pK_a, and is relatively lipophilic, but, based on nitro-containing X-ray structures, it seemed to be too large to bind with high affinity, barring a never-before-seen change in the P4 surface. This modification did not seem to impact Bcl-2/Bcl-xL potency ratios. Trifloyl compounds routinely outperformed nitro compounds going forward, and the latter group was eventually abandoned.

Extensive P2 ligand SAR work had already been performed on the terminal ring, but changes to the nonterminal phenyl had not been studied. Here, attempts were once again made to append polar groups to the solvent-exposed ring; and once again, these changes failed to improve pharmacokinetic properties and were often deleterious to potency. Changing the phenyl ring to an unsaturated or partially saturated heterocycle produced similar results. However, replacing the phenyl ring with cyclohexenes produced compounds that maintained the placement of the chlorophenyl group. These notably maintained the potency of the aromatic compounds, and also exhibited higher oral plasma levels (**25**, Table 4). The cyclohexene provided an opportunity to make ring modifications that were fundamentally different from those that were made to the aromatic ring in its place. Simply bulking up the ring by adding alkyl groups produced the dimethylcyclohexene **26**, which had still higher plasma levels, and also appeared to improve tissue/plasma distributions in various pharmacokinetic models.

At the third modification site, the consistent jump in AUC values of morpholine-containing compounds led to the hypothesis that, as with the acylsulfonamide, groups decreasing the amount of charged species present at a given moment and pH in the digestive tract should increase absorption. Several other oxygen-containing mono- and bicyclic amines were then targeted. Most of these produced

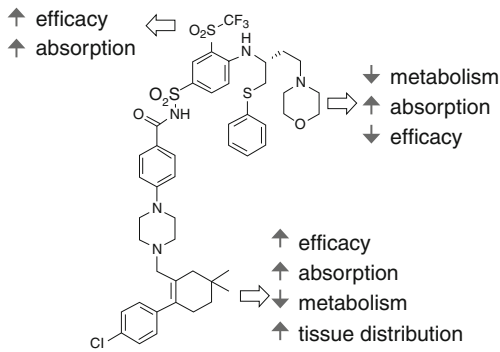

Fig. 6 Summary of changes made to ABT-737 (**21**) to produce navitoclax (**27**) (Reprinted with permission from Informa Healthcare, Wendt [24])

small improvements in absorption, but the morpholino group, with its roughly three-pK_b unit drop in basicity, regularly provided the highest oral exposures, albeit accompanied by a loss of potency. Bulkier alkylamines, such as isopropylmethyl or pyrrolidino, also improved PK parameters. All of these changes seemed to produce the additional benefit of a decreased metabolic liability relative to the dimethylamino group, as expected.

Ultimately, a select few compounds with combinations of the best functional groups were compared in various animal efficacy and PK/PD models. On the basis of these studies, **27** was chosen as the next development candidate, ABT-263, which was later renamed navitoclax [73]. As is summarized in Fig. 6, at the former nitro and phenyl positions, both potency and various pharmacokinetic inputs were improved, while the morpholine sacrificed some of the gained potency for a more critical further improvement in oral absorption. The end result is a compound with very similar activity to ABT-737, but a much improved pharmacokinetic profile.

In solving the pharmacokinetic issues associated with ABT-737, an even larger compound was produced. Navitoclax (**27**) has a MW of 974, is still highly protein bound ($\geq$99%) and has extremely low aqueous solubility, but is also more metabolically stable, has better tissue distribution and, most importantly, has a lower overall charge at physiologically relevant pH ranges. Navitoclax has low intravenous clearance values and low volumes of distribution across multiple species, and also has a very long dissolution rate-limited absorption phase as a result of its low solubility (Table 5) [74]. Additionally, the use of lipid-based formulations increases absorption and significantly enhances pharmacokinetic parameters.

Navitoclax, like ABT-737, has a very Bad-like binding profile, with high affinity for Bcl-2, Bcl-xL and Bcl-w, but not Mcl-1 or A1 (Table 6) [74]. Navitoclax is slightly more potent than ABT-737 against FL5.12/Bcl-2 cells (EC_{50}s 6 vs. 8 nM) and FL5.12/Bcl-xL cells (4 vs. 30 nM), and was very comparable to ABT-737 across a range of in vivo studies. Navitoclax induces complete tumor regressions in SCLC and ALL xenograft models, and potentiates clinically relevant regimens in lymphoma and multiple myeloma models [74–77]. Navitoclax is currently in

Table 5 Multispecies PK of navitoclax (**27**)

Species	Oral dose (mg/kg)	$t_{1/2}$(h)	C_{max} (μg/mL)	AUC (μg•h/mL)	F(%)
Mouse[a]	50	5.7	5.46	55	21
Rat[b]	5	6.5	0.67	7.5	22
Monkey[b]	2.5	n.d.	0.43	6.4	13
Dog[b]	2.5	5.6	3.67	27	22
Dog[c]	5	8.9	–	–	48

Reprinted with permission from Informa Healthcare, Wendt [24]
n.d. Unable to determine
[a]Delivered in 2% DMSO, 5% Tween80, 20% propylene glycol, 73% D5W solution
[b]Delivered in 10% DMSO in PEG-400
[c]Delivered in 10% EtOH, 30% PEG-400, 60% Phosal 50-PG solution

Table 6 Binding of hBad, ABT-737 (**21**) and navitoclax (**27**)

	FPA serum-free K_i (nM)				
	Bcl-xL	Bcl-2	Bcl-w	Mcl-1	A1
hBAD[a]	0.5	15	33	4,800	>10,000
ABT-737 (**21**)	<0.5	<1	0.9	>1,000	>1,000
navitoclax (**27**)	<0.5	<1	<1	550	>3,000

Adapted and reprinted by permission from the American Association for Cancer Research, Tse et al. [74]
[a]103–127: NLWAAQRYGRELRRMSDEFVDSFK

Phase II studies as a single agent for leukemia/lymphoma and in combination therapies for leukemia/lymphoma and solid tumors.

4 Perspective

As discussed above, the dominant characteristics of Bcl-2 family proteins, even when compared only to the family of pharma-targeted PPIs, are the size and hydrophobicity of the binding sites. This first impacted the project when trying to discover chemical matter. In addition to size and hydrophobicity contributing to the failure of HTS, a more specific feature – the large distance between hot spots for both Bcl-xL and Bcl-2 – can be seen as a separate, additional difficulty. As a comparison, a number of groups studying MDM2/p53 disruption were able to find lead compounds that accessed MDM2 hot spots through high-throughput screening protocols [78]. MDM2, like Bcl family proteins, binds to an α-helical segment of its binding partner, but the key side chain presentations of p53, corresponding to MDM2 hot spots, are separated by one helical turn, not two. Here, the compounds found were unworkable from a drug discovery standpoint, effectively necessitating the use of fragment screening. Moreover, it is not even clear that the compounds that were identified by HTS meaningfully accessed the key regions of the protein. As hot spots become further separated in space, the entropic, enthalpic or

pharmacokinetic costs inherent in a sufficiently large scaffold become increasingly prohibitive. With regard to Bcl-2 family proteins, investigators have searched for ways around the energetic aspects of this problem by employing organic synthesis-derived backbones with minimal degrees of freedom [79], and by rigidifying endogenous helical ligands [80]. Methods such as these may ultimately provide some generality as solutions to finding sufficiently druglike inhibitors of α-helix-binding proteins, but these structural approaches must also confer sufficiently drug-like characteristics upon their resulting molecules.

Proponents of the hot spot paradigm would note that the P2 and P4 hot spots were found by fragment screening, even though the fragments themselves were of insufficient size to induce local surfaces similar to those found in the native protein-ligand interaction, as a comparison of Figs. 2c and 5c, d illustrate. This contrasts with a typical enzyme-targeted process, where the active-site-binding moiety is normally established at the outset, whether as the result of screening or design, and is not radically modified unless ADMET issues necessitate it.

Both ABT-737 and navitoclax have extremely high affinities to their targets, with FRET K_i values of ~80 pM. One issue that has made many PPI targets unattractive to pharma is that the strength of the native binding event is either known, or assumed to be, extremely high. Surface plasmon resonance (SPR) measurements have shown ABT-737 to have affinity similar to or slightly better than a BH3 domain (130 vs. 140 pM for Bim BH3 by this method). High affinities toward hydrophobic targets require large molecules, as again, affinity must be disproportionately driven through relatively weak hydrophobic interactions. One point that may be overlooked is that it is primarily not the size of the binding regions of Bcl-xL/Bcl-2, but their character that is responsible for the need for inhibitors to be large. Although an inhibitor does not need to physically block the entire binding surface in order to disrupt protein binding, it is unlikely that a smaller compound could achieve affinities toward Bcl-2 and Bcl-xL necessary for biological activity without being so large. While it would be imprudent to suggest that inhibitors meaningfully more ligand-efficient than navitoclax cannot be found, it seems very unlikely that a sufficiently potent compound could be made that does not interact with both P2 and P4. As compounds in this series do not extend very far beyond P2 and P4, it also seems likely that any similar or more potent inhibitors of Bcl-xL/Bcl-2 would also be similar in size. If P2 or P4 possessed the capacity for polar interactions, a sufficiently potent inhibitor could perhaps be obtained by interacting with only one of P2 and P4, but in the real world, with nonpolar P2 and P4 pockets, such a state of affairs would probably produce a compound like **13**, which is not potent enough to show much biological activity.

Another way to look at the binding efficiency issue is to track the progression in size and potency of lead compounds throughout this effort. The ligand efficiency of compounds toward Bcl-xL – once the initial biphenyl acid hit was “optimized” to an acylsulfonamide – remained roughly constant, with small improvements when P4 and P2 optimization occurred. This result is in line with the findings of a study done at Abbott that examined progressive lead structures of a number of projects. This study showed that the efficiency of the ultimate clinical or preclinical

candidate is essentially "locked-in" at the initial lead stage [81], probably due to the common situation where the first lead structure already has in place a group making the strongest interaction possible within the binding pocket, with further elaboration consisting of matching of hydrophobic and hydrogen bonding surfaces. This again lays the problem of low ligand efficiency of ABT-737 and navitoclax at the feet of the absence of and impossibility of such a strong binding interaction in the hit compounds.

It is of note that as the project began with fragments obtained from NMR screening and ended with extremely potent compounds, the affinities of compounds ranged from K_i values of ~10^{-4} to $\ll 10^{-9}$. Because of this, several different assays drove the discovery process at different times. As affinity increased, the standard FPA gave way to versions of the FPA run in the presence of 1%, and then 10% serum. During this transition, cellular assays were introduced, and progressed from using FL5.12 cells in gelatin, to FL5.12 cells in 3% FBS, and eventually to more robust H146 cells in the presence of 10% serum. During the PK optimization phase of this program, as noted above, medicinal chemists were guided almost exclusively by the H146 cell assay and various PK and ADMET assays.

As discussed previously, NMR and X-ray crystal structures were very helpful to the medicinal chemistry effort. Initially, it was important to verify that fragment screening hits **1** and **2** did in fact find hydrophobic hot spots. Also, a great deal of chemists' time and effort would certainly have been misdirected had the Bcl-xL-bound structure of **3** with its surprising binding mode not been quickly determined. Likewise, the first structures showing the expanded P2 hot spot hastened the understanding of how the additional binding energies of compounds such as **16** and **21** were derived, and why some other large h2 fragments failed to accomplish the same thing. The medicinal chemistry team not only learned to rarely rule out a target compound due to a perceived lack of fit, but chemists actually began to consciously design compounds that would appear from previous structures not to fit into P2; i.e., work moved toward compounds that "challenged" the hot spot to distort itself further, becoming more concave and creating an opportunity for more efficient binding. The end result of this is that while P4 was efficiently liganded early in the drug discovery process, in a very short amount of time, true P2 optimization was gradual, and did not conclude until the synthesis of the last group of para-phenyl-substituted piperazine-series compounds, such as **21**. In general, the series of structures produced throughout this project repeatedly illustrated the now-familiar dynamic nature of the contact surfaces in and near the hydrophobic hot spots [44, 82].

As navitoclax and related orally bioavailable project compounds lie well outside the areas of compound space commonly designated as being druglike, it is worth discussing possible contributors to the "outlier" nature of navitoclax. First, while the molecular mass of 974 suggests a far larger molecule than is normally targeted, mass must be seen as a somewhat misleading proxy for molecular size. The trifloyl group of navitoclax adds a large amount of mass (87 Da) relative to the nitro group of ABT-737, but is only slightly larger. The hydrophobic collapse leading to the "bent-back" conformation not only reduces the effective surface area, but also effectively freezes several rotatable bonds. Additionally, several more of the

17 rotatable bonds of navitoclax are relatively trivial, i.e., those associated with rotation of the rings of the phenylpiperazine or the terminal chlorophenyl group. Only the bonds associated with the amine tail, and the bonds between the piperazine and chlorobiphenyl "create" much conformational space. Many of these points apply to ABT-737 and earlier compounds as well as to navitoclax, but post-ABT-737 work demonstrated that morpholino and nonnitro manifolds were heavily populated by compounds with significant plasma levels. Thus, the positive and negative charges on the molecules seem to be by far the largest contributors to poor bioavailability, and the broader class of these large, hydrophobic acylsulfonamides generally possesses low, but workable plasma levels.

As the above story makes clear, in the early stages of the project, the medicinal chemists put a great deal of effort into improving the water solubility of lead compounds. The lack of success in this venture was probably critical to the success of the project as a whole. While it is difficult to imagine a tight-binding Bcl-2/xL inhibitor with meaningful water solubility, such a molecule, if it did exist, would have had to possess a very high polar surface area (PSA). This probably would have in turn resulted in very poor oral absorption. Extensive literature attests to the importance of low polar surface area for orally bioavailable compounds [83–85]. Navitoclax, with a PSA of about 140 $Å^2$, is within the realm of acceptable values for this parameter, as <150 $Å^2$ is a common guideline [86]. While ideally the medicinal chemist wants both aqueous solubility and a low PSA, in practice it is difficult to satisfy both of these when the molecule in question is very large. Both of these are means to an end – good absorption – and not ends in themselves. By ultimately following that end directly during the last stage of the project, in performing first-pass pharmacokinetic assays on dozens of compounds, the group was left with low-solubility, high-lipophilicity compounds, probably the only plausible positive outcome. Also, the early concentration on targeting tolerated polarity toward minimization of protein binding was probably a good strategy.

It is not known whether navitoclax is transported in an active or passive manner. The clear dependence of oral bioavailability on charge state for this series of compounds constitutes suggestive evidence for the latter, and the repeated experience of seeing more polar compounds maintaining affinity but losing cell activity argues for a general loss of cell-penetrating ability. Nevertheless, active transport is certainly possible, as a number of already identified transporters are known to transport anionic high-molecular weight drugs [87], in particular the SLC22 [88] and OATP/SLCO [89] families. Regardless of the answer in this particular case, the possibility of active transport as a meaningful contributor to oral bioavailability for large lipophilic drugs in general remains.

In pursuit of PPI targets, several ideas and strategies have been popularized. The hot spot paradigm, alanine scanning, and fragment screening were all instrumental in the early part of this particular discovery effort. Later, structure-based design was of particular benefit in understanding how to approach the hydrophobic hot spots. Although the list of PPI drug targets that have yielded clinical candidates continues to grow, there are still very few inhibitors of noncontiguous-surface-interacting PPIs that have reached the clinic. It would be premature to draw conclusions based

on the experiences from a single project about the viability of this subgroup of PPIs as drug targets. Nevertheless, this example provides something of an indication that potential targets with similarities to Bcl-2 family proteins need not be automatically rejected, and the chances of success may be higher than were once believed.

References

1. Danial NN, Korsmeyer SJ (2004) Cell death: critical control points. Cell 116:205–219
2. Thompson CB (1995) Apoptosis in the pathogenesis and treatment of disease. Science 267:1456–1462
3. Reed JC (2000) Mechanisms of apoptosis. Am J Pathol 157:1415–1430
4. Strasser A, Huang DC, Vaux DL (1997) The role of the bcl-2/ced-9 gene family in cancer and general implications of defects in cell death control for tumorigenesis and resistance to chemotherapy. Biochim Biophys Acta 1333:F151–F178
5. Guchelaar HJ, Vermes A, Vermes I, Haanen C (1997) Apoptosis – molecular mechanisms and implications for cancer-chemotherapy. Pharm World Sci 19:119–125
6. Reed JC (1995) Bcl-2 family proteins: regulators of chemoresistance in cancer. Toxicol Lett 82 (83):155–158
7. Youle RJ, Strasser A (2008) The BCL-2 protein family: opposing activities that mediate cell death. Nat Rev Mol Cell Biol 9:47–59
8. Green DR, Evan GI (2002) A matter of life and death. Cancer Cell 1:19–30
9. van Delft MF, Huang DC (2006) How the Bcl-2 family of proteins interact to regulate apoptosis. Cell Res 16:203–213
10. Huang DCS, Strasser A (2000) BH3-only proteins – essential initiators of apoptotic cell death. Cell 103:839–842
11. Chittenden T (2002) BH3 domains: intracellular death-ligands critical for initiating apoptosis. Cancer Cell 2:165–166
12. Walensky LD, Gavathiotis E (2011) BAX unleashed: the biochemical transformation of an inactive cytosolic monomer into a toxic mitochondrial pore. Trends Biochem Sci 36:642–652
13. Dewson G, Kluck RM (2009) Mechanisms by which Bak and Bax permeabilize mitochondria during apoptosis. J Cell Sci 122:2801–2808
14. Certo M, Del Gaizo MV, Nishino M et al (2006) Mitochondria primed by death signals determine cellular addiction to antiapoptotic BCL-2 family members. Cancer Cell 9:351–365
15. Amundson SA, Myers TG, Scudiero D et al (2000) An informatics approach identifying markers of chemosensitivity in human cancer cell lines. Cancer Res 60:6101–6110
16. Sattler M, Liang H, Nettesheim D et al (1997) Structure of Bcl-xL-Bak peptide complex: recognition between regulators of apoptosis. Science 275:983–986
17. Petros AM, Nettesheim DG, Wang Y et al (2000) Rationale for Bcl-x(L)/Bad peptide complex formation from structure, mutagenesis, and biophysical studies. Protein Sci 9:2528–2534
18. Zhang H, Nimmer P, Rosenberg SA et al (2002) Development of a high-throughput fluorescence polarization assay for Bcl-xL. Anal Biochem 307:70–75
19. Petros AM, Medek A, Nettesheim DG et al (2001) Solution structure of the antiapoptotic protein Bcl-2. Proc Natl Acad Sci USA 98:3012–3017
20. Aouacheria A, Brunet F, Gouy M (2005) Phylogenomics of life-or-death switches in multicellular animals: Bcl-2, BH3-only, and BNip families of apoptotic regulators. Mol Biol Evol 22:2395–2416
21. Day CL, Chen L, Richardson SJ et al (2005) Solution structure of prosurvival Mcl-1 and characterization of its binding by proapoptotic BH3-only ligands. J Biol Chem 280:4738–4744
22. Muchmore SW, Sattler M, Liang H et al (1996) X-ray and NMR structure of human Bcl-xL, an inhibitor of programmed cell death. Nature 381:335–341

23. Denisov AY, Madiraju MSR, Chen G et al (2003) Solution structure of human BCL-w: modulation of ligand binding by the C-terminal helix. J Biol Chem 278:21124–21128
24. Wendt MD (2008) Discovery of ABT-263, a Bcl-family protein inhibitor. Observations on targeting a large protein-protein interaction. Expert Opin Drug Discov 3:1123–1143
25. Arkin MR, Wells JA (2004) Small-molecule inhibitors of protein-protein interactions; progressing towards the dream. Nat Rev Drug Discov 3:301–317
26. Chène P (2006) Drugs targeting protein-protein interactions. ChemMedChem 1:400–411
27. Coyne AG, Scott DE, Abell C (2010) Drugging challenging targets using fragment-based approaches. Curr Opin Chem Biol 14:299–307
28. Congreve M, Chessari G, Tisi D, Woodhead AJ (2008) Recent developments in fragment-based drug discovery. J Med Chem 51:3661–3680
29. Cuningham BC, Wells JA (1989) High-resolution epitope mapping of hGH-receptor interactions by alanine-scanning mutagenesis. Science 244:1081–1085
30. Clackson T, Wells JA (1995) A hot spot of binding energy in a hormone-receptor interface. Science 267:383–386
31. Clackson T, Ultsch MH, Wells JA, de Vos AM (1998) Structural and functional analysis of the 1:1 growth hormone:receptor complex reveals the molecular basis for receptor affinity. J Mol Biol 277:1111–1128
32. Hajduk PJ (2006) Applications of receptor-based NMR screening in drug discovery. Mod Magn Reson 2:1383–1389
33. Petros AM, Dinges J, Augeri DA et al (2006) Discovery of a potent inhibitor of the antiapoptotic protein Bcl-xL from NMR and parallel synthesis. J Med Chem 49:656–663
34. Oltersdorf T, Elmore SW, Shoemaker AR et al (2005) An inhibitor of Bcl family proteins induces regression of solid tumours. Nature 435:677–681
35. Wendt MD, Shen W, Kunzer A et al (2006) Discovery and structure-activity relationships of antagonists of B-cell lymphoma 2 family proteins with chemopotentiation activity in vitro and in vivo. J Med Chem 49:1165–1181
36. Mao H, Hajduk PJ, Craig R et al (2001) Rational design of diflunisal analogous with reduced affinity for human serum albumin. J Am Chem Soc 123:10429–10435
37. Curry S, Mandelkow H, Brick P, Franks N (1998) Crystal structure of human serum albumin complexed with fatty acid reveals an asymmetric distribution of binding sites. Nat Struct Biol 5:827–835
38. Hajduk PJ, Mendoza R, Petros AM et al (2003) Ligand binding to domain-3 of human serum albumin: a chemometric analysis. J Comput-Aided Mol Des 17:93–102
39. Shoemaker AR, Oleksijew A, Bauch J et al (2006) A small-molecule inhibitor of Bcl-xL potentiates the activity of cytotoxic drugs in vitro and in vivo. Cancer Res 66:8731–8739
40. Tsujimoto Y, Finger LR, Yunis J et al (1984) Cloning of the chromosomal breakpoint of neoplastic B cells with the t(14;18) chromosome translocation. Science 226:1097–1099
41. Petros AM, Olejniczak ET, Fesik SW (2004) Structural biology of the Bcl-2 family of proteins. Biochim Biophys Acta 1644:83–94
42. Wendt MD (2012) Targeting protein-protein interactions: dual inhibitors of Bcl-2 and Bcl-xL. In: Morphy JR, Harris CJ (eds) Designing multi-target drugs. RSC, Cambridge
43. Bruncko M, Oost TK, Belli BA et al (2007) Studies leading to potent, dual inhibitors of Bcl-2 and Bcl-xL. J Med Chem 50:641–662
44. Goh CS, Milburn D, Gerstein M (2004) Conformational changes associated with protein-protein interactions. Curr Opin Struct Biol 14:104–109
45. Lee EF, Czabotar PE, Smith BJ et al (2007) Crystal structure of ABT-737 complexed with Bcl-xL: implications for selectivity of antagonists of the Bcl-2 family. Cell Death Differ 14:1711–1713
46. Porter J, Payne A, de Candole B et al (2009) Tetrahydroisoquinoline amide substituted phenyl pyrazoles as selective Bcl-2 inhibitors. Bioorg Med Chem Lett 19:230–233
47. Castro AC, Grogan MJ, Holson EB et al US Patent App Publ 2007/0155705 A1, Jul 5 2007

48. Petros AM, Huth JR, Oost T et al (2010) Discovery of a potent and selective Bcl-2 inhibitor using SAR by NMR. Bioorg Med Chem Lett 20:6587–6591
49. Del Gaizo MV, Brown JR, Certo M et al (2007) Chronic lymphocytic leukemia requires BCL2 to sequester prodeath BIM, explaining sensitivity to BCL2 antagonist ABT-737. J Clin Invest 117:112–121
50. Vogler M, Dinsdale D, Sun S-M et al (2008) A novel paradigm for rapid ABT-737-induced apoptosis involving outer mitochondrial membrane rupture in primary leukemia and lymphoma cells. Cell Death Differ 15:820–830
51. Trudel S, Stewart AK, Li Z et al (2007) The Bcl-2 family protein inhibitor, ABT-737, has substantial antimyeloma activity and shows synergistic effect with dexamethasone and melphalan. Clin Cancer Res 13:621–629
52. Chauhan D, Velankar M, Brahmandam M et al (2007) A novel Bcl-2/Bcl-XL/Bcl-w inhibitor ABT-737 as therapy in multiple myeloma. Oncogene 26:2374–2380
53. Kline MP, Rajkumar SV, Timm MM et al (2007) ABT-737, an inhibitor of Bcl-2 family proteins, is a potent inducer of apoptosis in multiple myeloma cells. Leukemia 21:1549–1560
54. Kohl TM, Hellinger C, Ahmed F et al (2007) BH3 mimetic ABT-737 neutralizes resistance to FLT3 inhibitor treatment mediated by FLT3-independent expression of BCL2 in primary AML blasts. Leukemia 21:1763–1772
55. Konopleva M, Contractor R, Tsao T et al (2006) Mechanisms of apoptosis sensitivity and resistance to the BH3 mimetic ABT-737 in acute myeloid leukemia. Cancer Cell 10:375–388
56. Kuroda J, Puthalakath H, Cragg MS et al (2006) Bim and Bad mediate imatinib-induced killing of Bcr/Abl + leukemic cells, and resistance due to their loss is overcome by a BH3 mimetic. Proc Natl Acad Sci USA 103:14907–14912
57. Del Gaizo MV, Schlis KD, Sallan SE et al (2008) BCL-2 dependence and ABT-737 sensitivity in acute lymphoblastic leukemia. Blood 111:2300–2309
58. Tahir SK, Yang X, Anderson MG et al (2007) Influence of Bcl-2 family members on the cellular response of small-cell lung cancer cell lines to ABT-737. Cancer Res 67:1176–1183
59. Kaiser U, Schilli M, Haag U et al (1996) Expression of Bcl-2 protein in small cell lung cancer. Lung Cancer 15:31–40
60. Sartorius UA, Krammer PH (2002) Upregulation of Bcl-2 is involved in the mediation of chemotherapy resistance in human small cell lung cancer cell lines. Int J Cancer 97:584–592
61. Zhang YK, Fujita N, Tsuruo T (1999) p21(waf1/cip1) acts in synergy with Bcl-2 to confer multidrug resistance in a comptothecin-selected human lung-cancer cell line. Int J Cancer 83:790–797
62. Zangemeister-Wittke U, Schenker T, Luedke GH, Stahel RA (1998) Synergistic toxicity of bcl-2 antisense oligodeoxynucleotides and etoposide, doxorubicin and cisplatin on small-cell lung cancer cell lines. Br J Cancer 78:1035–1042
63. Higashiyama M, Doi O, Kodama K, Yokouchi H, Tateishi R (1996) Bcl-2 oncoprotein expression is increased especially in the portions of small cell carcinoma within the combined type of small cell lung cancer. Tumour Biol 17:341–344
64. Hann CL, Daniel VC, Sugar EA et al (2008) Therapeutic efficacy of ABT-737, a selective inhibitor of BCL-2, in small cell lung cancer. Cancer Res 68:2321–2328
65. Cragg MS, Harris C, Strasser A, Scott CL (2009) Unleashing the power of inhibitors of oncogenic kinases through BH3 mimetics. Nat Rev Cancer 9:321–326
66. Paoluzzi L, Gonen M, Bhagat G et al (2008) The BH3-only mimetic ABT-737 synergizes the antineoplastic activity of proteasome inhibitors in lymphoid malignancies. Blood 112:2906–2916
67. Lieber J, Eicher C, Wenz J et al (2011) The BH3 mimetic ABT-737 increases treatment efficiency of paclitaxel against hepatoblastoma. BMC Cancer 11:362
68. Deng J, Carlson N, Takeyama K et al (2007) BH3 profiling identifies three distinct classes of apoptotic blocks to predict response to ABT-737 and conventional chemotherapeutic agents. Cancer Cell 12:171–185

69. Huang S, Sinicrope FA (2008) BH3 Mimetic ABT-737 potentiates TRAIL-mediated apoptotic signaling by unsequestering Bim and Bak in human pancreatic cancer cells. Cancer Res 68:2944–2951
70. Chen S, Dai Y, Pei XY, Grant S (2009) Bim upregulation by histone deacetylase inhibitors mediates interactions with the Bcl-2 antagonist ABT-737: evidence for distinct roles for Bcl-2, Bcl-xL, and Mcl-1. Mol Cell Biol 29:6149–6169
71. Chen S, Dai Y, Harada H et al (2007) Mcl-1 down-regulation potentiates ABT-737 lethality by cooperatively inducing Bak activation and Bax translocation. Cancer Res 67:782–791
72. van Delft MF, Wei AH, Mason KD et al (2006) The BH3 mimetic ABT-737 targets selective Bcl-2 proteins and efficiently induces apoptosis via Bak/Bax if Mcl-1 is neutralized. Cancer Cell 10:389–399
73. Park C-M, Bruncko M, Adickes J et al (2008) Discovery of an orally bioavailable small molecule inhibitor of prosurvival B-cell lymphoma 2 proteins. J Med Chem 51:6902–6915
74. Tse C, Shoemaker AR, Adickes J et al (2008) ABT-263: a potent and orally bioavailable Bcl-2 family inhibitor. Cancer Res 68:3421–3428
75. Shoemaker AR, Mitten MJ, Adickes J et al (2008) Activity of the Bcl-2 family inhibitor ABT-263 in a panel of small cell lung cancer xenograft models. Clin Cancer Res 14:3268–3277
76. Ackler S, Mitten MJ, Foster K et al (2010) The Bcl-2 inhibitor ABT-263 enhances the response of multiple chemotherapeutic regimens in hematologic tumors in vivo. Cancer Chemother Pharmocol 66:869–880
77. Ackler S, Xiao Y, Mitten MJ et al (2008) ABT-263 and rapamycin act cooperatively to kill lymphoma cells *in vitro* and *in vivo*. Mol Cancer Ther 7:3265–3274
78. Shangary S, Wang S (2009) Small-molecule inhibitors of the MDM2-p53 protein-protein interaction to reactivate p53 function: a novel approach for cancer therapy. Ann Rev Pharmacol Toxicol 49:223–241
79. Kazi A, Sun J, Doi K et al (2011) The BH3 α-helical mimic BH3-M6 disrupts Bcl-XL, Bcl-2, and MCL-1 protein-protein interactions with Bax, Bak, Bad, or Bim and induces apoptosis in a Bax- and Bim-dependent manner. J Biol Chem 286:9832–9842
80. Pitter K, Bernal F, Labelle J, Walensky LD (2008) Dissection of the BCL-2 family signaling network with stabilized alpha-helices of BCL-2 domains. Methods Enzymol 446:387–408
81. Hajduk P (2006) Fragment-based drug design: how big is too big? J Med Chem 49:6972–6976
82. Eyrisch S, Helms V (2007) Transient pockets on protein surfaces involved in protein-protein interactions. J Med Chem 50:3457–3464
83. Palm K, Luthman K, Ungell A-L, Strandlund G, Artursson P (1996) Correlation of drug absorption with molecular surface properties. J Pharm Sci 85:32–39
84. Palm K, Stenberg P, Luthman K, Artursson P (1997) Polar molecular surface properties predict the intestinal absorption of drugs in humans. Pharm Res 14:568–571
85. Egan WJ, Lauri G (2002) Prediction of intestinal permeability. Adv Drug Deliv Rev 54:273–289
86. Martin Y (2005) A bioavailability score. J Med Chem 48:3164–3167
87. Dobson PD, Kell DB (2008) Carrier-mediated cellular uptake of pharmaceutical drugs: an exception or the rule? Nat Rev Drug Discov 7:205–220
88. Koepsell H, Endou H (2004) The SLC22 drug transporter family. Pflugers Arch 447:666–676
89. Hagenbuch B, Meier PJ (2004) Organic anion transporting polypeptides of the OATP/LSC21 family: phylogenetic classification as OATP/SLCO superfamily, new nomenclature and molecular/functional properties. Pflugers Arch 447:653–665

Index